Steffen STELZER

Dissertation

“…we are hesitant but cannot resist the temptation to draw a straight line..."

(Paris and Erdogan introducing their Paris law,1963)

Steffen STELZER

Dissertation

Optimized experimental methods for the description of the delamination and failure behavior of high performance composites and joints

December 2014

Institute of Materials Science and Testing of Polymers

Department Polymer Engineering and Science, Montanuniversitaet Leoben

About the Dissertation

This cumulative Dissertation was authored by

DI Steffen STELZER
born April 14, 1985
in Leoben (Steiermark, Austria)

Submitted to

Institute of Materials Science and Testing of Polymers
Department Polymer Engineering and Science
Montanuniversitaet Leoben

Conducted at

Institute of Materials Science and Testing of Polymers
Department Polymer Engineering and Science
Montanuniversitaet Leoben

Academic Supervisor

Univ.-Prof. Dr. Gerald PINTER
Institute of Materials Science and Testing of Polymers
Department Polymer Engineering and Science
Montanuniversitaet Leoben

AFFIDAVIT

I declare in lieu of oath, that I wrote this thesis and performed the associated research myself, using only literature cited in this volume.

Leoben, December 2014 (Steffen Stelzer)

FUNDING

Funding of the Austrian Research Promotion Agency for project 830384 “Composite+composite Joints with Enhanced damage toleranCe (CoJEC)” is gratefully acknowledged as well as the support of the involved project partners FACC AG, Fronius International GmbH, Rübig GmbH & Co KG, Fill GmbH, RECENDT GmbH and LKR Leichtmetall Kompetenzzentrum Ranshofen.

ACKNOWLEDGMENTS

Many people have helped me to finish this PhD thesis and I would like to hereby express my gratitude.

First of all I want to thank my supervisor Univ.-Prof. Dr. Gerald Pinter (Institute of Materials Science and Testing of Polymers, Department Polymer Engineering and Science, Montanuniversitaet Leoben, AT) for his help, motivation, professional input and friendship. He has been a very good mentor. His ways to inspire me in finding new ways to improve my work are exceptional. Besides starting up the Institute in the new building he always had time to talk and never lost his positive attitude. He pushed me to achieve goals that seemed beyond reach, but also stood by my side, when times were rough.

I thank Univ.-Prof. Dr.-Ing. Ralf Schledjewski (Institute for Processing of Composites, Department Polymer Engineering and Science, Montanuniversitaet Leoben, AT) for supervising my elective subject and giving relevant input towards processing of composite materials.

I would like to express my gratitude to Dr. Andreas Brunner (EMPA, Swiss Federal Laboratories for Materials Science and Technology, CH) for co-authoring many of my publications and for being a very important scientific partner throughout my PhD.

Regular meetings with the members of the European Structural Integrity Society, Technical Committee 4 on Polymers and Composites improved my understanding of fracture mechanics in polymers. Numerous discussions with leading researchers in the field of fracture mechanics gave me the opportunity to learn from their experience. I would like to thank Prof. Gordon Williams (Imperial College London, UK), Prof. Anthony Kinloch (Imperial College London, UK) and Prof. Ian Horsefall (Cranfield University, UK) among others for letting me be part of the committee and doing me the great honor of assigning me to the lead of the work area on composite fatigue. Also, I would like to thank Univ.-Prof. Gerald Pinter for giving me the opportunity to join the regular ESIS TC4 meetings.

Dr. Stephan Ucsnik (Leichtmetallkompetenzzentrum Ranshofen) was project leader of the funded project “composite-composite joints with enhanced damage tolerance” (CoJEC). Based on his knowledge on joining metal to carbon fiber

reinforced polymers it was possible to successfully develop a hybrid joining technology for joining composites to composites. Furthermore I would like to thank Dipl.-Ing. Harald Sehrschön (Fill GmbH, Gurten), Gerhard Sieglhuber (Fill GmbH, Gurten), Martin Schickbauer (Fill GmbH), Andreas Waldhoer (Fronius GmbH, Wels) and Dipl.-Ing. (FH) Jürgen Tauchner (FACC AG, Ried im Innkreis) among other persons that were involved in the successful development of a new composite-composite joining technology within the project CoJEC.

I thank all my co-authors that supported me in the preparation of the publications presented in this thesis. Also, I thank Dipl.-Ing. Georg Singer, Dipl.-Ing. Christian Schillfahrt, Dipl.-Ing. Thomas Unger and Georg Kaltenegger, who carried out their Bachelor and Master Theses within CoJEC and other projects.

I thank my colleague in office, Dipl.-Ing. Peter Guttmann, and all the members of the Institute for Materials Science and Testing of Polymers for numerous conversations and content related input. I thank them for their support in the lab and for all the little things that are necessary to successfully bring a PhD thesis to an end. I especially thank Jürgen Grosser, Jürgen Föttinger and Stefan Hinterdorfer for their commitment in the fatigue laboratory. They provided hands, where more than two were necessary.

I thank all my friends for their understanding and their patience during the last time of my thesis.

Most of all I thank my parents. For the lifelong support they gave me and their firm trust in my abilities. Because of them I got the opportunity to study. They fostered my interest in science and did not hesitate to accept personal cutbacks to my benefit. I know I only need to ask and they do anything to help me.

Finally I would like to thank my girlfriend Claudia Steinmetz. She has been there for me in hard times and celebrated with me in the good times. She gave me strength and distracted me, when I was getting lost in thoughts. With her never ending support, she had great part in the successful completion of this thesis.

ABSTRACT

This thesis deals with the characterization of the delamination behavior of endless fiber reinforced polymer (FRP) composites and with through-the-thickness reinforcements that suppress the evolution of such delaminations in composites.

Delamination is a common problem occurring in FRP composites because of their layered structure. Yet, there are no standards dealing with the fatigue delamination growth in composite materials. One part of this thesis is the characterization of the fatigue delamination behavior of composites in mode I and mode II. Round robin exercises were carried out to evaluate the potential of fatigue delamination tests for standardization.

Test campaigns were conducted within subcommittee D30.06 of the American Society for Testing and Materials (ASTM), and committee TC4 within the European Structural Integrity Society (ESIS). The tests were carried out on four carbon fiber reinforced epoxy composites, on one glass fiber reinforced epoxy composite and one carbon fiber reinforced poly-ether-ether-ketone (PEEK). They showed the reproducibility and in- and inter-laboratory scatter and also highlighted the limits of fatigue delamination tests.

Round robin activities within ESIS TC4 and ASTM D30.06 emphasized the need to find new ways for data presentation in order to make the data accessible for design purposes. The three major questions are: (1) is it possible to reduce the scatter of the fatigue crack growth curves, (2) how can the slope of the Paris law curve be reduced and (3) is the detection of a threshold value feasible in composite materials? These questions are faced in this thesis by introducing a new way of data presentation. A Hartman-Schijve based approach, where the crack growth rate is dependent on the amount by which the strain energy release rate exceeds the threshold value, seems to be a reliable and physically feasible way to receive Paris like fatigue crack growth curves with slope values around 2. This is significantly less than slope values of around 10 seen in classical Paris law data presentations. With small slope values the errors in predicted crack growth rate are reduced when considering certain load cases in a composite component. This can lead to reliable lifetime predictions.

Further, based on the experiences from the international test campaigns, fatigue delamination tests were carried out on carbon fiber reinforced epoxy composites,

which were produced via different manufacturing routes. These tests revealed that fatigue delamination tests can even pick up small changes in the fiber distribution, which are caused by changes in the preforming process.

Another focus of this work was put on suppression of delaminations in composites and composite to composite joining. A novel joining technology based on 3D shaped metallic pins, which are produced via cold metal transfer (CMT) welding, is presented in this thesis. An integral part of this technology is the form fit connection between the metal and the surrounding CFRP, which is provided by the 3D shape of the CMT pin. The CMT pins are welded onto thin metal sheets, which act as carrier elements and ease the positioning of the pins in the joint. Composite-composite joints were reinforced with CMT pins with the aim to suppress/delay the initiation and growth of delaminations in the joint area by making use of the pins' form-fit connection and to increase the damage tolerance of the joint by plastic deformation of the CMT pins.

In a first test campaign, tests were carried out on co-cured specimens without CMT pin reinforcement. Numerical simulations of these tests helped to get a basic understanding of the failure behavior of co-cured single lap shear (SLS) specimens, to localize areas of increased interlaminar stresses and to find optimum positions for through-the-thickness reinforcements. Detailed investigations of quasi-static tensile tests on CMT pin reinforced SLS specimens with different pretreatment yielded a failure model for the complex loading behavior of CMT pin reinforced SLS specimens. In a next step, the knowledge gained from this first test campaign was transferred to other types of pin reinforcements. CMT titanium pin reinforced specimens were investigated as well as titanium z-pin reinforced specimens. Finally, the fatigue behavior of unreinforced and through-the-thickness reinforced composite-composite joints was evaluated.

Tests under both, quasi-static and fatigue loading, showed the high potential of CMT pin reinforcements for the suppression of delamination in the bond line of composite-composite joints. The pin reinforcements transfer loads between two composite adherends even after adhesive failure of the bond line in the joint. Final failure in CMT pin reinforced specimens occurs at high levels of strain and necessitates significantly higher amounts of energy than in unreinforced specimens.

KURZFASSUNG

Diese Dissertation beschäftigt sich mit dem Delaminationsverhalten von endlos faserverstärkten Kunststoffverbunden (FKV) und mit der Vermeidung von Delaminationen in FKV durch das gezielte Einbringen von Verstärkungen in die Dickenrichtung (translaminare Verstärkungen).

Delaminationen treten in FKV aufgrund deren Schichtstruktur und der geringen interlaminaren Festigkeiten auf. Obwohl Delamination in FKV ein bekanntes und relativ gut erforschtes Problem ist, existieren nach wie vor keine standardisierten Prüfmethoden für die Bestimmung des Delaminationsverhaltens von FKV unter Ermüdungslasten. Deshalb befasst sich ein Teil dieser Dissertation mit der Durchführung zyklischer Delaminationsversuche und der Organisation von Ringversuchen, um das Potential von Delaminationsversuchen für eine Standardisierung zu evaluieren.

Internationale Versuchskampagnen wurden innerhalb der „American Society for Testing and Materials“ (ASTM), Subkommitee D30.06, und der „European Structural Integrity Society“ (ESIS), technisches Komitee 4, organisiert und durchgeführt. Delaminationsversuche an vier verschiedenen kohlenstoff-faserverstärkten Epoxidharzen, einem glasfaserverstärkten Epoxidharz und einem kohlenstofffaserverstärkten Polyetheretherketon zeigten die bei diesen Versuchen auftretenden Streuungen (v.a. im Vergleich mehrerer Labors). Es offenbarten sich dabei die Grenzen der Anwendbarkeit dieser Versuche, vor allem hinsichtlich der Bestimmung des Schwellenwertes und der Anwendbarkeit der Ergebnisse klassischer Darstellungen des Risswachstumsverhaltens auf Basis des Gesetzes von Paris im Design von FKV.

Die Ringversuche innerhalb ESIS TC4 und ASTM D30.06 zeigten die Notwendigkeit, neue Auswerteroutinen für zyklische Delaminationsversuche zu finden, um (1) die Streuung der Delaminationswachstumskurven zu verringern, (2) die hohen Steigungswerte der Delaminationswachstumskurven zu verringern und (3) Schwellenwerte besser erfassen zu können. Diesen Punkten wird in dieser Dissertation mit einer neuen Art der Datendarstellung begegnet. Die Darstellung der Energiefreisetzungsraten auf Basis eines modifizierten Hartman-Schijve Ansatzes lieferte Delaminationswachstumskurven mit Steigungswerten von etwa 2. Solch niedrige Steigungswerte können Fehler bei der Vorhersage von Risswachstumsraten auf Basis von Delaminationswachstumskurven verringern

und könnten so zur Verwendung dieser Daten im Design von FKV Strukturen führen.

Auf Basis der Erfahrungen, die in den internationalen Ringversuchen gemacht wurden, wurden zyklische Delaminationsversuche angewendet, um den Einfluss verschiedener Preformingprozesse auf das Delaminationsverhalten von kohlenstofffaserverstärkten Epoxidharzen zu untersuchen. Das Delaminations-wachstum wurde dabei signifikant durch die Verarbeitungsvorgeschichte beeinflusst und es war möglich, diese Unterschiede mit zyklischen Delaminationsversuchen zu erfassen.

Ein weiterer Fokus dieser Arbeit lag auf der Unterdrückung von Delaminationen in FKV-FKV Verbindungen. Zu diesem Zweck wurde im Rahmen dieser Arbeit eine neuartige Verbindungstechnik für FKV untersucht. Diese basiert auf kleinen metallischen Stiften, die mit dem FKV eine formschlüssige Verbindung eingehen. Diese metallischen Stifte werden mittels „Cold Metal Transfer“ (CMT) Schweißen, hergestellt. Dabei werden die „CMT Pins“ auf dünne, metallische Bleche aufgeschweißt, welche als Trägerelement und Positionierungshilfe im Fügeprozess dienen. Das Ziel bei der Verwendung der CMT Pins liegt, neben der Unterdrückung/Verzögerung von Delaminationen durch den Formschluss, in der Erhöhung der Schadenstoleranz durch die plastische Deformation des Metalls.

In einem ersten Versuchsdurchlauf wurde das Versagensverhalten von co-gehärteten einschnittigen FKV-FKV Verbindungen experimentell und numerisch untersucht. Auf Basis der dabei gewonnenen Erkenntnisse wurden bevorzugte Positionen für translaminare Verstärkungen in FKV-FKV Verbindungen ermittelt. Darauf folgende detaillierte Untersuchungen an translaminar verstärkten FKV-FKV Verbindungen mündeten in einem Versagensmodell für CMT-Pin verstärkte Verbindungen. Versuche an mit CMT Pins translaminar verstärkten FKV-FKV Verbindungen unter quasi-statischen und Ermüdungslasten zeigten das Potential dieser Verbindungstechnologie auf. Nach dem adhäsiven Versagen der Verbindung übernahmen die metallischen Pins die Lasten und führten zu einer signifikanten Erhöhung der Schadenstoleranz.

TABLE OF CONTENTS

PART I:

Introduction and Scope

1 INTRODUCTION TO THE THESIS

1.1 MOTIVATION

Fiber reinforced polymer (FRP) composites combine high strength and stiffness with low density and therefore provide excellent specific mechanical material properties. They typically consist of glass, carbon or aramid fibers that are embedded in thermoset (e.g. epoxy) or thermoplastic (e.g. poly-ether-ether-ketone) matrix resins. Typically, layers of fibers are disposed on each other to achieve properties that match the loading situation present in a composite structure. Ideally, these loads occur in plane with the layers of fibers. Loads occurring perpendicular to this plane (e.g. caused by changes in geometry) can cause interlaminar crack initiation and growth [1]. Various authors have shown that in structural applications under fatigue loads, delaminations can initiate and grow to a critical size, when not monitored and repaired [2–12].

In the preface of the proceedings of the first European Conference of Composite Materials Prof. Ingnazio Crivelli-Visconti mentioned that major advances had been made in the use of fracture mechanics for design of composite materials [13] (in this thesis, the term “composite material” is limited to endless fiber-reinforced polymers). This was in 1985. Yet, there is still no standard for the characterization of fatigue delamination properties of composite materials available in 2014. Consequently, designs of composite structures are not based on the knowledge of delamination growth. For certification purposes current designs are such that any delamination will not grow. Nevertheless, various authors mentioned cases, where delaminations occurred in composite structures, despite these design philosophies [3,14,15]. The importance of delamination in composite structures was highlighted by Schön et al. [14], who stated:

> *“During certification of the AIRBUS A320 vertical fin, no delamination growth was detected during static loading. The following fatigue loading of the same component had to be interrupted due to large delamination growth. The delamination grew due to out-of-plane loads.“*

Also, for the estimation of inspection intervals a reliable relation between delamination growth rates and applied loads needs to be established.

Jones et al. [15] stated:

> *"…the delamination growth seen in various full scale fatigue tests also highlight the need to develop a methodology that can be used to accurately and reliably predict the inspection intervals associated with delamination growth arising from small naturally occurring defects."*

However, besides the lack of a standard for fatigue delamination measurements, there does not exist data showing the in- and inter-laboratory scatter of delamination fatigue measurements. This will be essential for the estimation of safety factors, if fatigue crack growth (FCG) curves are to be used in the design of composite structures.

Further, new methods for data presentation are needed, because in contrast to metals, composite materials give fatigue crack growth curves with high values of the exponent of the power law given in equation (1.1). This power law by Paris and Erdogan [16,17] relates the range of the stress intensity factor to the crack growth rate. It describes the linear relationship between crack growth rate, da/dN and the stress intensity factor, K, in a double logarithmic diagram ('Paris curve'):

$$da/dN = B\,(\Delta K)^n \tag{1.1}$$

where B and n are constants of the power law. The stress intensity factor was later replaced by the strain energy release rate, G, in order to account for the complex stress ahead of the crack tip in composite materials [18–20]:

$$da/dN = A\,(\Delta G)^m \tag{1.2}$$

where A and m again are constants of the power law. With large exponents, small errors in the applied load lead to large errors in the predicted growth rate. Since composite materials do give rather steep Paris curves, it is necessary to find data presentations for fatigue delamination growth curves with smaller exponents [19].

Areas that are especially susceptible to delaminations are joints. Cracks can initiate at ply drops, free edges, or holes due to interlaminar stresses [1]. Many research groups have focused on reducing interlaminar stresses by reinforcing the laminate with through-the-thickness reinforcements. Stitching [21–26], z-pinning [27–32] and tufting [33,34] are the most common through-the-thickness reinforcement techniques.

These reinforcements are based on glass [33,34], carbon [33,35,36] or polymeric fibers [37–39]. Recent research works investigated the potential of metallic reinforcements [40–46]. Metallic reinforcements additionally contribute to the damage tolerance of the joint by plastic deformation of the metal. Furthermore, metals allow to form shapes that create a form-fit connection between the through thickness reinforcement and the surrounding composite.

1.2 OBJECTIVES

With regard to the considerations mentioned above, the objectives of this dissertation were defined in the following manner:

1. Development of a test procedure for fatigue delamination.
   - Comprehensive investigation of test parameters, such as test frequency, specimen geometry and type of control mode.
2. Investigation of the in- and inter-laboratory reproducibility of fatigue crack growth curves of composite materials.
   - Organization of international round robin exercises in mode I and mode II.
   - Investigation of the applicability of common data reduction schemes to fatigue delamination growth data.
3. Investigation of the applicability of fatigue crack growth data to design of composite structures.
   - Assessment of state of the art data reduction schemes.
   - Development of alternative data presentation techniques for delamination growth curves.
4. Suppression of delaminations in composites and composite-composite joints.
   - Investigation of the effect of pin reinforcement on damage tolerance of composite-composite joints.
   - Evaluation of the effect of pin reinforcement on the fatigue properties of composite-composite joints.

1.3 STRUCTURE OF THE THESIS

According to the objectives outlined above, this thesis presents a series of subsequent publications illustrating the progress in developing optimized experimental methods for the description of the delamination and failure behavior of high performance composites and joints. The thesis is divided into four parts:

1. Introduction to the thesis
2. Delamination of composite materials
3. Delamination suppression and joining
4. Summary and outlook

The first part gives an introduction to the topics dealt with in this thesis. Based on the motivation, the objectives of the thesis are outlined and the structure of the thesis is presented.

Part two is dedicated to the measurement of the delamination behavior of composite materials and addresses points 1 to 3 of the objectives. The main focus is the development of a standardized test procedure for the measurement of FCG curves in endless fiber reinforced composite materials. In **publication 1** parameter studies are carried out in mode I, which is the tensile crack opening mode. These are done in order to evaluate which testing parameters are significant in the measurement of FCG curves of composites. **Publications 2 and 3** present pre-standardization tests in mode I fatigue that were carried out within subcommittee D30.06 of the American Society for Testing and Materials (ASTM), and technical committee 4 (TC4) within the European Structural Integrity Society (ESIS).. **Publication 4** shows preliminary results from round robin activities in mode II, where shear loads are imposed on the crack tip. In **publication 5** the mode I fatigue testing procedure is applied to differently manufactured CFRP. The sensitivity of this testing method to small changes in the fiber distribution is illustrated.

The tests carried out in **publications 1 - 4** show that some factors limit the use of FCG data for design. Therefore, **publication 6** presents a method that aims at overcoming problems related to fracture mechanics based design in composites.

The third part of this thesis addresses point 4 of the objectives. It deals with delamination suppression in and joining of composite materials. A novel joining technology for composite materials based on metallic pins aims at the suppression of delaminations in the bonding area of composite to composite joints. This novel joining technology is introduced in **publication 7**. In this manuscript the main

failure mechanisms are investigated. In **publication 8** the authors evaluate the effect of various through-the-thickness reinforcements on the strength and damage tolerance of composite-composite joints under quasi-static loading conditions. **Publication 9** studies the effect of through-the-thickness reinforcements on the fatigue performance of composite-composite joints.

In the fourth part, the thesis is reviewed, the key findings of the thesis are presented and an outlook to future investigations is given. The appendix of this thesis shows the abbreviations and symbols used in this thesis.

In the following, the publications presented in this thesis are listed:

Publication 1: Cyclic interlaminar crack growth in unidirectional and braided composites

Publication 2: Mode I delamination fatigue crack growth in unidirectional fiber reinforced composites: development of a standardized test procedure

Publication 3: Mode I delamination fatigue crack growth in unidirectional fiber reinforced composites: Results from ESIS TC4 round-robins

Publication 4: Mode II fatigue delamination resistance of advanced fiber-reinforced polymer-matrix laminates: Towards the development of a standardized test procedure

Publication 5: Influence of fiber placement and architecture on fracture mechanical properties of carbon fiber reinforced composites

Publication 6: Mode I, II and Mixed Mode I/II delamination growth in composites

Publication 7: Mechanical characterization of a novel composite-composite joining technology with through-the-thickness reinforcement for enhanced damage tolerance

Publication 8: Strength and damage tolerance of composite-composite joints with metallic through-the-thickness reinforcements

Publication 9: Fatigue behavior of CMT pin reinforced composite-composite joints

1.4 REFERENCES

[1] Sierakowski RL, Newaz GM. Damage tolerance in advanced composites. Basel: Technomic Publishing AG; 1995.

[2] Cairns DS, Riddle T, Nelson J. Wind Turbine Composite Blade Manufacturing: The Need for Understanding Defect Origins, Prevalence, Implications and Reliability. Sandia Report 2011;1094.

[3] Chalkley P, Geddes R. Service history of the F-111 wing pivot fitting upper surface boron/epoxy doublers: DSTO-TN-0168. Department of Defence, September 1998.

[4] Savage G. Sub-critical crack growth in highly stressed Formula 1 race car composite suspension components. Engineering Failure Analysis 2009;16(2):608–17.

[5] Schön J, Nyman T, Blom A, Ansell H. A numerical and experimental investigation of delamination behaviour in the DCB specimen. Composites Science and Technology 2000;60(2):173–84.

[6] Greenhalgh ES. Delamination growth in carbon-fibre composite structures. Composite Structures 1993;23(2):165–75.

[7] Greenhalgh ES, Hiley M. The assessment of novel materials and processes for the impact tolerant design of stiffened composite aerospace structures. Composites Part A: Applied Science and Manufacturing 2003;34:151–61.

[8] Tay TE. Characterization and analysis of delamination fracture in composites: An overview of developments from 1990 to 2001. Applied Mechanics Reviews 2003;56:1–31.

[9] Gilchrist MD, Kinloch AJ, Matthews FL. Mechanical performance of carbon-fibre- and glass-fibre-reinforced epoxy I-beams: III. fatigue performance. Composites Science and Technology 1999;59(2):179–200.

[10] Gilchrist MD, Kinloch AJ, Matthews FL. Mechanical performance of carbon-fibre and glass-fibre-reinforced epoxy I-beams: II. Fractographic failure observations. Composites Science and Technology 1996;56(9):1031–45.

[11] Bolotin VV. Delaminations in composite structures: Its origin, buckling, growth and stability. Composites Part B: Engineering 1996;27(2):129–45.

[12] Martin RH. Incorporating interlaminar fracture mechanics into design. Proceedings of the Institution of Mechanical Engineers, Part L: Journal of Materials Design and Applications 2000;214(2):91–7.

[13] Crivelli-Visconti I. A sensible approach to composite structures. In: Brunsell AR, Lamicq P, Massiah A, editors. Development in the sicence and technology of composite materials. Bordeaux; 1985, p. 27–31.

[14] Schön J, Nyman T, Blom A, Ansell H. A numerical and experimental investigation of delamination behaviour in the DCB specimen. Composite Science and Technology 2000;60:173–84.

[15] Jones R, Pitt S, Brunner A, Hui D. Application of the Hartman–Schijve equation to represent mode I and mode II fatigue delamination growth in composites. Composite Structures 2012;94(4):1343–51.

[16] Paris PC, Gomez MP, Anderson WE. A Rational Analytic Theory of Fatigue. The Trend in Engineering 1961;13:9–14.

[17] Paris P, Erdogan F. A Critical Analysis of Crack Propagation Laws. Journal of Basic Engineering 1963;85(4):528–33.

[18] Whitcomb JD. Strain energy release rate analysis of cyclic delamination growth in compressively loaded laminates. NASA Technical Memorandum 1983(84598):1–37.

[19] Asp LE, Sjögren A, Greenhalgh ES. Delamination Growth and Thresholds in a Carbon/Epoxy Composite under Fatigue Loading. Journal of Composites Technology & Research 2001;23(2):55–68.

[20] Sjögren A, Asp LE. Effects of temperature on delamination growth in a carbon/epoxy composite under fatigue loading. International Journal of Fatigue 2002;24(2-4):179–84.

[21] Aymerich F, Priolo P, Sun C. Static and fatigue behaviour of stitched graphite/epoxy composite laminates. Composites Science and Technology 2003;63(6):907–17.

[22] Dransfield K, Baillie C, Mai Y. Improving the delamination resistance of CFRP by stitching—a review. Composites Science and Technology 1994;50(3):305–17.

[23] Dransfield KA, Jain LK, Mai Y. On the effects of stitching in CFRPs - I. Mode I delamination toughness. Composites Science and Technology 1998;58:815–27.

[24] Mouritz A, Leong K, Herszberg I. A review of the effect of stitching on the in-plane mechanical properties of fibre-reinforced polymer composites. Composites Part A: Applied Science and Manufacturing 1997;28:979–91.

[25] Dickinson LC, Farley GL, Hinders MK. Translaminar Reinforced Composites: A Review. Journal of Composites Technology & Research 1999;21(1):3–15.

[26] Hinders M, Dickinson L. Trans-laminar-reinforced (TLR) composites. NASA GRANT 1997;1-1647:1–226.

[27] Allegri G, Zhang X. On the delamination and debond suppression in structural joints by Z-fibre pinning. Composites Part A: Applied Science and Manufacturing 2007;38(4):1107–15.

[28] Cartié D, Brunner AJ, Partridge IK. Effects of mesostructure on crack growth control characteristics in z-pinned laminates. In: Blackman BRK, Pavan A, Williams JG, editors. Fracture of polymers, composites, and adhesives II: ESIS Publication 32. Amsterdam: Elsevier; 2003, p. 503–14.

[29] Cartié DD, Troulis M, Partridge IK. Delamination of z-pinned carbon fibre reinforced laminates. Composites Science and Technology 2006;66(6):855–61.

[30] Partridge IK, Cartié DD. Delamination resistant laminates by Z-Fiber® pinning: Part I manufacture and fracture performance. Composites Part A: Applied Science and Manufacturing 2005;36(1):55–64.

[31] Cox BN, Sridhar N. A Traction Law for Inclined Fiber Tows Bridging Mixed-Mode Cracks. Mechanics of Advanced Materials and Structures 2002;9(4):299–331.

[32] Grassi M, Cox B, Zhang X. Simulation of pin-reinforced single-lap composite joints. Composites Science and Technology 2006;66(11-12):1623–38.

[33] Cartié DD, Dell'Anno G, Poulin E, Partridge IK. 3D reinforcement of stiffener-to-skin T-joints by Z-pinning and tufting. Engineering Fracture Mechanics 2006;73(16):2532–40.

[34] Dell'Anno G, Cartié DD, Partridge IK, Rezai A. Exploring mechanical property balance in tufted carbon fabric/epoxy composites. Composites Part A: Applied Science and Manufacturing 2007;38(11):2366–73.

[35] Cartié DD, Laffaille J, Partridge IK, Brunner AJ. Fatigue delamination behaviour of unidirectional carbon fibre/epoxy laminates reinforced by Z-Fiber® pinning. Engineering Fracture Mechanics 2009;76(18):2834–45.

[36] Rugg KI, Cox BN, Massabò R. Mixed mode delamination of polymer composite laminates reinforced through the thickness by z-fibers. Composites Part A: Applied Science and Manufacturing 2002;33:170–90.

[37] Aymerich F. Experimental investigation into the effect of edge stitching on the tensile strength and fatigue life of co-cured joints between cross-ply adherends. Advanced Composites Letters 2004;13(3):151–61.

[38] Plain KP, Tong L. An experimental study on mode I and II fracture toughness of laminates stitched with a one-sided stitching technique. Composites Part A: Applied Science and Manufacturing 2011;42(2):203–10.

[39] Rys T, Sankar BV, Ifju PG. Investigation of fracture toughness of laminated stitched composites subjected to mixed mode loading. Journal of Reinforced Plastics and Composites 2010;29(3):422–30.

[40] Cartié D, Cox B, Fleck NA. Mechanisms of crack bridging by composite and metallic rods. Composites Part A: Applied Science and Manufacturing 2004;35(11):1325–36.

[41] Graham D, Rezai A, Baker D, Smith PA, Watts JF. A hybrid joining scheme for high strength multi-material joints. In: Proceedings of the 18th International Conference on Composite Materials. Jeju, South Corea; 2011.

[42] Löbel T, Kolesnikov B, Scheffler S, Stahl A, Hühne C. Enhanced tensile strength of composite joints by using staple-like pins: Working principles and experimental validation. Composite Structures 2013;106:453–60.

[43] Son H, Park Y, Kweon J, Choi J. Fatigue behaviour of metal pin-reinforced composite single-lap joints in a hygrothermal environment. Composite Structures 2014;108:151–60.

[44] Heimbs S, Nogueira A, Hombergsmeier E, May M, Wolfrum J. Failure behaviour of composite T-joints with novel metallic arrow-pin reinforcement. Composite Structures 2014;110:16–28.

[45] Jürgens M, Noguiera AC, Lang H, Hombergsmeier E, Drechsler K. Influence of an optimized 3D-reinforcement layout on the structural mechanics of co-bonded CFRP joints. In: Proceedings of the 16th European Conference on Composite Materials, 22.06. - 26.06.2014.

[46] Noguiera AC, Drechsler K, Hombergsmeier E, Furfari D, Pacchione M. Investigation of a hybrid 3D-reinforced joining technology for lightweight structures. In: Ferreira (Hg.) 2011 – 16th International Conference on Composite Materials.

Part II:

Delamination of Composite Materials

2 INTRODUCTION TO DELAMINATION OF COMPOSITE MATERIALS

2.1 GENERAL BACKGROUND TO DELAMINATION OF COMPOSITES

Part II of the thesis deals with the characterization of the delamination behavior of composite materials. Delamination, or interlaminar fracture, is one of the instances where fracture mechanics formalisms are applicable to fiber-reinforced composites on a global scale. The crack is confined to the matrix material between two plies, the continuum theory is applicable and the crack growth is self-similar [1]. Yet, as mentioned in Part I, the commonly used stress intensity factor cannot be applied to composite materials, due to the complex stress state in front of the crack tip [2–4]. Thus, the calculation of the toughness of composite materials is based on the strain energy release rate, G, which is also part of the linear elastic fracture mechanics (LEFM) concept. The strain energy release rate describes the amount of energy that is dissipated during rupture per unit of newly created fracture area [5–7]:

$$G = -\frac{1}{b}\left(\frac{dU}{da}\right) \tag{2.1}$$

where U is the potential energy available for crack growth, b the specimen width and a the crack length. This energy based LEFM method of G calculation is commonly referred to as area method [8].

Another approach for calculating G is the compliance method based on the Irwin-Kies equation [9,10]:

$$G = \frac{P^2}{2b}\frac{dC}{da} = \frac{\delta^2}{2bC^2}\frac{dC}{da} \tag{2.2}$$

where C is the specimen compliance.

Fracture testing can be carried out in various loading modes. Mode I is the opening, or tensile mode, where the crack surfaces move directly apart. Mode II is the in-plane shear mode, where the crack surfaces slide over one another in a direction perpendicular to the leading edge of the crack. Mode III is the anti-plane shear mode, where the crack planes move relatively to one another and parallel to the leading edge of the crack [11], see Figure 2.1.

For composite materials, the most common specimen configuration is the double cantilever beam (DCB) specimen. Its geometry essentially permits to carry out

tests in mode I, mode II (end-notched flexure, ENF, or end-loaded split, ELS) and mixed mode I/II (fixed ratio mixed mode, FRMM), see Figure 2.2.

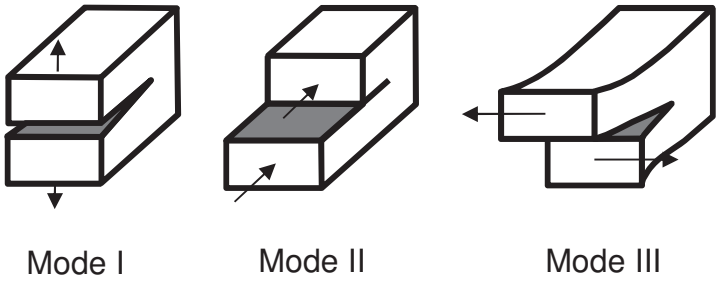

Figure 2.1: Basic modes of loading in fracture mechanical tests: (a) opening, or tensile mode, (b) sliding, or in-plane shear mode, (c) tearing, or anti-plane shear mode.

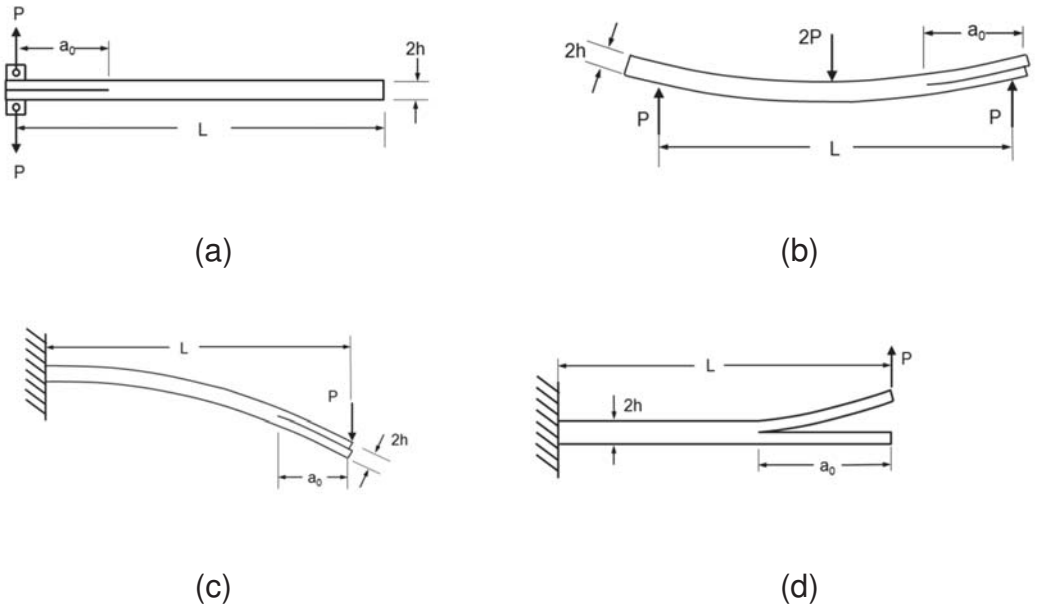

Figure 2.2: Common configurations for evaluating interlaminar fracture toughness: (a) double cantilever beam specimen for pure mode I, (b) end-notched flexure specimen for pure mode II, (c) end-loaded split specimen for pure mode II, (d) fixed ratio mixed mode for mixed mode I/II (I:II = 4:3)

2.1.1 Data reduction for mode I loading situations

Besides the energy based LEFM method of G calculation presented in equation (2.1), the strain energy release rate can also be calculated via elastic beam theory, which is also called simple beam theory (SBT). This yields equation (2.3) [7]:

$$G_{I,DCB} = \frac{P_I{}^2 a^2}{bE_1 I} = \frac{12 P_I{}^2 a^2}{b^2 h^3 E_1} = \frac{3 P_I \delta}{2ba} = \frac{9 E_1 I \delta^2}{4ba^4} \tag{2.3}$$

with P_I being the load in tensile direction, δ the displacement of the point of load application, a the crack length, b the specimen width, E_1 the material's flexural modulus and I the area moment of inertia.

Since the methods mentioned above do not include correction factors for neither large displacements, nor for load blocks, various authors extended the above mentioned methods to account for these effects.

Large displacements lead to changes in geometry, particularly a shortening of the bending arms. Load blocks are needed for transferring tensile loads to the specimen, but when rotated, they change the moment arm. Further, corrections for the orthotropic material behavior of composites[1] are needed, because it leads to a larger relative contribution of transverse shear to the deformation beyond the crack tip [9,10].

For mode I loads these corrections are included in both the corrected beam theory (CBT) by Williams [9,10,12] see equation (2.4), and the modified compliance calibration (MCC) by Kageyama et al. [13], see equation (2.5):

$$G_{I,DCB,CBT} = \frac{3P\delta}{2b(a+\Delta)} \frac{F}{N} \tag{2.4}$$

$$G_{I,DCB,MCC} = \frac{3m}{2(2h)} \left(\frac{P}{b}\right)^2 \left(\frac{bC}{N}\right)^{2/3} F \tag{2.5}$$

where F is the large displacement correction [14,15], N the load block correction [10,15] and Δ the correction for effects of transverse shear beyond the crack tip (see Figure 2.3 (a)) [10]. m is the slope of the plot depicted in Figure 2.3 (b).

[1] While for isotropic materials the ratio of axial modulus to shear modulus E/G $\approx$ 2.6, this ratio can be up to 50 for composite laminates [10].

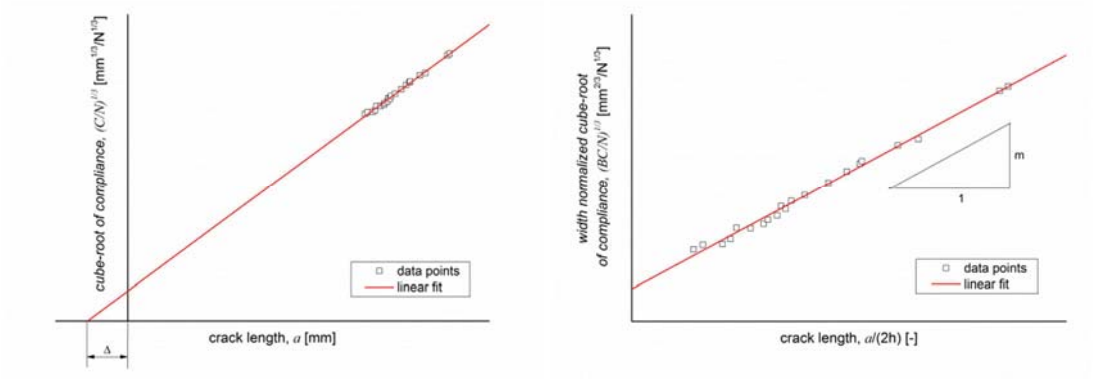

(a) (b)

Figure 2.3: (a) Determination of the correction factor Δ for CBT.
(b) Determination of the slope value m for MCC.

2.1.2 Data reduction for mode II loading situations

Applying simple beam theory to ELS specimens yields equation (2.6) [7,16]:

$$G_{II,ELS} = \frac{9P_{II}^2 a^2}{4b^2 h^3 E_1} \tag{2.6}$$

with P_{II} being the load in shear direction, a the crack length, b the specimen width and h the thickness of one beam of the specimen (2h = specimen thickness).

$$G_{II,3ENF} = \frac{9a^2 P_{II}\delta}{2b\left(\frac{1}{4}L^3+3a^3\right)} \tag{2.7}$$

where L is the span length in a three point bending, end loaded split test (3ENF).

CBT and MCC are compliance based methods commonly used for mode I loading situations. For mode II loading in an ELS test experimental compliance method (ECM, equation (2.8)) and corrected beam theory with effective crack length (CBTE, equation (2.9)) are the most common compliance based data reduction methods:

$$G_{II,ELS,ECM} = \frac{3P^2 a^2 m}{2b} \tag{2.8}$$

$$G_{II,ELS,CBTE} = \frac{3P^2 a_e^2}{16bE_1 I} = \frac{9P^2 a_e^2}{4b^2 h^3 E_1} \tag{2.9}$$

with a_e the effective crack length accounting for the compliance of the test rig, transverse shear effects and rotations at the crack tip and the clamping point. m is the slope of a cubic relationship between the cube of the measured crack length and the specimen compliance (for details see [7,16,17]).

For ENF tests corrections are needed, when large displacements are applied. These corrections account for changes in the moment arm due to deflection of the specimen and for changes in compliance due to changes in the specimen length during deflection of the specimen[2] [17,18]:

$$G_{II,3ENF,CBT} = \frac{9P\delta}{2ba}\left[\frac{3\left(\frac{a}{L}\right)^3}{2+3\left(\frac{a}{L}\right)^3}\right]\left(\frac{F^*}{N^*}\right) \tag{2.10}$$

where F* is a correction for the curved shape of the crack in the loaded stage and N^* is a correction for changes in the compliance due to changes in the specimen length (for details see [7,17,18]).

2.1.3 Data reduction for mixed mode I/II loading situations

Mixed mode loading situations can be realized in a FRMM set-up as depicted in Figure 2.2 (d). This set-up allows to test with a constant mode I to mode II ratio of I:II = 4:3 [12,19–25]. The total mixed-mode energy release rate can be partitioned into mode I and mode II components G_I^{mixed} and G_{II}^{mixed}, respectively, such that:

$$G_m = G_I^{mixed} + G_{II}^{mixed} \tag{2.11}$$

$$G_I^{mixed} = \frac{3P^2(a+\Delta_I)^2}{b^2E_1h^3}F \tag{2.12}$$

$$G_{II}^{mixed} = \frac{9P^2(a+\Delta_{II})^2}{4b^2E_1h^3}F \tag{2.13}$$

where Δ_I and Δ_{II} are the correction factors for mode I and mode II respectively.

Other mode ratios can be realized using the so-called mixed mode bending set-up by Crews and Reeder [26,27].

2.2 QUASI-STATIC DELAMINATION TESTS

An overview of standards for quasi-static delamination tests on endless fiber reinforced polymers is given in Table 2.1. It can be seen that delamination testing under quasi-static loading conditions in mode I and mode II is standardized internationally. For mode I, the data reduction methods used in these standards are either based on the area method presented in equation (2.1), or on compliance based methods as presented in equation (2.2). While data reduction based on area method (AITM 1-0005, EN 6033, HB 7402, BSS 7273) cannot be easily

[2] The span length is fixed and the specimen is allowed to slide over the supports [18].

applied to cyclic test methods, data reduction based on the compliance method (ISO 15024, ASTM D5528, JIS K 7086) is applicable to cyclic delamination tests.

Mode II tests are either based on a 3ENF test set-up (JIS K 7086, AITM 1-0006, EN 6034) or on an ELS test set-up (ISO 15114). Basically, both test set-ups can be used for tests in fatigue. But while the 3ENF test set-up is prone to shifting of the specimen, there is no such problem with the ELS test set-up. Furthermore, the ELS set-up allows for small crack opening displacements, which ease the measurement of the crack length. By inverting the loading direction of the ELS test, a fixed ratio mixed mode I/II test can be carried out.

Table 2.1: Quasi-static delamination test methods for endless fiber reinforced polymers.

Mode	Standard test method	Standard test in preparation
I	JIS K 7086 [28] ASTM D 5528 [29] ISO 15024 [30] HB 7402 [31] AITM 1-0005 [32] BSS 7273 [33] EN 6033 [34]*	-
II	JIS K 7086 [28] AITM 1-0006 [35] ISO 15114 [36] EN 6034 [37]*	ASTM WK 22949
III	not available	ASTM round robins 1999 ff. (no current work item)
I/II	ASTM D6671 [38]	ESIS round robins 1994 ff. (no current activity)
I/III	not available	-
II/III	not available	-
I/II/III	not available	-

* withdrawn in 2009

ASTM D6671 is the only standardized test method for determining the mixed mode delamination behavior of composite materials. The tests are based on a mixed mode bending (MMB) set up, which allows to test in various mode I to mode II ratios [38].

2.3 FATIGUE DELAMINATION TESTS

In contrast to quasi-static loading, there are no standards available for fatigue delamination growth in composites, see Table 2.2. ASTM D 6115 [39] is the only standard related to delamination fatigue. It deals with the determination of onset values for delamination. In ASTM D 6115 the delamination onset is defined by an increase in specimen compliance (either a 1 % or 5 % increase). Testing at various levels of strain energy release rate results in a G-N curve describing the onset values of delamination for each level of strain energy release rate.

In contrast to the determination of the delamination onset, it is necessary to record both the crack length and the compliance for the determination of delamination growth curves. Crack growth curves are commonly referred to as Paris curves. In 1963 Paris and Erdogan presented equation (1.1) to describe a linear relationship between the crack growth rate and the stress intensity factor [40,41]. In this relationship, the stress intensity factor was later replaced by the strain energy release rate [2].

Figure 2.4 shows schematic Paris plots for two materials. The Paris law, see equation (1.1), describes the crack growth behavior in region 2 of the curve [40,41]. Region 1 is characterized by very slow crack growth, where the average delamination growth rate decreases at constant applied strain energy release rate, and is called threshold region. In region 3, the strain energy release rate reaches a critical value and catastrophic failure occurs within one single load cycle.

Increasing the material's properties can be realized by increasing the threshold value of strain energy release rate, G_{th}, or by increasing the critical strain energy release rate value G_c. Decreasing the slope of the crack growth curve of a material, at a constant (or higher) threshold value, increases the time that is available for inspection, because the crack takes longer to grow through the material. Also, a decrease in slope makes it easier to calculate the crack growth behavior in cracked structures, because a small error in the load leads to small errors in the crack growth rate. With steep Paris curves on the other hand, small errors in the load lead to large uncertainties in the predicted crack growth rate [3].

Table 2.2: Cyclic fatigue delamination test methods for endless fiber reinforced polymers.

Mode	Standard test method	Standard test in preparation
I (onset)	ASTM D 6115 [39]	
I (propagation)	not available	ESIS TC4 round robins, see **publications 2 and 3** [42,43] ASTM D30.06 round robin, see **publication 2** [42]
II	not available	ESIS TC4 round robins, see **publication 4** [44]
III	not available	
I/II	not available	
I/III	not available	
II/III	not available	
I/II/III	not available	

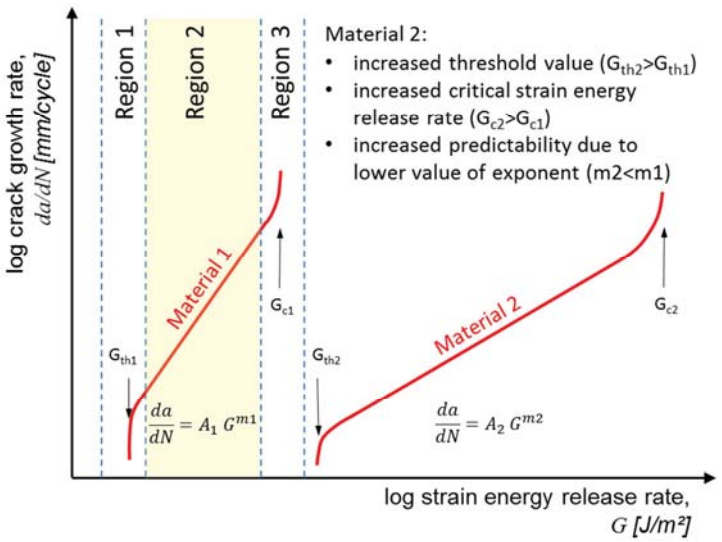

Figure 2.4: Schematic Paris curves for two materials.

In fatigue tests, the specimen can be loaded in either displacement, or load control. Both types of test configurations lead to tests with increasing compliance. This is due to crack growth in the specimen (see correlation between crack length and compliance in Figure 2.3). While in load control, the compliance stays the same until onset of delamination, in displacement control the compliance increases significantly at the beginning and levels off in the course of the test, see Figure 2.5. In load control, the crack growth accelerates until finally catastrophic failure happens within one single load cycle.

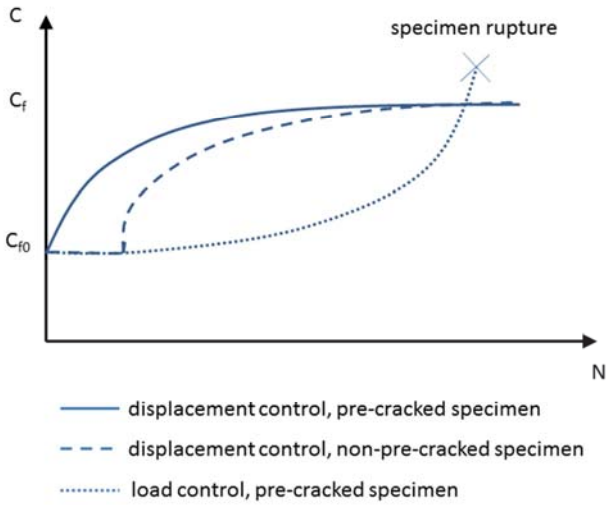

Figure 2.5: Evolution of the compliance against number of cycles in a fatigue delamination test (adapted from [45]).

2.4 REFERENCES

[1] Anderson TL. Fracture mechanics: Fundamentals and applications. 3rd ed. Boca Raton, FL: Taylor & Francis; 2005.

[2] Whitcomb JD. Strain energy release rate analysis of cyclic delamination growth in compressively loaded laminates. NASA Technical Memorandum 1983(84598):1–37.

[3] Asp LE, Sjögren A, Greenhalgh ES. Delamination Growth and Thresholds in a Carbon/Epoxy Composite under Fatigue Loading. Journal of Composites Technology & Research 2001;23(2):55–68.

[4] Sjögren A, Asp LE. Effects of temperature on delamination growth in a carbon/epoxy composite under fatigue loading. International Journal of Fatigue 2002;24(2-4):179–84.

[5] Rivlin RS, Thomas AG. Rupture of rubber. I. Characteristic energy for tearing. Journal of Polymer Science 1953;10(3):291–318.

[6] Irwin GR, Kies JA. Journal of Welding 1954;33:193.

[7] Hashemi S, Kinloch AJ, Williams JG. The analysis of interlaminar fracture in uniaxial fibre-polymer composites. Proc. R. Soc. London A. 1990;427:173–99.

[8] Hashemi S, Kinloch AJ, Williams JG. Corrections needed in double-cantilever beam tests for assessing the interlaminar failure of fibre-composites. Journal of Materials Science Letters 1989;8:125–9.

[9] Williams JG. On the calculation of energy release rates for cracked laminates. International Journal of Fracture 1988;36:101–19.

[10] Williams JG. The fracture mechanics of delamination tests. Journal of Strain Analysis for Engineering Design 1989;24(4):207–14.

[11] Hertzberg RW. Deformation and fracture mechanics of engineering materials. 5th ed. New York, NY: John Wiley and Sons Inc; 2012.

[12] Hashemi S, Kinloch AJ, Williams JG. The Effects of Geometry, Rate and Temperature on the Mode I, Mode II and Mixed-Mode I/II Interlaminar Fracture of Carbon-Fibre/Poly(ether-ether ketone) Composites. Journal of Composite Materials 1990;24(9):918–56.

[13] Kageyama K, Kobayashi T, Chou T. Analytical compliance method for mode I interlaminar fracture toughness testing of composites. Composites 1987;18(5):393–9.

[14] Naik RA, Crews JH, Shivakumar KN. Effects of T-Tabs and Large Deflections in Double Cantilever Beam Specimen Tests. In: O'Brien TK, editor. Composite materials: Fatigue and fracture (third volume), 3rd ed. Philadelphia, PA: ASTM; 1991, p. 169–86.

[15] Williams JG. Large Displacement and End Block Effects in the 'DCB' Interlaminar Test in Modes I and II. Journal of Composite Materials 1987;21(4):330–47.

[16] Blackman B, Brunner AJ. Fibre-composites- The determination of the mode II fracture resistance, GIIC, of unidirectional fibre-composites using the cal. ESIS TC4 test protocol 2009.

[17] Wang Y, Williams JG. Corrections for mode II fracture toughness specimens for composite materials. Composites Science and Technology 1992;43:251–6.

[18] Williams JG. A note on finite displacement correction factors for the end notch flexure (ENF) test. Composites Science and Technology 1990;39:279–82.

[19] Blackman B, Brunner AJ, Davies P. Delamination fracture of continuous fibre composites: Mixed-mode fracture. In: Moore DR, Pavan A, Williams JG, editors. Fracture Mechanics Testing Methods for Polymers, Adhesives and Composites: ESIS Publication 28. Amsterdam: Elsevier; 2001, p. 335–59.

[20] Blanco N, Gamstedt EK, Costa J, Trias D. Analysis of the mixed-mode end load split delamination test. Composite Structures 2006;76(1-2):14–20.

[21] Charalambides MN, Kinloch AJ, Wanng Y, Williams JG. On the analysis of mixed-mode failure. International Journal of Fracture 1992;54:269–91.

[22] Choi NS, Kinloch AJ, Williams JG. Delamination Fracture of Multidirectional Carbon-Fiber/Epoxy Composites under Mode I, Mode II and Mixed-Mode I/II Loading. Journal of Composite Materials 1999;33(1):73–100.

[23] Dyson IN, Kinloch AJ, Okada A. The interlaminar failure behaviour of carbon fibre/polyetheretherketone composites. Composites 1994;25(3):189–96.

[24] Hashemi S, Kinloch AJ, Williams JG. Mixed-mode fracture in fiber-polymer composite laminates. In: O'Brien TK, editor. Composite materials: Fatigue and fracture (third volume), 3rd ed. Philadelphia, PA: ASTM; 1991, p. 143–68.

[25] Kinloch AJ, Wang Y, Williams JG, Yayla P. The mixed-mode delamination of fibre composite materials. Composites Science and Technology 1993;47:225–37.

[26] Crews JH, Reeder JR. A mixed-mode bending apparatus for delamination testing. NASA Technical Memorandum 1988;100662:1–42.

[27] Reeder JR, Crews JR. Mixed-mode bending method for delamination testing. AIAA Journal 1990;28(7):1270–6.

[28] JIS - Japanese Standards Association. JIS K 7086:1993 Testing methods for interlaminar fracture toughness of carbon fibre reinforced plastics(K 7086); 1993.

[29] ASTM - American Society for Testing and Materials. D5528:2001 - Standard test method for mode I interlaminar fracture toughness of unidirectional fiber-reinforced polymer matrix composites(D5528:2001).

[30] ISO - International Organization for Standardization. ISO 15024 - Fibre-reinforced plastic composites — Determination of mode I interlaminar fracture toughness, GIC, for unidirectionally reinforced materials(15024); 2001.

[31] China Aviation Industry Standard. HB 7402:96 - Test method for mode I interlaminar fracture toughness GIC of carbon fibre reinforced composite laminates.

[32] AITM - Airbus Test Method. 1-0005: Determination of interlaminar fracture toughness Mode I ; 1994.

[33] BSS - Boeing Specification Support Standard. 7273:94 - GIC interlaminar fracture toughness fiber-reinforced composites(7273).

[34] EN - European Standard. 6033 - Aerospace series - Carbon fiber reinforced plastics - Determination of interlaminar fracture toughness energy - Mode I - GIC .

[35] AITM - Airbus Test Method. 1 0006 - Determination of interlaminar fracture toughness energy Mode II; 1994.

[36] ISO - International Organization for Standardization. ISO 15114 - Fibre-reinforced plastic composites — The determination of the Mode II fracture resistance, GIIC, for unidirectionally reinforced materials using the calibrated end loaded split (C-ELS) test and an effective crack length approach(15114); 2011.

[37] EN - European Standard. 6034 - Aerospace series - Carbon fiber reinforced plastics - Determination of interlaminar fracture toughness energy - Mode II - GIIC.

[38] ASTM - American Society for Testing and Materials. D6671–01 - Standard Test Method for Mixed Mode I-Mode II Interlaminar Fracture Toughness of Unidirectional Fiber Reinforced Polymer Matrix Composites(D6671-01).

[39] ASTM - American Society for Testing and Materials. D6115:1997 - Standard test method for mode I fatigue delamination growth onset of unidirectional fiber-reinforced polymer matrix composites(D6115:1997).

[40] Paris P, Erdogan F. A Critical Analysis of Crack Propagation Laws. Journal of Basic Engineering 1963;85(4):528–33.

[41] Paris PC, Gomez MP, Anderson WE. A Rational Analytic Theory of Fatigue. The Trend in Engineering 1961;13:9–14.

[42] Stelzer S, Brunner AJ, Argüelles A, Murphy N, Pinter G. Mode I delamination fatigue crack growth in unidirectional fiber reinforced composites: Development of a standardized test procedure. Composites Science and Technology 2012;72(10):1102–7.

[43] Stelzer S, Brunner A, Argüelles A, Murphy N, Cano G, Pinter G. Mode I delamination fatigue crack growth in unidirectional fiber reinforced composites: Results from ESIS TC4 round-robins. Engineering Fracture Mechanics 2014;116:92–107.

[44] Brunner A, Stelzer S, Pinter G, Terrasi G. Mode II fatigue delamination resistance of advanced fiber-reinforced polymer–matrix laminates: Towards the development of a standardized test procedure. International Journal of Fatigue 2013;50:57–62.

[45] Renart J, Costa J, Sarrado, C. Budhe, S., Turon A, Rodriguez-Bellido A. Mode I fatigue behaviour and fracture of adhesively bonded fibre-reinforced polymer (FRP) composite joints for structural repairs. In: Vassilopoulos AP, editor. Fatigue and fracture of adhesively-bonded composite joints. Cambridge: Woodhead Publishing; 2015, p. 121–47.

3 DEVELOPMENT OF STANDARDIZED TEST PROCEDURES FOR FATIGUE DELAMINATION TESTING

3.1 INTRODUCTION

From the early development of delamination tests in composite materials [1–7], via the calculation of correction factors [8–10], it took some time to the evolution of standards for quasi-static mode I delamination tests. This evolution is illustrated in references [11–13] for the ISO standard [14] and in reference [15] for the ASTM standard [16] on mode I interlaminar fracture toughness of unidirectionally reinforced composite materials. Both standards, ASTM D5528 and ISO 15024 were preceded by extensive round robin testing, see references [12,15,17]. The same accounts for mode II loading. Rigorous round robin exercises [17–20] led to the development of a test procedure [21] that was subsequently converted into ISO standard 15114 [22].

Although there are yet no standards for fatigue delamination testing, various authors have investigated the fatigue delamination properties of composites in the past. Overviews are given in references [23–28]. First inter-laboratory comparisons were carried out by Brunner et al. [29].

When developing a standardized test procedure, it is essential to ensure the repeatability of the test results and to minimize scatter. Before carrying out round robin activities, it is important to provide a test procedure that gives consistent results. The impact of the main influence factors on the measurement results has to be investigated. In the case of fatigue delamination tests at a fixed load ratio and temperature, they are (1) testing frequency, (2) specimen thickness, (3) initial crack length, (4) type of test machine, (5) specimen material and (6) control mode of the test machine. The influences of these parameters are investigated in **publication 1** [30].

Based on the parameter studies carried out in **publication 1**, a final test protocol was developed. Together with test materials, this protocol was distributed to the participating laboratories. The raw data of all round robin tests was processed in Leoben based on Matlab (MathWorks, Natick, USA) and VisualBasic (Microsoft Corporation, Redmond, USA) codes. These codes were written by the author of this thesis in order to provide objective and fast data evaluation.

Results from international round robin delamination tests in mode I loading based on the test protocol are given in **publications 2 and 3** [31,32]. **Publication 4** presents results from pre-standardization delamination tests in mode II loading [33].

3.1.1 References

[1] Newaz GM, Ahmad J. A simple technique for measuring mode I delamination energy release rate in polymeric composites. Engineering Fracture Mechanics 1989;33(4):541–52.

[2] O'Brien T, Johnston NJ, Morris DH, Simonds RA. A simple test for the interlaminar fracture toughness of composites. Proc. 27th National Sampe Symposium 1982:8–15.

[3] Wang SS, Choi I. The mechanics of delamination in fiber-reinforced composite materials. Part I: Stress singularities and solution structure. NASA Contractor Report 1983;172269:1–44.

[4] Wang SS, Choi I. The mechanics of delamination in fiber-reinforced composite materials. Part 2: Delamination behavior and fracture mechanics parameters. NASA Contractor Report 1983;172270:1–60.

[5] Whitney JM, Browning CE, Hoogsteden W. A double cantilever beam test for characterizing mode I delamination of composite materials. Journal of Reinforced Plastics and Composites 1982;1:297–313.

[6] Williams JG. On the calculation of energy release rates for cracked laminates. International Journal of Fracture 1988;36:101–19.

[7] Williams JG. The fracture mechanics of delamination tests. Journal of Strain Analysis for Engineering Design 1989;24(4):207–14.

[8] Kageyama K, Kobayashi T, Chou T. Analytical compliance method for mode I interlaminar fracture toughness testing of composites. Composites 1987;18(5):393–9.

[9] Williams JG. Large Displacement and End Block Effects in the 'DCB' Interlaminar Test in Modes I and II. Journal of Composite Materials 1987;21(4):330–47.

[10] Williams JG. End corrections for orthotropic DCB specimens. Composites Science and Technology 1989;35:367–76.

[11] Blackman BRK, Brunner AJ, Davies P. The evolution of an ISO standard for the mode I delamination toughness of laminates. Proc. 12th Biennel Conference on Fracture - ECF 12 1998:1369–75.

[12] Brunner AJ, Tanner S, Davies P, Wittich H. Interlaminar fracture testing of unidirectional fibre-reinforced composites: results from ESIS-round robins. Proc. 2nd European Conference on Composite Materials, Composite Testing and Standardization 1994:523–31.

[13] Williams JG, Davies P, Brunner AJ. Standard tests for the toughness of composite laminates - Some bones of contention. Proc. 10th International Conference on Composite Materials 1995:71–5.

[14] ISO - International Organization for Standardization. ISO 15024 - Fibre-reinforced plastic composites — Determination of mode I interlaminar fracture toughness, GIC, for unidirectionally reinforced materials(15024); 2001.

[15] O'Brien TK, Martin R. Results of ASTM Round Robin Testing for Mode I interlaminar Fracture toughness of Composite Materials. NASA Technical Memorandum 1992;104222.

[16] ASTM - American Society for Testing and Materials. D5528:2001 - Standard test method for mode I interlaminar fracture toughness of unidirectional fiber-reinforced polymer matrix composites(D5528:2001).

[17] Davies P, Kausch HH, Williams JG, Kinloch AJ, Charalambides MN, Pavan A et al. Round-robin interlaminar fracture testing of carbon-fibre-reinforced epoxy and PEEK composites. Composites Science and Technology 1992;43:129–36.

[18] Davies P, Sims GD, Blackman BRK, Brunner AJ, Kageyama K, Hojo M et al. Comparison of test configurations for the determination of GIIC: An international round robin. Proc. 2nd European Conference on Cognitive Modelling 1998:180–5.

[19] Davies P., Blackman BRK, Brunner AJ. Mode II delamination. In: Moore DR, Pavan A, Williams JG, editors. Fracture Mechanics Testing Methods for Polymers, Adhesives and Composites: ESIS Publication 28. Amsterdam: Elsevier; 2001, p. 307–33.

[20] Blackman BRK, Brunner AJ, Williams JG. Mode II fracture testing of composites: a new look at an old problem. Engineering Fracture Mechanics 2006;73(16):2443–55.

[21] Davies P, Ducept F, Brunner AJ, Blackman BRK, Morais A de. Development of a standard mode II shear fracture test procedure. In: Harris B, editor. Fatigue in Composites. Cambridge: Woodhead Publishing Limited; 2000, p. 9–15.

[22] ISO - International Organization for Standardization. ISO 15114 - Fibre-reinforced plastic composites — The determination of the Mode II fracture resistance, GIIC, for unidirectionally reinforced materials using the calibrated end loaded split (C-ELS) test and an effective crack length approach(15114); 2011.

[23] Dahlen C, Springer GS. Delamination growth in composites under cyclic loads. Journal of Composite Materials 1994;28(8):732–81.

[24] Tay TE. Characterization and analysis of delamination fracture in composites: An overview of developments from 1990 to 2001. Applied Mechanics Reviews 2003;56:1–31.

[25] Mall S, Yun KT, Kochhar NK. Characterization of Matrix Toughness Effect on Cyclic Delamination Growth in Graphite Fiber Composites. In: Lagace PA, editor. Composite Materials: Fatigue and Fracture: ASTM STP 1012. West Conshohocken, PA: American Society for Testing and Materials; 1989, p. 296–310.

[26] Martin RH, Murri GB. Characterization of mode I and mode II delamination growth and thresholds in AS4/PEEK composites. In: Garbo S, editor. Composite Materials: Testing and Design: ASTM STP 1059. West Conshohocken, PA: American Society for Testing and Materials; 1990, p. 251–70.

[27] Martin RH, Murri GB. Characterization of mode I and mode II delamination growth and thresholds in graphite/PEEK composites. NASA Technical Memorandum 1988;100577.

[28] Whitcomb JD. Strain energy release rate analysis of cyclic delamination growth in compressively loaded laminates. NASA Technical Memorandum 1983(84598):1–37.

[29] Brunner AJ, Murphy N, Pinter G. Development of a standardized procedure for the characterization of interlaminar delamination propagation in advanced composites under fatigue mode I loading conditions. Engineering Fracture Mechanics 2009;76(18):2678–89.

[30] Stelzer S, Pinter G, Wolfahrt M, Brunner AJ, Noisternig J. Cyclic interlaminar crack growth in unidirectional and braided composites. In: Yao W, Renard J, Himmel NA, editors. Fatigue behaviour of fiber reinforced polymers. Pennsylvania, U.S.A.: DEStech Publications, Inc; 2010, p. 49–63.

[31] Stelzer S, Brunner AJ, Argüelles A, Murphy N, Pinter G. Mode I delamination fatigue crack growth in unidirectional fiber reinforced composites: Development of a standardized test procedure. Composites Science and Technology 2012;72(10):1102–7.

[32] Stelzer S, Brunner A, Argüelles A, Murphy N, Cano G, Pinter G. Mode I delamination fatigue crack growth in unidirectional fiber reinforced composites: Results from ESIS TC4 round-robins. Engineering Fracture Mechanics 2014;116:92–107.

[33] Brunner A, Stelzer S, Pinter G, Terrasi G. Mode II fatigue delamination resistance of advanced fiber-reinforced polymer–matrix laminates: Towards the development of a standardized test procedure. International Journal of Fatigue 2013;50:57–62.

3.2 PUBLICATION 1

CYCLIC INTERLAMINAR CRACK GROWTH IN UNIDIRECTIONAL AND BRAIDED COMPOSITES

3.2.1 Bibliographic Information

- Authors and their relevant contributions to the publication:
  - Steffen Stelzer[1]
    Preparation and submission of the manuscript, execution and analysis of the tests in laboratory A.
  - Gerald Pinter[1]
    Academic supervision of the work carried out in this publication.
  - Markus Wolfahrt[2,4]
    Project co-ordination and co-supervision of the work.
  - Andreas J. Brunner[3]
    Execution and analysis of the tests in laboratory B.
  - Johannes Noisternig[4]
    Organization of specimen production at FACC AG.
- Affiliations:
  [1] Institute of Materials Science and Testing of Polymers, Montanuniversitaet Leoben, Leoben, Austria
  Polymer Competence Center Leoben, Austria
  [2] EMPA, Swiss Federal Laboratories for Materials Science and Technology, CH-8600 Dübendorf, Switzerland
  [3] FACC AG, Fischerstrasse 9, A-4910 Ried im Innkreis, Austria

- Source: Fatigue Behavior of Fiber Reinforced Polymers
- ISBN: 978-1-60595-091-4

Statement with regard to publication: The manuscript presented here is an adapted accepted manuscript in order to fit the formatting of the thesis and does not necessarily reflect the actually published version.

3.2.2 Abstract

Since there is still no standard test method for the investigation of the fatigue delamination propagation behavior of fiber reinforced composites, this paper aims at examining some of the parameters that can influence this kind of measurements. Therefore unidirectionally reinforced composites were tested under displacement control and double cantilever beam specimens were used to realize mode I tensile opening loads in the material. A comparison of the effect of different parameters on this type of measurements was carried out including machine parameters (frequency, control mode, type of machine) and specimen parameters (initial crack length, thickness, material). The comparison of the results with the results from a second laboratory yielded promising results. Furthermore the damage tolerance of braided composites with different braid architectures (i.e. braiding angle) was studied.

3.2.3 Introduction

High performance fiber composites feature outstanding specific properties and therefore have an indisputable potential for applications in design of lightweight structures. Nevertheless their application is limited especially because of their susceptibility to delamination. Delaminations can grow to a critical size under cyclic loading conditions, even at loads below the static strength of the material and can thus trigger the failure of the structure. To be able to avoid such a failure key data to describe the initiation and growth of delaminations for design purposes have to be created and approaches for the enhancement of the material performance have to be found.

In ASTM D 6115 a standard test method for the mode I fatigue delamination growth onset of unidirectional fiber reinforced (UD)-polymer matrix composites was introduced [1]. But for estimating the behavior of existing delaminations under fatigue loads or for comparing different laminates with respect to their delamination propagation under fatigue loads and for design purposes, this is not sufficient. Therefore it is an aim to establish a test method for the characterization of the delamination growth under mode I fatigue loads. In order to allow its application in an industrial environment short test durations below 24 hours are desired. To be able to receive threshold values however, the test duration has to be increased significantly. For this reason the determination of the threshold value should not be the main goal, but an option of a test procedure [2].

Due to the possibility to automatically manufacture large structures with complex shape and high production rates, braided composites produced with liquid resin infusion technology are increasingly considered for structural commercial aircraft components. Furthermore by using braided structures the impact and delamination resistance can be improved [3,4]. Biaxial braids consist of two yarns located at an angle of ± θ to the longitudinal direction along the mandrel axis. By adding fibers in the longitudinal direction a triaxial braid can be achieved [5]. Since the braid geometry has an influence on the mechanical properties of a part it is imperative to evaluate the differences in the performance of different braid geometries. In a previous study the effect of different braid geometries on the mechanical properties of specimens loaded in tension, without holes, and compression, with and without holes, applying standardized test methods, were examined [6]. So far there are no reported fundamental fracture tests for braided composites [7].

The overall objective of the present work was to create a test protocol for mode I delamination testing of UD-laminates which is applicable in an industrial test environment (short test duration, automated data acquisition and analysis) and to study the damage tolerance of braids by fatigue crack growth tests and classical CAI tests.

3.2.4 Experimental

3.2.4.1 Materials and test specimens

The tests were carried out in two laboratories which will be further referred to as laboratories A and B. For the UD-laminates used at laboratory A prepreg type materials were used. A 180°C-cureable interleaf-type toughened epoxy resin system, Rigidite 5276-1 (R5276), supplied by BASF AG (Ludwigshafen, Germany) and a 380°C-processable thermoplastic poly-ether-ether-ketone (PEEK) matrix supplied by ICI (Östringen, Germany) were utilized. The epoxy resin was reinforced with carbon fibers of the type Celion G30-500 from BASF Structural Materials (Charlotte, USA) and the PEEK matrix with carbon fibers of the type AS4 from Hercules Inc. (Magna, USA). The two types of carbon fibers were similar in terms of fiber diameter, modulus and ultimate fiber strength and strain. In order to initiate interlaminar crack growth, a Teflon® film with a thickness of 20 µm was placed at the laminate mid thickness at one end of the specimen. The epoxy resin was cured in an autoclave using vacuum bag technique and the PEEK laminates were produced using a diaphragm forming process. Double cantilever beam (DCB) specimens, 145 mm long and 20 mm wide, were machined from the

laminates with a diamond saw so that the fibers were oriented along the specimen length. The specimens had a thickness (2h) of 4 mm [8].

The UD-specimens tested at laboratory B were made of a 180°C-cureable highly toughened epoxy resin system, Cycom 5276-1 (C5276), reinforced with carbon fibers of the type G40-800. The material was supplied by Cytec Engineered Materials (Anaheim, USA). A polymer film with a thickness below 13 µm and a length of 50 mm, as required by ISO 15024 [9], was used to create a crack at specimen mid-thickness. The DCB specimens had a width of 20 mm, a length of 150 mm and a thickness of 3.5 mm. The unidirectionally reinforced epoxy resins tested at laboratories A and B had similar mechanical properties.

In laboratory A the procedure was additionally applied to braided composites. A high-tenacity, standard modulus carbon fiber from Toho Tenax Europe GmbH (Wuppertal, D) was used for all braided preforms which were formed over a cylindrical mandrel. Afterwards the braids were removed from the mandrel, slit along the 0° fiber direction, flattened and placed in a mold. To obtain the final thickness (4 mm) of the test panels, the biaxial preforms consisted of 8 layers, while the triaxial preforms were made of 6 layers. Laminates with 300 mm in width and 500 mm in length were infused with the epoxy resin RTM 6 from Hexcel Composites (Dagneux, F) using Vacuum-Assisted Resin Transfer Molding (VARTM). All test panels were inspected ultrasonically and found to be free of voids and micro cracks. DCB specimens in the dimension of 250 x 25 mm were cut out from the laminate plates for the fracture tests using a cutting machine with a diamond-coated cutting blade. To be able to examine the influence of the crack growth direction on the delamination behavior, the specimens were cut out in 0° (longitudinal) and 90° (transversal) direction. A Teflon® film was placed at laminate mid-thickness as starter crack at one edge of the specimens. For the compression after impact tests specimens with a length of 150 mm and a width of 100 mm were cut out of the test panels. The specimens with triaxial braid geometry were cut out in longitudinal and transversal direction like the specimens for the delamination testing. The biaxial samples, however, were only cut out in longitudinal direction.

3.2.4.2 Test methods

At laboratory A the fatigue crack growth measurements under mode I loading conditions were carried out on a servo-hydraulic test machine (MTS 858, MTS Systems Corporation, Berlin, Germany) and on an electro-dynamic test machine (ElectroForce 3200, Bose Corporation, Eden Prairie, USA) using the DCB

specimens. The servo-hydraulic test machine had a 15 kN load cell calibrated in a load range from 0 to 400 N. The electro-dynamic test machine had a load cell with a load capacity of 450 N. An R-ratio of 0.1 was used in all the measurements and the tests were carried out under displacement control. To be able to start the measurements at high crack growth rates just below G_{IC} a quasi-static mode I test for pre-cracking was carried out as a G_{IC}-test at a testing velocity of 3 mm/min. The displacement value at which pre-cracking was stopped, was then taken as the δ_{max} value for fatigue loading Figure 3.1). Furthermore potential influences of resin-rich areas at the end of the Teflon® foil were avoided by performing this quasi-static test. The initial crack length for the cyclic test, a_0, equals the crack length reached after the quasi-static test. The cyclic test was started at 5 or 10 Hz using the pre-cracked specimens and continued until a crack growth rate of about 10^{-6} mm/cycle was reached. The crack length was obtained via visual observation of the crack through a traveling microscope (magnification 40x). The tests were carried out in a laboratory environment of 23°C and 50% relative humidity.

The tests at laboratory B were performed on a servo-hydraulic test machine (Instron type 1273, Instron, High Wycombe, United Kingdom) with a 1 kN load cell calibrated in the load range from 0 to 100 N. The tests were performed under displacement control with a frequency of 3 Hz and an R-ratio of 0.1. No quasi-static mode I pre-cracking was done since the polymer film of the specimens used in laboratory B was sufficiently thin. Hence the initial crack length for cyclic testing, a_0, equaled the length of the polymer film insert. The delamination lengths were monitored with a traveling microscope and the tests were done in a climate controlled laboratory (+23°C, 50% relative humidity).

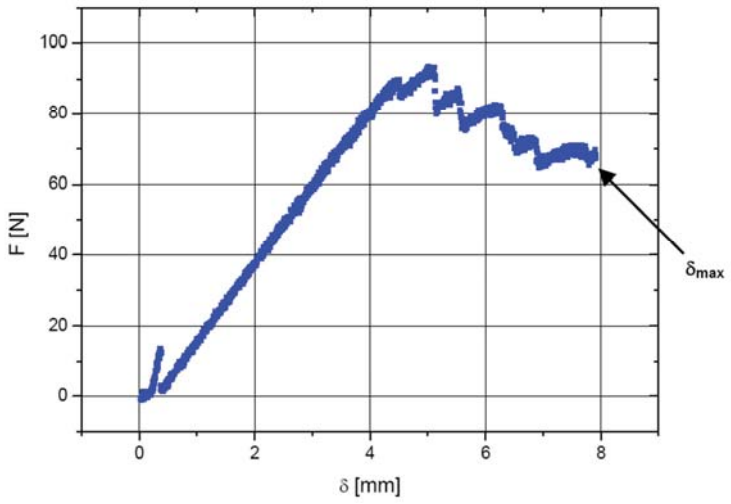

Figure 3.1: Force over displacement curve of a quasi-static pretest to determine δ_{max}.

At both laboratories the strain energy release rates were calculated using the modified compliance calibration (MCC) [10] and additional crack lengths were computed from the compliance data recorded during the measurements by using the calibration equation of the MCC method. By plotting da/dN over G_{Imax} in a double logarithmic scale a so called Paris plot was achieved [11, 12]. G_{Imax} was used instead of ΔG_I in order to avoid an influence of facial interference on the results of the measurements [13]. All the calculations were made using an Excel-VBA-Macro provided by laboratory A.

Compression after impact tests on braided composites were carried out at laboratory A using an universal test machine (Z250, Zwick GmbH & Co. AG, Ulm, Germany) after the specimens were subjected to impacts at defined ranges of impact energies with a falling weight impact tester (Fractovis Plus S.p.A, CEAST, Pianezza, Italy). The residual compressive strengths of the specimens were assessed [14].

3.2.5 Results and discussion

3.2.5.1 Fracture testing

In Figure 3.2 a comparison of two types of crack length determination is depicted. On the one hand the crack lengths were measured optically by using a traveling microscope. On the other hand the crack lengths were computed from compliance data which was recorded by the test machine automatically. It is shown that the two calculation methods give comparable crack growth curves. In the following diagrams compliance calibration is applied for the calculation of the crack growth curves.

According to the literature [2, 7, 15, 16] a scatter of the data of up to one decade of the crack growth rate can be expected, when an interlaminar crack growth curve is recorded. Figure 3.3 shows the amount of scatter that was received without varying any test parameters at laboratory A.

The length of the starter crack has an influence on the crack opening displacement, on the compliance of the specimen and on the amount of fiber bridging occurring during the test [17]. Considering this it is very important to examine the influence of the length of the starter crack on the results of the measurements.

In Figure 3.4 the fatigue crack growth curves for starter cracks with 30 and 50 mm can be found. To receive longer starter crack lengths, the quasi-static mode I test

was carried on until the desired crack length was reached. During the measurements it was found that an increase of the length of the starter crack made it necessary to decrease the test frequencies, because a higher piston stroke was required. Hence the test frequency for the specimens with a starter crack length of 50 mm was limited to 5 Hz. Additional problems with the 50 mm starter crack occurred at crack growth rates below 10^{-4} mm/cycle. The forces fell below a level that made it difficult to record them at the 15 kN servo-hydraulic test machine. This led to a big scatter in the recorded forces.

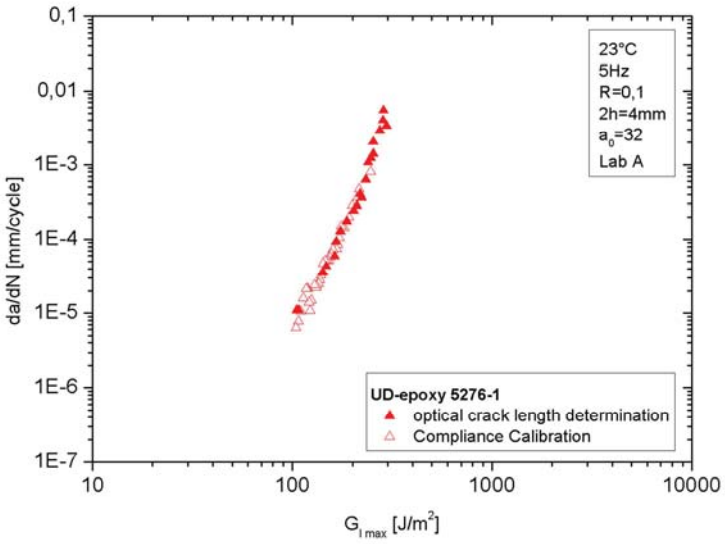

Figure 3.2: Effect of crack length determination (optical vs. compliance calibration) on interlaminar fatigue crack growth.

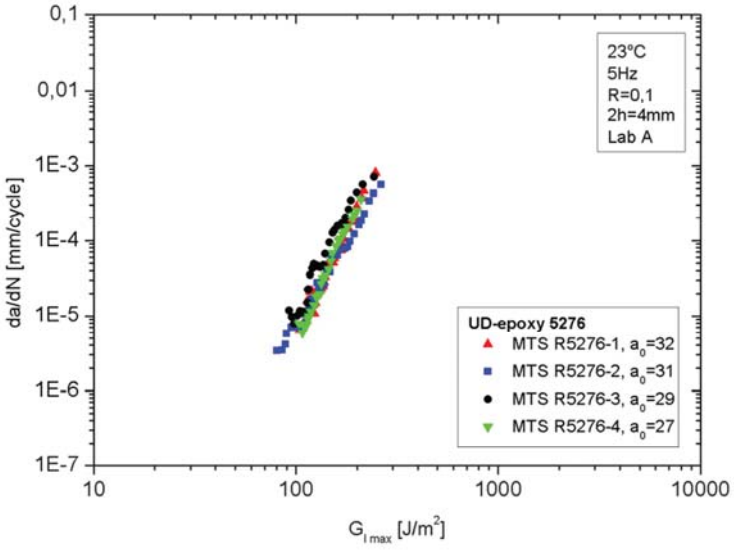

Figure 3.3: Reproducibility of interlaminar fatigue crack growth tests.

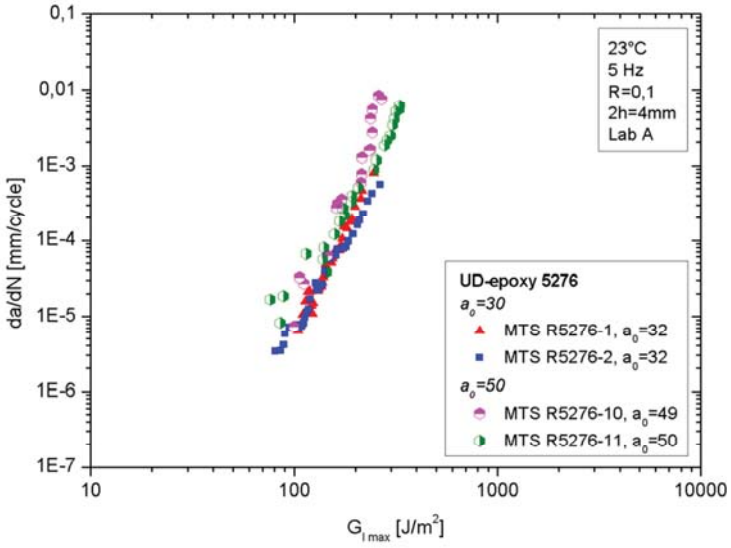

Figure 3.4: Effect of the length of the starter crack on interlaminar fatigue crack growth.

An increase of the test frequency can, on the one hand, have a negative influence on the results of the measurements by leading to hysteretic heating of the specimen. On the other hand an increase of the test frequency, such as from 5 to 10 Hz, leads to a drastic reduction in the testing time and therefore reduces testing costs. In previous studies on CF-epoxy, 10 Hz did not result in hysteretic heating of the sample [2].

In Figure 3.5 it is shown that there was no significant influence of the test frequency on the results of the measurements, when the frequency was raised from 5 to 10 Hz.

Figure 3.6 shows the influence of specimen thickness on the results of the measurements. By doubling the thickness of the specimen the bending stiffness is increased eight-fold. This leads to smaller crack opening displacements and makes it difficult to read the crack lengths with the traveling microscope. It is assumed that this leads to a bigger amount of scatter when testing the thicker specimens. On the other hand the smaller crack opening displacements make it possible to test at higher frequencies. Thus test frequencies of 10 Hz were used for the thicker specimens. Nevertheless these effects need to be examined in more detail and exclude the use of specimens with a thickness of 8 mm for the characterization of the interlaminar fatigue crack growth behavior for now.

In Figure 3.7 the results of the measurements under displacement control are compared to the results achieved from testing in load control. Therefore all other

test parameters were kept constant. It can be seen that the two test control modes yielded similar results.

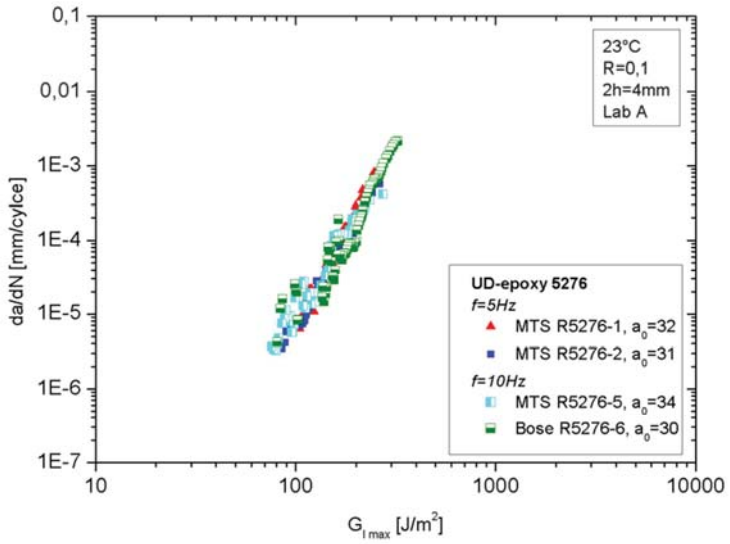

Figure 3.5: Effect of frequency on interlaminar fatigue crack growth.

Testing in displacement control has the following advantages compared to testing in load control:

- Fast crack growth occurs at the beginning of the measurements.
- There is no need to be present all the time and the tests can be left alone over night or even for a couple of days. Crack lengths can be computed from the compliance data recorded continuously by the test machine.
- The detection of the threshold is a matter of testing time (given that no fiber bridging occurs and that the plastic zones remained small).

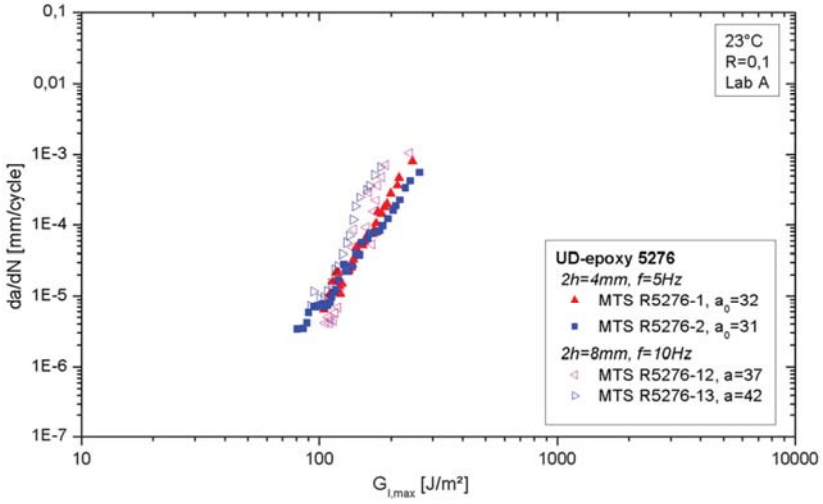

Figure 3.6: Effect of specimen thickness (2h) on interlaminar fatigue crack growth.

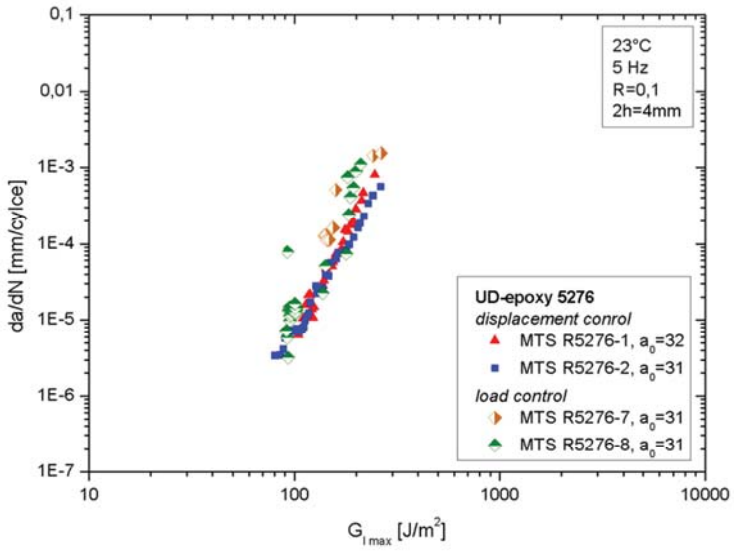

Figure 3.7: Effect of control mode (displacement control and load control) on interlaminar fatigue crack growth.

Because the reproducibility of the results of standardized tests is enormously important, it is examined whether this test method can be carried out on other test machines. The results of this intra-laboratory comparison of the tests carried out on different types of test machines can be seen in Figure 3.8. Both machines yielded similar results, although the electro-dynamic test machine had some problems with the tuning. The low load capacity of the machine made it necessary to regularly adjust the tuning of the machine due to the change of specimen compliance during crack growth.

The results of an ongoing inter-laboratory comparison of this type of measurements in the framework of the European Structural Integrity Society, Technical Committee 4 (ESIS TC4) are not yet available. First results of tests on similar materials at laboratory B (s. Figure 3.9), however, indicate, that an inter-laboratory comparability of this type of measurements is given.

This kind of measurements works very well with other materials too, as can be seen in Figures 7.10, 7.11 and 7.13. Figure 3.10 shows the interlaminar fatigue crack growth behavior of UD-PEEK. In Figure 3.11 the fatigue crack growth behavior of a biaxial braid is depicted in the log da/dN versus log G_{Imax}-diagram. This figure shows some scatter in the values of G_{Imax}, which can be ascribed to two mechanisms. On the one hand, the crack growth is stopped at fibers not oriented in growth direction and the crack is deflected from its nominal growth plane (crack deflection). On the other hand a second crack plane is created (crack

branching). In Figure 3.12 these mechanisms are shown in a picture taken during the measurements on the biaxial braids. It has to be mentioned, that the results shown here were calculated based on equations that require the ideal case of one single and even crack plane. Hence, the results are not fully valid. Nevertheless they were reproducible and can thus be used for the comparison of the two different braid architectures.

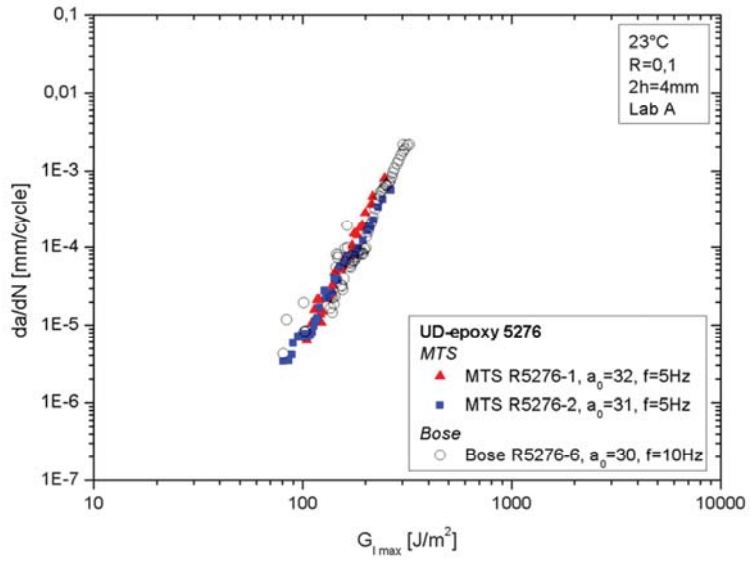

Figure 3.8: Effect of machine type (servo-hydraulic and electro-dynamic) on interlaminar fatigue crack growth.

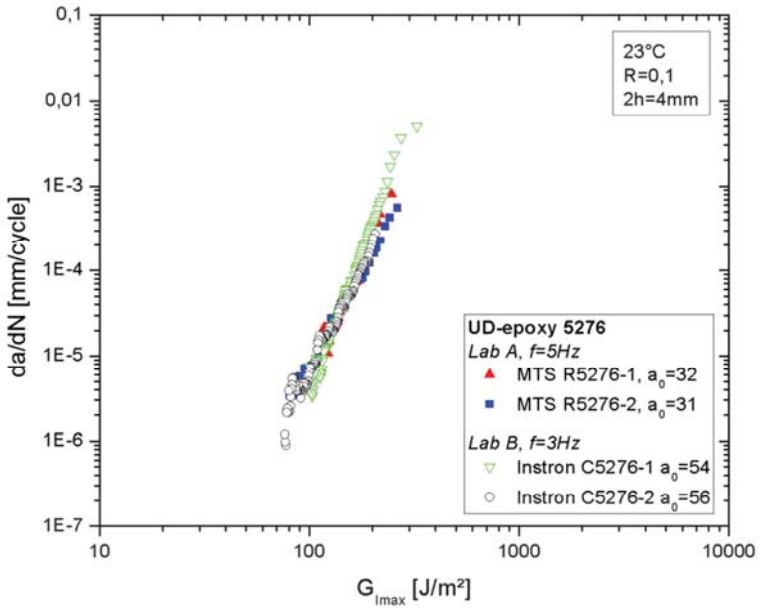

Figure 3.9: Comparison of the results from laboratory A with results from laboratory B.

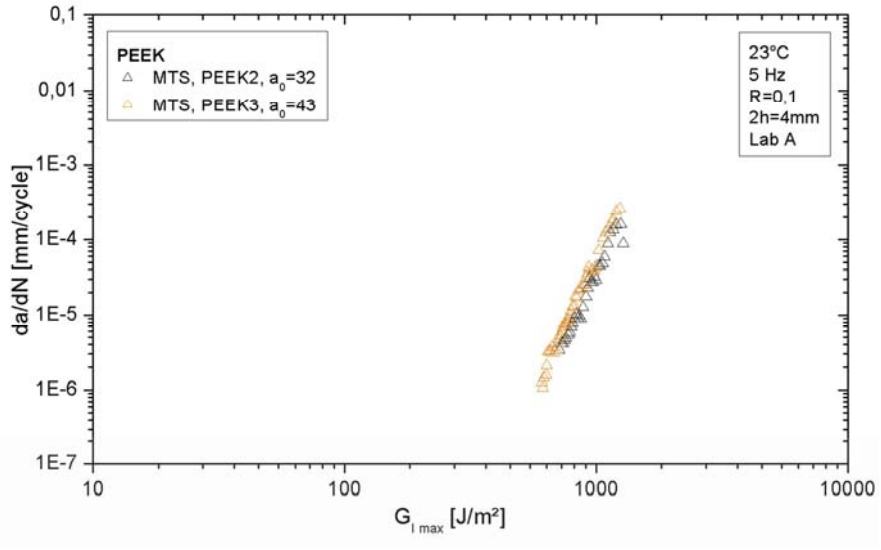

Figure 3.10: Interlaminar fatigue crack growth behavior of UD-PEEK laminates.

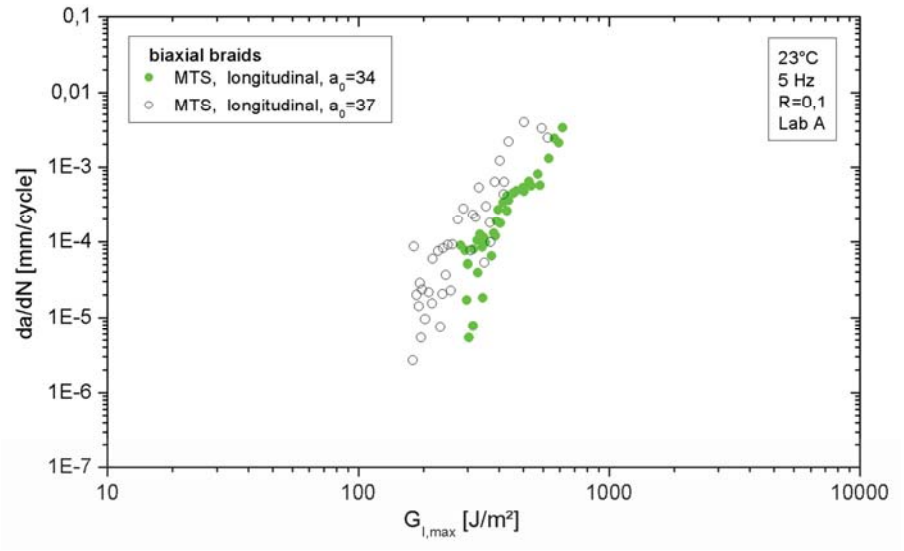

Figure 3.11: Interlaminar fatigue crack growth behavior of biaxial braids.

In Figure 3.13 the fatigue crack growth behavior of triaxial braids is illustrated both for longitudinal and transversal test direction. The triaxial braids tested in longitudinal direction show a smaller influence of both crack deflection and crack branching on the fatigue crack growth data (less scatter) than those tested in transversal direction. The difference between the two different test directions is within the scatter of the data. Compared to the biaxial braids, the triaxial braids show no significant difference in the mode I fatigue crack growth behavior.

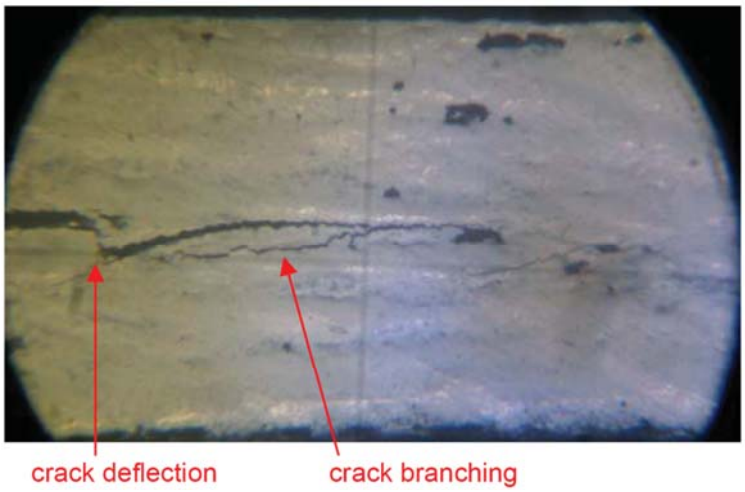

Figure 3.12: Crack deflection and crack branching in the biaxial braid.

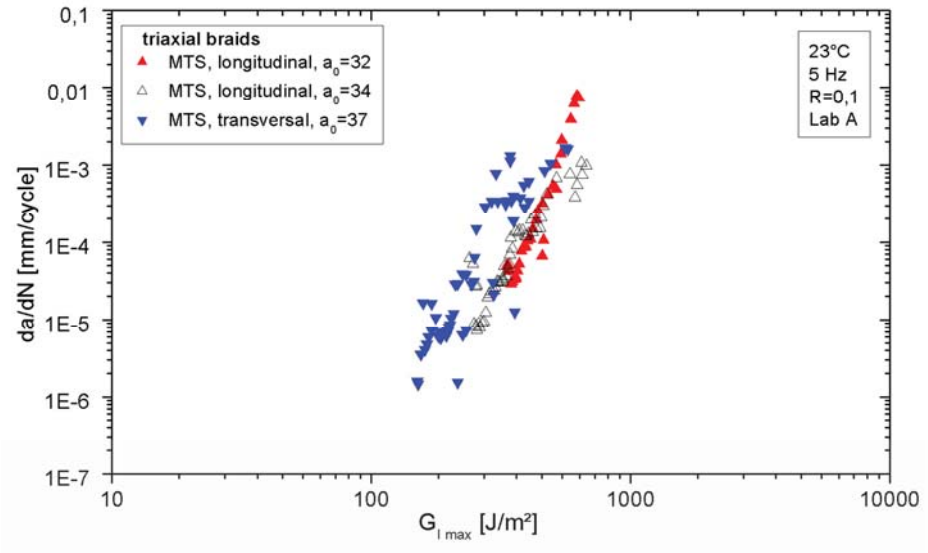

Figure 3.13: Interlaminar fatigue crack growth behavior of triaxial braids.

3.2.5.2 Compression after impact testing

In Figure 3.14 the residual strength of the braided composites is plotted as a function of the impact energy. Similar results were obtained for the triaxial braids tested in transversal direction and the biaxial braids which were tested in longitudinal direction. The residual strength values of the triaxial braids which were tested in the longitudinal direction, however, are at a significantly higher level than the triaxial ones tested in transversal direction. Hence the addition of 0° yarns leads to an increase of the compressive strength after impact when specimens are loaded in longitudinal direction.

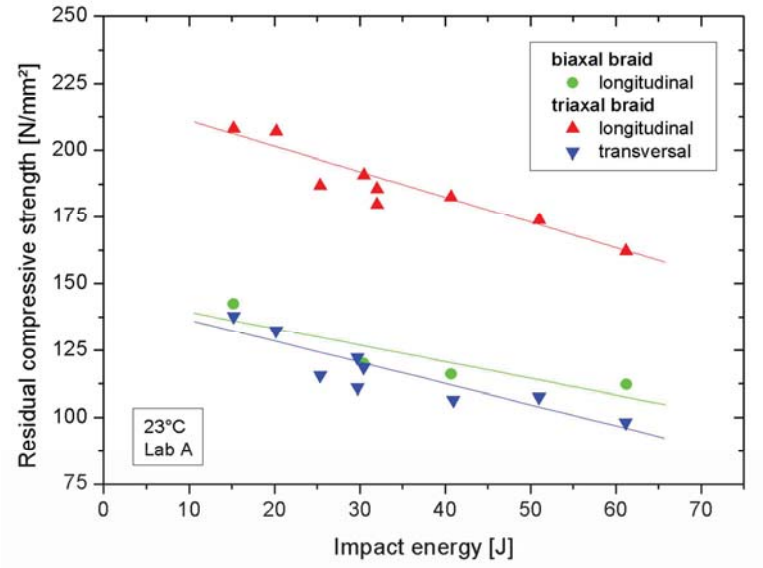

Figure 3.14: Effect of braid architecture on the residual compressive strength of braided composites.

3.2.6 Conclusions

The presented procedure for the characterization of the interlaminar crack growth in fiber reinforced composites proved to be an appropriate way to measure the growth of delaminations. The fatigue crack growth behavior of unidirectionally reinforced polymer laminates with matrices made of either poly-ether-ether-ketone or epoxy resin could be well compared. The machine parameters frequency, control mode and type of machine showed no significant influences on the results of the measurements on UD-reinforced epoxy resins. When varying the specimen parameters initial crack length and thickness, however, the results indicate the need for guidelines concerning these parameters to be able to receive reproducible results. An inter-laboratory comparison of the results of this kind of measurements provided promising results. Round robin measurements have been initialized to prove these findings and will be carried out by members of ESIS TC4. [2, 18]. The interlaminar crack growth behavior of UD-PEEK samples could be measured reproducibly and the PEEK samples proved to be much tougher than the epoxy resin samples.

Furthermore an experimental investigation of the interlaminar crack growth in braided composites under fatigue loading conditions shows that crack branching occurs in multi-directional composites. This increases the dissipation of fracture energy in the specimen. All the braided samples showed stick slip effects, leading

to crack growth curves with a greater amount of scatter compared to the unidirectional reinforced laminates. This can be ascribed to the delamination crack interacting with the braid structure, especially with transverse fibers [19]. Nevertheless no significant difference in the fatigue delamination behavior of biaxial and triaxial braided composites could be found. Compression after impact measurements were made to study damage tolerance of the braided composites. It was found that the fiber orientation has a great influence on the compression after impact behavior.

In all cases the mode I fatigue delamination propagation measurements under displacement control provided very reproducible results and seem to be a promising tool to characterize the delamination behavior of polymer laminates under mode I fatigue loading conditions.

3.2.7 Acknowledgement

Part of the research work of this paper was performed at the Polymer Competence Center Leoben GmbH (PCCL, Austria) within the framework of the Kplus-program of the Austrian Ministry of Traffic, Innovation and Technology with contributions by the Montanuniversität Leoben (Institute of Materials Science and Testing of Polymers) and FACC AG (Ried im Innkreis, A). The PCCL is funded by the Austrian Government and the State Governments of Styria and Upper Austria. The authors would like to thank Mr. M. Stuart and Cytec (New Jersey, USA) for supplying UD-specimens for the measurements at Empa and Toho Tenax Europe GmbH (Wuppertal, D) for providing the carbon fibers for the braids. Test set-up, test performance and data acquisition by Mr. D. Völki at Empa is also acknowledged.

3.2.8 References

[1] ASTM E 647–00, Standard test method for measurement of fatigue crack growth rates, West Conshohocken, USA: American Society for Testing and Materials International (2008).

[2] A.J. Brunner, N. Murphy, G. Pinter, Development of a standardized procedure for the characterization of interlaminar delamination propagation in advanced composites under fatigue mode I loading, Engineering Fracture Mechanics 76 (2009) 2678-2689.

[3] J.E. Masters, P.G. Ifju, A phenomenological study of triaxially braided textile composites loaded in tension, Composites Science and Technology, 56 (1996) 347-358.

[4] L.V. Smith, , S.R. Swanson, Strength design with 2-D triaxial braid textile composites, Composites Science and Technology, 56 (1996) 359-365.

[5] C. Ayranci, J. Carey, 2D braided composites: A review for stiffness critical applications, Composite Strucures, 85 (2008) 43-58.

[6] M. Wolfahrt., G. Pinter, S. Zaremba, T. von Reden, C. Ebel, Effect of preform architecture on the mechanical and fatigue behavior of braided composites for generating design allowables. in 'Proceedings of SAMPE Europe. Paris, France', Vol. 30 (2009) 277-282.

[7] J. Chen, E. Ravey, S. Hallett, M. Wisnom, M. Grassi, Prediction of delamination in braided composite T-piece specimens, Composite Science and Technology 69 (2009) 2363-2367

[8] M.-K. Cvitkovich, Polymer matrix effects on interlaminar crack growth in advanced composites under monotonic and fatigue mixed-mode I/II loading conditions, PhD Thesis, University of Leoben, Austria (1995) 56-57.

[9] ISO 15024, Fibre-reinforced plastic composites – Determination of mode I interlaminar fracture toughness, GIC, for unidirectionally reinforced materials (2001).

[10] K. Kageyama, M. Hojo, Proc. 5th Japan-US Conference on Composite Materials (1990) 227-234

[11] P.C. Paris, F. Erdogan, A critical analysis of crack propagation laws, Journal of Basic Engineering 85 (1963) 528-534

[12] D.J. Wilkins, J.R. Eisenmann, R.A. Camin, W.S. Margolis, R.A. Benson, Characterizing delamination growth in graphite-epoxy, in K.L. Reifsnider (Ed.) Damage in Composite Materials, ASTM Publications, Philadelphia, USA, 1982, pp. 168-183.

[13] R.H. Martin, G.B. Murri, Characterization of mode I and mode II delamination growth and thresholds in graphite/peek composites, NASA technical memorandum 100577 (1988) 1-52.

[14] AITM 1-0010: Determination of compression strength after impact, Blagnac, France (2003).

[15] R.H. Martin, G.B. Murri, Characterization of Mode I and Mode II delamination growth and thresholds in AS4/PEEK composites, in S.P. Garbo (Ed.) Composite Materials: Testing and Design, Vol.9, ASTM Publications, Philadelphia, USA, 1990, pp. 251-270.

[16] A. Argüelles, J. Vina, A.F. Canteli, M.A. Castrillo, J. Bonhomme, Interlaminar crack initiation and growth rate in a carbon-fibre epoxy composite under mode-I fatigue loading, Composite Science and Technology 68 (2008) 2325-2331

[17] M. Hojo, S. Ochiai, T. Aoki, H. Ito, New simple and practical test method for interlaminar fatigue threshold in cfrp laminates, 2nd ECCM-Composites, Testing & Standardization, (1994a) 553-561

[18] A.J. Brunner, I. Paris, G. Pinter, Fatigue Propagation Test Development for Polymer-Matrix Fibre-Reinforced Laminates, in 'Proceedings of 12th International Conference on Fracture Ottawa, Canada', (2009).

[19] N. Alif, L.A. Carlsson, L. Boogh, The effect of weave pattern and crack propagation direction on mode I delamination resistance of woven glass and carbon composites, Composites Part B: Engineering 29B (1998) 603-611

3.3 PUBLICATION 2

MODE I DELAMINATION FATIGUE CRACK GROWTH IN UNIDIRECTIONAL FIBER REINFORCED COMPOSITES: DEVELOPMENT OF A STANDARDIZED TEST PROCEDURE

3.3.1 Bibliographic Information

- Authors and their relevant contributions to the publication:
  - Steffen Stelzer[1]
    Preparation and submission of the manuscript, organization of the round robin exercise, material distribution, execution of the tests in laboratory A, calculation and analysis of all test results.
  - Andreas J. Brunner[2]
    Execution of the tests in laboratory B.
  - Antonio Argüelles[3]
    Execution of the tests in laboratory C.
  - Neal Murphy[4]
    Execution of the tests in laboratory D.
  - Gerald Pinter[1,5]
    Academic supervision of the work carried out in this publication.
- Affiliations:
  [1] Institute of Materials Science and Testing of Polymers, Montanuniversitaet Leoben, Leoben, Austria
  [2] EMPA, Swiss Federal Laboratories for Materials Science and Technology, CH-8600 Dübendorf, Switzerland
  [3] Department of Construction and Manufacturing Engineering, Universidad de Oviedo, Campus de Viesques, Gijón 33203, Spain
  [4] School of Electrical, Electronic and Mechanical Engineering, UCD Engineering and Materials Science Centre, University College Dublin, Belfield Dublin 4, Ireland
  [5] PCCL, Polymer Competence Center Leoben, Roseggerstrasse 12, A-8700 Leoben, Austria

- Periodical: Composites Science and Technology
- DOI: 10.1016/j.compscitech.2011.11.033

Statement with regard to publication: The manuscript presented here is an adapted accepted manuscript in order to fit the formatting of the thesis and does not necessarily reflect the actually published version.

3.3.2 Abstract

Selected mode I fatigue data from five different types of fiber-reinforced, polymer-matrix composites tested in two round robins organized by the American Society for Testing and Materials subcommittee D30.06 and European Structural Integrity Society Technical Committee 4, respectively, are analyzed and discussed. The focus is on experimental scatter (in-laboratory and inter-laboratory) and on schemes for quantitative data analysis. It is shown that in spite of considerable scatter different composites can be distinguished and, under certain assumptions, a relative ranking be established. Further, effects from limited experimental measurement resolution are noted and implications for the test procedure and use of the test data in design of composite structures discussed. For comparative purposes, a rough ranking of different composites is feasible with test data generated within 24 hours per specimen in an industrial test environment.

3.3.3 Introduction

Characterization of delamination resistance of fiber-reinforced polymer-matrix composites (FR-PMC) under quasi-static and cyclic fatigue loads is important for development of laminates with improved damage tolerance as well as for designing composite structures and, therefore, has been an active area of research for quite a while (see e.g., [1, 2] for a summary). While this has resulted in standardized test procedures or at least in standardization activities for quasi-static loading in different modes [3], this is not the case for cyclic fatigue yet. A procedure for mode I tensile opening cyclic fatigue testing of FR-PMC was evaluated in a first round robin test involving three laboratories and was shown to yield sufficiently reproducible results [4] and additional testing showed sufficient discrimination between selected, different types of FR-PMC [5]. Recently, additional round robin testing on mode I cyclic fatigue was performed, both within subcommittee D30.06 on interlaminar properties of composite materials of the American Society for Testing and Materials (ASTM) International and committee TC4 on fracture of polymers, composites and adhesives of the European Structural Integrity Society (ESIS). The present contribution evaluates selected results from these round robins and focuses on approaches for quantitative data analysis on one hand, and on experimental scatter and measurement resolution on the other. Implications for the test procedure under development will be discussed.

3.3.4 Experimental

3.3.4.1 Materials and specimens

The materials used in the two round robin programs are listed in Table 3.1 for ASTM D30.06 and in Table 3.2 for ESIS TC4. All tests were performed using double cantilever beam (DCB) specimens (according to ASTM D5528 or ISO 15024) with a total length of about 152 mm (ASTM) and of 145 mm (ESIS), a width of 20 mm and thicknesses as listed in Tables 8.1 and 8.2. Starter cracks were realized by using a PTFE film insert (about 5 µm for ASTM and about 20 µm thick for ESIS) at the laminate mid-plane. Aluminum load-blocks (about 6 mm thick, 12.8 mm long and 20 mm wide, with a pin-hole with a diameter around 3.8 mm located towards the crack tip for ASTM, and 10 mm thick, 15 mm long and 20 mm wide with centered pin-hole with a diameter of 4 mm for ESIS) were mounted for load introduction.

Table 3.1: Materials used in the ASTM D30.06 round robin

	C1	C2	G1
Fiber	Carbon, IM7	Carbon, G40-800 12k	Glass, S2
Matrix resin	Epoxy, 977-3	Epoxy, 5276-1	Epoxy, 5216
Lay-up	$[0]_{26}$	$[0]_{26}$	$[0]_{18}$
Thickness (mm)	3.5 (nominal 3.5)	3.4 (nominal 3.7)	4.1 (nominal 4.0)

Table 3.2: Materials used in the ESIS TC4 round robin

	C3	C4
Fiber	Carbon, G30-500 12k	Carbon, AS4
Matrix resin	Epoxy, Rigidite 5276	PEEK
Lay-up	$[0]_{24}$	$[0]_{24}$
Thickness (mm)	4.0	3.0

3.3.4.2 Procedure

The ASTM test procedure first asked for drying the specimens according to ASTM D5229/D5229M and then storing them in a desiccator before testing under standard laboratory conditions of (23±3)°C and (50±10) % relative humidity. The mode I fatigue test shall be performed without precracking at 10 Hz (if possible); at laboratory B tests were run with 3 Hz due to large displacements and with a R-ratio of 0.1. Testing shall be continued until a delamination rate below 10^{-6} mm/cycle is reached in order to determine a threshold value. For determining the maximum cyclic displacement δ_{max}, a series of quasi-static tests shall be performed on a separate set of nominally identical specimens up to a delamination length of 75 mm beyond the initial crack tip. The quasi-static results shall be used to calculate δ_{max} from the following relation (3.1):

$$\frac{\delta^2{}_{\max}}{[\delta_{cr}]^2{}_{av}} = \frac{G_{\mathrm{Im}ax}}{G_{Ic}} = 0.8 \tag{3.1}$$

$$\text{, i.e., } \delta_{\max} = \sqrt{0.8[\delta_{cr}]^2{}_{av}} \tag{3.2}$$

where G_{Ic} is the critical strain energy release rate, $[\delta_{cr}]^2_{av}$ is the average of the squared critical displacement values at G_{IC} from the quasi-static tests and G_{Imax} is the maximum cyclic strain energy release rate. Effectively, at laboratory B, a factor of 0.8 proved to be too low to get the delamination propagation started from the initial crack within a sufficiently low number of cycles and a factor around 1.0 was used for most tests. The quasi-static data are summarized in Table 3.3. One laboratory also tested additional specimens for delamination growth onset according to ASTM D6115 based on developments reported in [6].

The ESIS procedure specified that in order to start the measurements at high crack growth rates just below G_{IC} a quasi-static mode I test for pre-cracking was done as a G_{IC} -test at a cross-head speed between 1 and 5 mm/min. The displacement value at which pre-cracking was stopped was then taken as the δ_{max} value for fatigue loading. The cyclic test was started and continued until a crack growth rate of about 10^{-6} mm/cycle was reached. An R-value of 0.1 was used in all the measurements and the tests were done under displacement control.

Fatigue loading could be stopped to perform visual observation of delamination lengths with a travelling microscope. In order to avoid errors during the calculation of the results a spreadsheet macro file was created which was used by all the participants for the calculation of da/dN and G_{Imax}.

Table 3.3: Quasi-static Mode I averages from the ASTM D30.06 round robin (Laboratory B, 5 specimens each)

	C1	C2	G1
Initiation G_{IC} (NL) ± standard deviation [J/m^2]	120 ± 9.7	253 ± 23.8	147 ± 11.8
Initiation G_{IC} (MAX/5%) ± standard deviation [J/m^2]	145 ± 12.1	290 ± 11.8	172 ± 11.9
Average Propagation ± standard deviation [J/m^2]	174 ± 16.5	337 ± 27.1	432 ± 27.7
Maximum Propagation ± standard deviation [J/m^2]	184 ± 17.2	357 ± 34.2	574 ± 26.9
Back-calculated E-modulus ± standard deviation [GPa]	122 ± 5.8	142 ± 12.5	59 ± 13.3

Data from visual observation of delamination propagation and from recorded machine compliance can be used to evaluate G_{Imax} and the corresponding delamination rate da/dN. G_{Imax} is evaluated using simple beam theory, corrected beam theory and modified compliance calibration and the da/dN-values are calculated in a secant (point-wise) approximation or with a seven point polynomial fit (according to ASTM D647). The number of machine compliance data points can be reduced by specifying a minimum delamination length increment between subsequent data points in the data presentation graphs (typically 50 µm was used). The same spreadsheet was used to analyze the ASTM round robin data from laboratory B. A typical set-up for mode I fatigue testing (laboratory B) is shown in Figure 3.15.

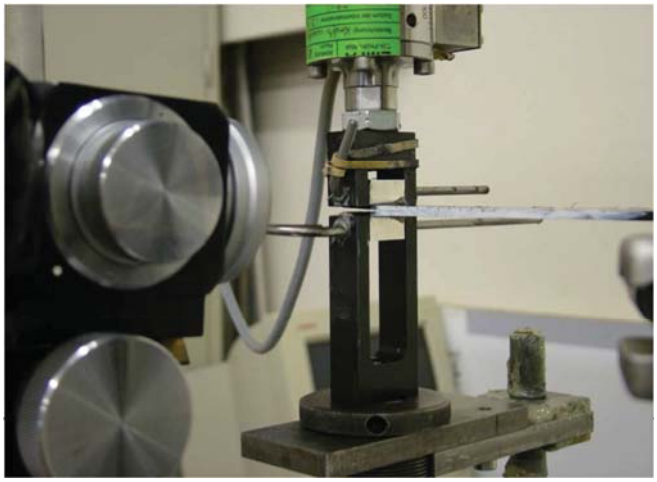

Figure 3.15: DCB-specimen for mode I fatigue testing mounted in the fixture (laboratory B) without applied load; the travelling microscope for visually identifying the delamination tip is seen on the left.

3.3.5 Results and Discussion

3.3.5.1 ASTM Round Robin

Only data from laboratory B are available for the analysis and hence, no information on inter-laboratory scatter can be derived. On the other hand, as shown in Figure 3.16, the in-laboratory scatter of the data from visually recorded delamination lengths using a travelling microscope is such that it is somewhat difficult to even distinguish trends among the three laminates. This is different from the data presented in [5] where various carbon- and glass FR-PMC could easily be distinguished. It has to be noted that G_{Imax} values are determined from the modified compliance calibration method (MCC, see [7]).

As a second step in the analysis, the same data are plotted using delamination lengths calculated from recorded machine compliance data (machine load and displacement, respectively) [4] instead of visually determined delamination lengths (Figure 3.17). Since machine data have been recorded every 500 cycles, the number of data points is reduced by requiring a minimum delamination length increment of 50 μm between individual data points in the spreadsheet used for data analysis.A 50 μm delamination length increment roughly corresponds to the resolution of the visual delamination length measurement obtained with the microscope at laboratory B.

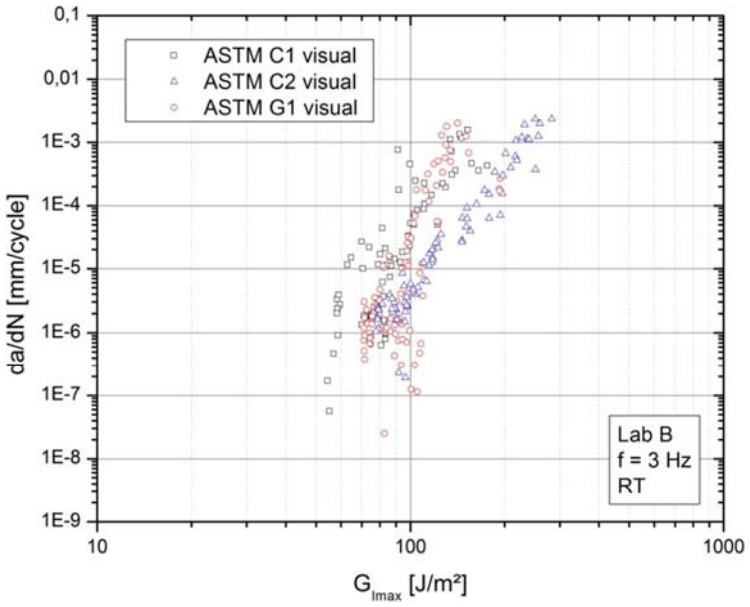

Figure 3.16: Paris plot of all visual data recorded by laboratory B for three types of laminates used in the ASTM round robin, G_{Imax} has been evaluated by the modified compliance calibration (MCC) method.

This allows distinguishing differences in slope of the Paris plots for each group of laminate. In a next step, the data points for each specimen are replaced by a power law fit, $\frac{da}{dN} = A \cdot {G_{Imax}}^{m}$, which yields a quantitative result, namely the exponent m, which represents the slope of the linear regime in the double logarithmic diagram. It has to be noted that these fits include all data points and hence may be affected by possible deviations from linear behavior at both, high and low delamination rates. In a further step, the power law fits for each material are presented individually, this time including the non-linear (NL) and maximum or 5% (MAX/5%) initiation values from quasi-static testing of specimens of these laminates (again determined by the MCC method).

From the four graphs in Figure 3.18, the following conclusions can be drawn: (1) Laminates C1 and G1 show a larger scatter in slopes than laminate C2, (2) laminate C2 clearly shows the lowest slope, while C1 and G1 seem to yield similar slopes, (3) laminates C1 and C2 show at least one fit with a distinctly different slope among the five data sets, and (4) for laminate C1, all linear fits except one reach the average MAX/5% initiation value determined from quasi-static tests, whereas for C2 and G1 only one linear fit each exceeds the average NL value from the same tests.

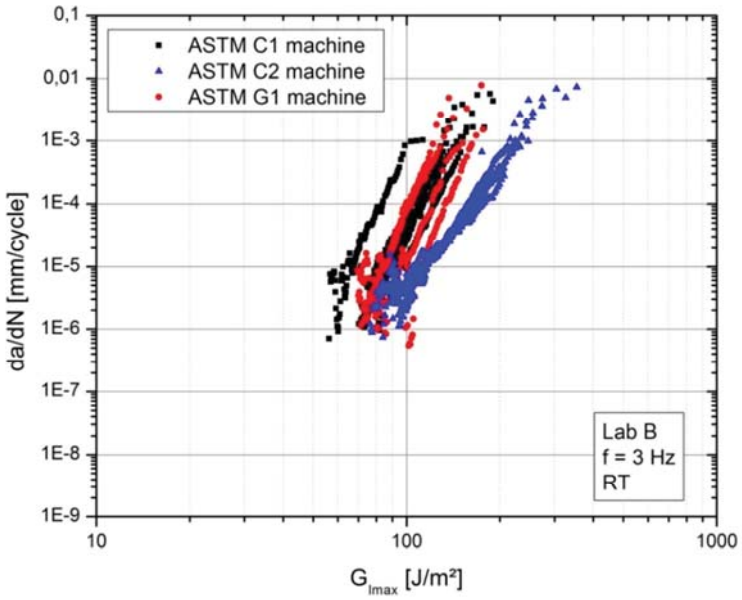

Figure 3.17: Paris plot of the same data shown in Figure 3.16 but using delamination lengths back-calculated from machine compliance instead of visually determined delamination lengths. The number of data points has been reduced by requiring a minimum delamination length of 50 micrometer between each data point.

It can also be noted that the highest observed delamination rates da/dN for all three laminates are on the order of about $5x10^{-3}$ mm/cycle. If the values of the slopes from the different specimens are compared in a bar-plot (Figure 3.19) it is evident that in spite of some scatter laminate C2 yields the lowest, C1 intermediate and G1 the highest values for the slopes. In this respect, the three laminates can clearly be distinguished.

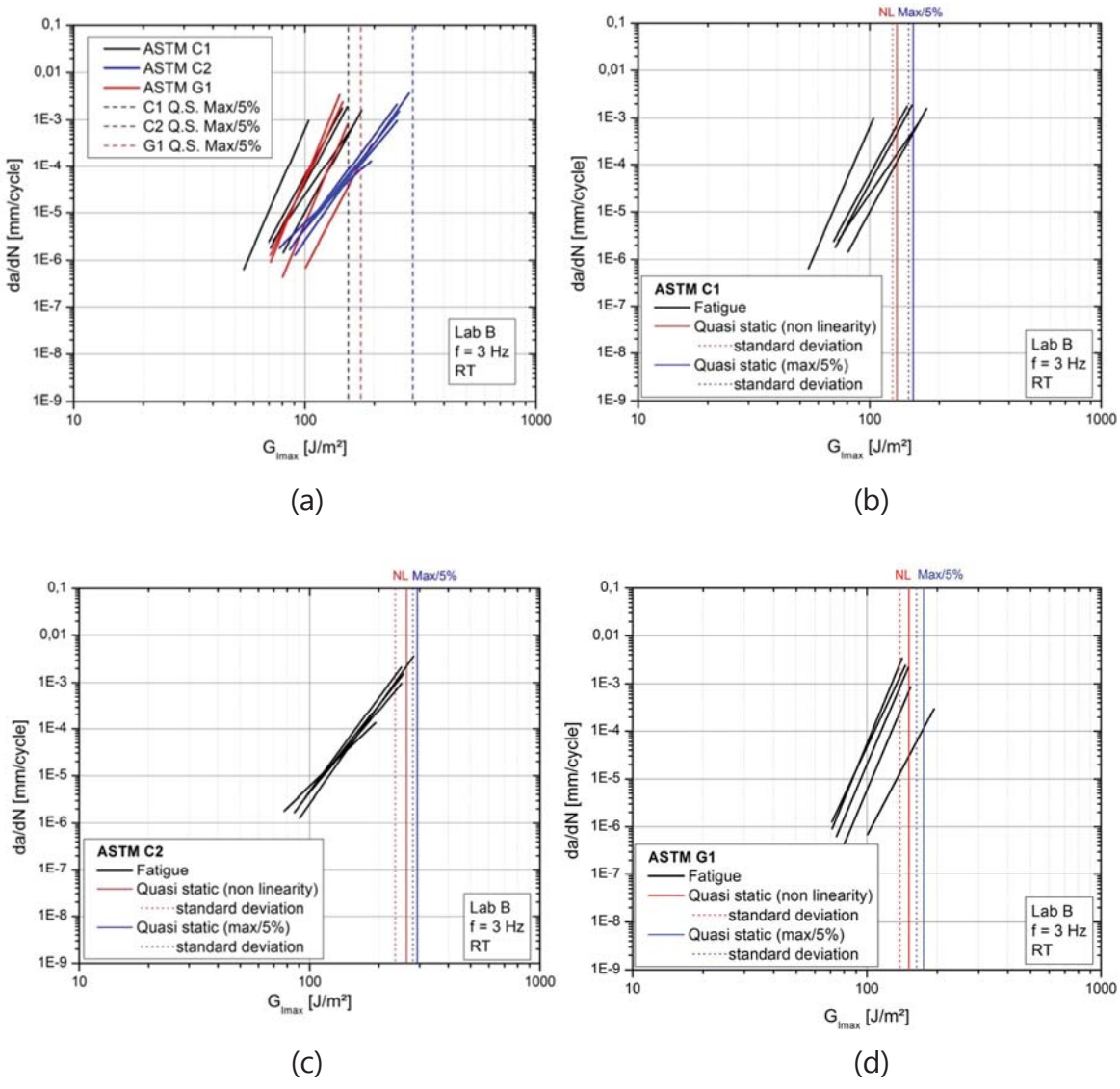

Figure 3.18: Paris plots of the fatigue data represented by linear fits for each specimen, (a) for all three laminates, (b) for laminate type C1, (c) for laminate type C2, and (d) for laminate type G1. The average non-linear and maximum or 5% initiation values determined from quasi-static tests are shown as thick dotted lines with thin dotted lines indicating the lower standard deviation (averages and standard deviations from testing 5 separate specimens per laminate).

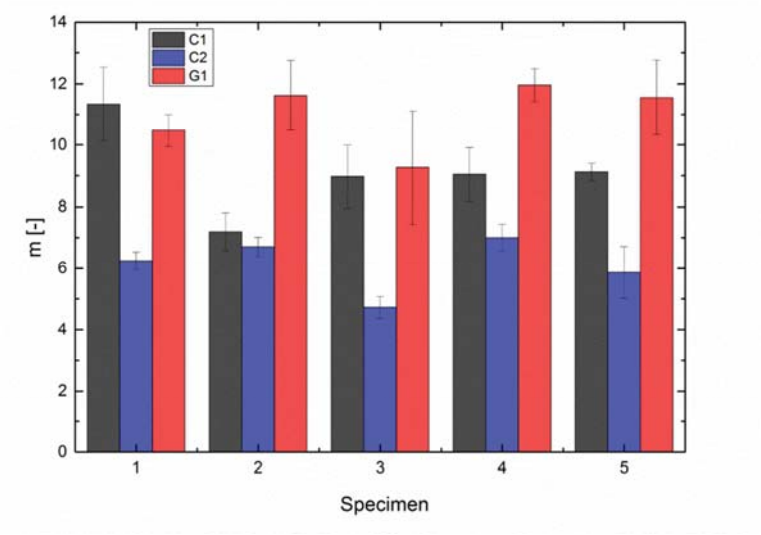

Figure 3.19: Comparison of the slopes (m) obtained from linear fits of the Paris plots for each specimen.

However, a comparison of slopes is not sufficient for ranking the laminates with respect to their delamination resistance performance. A steep slope does indicate that a laminate may exhibit a significant increase in delamination-rate even for a small increment of the applied load (equivalent to G_{Imax}) [8].

On the other hand, it is debatable whether a low slope will really be preferable since such a laminate may yield higher delamination-rates at relatively low applied loads.

A linear fit that, for a given delamination-rate da/dN, corresponds to a “high” value of applied load G_{Imax} may, in the end indicate a better delamination resistance than one for which the applied load is much smaller (at the same rate) independent of the slope. Taking an arbitrary delamination-rate of 10^{-5} mm/cycle and comparing the three laminates in Figure 3.20 yields lowest applied loads G_{Imax} of 69, 111, and 86 J/m^2 for C1, C2 and G1, respectively. This coincides with the relative ranking obtained from quasi-static mode I testing of the same laminates. Of course, if the same comparison were made at 10^{-7} mm/cycle and assuming that no threshold-like effects would come into play at this rate, the ranking may look different with C2 yielding the lowest values (from extrapolation of the linear fits). These examples show that under certain assumptions, a relative ranking of the delamination resistance of different laminates can be established using the type of data analysis outlined above. A detailed statistical analysis of the results would in principle even yield confidence intervals for the values describing the ensemble of test data.

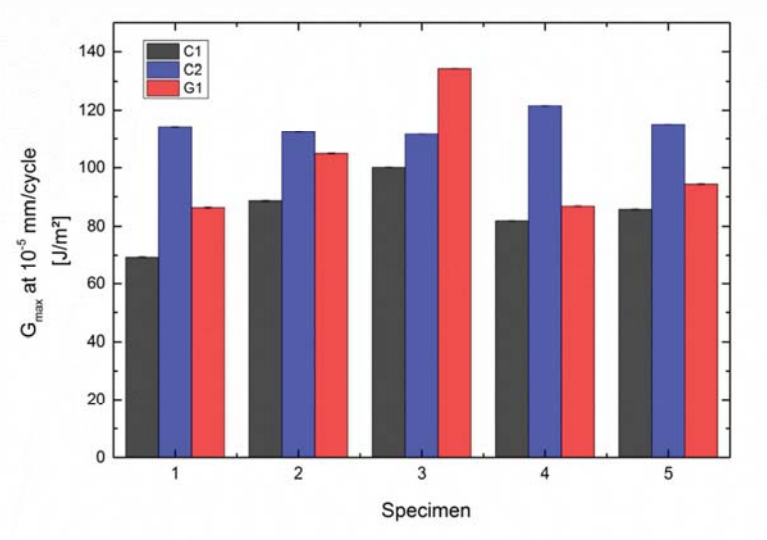

Figure 3.20: Comparison of the G_{Imax} values at 10^{-5} mm/cycle obtained from linear fits of the Paris plots for each specimen.

It has, however, to be pointed out that before using any of these values for designing a composite structure, their validity will have to be firmly established (at least in an analysis of the full data set from the ASTM round robin) and in- and inter-laboratory scatter will have to be assessed in detail for determining suitable safety factors. As already noted above, steep slopes of the fatigue curves yield large uncertainties in predicted delamination growth rates for relatively small uncertainties in the applied load [8]. The same holds for large scatter in the slopes, if delamination growth rates are, e.g., used in design. Threshold values [6, 9] for mode I fatigue used in a “no-growth” design concept could be considered as an alternative, however, determination of such values may require long test duration, especially at low frequencies or large displacements. It might be advisable to change recommended specimen geometries from that of the quasi-static mode I tests (ASTM D5528 or ISO 15024) to less compliant beams for that. Further, as noted earlier [4], it is not clear whether such threshold values do exist or whether they appear due to limited experimental measurement resolution [10]. Evidence for effects caused by limited measurement resolution from selected ESIS round robin data will be presented and discussed below.

3.3.5.2 ESIS Round Robin

Analogous to the approach for data analysis of the ASTM round robin, all raw data from all participants (laboratories A,B,C; and D) obtained on two carbon FR-PMC (one thermoset epoxy and one thermoplast, i.e., PEEK) are compiled in Figure 3.21. In this case, the data for the thermoset and thermoplastic composites are

readily distinguishable. At first sight, it is also clear that the thermoplastic shows a larger scatter than the thermoset laminate (neglecting one thermoset data set on the far left with a very steep slope). The full analysis of the data will be published elsewhere [11], but selected aspects will be discussed in this section. Performing the same linear fitting procedure described above and comparing the slopes of the linear fits for the thermoplastic AS4/PEEK laminate (Figure 3.22) shows that there is considerable in-laboratory as well as inter-laboratory scatter. Neglecting three extreme values of about -0.9, 63.5 and 11.8 (laboratories B, C and D, not shown) the average slope is roughly similar to that of laminate C2. Since all fits are located at applied loads G_{Imax} above 200 J/m^2, it is expected that the delamination resistance performance of the thermoplastic composite is superior to that of the thermoset.

A plot of machine load peak values and calculated delamination length is shown for one specimen of carbon FR-epoxy for laboratory A and B, respectively in Figure 3.23. The noise in the load signal clearly differs for the two laboratories due to the different load cells used. This noise in the load signal is reflected in a corresponding noise in the delamination lengths calculated from the machine data. This finally results in significant scatter in the Paris plot for the specimen tested in laboratory A at delamination-rates around 10^{-5} mm/cycle.

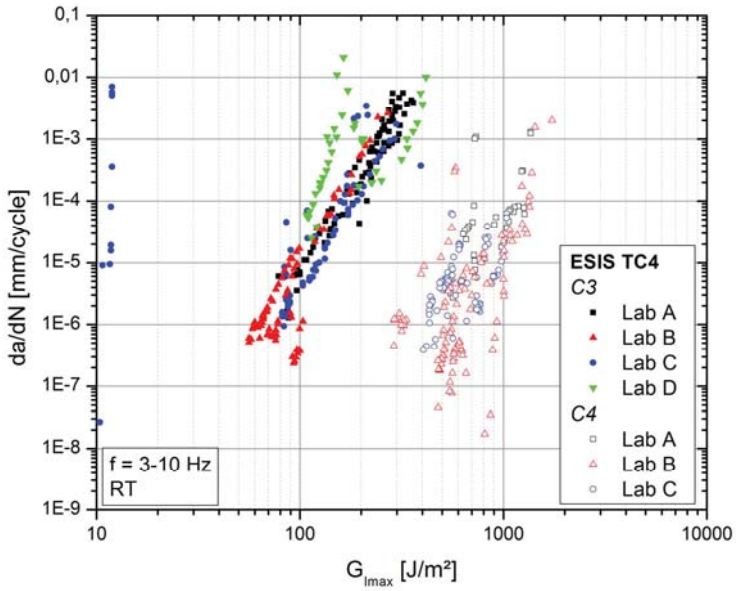

Figure 3.21: Paris plot of all visual data recorded by laboratories A, B, C and D for two types of laminates used in the ESIS round robin, G_{Imax} has been evaluated by the modified compliance calibration (MCC) method.

The same composite tested in laboratory B still yields a straight Paris plot at these rates. However, similar scatter to that found for laboratory A at 10^{-5} mm/cycle is observed for specimens tested at laboratory B for delamination-rates around 10^{-6} mm/cycle and lower (Figure 3.24). This constitutes strong evidence that determination of Paris plots at low delamination-rates may be affected by measurement resolution, in particular by the choice of the load cell or calibrated load-cell range. At sufficiently low rates, an analogous and cumulative effect from variation in the displacement control of the test machines is expected to come into play as well. It is hypothesized that these effects may put limitations on the determination of mode I fatigue threshold values for composite laminates, even though this has not been attempted in the present round robin tests.

Close inspection of the calculated and visually determined delamination lengths as a function of cycle numbers (Figure 3.23) also indicates that stopping the test machines for visually reading delamination lengths may induce slight shifts in the load signals upon restarting the cyclic loads. This will ultimately also affect the accuracy of the determination of the Paris plot behavior.

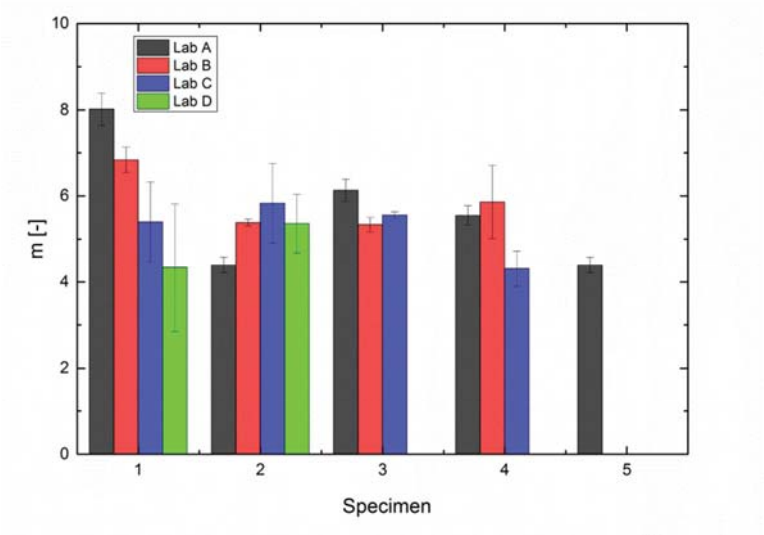

Figure 3.22: Comparison of the slopes (m) obtained from linear fits of the Paris plots for each specimen from the G30-500/R5276 laminate.

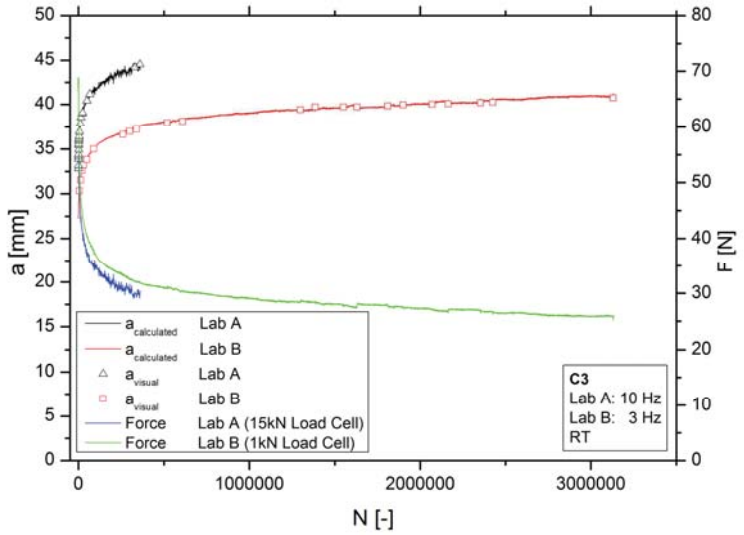

Figure 3.23: Machine load and calculated delamination length versus cycle number (laboratory A and B) for the carbon FR-PMC. Visually determined delamination lengths (machine stopped) are also indicated (see text for details).

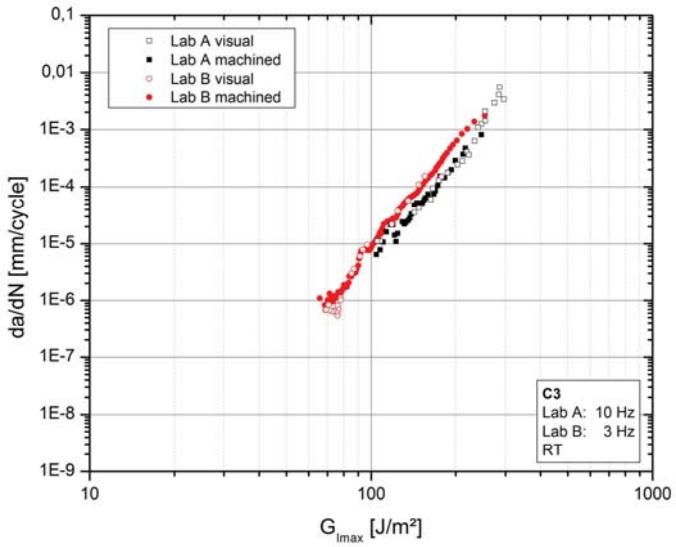

Figure 3.24: Paris plot for one specimen of carbon FR-PMC for laboratory A and B, respectively.

Since laminate type C2 from the ASTM round robin uses an epoxy type 5276-1 and material A from the ESIS round robin is using a similar epoxy (R5276), however with different carbon fiber types (G40-800 12k in C2 versus G30-500 12k), the slopes of the linear fits for the two laminates can be compared (Figure 3.25). For the same delamination-rates, the fits for laminate C2 tend to be

shifted to slightly higher values of applied load (G_{Imax}). The data also seem to indicate a slightly higher slope for laminate C2 compared with laminate type A. This could be interpreted as indication of improved performance, but the data base for comparing averages and scatter is limited (5 specimens each tested at one single laboratory). It has to be noted that material A has been stored for an extended period of time and hence may be affected by ageing. Nevertheless, it will be of interest to compare the full data set from all laboratories for each of the two materials, once the data are available.

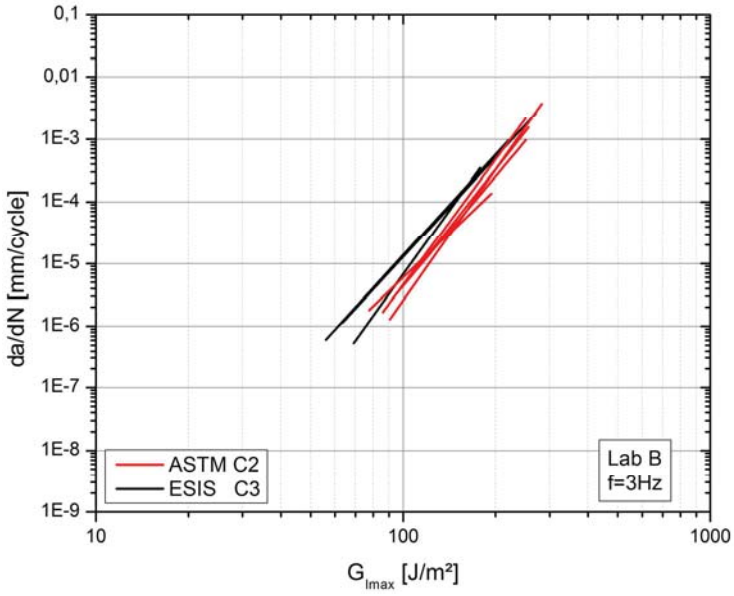

Figure 3.25: Comparison of Paris plots for laminate types C2 and C3 using a similar epoxy matrix (all test data from laboratory B).

3.3.6 Conclusions

The round robin data presented in this paper have shown the need for establishing structured data processing and analysis, if different laminates shall be compared with respect to their mode I cyclic fatigue delamination resistance behavior. Due to the inherently large scatter, both in-laboratory as inter-laboratory, it may be difficult or virtually impossible to rank different laminates, if only raw data are used in the Paris plot. While the analysis methodology proposed in the present paper will provide a rough ranking, quite likely further detailed analyses will have to be performed for obtaining statistical confidence limits before using the data for design. Testing five specimens per laminate type may constitute a lower limit and more specimens may have to be tested for sufficient discrimination and statistical confidence. Testing at higher frequencies (up to 10 Hz) may require stiffer specimens than those recommended by the quasi-static test procedures. The analysis has also indicated limitations arising from the resolution of machine load and displacement measurements which may affect determination of the so-called threshold behavior of the laminates. Further research will be necessary to resolve these issues.

3.3.7 Acknowledgments

The support of Dr. Isabelle Paris (organizer of the ASTM D30.06 round robin) and of Dr. Mike Stuart (Cytec USA, for providing the additional specimens) as well as technical assistance with testing at Empa by Mr. Daniel Völki is gratefully acknowledged.

3.3.8 References

[1] P. Davies, B.R.K. Blackman, A.J. Brunner “Standard test methods for delamination resistance of composite materials: Current status”, Appl. Comp. Mats. 5 (1998) 345-364.

[2] T.E. Tay “Characterization and analysis of delamination fracture in composites: a review of developments from 1990 to 2001”, Appl. Mech. Rev. 56 (2003) 1-23.

[3] A.J. Brunner, B.R.K. Blackman, P. Davies “A status report on delamination resistance testing of polymer-matrix composites”, Eng. Fract. Mech. 75 (2008) 2779-2794.

[4] A.J. Brunner, N. Murphy, G. Pinter “Development of a standardized procedure for the characterization of interlaminar delamination propagation

in advanced composites under fatigue mode I loading", Eng. Fract. Mech. 76 (2009) 2678-2689.

[5] A.J. Brunner, I. Paris, G. Pinter "Fatigue propagation test development for polymer-matrix fibre-reinforced laminates", Proc. 12th Intl. Conf. on Fracture ICF-12, paper No. 00371 (2009), pp. 1-8.

[6] R.H. Martin, G.B. Murri "Characterization of mode I and mode II delamination growth and thresholds in AS4/PEEK composites", in: Composite Materials: Testing and Design, ASTM STP 1059 (S.P. Garbo, ed.), American Society for Testing and Materials (1990) 251-270.

[7] A.J. Brunner, B.R.K. Blackman, P. Davies "Mode I Delamination" Chapter 4.1 in: Fracture Mechanics Testing Methods for Polymers, Adhesives and Composites (D.R. Moore, A. Pavan, J.G. Williams, eds.) Elsevier (2001) 271-305.

[8] L.E. Asp, A. Sjögren, E.S. Greenhalgh "Delamination growth and thresholds in a carbon/epoxy composite under fatigue loading", J. Compos. Technol. & Res. 23 (2001) 55-68.

[9] M. Hojo, S. Ochiai, K. Tanaka "Near-threshold propagation of delamination fatigue cracks in unidirectional CF/PEEK laminates in air and in water", Mater. Sci. Res. 1 (1995) 100-107.

[10] G. Allegri, M.I. Jones, M.R. Wisnom, S.R. Hallett "A new semi-empirical model for stress ratio effect on mode II fatigue delamination growth", Compos. A: Appl. Sci. & Manuf. A 42 (2011) 733-740.

[11] S. Stelzer, A.J. Brunner, A. Argüelles, N. Murphy, G. Pinter, Proceedings 6th ESIS Conference (2011), in preparation.

3.4 PUBLICATION 3

MODE I DELAMINATION FATIGUE CRACK GROWTH IN UNIDIRECTIONAL FIBER REINFORCED COMPOSITES: RESULTS FROM ESIS TC4 ROUND-ROBINS

3.4.1 Bibliographic Information

- Authors and their relevant contributions to the publication:
  - Steffen Stelzer[1]
    Preparation and submission of the manuscript, organization of the round robin exercise, material distribution, execution of the tests in laboratory A, calculation and analysis of all test results.
  - Andreas J. Brunner[2]
    Execution of the tests in laboratory C.
  - *Antonio Argüelles*[3]
    Execution of the tests in laboratory B.
  - Neal Murphy[4]
    Execution of the tests in laboratory D.
  - Gema Maudes Cano[5]
    Execution of the tests in laboratory E.
  - Gerald Pinter[1,6]
    Academic supervision of the work carried out in this publication
- Affiliations:
  [1] Institute of Materials Science and Testing of Polymers, Montanuniversitaet Leoben, Leoben, Austria
  [2] EMPA, Swiss Federal Laboratories for Materials Science and Technology, CH-8600 Dübendorf, Switzerland
  [3] Department of Construction and Manufacturing Engineering, Universidad de Oviedo, Campus de Viesques, Gijón 33203, Spain
  [4] School of Electrical, Electronic and Mechanical Engineering, UCD Engineering and Materials Science Centre, University College Dublin, Belfield Dublin 4, Ireland
  [5] Instituto Nacional de Técnica Aerospacial, Carretera de Ajalvir, Km 4, 28850 Torrejón de Ardoz, Spain
  [6] PCCL, Polymer Competence Center Leoben, Roseggerstrasse 12, A-8700 Leoben, Austria

- Periodical: Engineering Fracture Mechanics
- DOI: 10.1016/j.engfracmech.2013.12.002

Statement with regard to publication: The manuscript presented here is an adapted accepted manuscript in order to fit the formatting of the thesis and does not necessarily reflect the actually published version.

3.4.2 Abstract

Two round robins on mode I fatigue delamination propagation organized by Technical Committee 4 of the European Structural Integrity Society compared three unidirectional carbon fiber reinforced composites, one with thermoplastic (poly-ether-ether-ketone) and two with thermoset (epoxy) matrix tested at five laboratories. Different approaches for data evaluation and their effect on the in- and inter-laboratory scatter are discussed and compared. Calculated delamination rates da/dN and applied G_{Imax} from displacement controlled tests are sensitive to small scatter in the load signal, and, therefore, a new route to evaluate the crack growth rate from pairs of load and displacement data is presented.

3.4.3 Introduction

In recent years fiber reinforced polymer composites have gained in importance, especially due to the growing interest of the transportation industry in lightweight structures [1–4]. But notwithstanding their many advantages, the biggest disadvantage of using fiber-reinforced polymer-matrix (FRP) composite materials is their susceptibility to delamination initiation and to growth of these interlaminar delaminations (see, e.g., [5, 6] for recent reviews). To account for the need to characterize the delamination resistance of FRPs under monotonic mode I loading conditions a significant research effort was carried out in the last three decades [5–13]. Several research groups have further published results of cyclic mode I delamination measurements on FRP [12, 14–25]. There are approaches for incorporating delamination properties into structural design [26] and quasi-static as well as cyclic fatigue fracture mechanics data from composite laminates have been used to predict the delamination behavior of composite structures [27–31].

Standards considering the determination of the critical value of the interlaminar fracture toughness, G_{IC}, for unidirectionally reinforced polymer composites under quasi-static load were published [32–34]. Furthermore a standard for the measurement of delamination fatigue growth onset was issued in 2008 [35]. Recently, European Structural Integrity Society Technical Committee 4 (ESIS TC4) and American Society for Testing and Materials, International, Subcommittee D30.06 (ASTM D30.06) carried out separate round-robin test programs on mode I (tensile opening) fatigue delamination growth. Selected results and additional references have been compiled in [36–38], but so far no standards considering mode I fatigue crack propagation in unidirectionally reinforced (UD) polymer composites have been published. The applicability of mode I fatigue test procedures to glass fiber-reinforced polymer-matrix (GFRP) laminates was

investigated [22, 27] and it was shown that different types of FRP laminates could be discriminated [37]. The 2009 round robin exercise carried out by ESIS TC4 investigated the influences of control mode (load vs. displacement control), test frequency and test duration on the overall test results [36] performed at three laboratories. None of these test parameters was found to exert a significant influence when testing a carbon fiber reinforced epoxy laminate (IM7/977-2). Selected results from preliminary testing and of a first round robin of ESIS TC4 and ASTM D30.06 published in [38] focused on discrimination between different composite laminates and, in part, on determination of threshold values. A second ESIS TC4 round robin performed in 2010-2011 focused on material dependent inter-laboratory scatter by testing one carbon fiber epoxy laminate (G30-500 12k/R5276) and one carbon-fiber poly-ether-ether-ketone (AS4/PEEK) laminate at five laboratories. Possible sources of inter-laboratory scatter include different types of test machines used at participating laboratories, different test set-ups and frequencies, and different operators recording the visually determined delamination lengths.

Compared with tests described in the literature so far, a round robin with several participating laboratories for the first time allows the determination of inter-laboratory scatter. The in-laboratory scatter can be compared to previously published literature for the same or similar composite laminates. In order to have comparable results, a number of test parameters were prescribed (see below for details).

In order to facilitate testing in an industrial test environment particular emphasis was placed on short test duration and automated data acquisition [36]. Therefore, threshold determination was not an aim of the round robins. As discussed in [38], threshold value determination may require higher resolution of load and displacement than mode I fatigue delamination propagation. The present paper for the first time compiles all data sets from the mode I fatigue delamination propagation round robins performed within ESIS TC4.

3.4.4 Experimental

3.4.4.1 Materials and specimens

Three materials, listed in Table 3.4, were tested within the ESIS TC4 mode I fatigue round robin exercises. DCB specimens based on prescriptions and recommendations in [34] with a total length of about 145 mm, a width of 20 mm and thicknesses as listed in Table 3.4 were used. For starting the crack a poly-

tetra-fluoro-ethylene (PTFE) film (about 20 µm thick), inserted at the laminate mid-plane, was used in materials A and B, and a fluorinated ethylene propylene (FEP) film (about 10 µm thick) in material C. [34] recommends the use of film inserts with less than 13 µm thickness in order to simulate a sharp crack. In the ESIS TC4 round robin a monotonic precrack was generated prior to fatigue testing in order to avoid an influence of the film insert on the crack growth. Aluminum load-blocks were mounted for load introduction.

3.4.4.2 Procedure

The round robin test procedure and the results presented here are based on the experience from published literature [7–25] and preliminary testing at selected laboratories [37]. The 2011 test procedure in principle allows testing at different stress ratios, R, test frequencies and under load or displacement control. For ease of comparison in the round robin, testing was limited to displacement control based on a comparison between load and displacement control from the first round robin [36]. Test frequencies shall be chosen as high as possible, but possible heating effects would have to be investigated for frequencies of 10 Hz or higher. Data will be presented as a function of G_{Imax} rather than ΔG for eliminating scatter due to possible facial interference and the prescribed stress ratio of R=0.1 will yield conservative results when using G_{Imax} [14].

Table 3.4: Materials used in the ESIS TC4 round robins.

	A	B	C
Fiber	Carbon, G30-500 12k	Carbon, AS4	Carbon, IM7
Matrix resin	Epoxy, Rigidite 5276	PEEK	Epoxy, 977-2
Lay-up	[0]	[0]	[0]
Thickness (mm)	4.0	3.0	4.0
Starter film type and thickness	PTFE, 20 µm	PTFE, 20 µm	FEP, 10 µm

Facial interference comprises a combination of effects including fiber bridging (e.g., fibers of both crack faces interfere during the crack closing step), a plasticity

zone wake (usually called crack closure in metals), rough surface and debris [18]. The ESIS TC 4 procedure specified that in order to start the measurements at high crack growth rates just below G_{IC}, a quasi-static mode I test for pre-cracking was performed as a G_{IC}-test at a cross-head speed of between 1 and 5 mm/min, ideally to obtain a short, i.e., a few mm long precrack. Cyclic fatigue loading was then started with the last displacement value from the quasi-static test, since choosing a maximum displacement from the average of all quasi-static tests, e.g., according to equation (3.3) as required by the ASTM D30.06 procedure proved difficult because of the scatter among specimens (mainly due to stiffness variation).

$$\delta_{\max} = \sqrt{[0.8 \cdot \delta_{cr}]^2_{av}} \tag{3.3}$$

where δ_{max} is the maximum displacement in the cyclic test and δ_{cr} is the critical displacement in the quasi-static test. The fatigue tests were continued until a crack growth rate of about 10^{-6} mm/cycle was reached. Fatigue loading could be stopped to perform visual observation of delamination lengths with a travelling microscope. In order to avoid errors during the calculation of the results a spreadsheet macro file was created which was used by all the participants for the calculation of the so-called Paris plot, i.e., da/dN as a function of G_{Imax}. The tests were carried out in five different laboratories (labeled A,B,C,D,E) using five different test machines. Laboratory A used a servo-hydraulic test machine (type MTS 858) with a 15 kN load cell calibrated to a load range between 0 and 400 N. The tests at laboratory B were done on a servo-hydraulic test machine (type MTS Bionix) with a 15 kN load cell. Laboratory C used a servo-hydraulic test machine (type Instron 1273) with a 1 kN load cell, calibrated to a load range between 0 and 500 N. Laboratory D used a servo-hydraulic test machine (type Instron 8502) with a load cell capacity of 5 kN. Laboratory E carried out the tests on a servo-hydraulic test machine (type Instron 8872) with a 5 kN load cell. Laboratories A and B performed the tests at a maximum frequency of 10 Hz, laboratory C at 3 Hz and laboratories D and E at 5 Hz. Labs A, B and D had to reduce the test frequency when testing the more compliant PEEK specimens due to the greater piston displacement that was needed to keep the interlaminar crack growing.

3.4.4.3 Crack length detection

The crack length, a, was determined using three different approaches. All round robin participants used a travelling microscope with a sufficient resolution for visual crack length detection as defined in [34] as first method. Based on these visually observed crack lengths and the corresponding machine data, a compliance based approach (see equation 3.4) was used as second method to calculate crack lengths from every pair of load and displacement values recorded by the test machine at selected intervals during the test as explained in [36].

$$a = \left(\frac{C}{B} \right)^{\frac{1}{m'}} \tag{3.4}$$

where C is the compliance determined from machine load and displacement and B and m' are constants of a power-law fit. Figure 3.26(a) shows such a power law fit and Figure 3.26(b) the resulting crack length as a function of the number of cycles after applying this compliance calibration to load and displacement data recorded by the test machine.

As third method, the so-called "effective" crack length method can be applied in order to back-calculate crack lengths from the measured compliance of the specimen and independent measurements of the flexural modulus, E_1, rather than visually measuring crack lengths (see [39] for details of the calculations). Using this method for the determination of crack lengths would facilitate fatigue delamination measurements on FRP because after starting the test it would only be necessary to stop the test when a sufficiently low crack growth rate is reached. Simultaneously, possible shifts in machine data recording from stopping and restarting the fatigue loading and operator dependent visual determination of delamination length would be eliminated. Effective crack lengths, a_{eff}, were calculated via equation (3.5), which is derived from corrected beam theory:

$$a_{eff} = \frac{h}{2} \left(\frac{E_1 C b}{N} \right)^{\frac{1}{3}} \tag{3.5}$$

where h is half the thickness of the specimen, E_1 the flexural modulus, b the width of the specimen and N a finite displacement correction to account for load-block effects. The flexural moduli of materials A and B were measured on a tensile testing machine (type Zwick Roell Z250) with a 10 kN load cell in laboratory A according to [40] while the value for material C was obtained from [41].

3.4.4.4 Calculation of da/dN

The crack growth rate, da/dN, was calculated using a seven point averaging method as described in ASTM E 647 [42]. This is an incremental polynomial method fitting a second order polynomial (parabola) to sets of (2n+1) successive data points, where n is 1, 2 or 3. The first and last pair of data points are evaluated using the secant or 2 point technique, where two points are connected with a straight line and the crack growth rate is the slope of this line. In order to examine a possible influence of the number of fitted data points on the calculation of da/dN the authors also calculated da/dN by using this 2 point technique and a 5 point technique, where n=2. With the aim of reducing the scatter in the compliance based calculation of da/dN observed in the first round robin [36] and illustrated in Fig. 3.26(b), two approaches were selected. The first is to eliminate all data points which do not correspond to a delamination length increase of more than 0.1 mm (see Fig. 3.26(c)). The second uses a second order power law fit of the crack lengths calculated from compliance, which is plotted versus cycle number (see Fig. 3.26(d)).

3.4.4.5 Calculation of the strain energy release rate

The strain energy release rate in mode I, G_I, can also be calculated in various ways. The simplest method is to calculate it using so-called “simple beam theory” (SBT), see equation (3.6):

$$G_I = \frac{3P\delta}{2ba} \tag{3.6}$$

where P is the load and δ is the displacement. Since [34] recommends the use of corrected beam theory (CBT, see equation 3.7) and modified compliance calibration (MCC, see equation 3.8) for the calculation of G_I, these two calculation methods are also evaluated in this paper.

$$G_I = \frac{3P\delta}{2b(a+|\Delta|)}\frac{F}{N} \tag{3.7}$$

where Δ is a correction factor to account for the effects of transverse shear and for deformation beyond the crack tip [43] and F is a correction factor to account for large displacements and N the load-block correction [34, 44].

$$G_I = \frac{3n}{2(2h)}\left(\frac{P}{b}\right)^2\left(\frac{bC}{N}\right)^{2/3}F \tag{3.8}$$

where n is the slope of the linear fit of $(bC/N)^{1/3}$ over (a/2h).

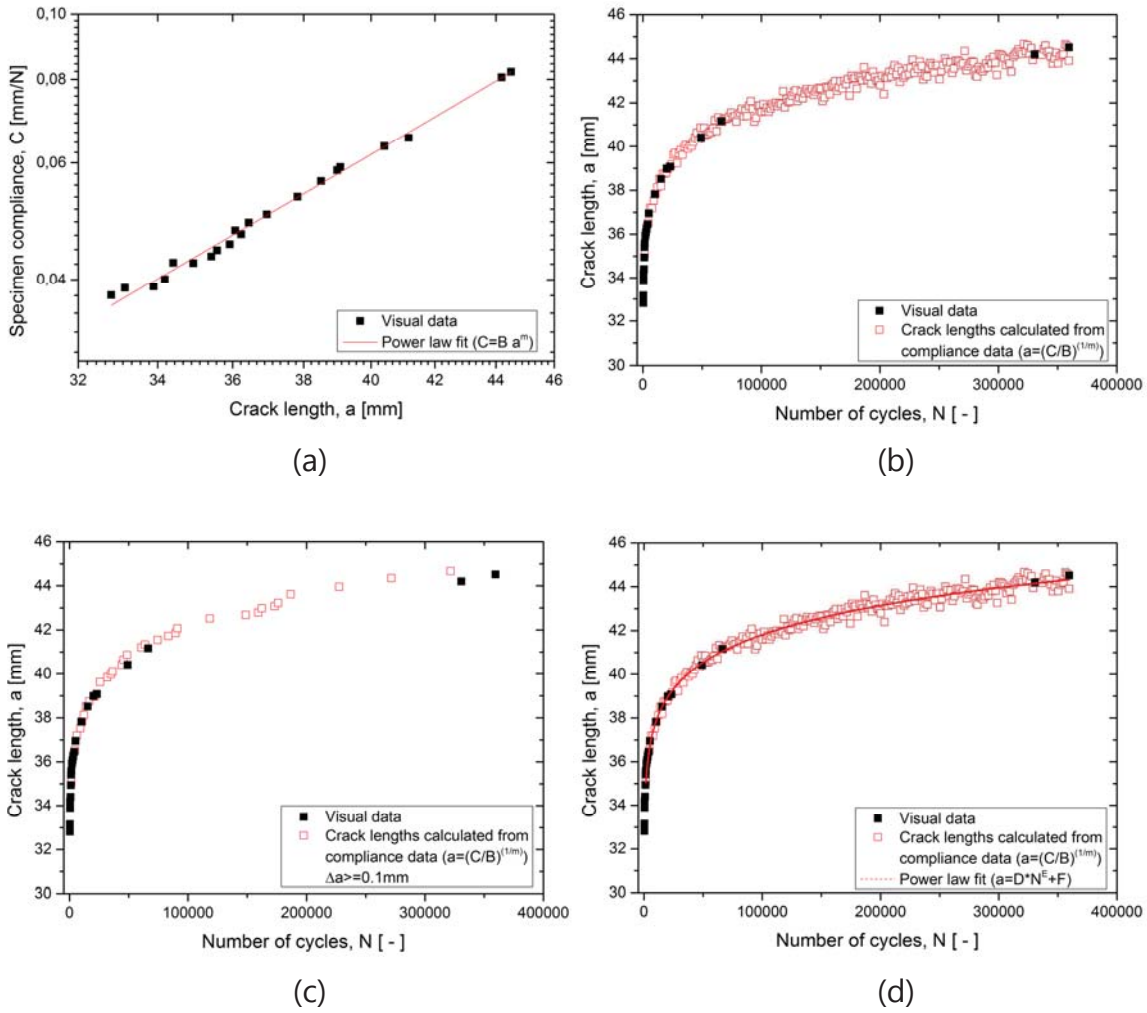

Figure 3.26: Calculation of crack lengths from load and displacement data recorded by the test machine (Lab A and material A).

(a) Correlation between specimen compliance and visually measured crack lengths.

(b) Visually measured crack lengths and crack lengths calculated from compliance data versus number of cycles.

(c) Visually measured crack lengths and crack lengths calculated from compliance data versus number of cycles after data reduction ($\Delta a > 0.1$ mm).

(d) Visually measured crack lengths, crack lengths calculated from compliance data and a fit of crack lengths calculated via compliance.

3.4.5 Results and Discussion

Figure 3.27 shows the results of all laboratories using visually observed crack lengths for the determination of the crack growth rate, da/dN. The strain energy release rate was calculated via (a) SBT, (b) CBT and (c) MCC. In case of material A, taking all data from all laboratories into account, the inter-laboratory scatter of the data calculated via SBT is in the order of one third of a decade of the strain energy release rate (or of two decades of the crack growth rate da/dN). The in-laboratory scatter for the different labs is comparable and also amounts to about one third of a decade of the strain energy release rate (or again of two decades in da/dN). When using compliance based methods for the calculation of the strain energy release rate, namely CBT and MCC, the scatter increases and can even reach up to about half a decade of the strain energy release rate (or two-and-one-half decades in da/dN). A factor that can play a role in the compliance based analysis schemes is the development of the fracture process zone with increasing number of fatigue cycles. Starting cyclic fatigue from a relatively short, quasi-static mode I precrack (a few mm long) may, depending on the type of composite, not necessarily correspond to starting from a steady-state crack tip with fully developed fracture process zone. Increasing the fracture process zone in the wake of the delamination tip can affect the compliance of the specimens.

The slope of the Paris plot, which is described by the exponent m (see equation 3.9) agrees fairly well for laboratories A, B, C, D and E in the da/dN-range between 10^{-3} and 10^{-6} mm/cycle for data calculated from visually observed crack lengths (see Figure 3.28(a)). The level for valid fits was arbitrarily defined by requiring a value for the coefficient of determination R^2 above 0.95. The results of laboratories D and E show significant scatter in the values of m and therefore contribute significantly to the inter-laboratory scatter mentioned above (see Figures 3.28(a), (b) and (c)).

$$\frac{da}{dN} = A \cdot G_{\mathrm{Im}\,ax}{}^{m} \tag{3.9}$$

For material B the in-laboratory and inter-laboratory scatter in da/dN in the Paris plot is larger than for material A, but similar for all participating labs. One of the causes of this increase in scatter is the partly unstable delamination behavior of material B.

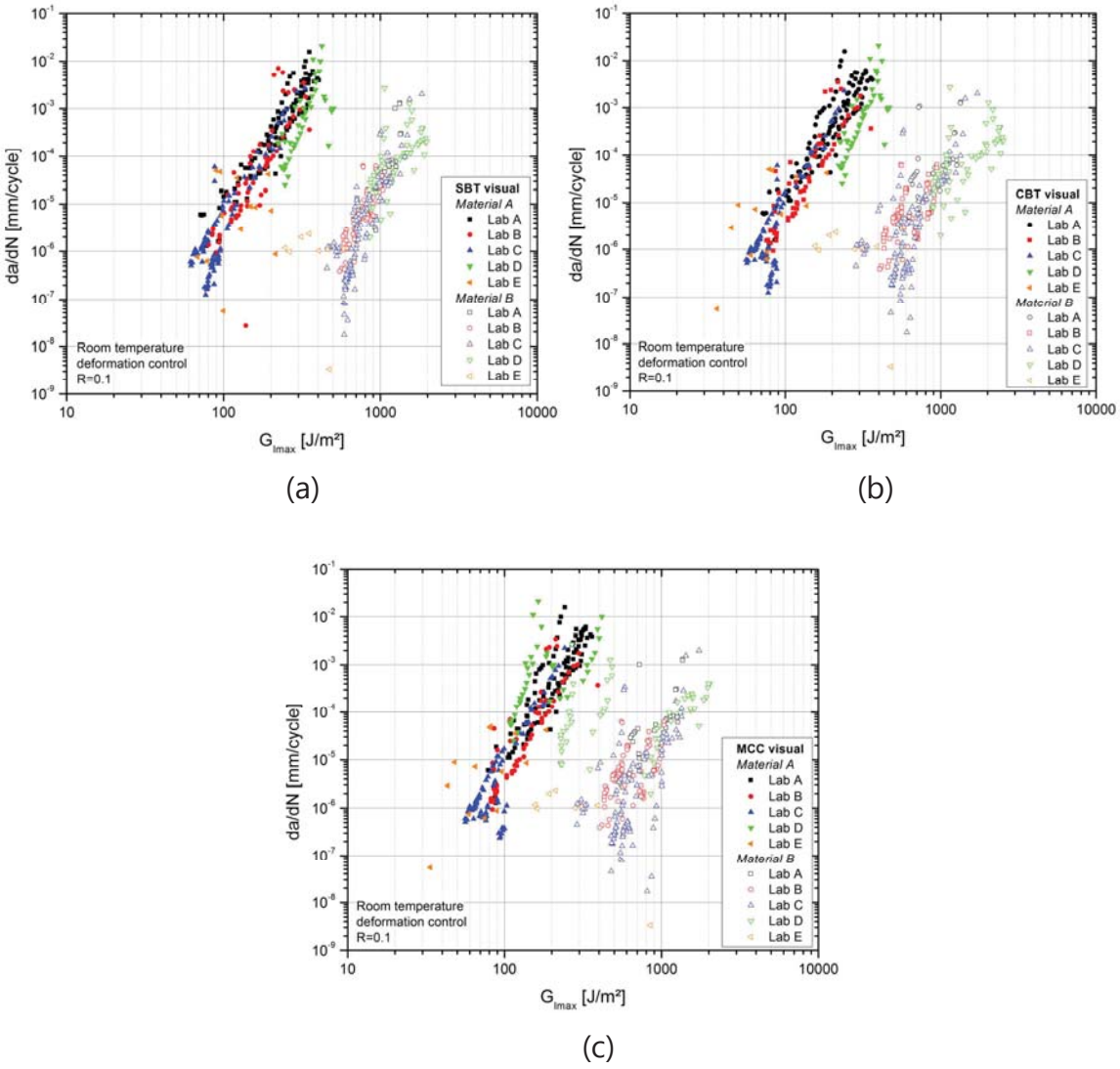

Figure 3.27: Paris plots from visually observed crack lengths.
(a) Paris plots with G_I calculated via simple beam theory.
(b) Paris plots with G_I calculated via corrected beam theory.
(c) Paris plots with G_I calculated via modified compliance calibration.

The crack did not grow continuously, but showed stochastic arrest effects. This has an influence on the linearization of a compliance based term over a crack length based term in both CBT and MCC. Again the scatter in strain energy release rate clearly increases when compliance based methods (namely CBT and MCC) were used to calculate G_{Imax}, this time going up from roughly one third of a decade in G_{Imax} (or one-and-one-half decades in da/dN) to one decade in G_{Imax} (and several decades in da/dN, respectively).

The variation in slope for Material B in the case of visually observed crack lengths can be seen in Figure 3.28(b). While data from laboratory D yielded results with the highest values for m, laboratory E did not deliver data that were considered valid at all based on the arbitrarily chosen correlation criterion (R^2>0.95). The average value from the valid round robin data of 8.63 is higher than that of 6.14 determined by [18]. However, literature data cited in [18] cover a range of slopes between 3.0 and 10.5, i.e., an apparent inter-laboratory scatter of roughly ± 3, i.e. comparable with the ± 2.28 found in the present round robin. The larger scatter observed in the position of the Paris plot on the G_{Imax} axis for material B, on the other hand, makes it questionable whether such data can be used in design (unless unrealistically large safety factors are applied).

Figure 3.29 shows the course of da/dN versus G_{Imax} values calculated with MCC from pairs of load and displacement data via the compliance based crack length approach. Compared to the graphs shown in Figure 3.27, and specifically Fig. 3.27(a) with crack length from visual observation, the scatter is larger than any of these types of G_{Imax} calculation.

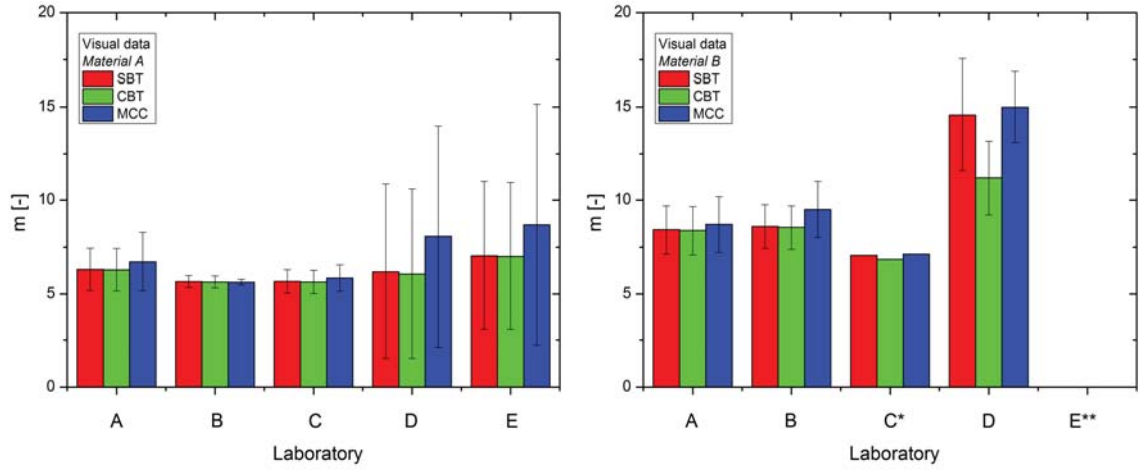

Figure 3.28: Slopes m of the Paris plots (visually measured crack lengths). The data were fitted with a power law relationship as shown in equation (3.9). All fits that did not meet an arbitrary minimum R^2 of 0.95 were rejected.
(a) Values of exponent m for material A.
(b) Values of exponent m for material B.
* Fit for one specimen. For all other specimens the value of determination of the fits was too low.
** No valid fits could be created for data of laboratory E.

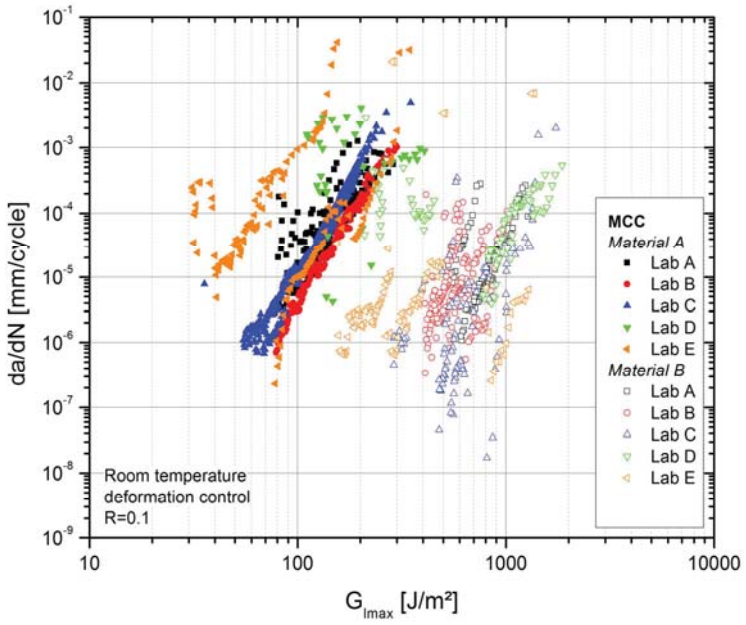

Figure 3.29: Paris plots from crack lengths calculated via compliance calibration. Paris plots with G_I calculated via modified compliance calibration.

This indicates that the use of compliance data for the calculation of either da/dN or G_{Imax} is directly responsible for the scatter in the plots. Since compliance is calculated from displacement and load which are machine parameters influenced by test set-up, it is important to use a sufficiently stiff test machine, a load cell within a load range just above the maximum loads appearing in the test (in this case about 500N) and preferably local displacement measurement (e.g. clip on extensometers). Asp et al. [23] carried out cyclic delamination tests on HTA/6376C and used a 250 N load cell range. Still, the scatter in the da/dN versus G_{Imax} curve was roughly one third of a decade of G_{Imax} (or one decade of da/dN) in the lower crack growth rate regime. Figures 3.30(a) and 3.30(b) and Tables 3.5 and 3.6 again show values for the slopes of the Paris plots, for material A and B, respectively, in this case for the results calculated via the compliance based crack length approach. The values agree quite well with those calculated from visually observed crack lengths in Figures 3.28(a) and 3.28(b). Only one valid fit (R^2>0.95) could be generated with data from laboratory D for both materials A and B. The same holds for material B of laboratory E. Tables 3.5 and 3.6 show values of the exponent m (see equation 3.9) for power law fits of Paris plots for materials A and B respectively. Two types of da/dN calculation are compared. 7 point fitting as described in [42] and fitting of crack length data with a second order power law fit as described above. All data that was calculated via the latter route was further refined by setting an arbitrary limit for the coefficient of determination (R^2) of 0.95.

All data that did not meet this criterion was rejected. Thereby the in- and inter-laboratory scatter of the slope values could be greatly reduced. In both cases the scatter of the slope value increases when using compliance based methods to calculate the strain energy release rate.

In Figure 3.31 the Paris plots for the case of crack lengths calculated via the effective crack length approach are shown. The flexural modulus for the determination of the effective crack length was measured on 10 specimens for each material. E_1 amounted to 118±7 GPa for material A, to 120±6 GPa for material B and to 120±2 GPa for material C [41]. In contrast to the results shown above (Fig. 3.27(c) and Fig. 3.29, i.e., crack length determined from visual observation and compliance measurements) the results calculated via MCC and a_{eff} show less scatter. While the comparison between the different methods (i.e., SBT, CBT and MCC) in the Figures includes the correction factors F and N only in the case of CBT and MCC but not for SBT, their effect is essentially negligible (yielding G_{IC} values that differ at most by 1-2 % if F and N are set to 1). No clear explanation can hence be given for this phenomenon.

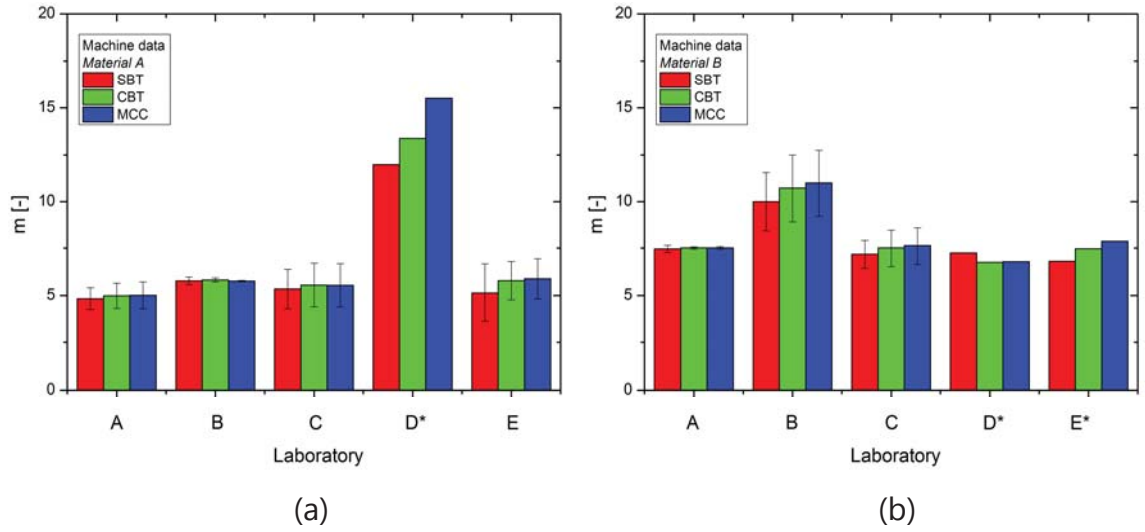

Figure 3.30: Slopes m of the Paris plots (crack lengths calculated from compliance data). The data were fitted with a power law relationship as shown in equation (3.9). All fits that did not meet a minimum R^2 of 0.95 were rejected.
(a) Values of exponent m for material A.
(b) Values of exponent m for material B.
* fit for only one specimen. For all other specimens the value of determination of the fits was too low.

Table 3.5: Slope values obtained from fits of Paris plots of material A. All results calculated from machine data. Values for standard deviations in brackets.

Strain energy release rate calculation		Simple Beam Theory		Corrected Beam Theory		Modified Compliance Calibration	
da/dN calculation		7-point	Full fit	7-point	Full fit	7-point	Full fit
Laboratory	A	4.17 (0.86)	4.83 (0.58)	4.32 (0.93)	4.98 (0.67)	4.30 (0.93)	5.01 (0.71)
	B	0.49 (6.72)	5.77 (0.20)	-6.67 (23.07)	5.82 (0.11)	-6.85 (23.48)	5.76 (0.03)
	C	3.69 (3.16)	5.34 (1.04)	3.85 (3.27)	5.55 (1.15)	4.04 (2.41)	5.54 (1.14)
	D	0.41 (3.06)	11.95 [a]	0.40 (3.05)	13.38 [a]	0.15 (3.27)	15.50 [a]
	E	3.08 (2.13)	5.13 (1.54)	3.34 (2.34)	5.78 (1.01)	3.41 (2.22)	5.88 (1.06)
Mean value of all tests		2.46 (3.87)	5.65 (2.01)	0.87 (11.41)	5.99 (2.27)	0.83 (11.59)	6.17 (2.81)

7-point.....Seven point averaging method for the calculation of da/dN as described in ASTM E647 [42]

Full fit .....Fitting the full range of crack length data versus number of cycles with a second order power law fit

[a] .....Only one valid specimen (R^2>0.95)

Table 3.6: Slope values obtained from fits of Paris plots of material B. All results calculated from machine data. Values for standard deviations in brackets.

Strain energy release rate calculation		Simple Beam Theory		Corrected Beam Theory		Modified Compliance Calibration	
da/dN calculation		7-point	Full fit	7-point	Full fit	7-point	Full fit
Laboratory	A	7.57 (0.72)	7.46 (0.19)	7.92 (1.24)	7.51 (0.06)	7.92 (1.24)	7.51 (0.07)
	B	7.14 (2.67)	10.00 (1.54)	7.52 (2.73)	10.72 (1.79)	7.48 (2.68)	10.99 (1.76)
	C	9.47 (5.45)	7.17 (0.74)	10.35 (6.14)	7.51 (0.99)	10.94 (8.14)	7.63 (0.99)
	D	2.01 (4.69)	7.24[a]	1.81 (3.95)	6.75[a]	1.72 (4.45)	6.78[a]
	E	9.10 (5.71)	6.80[a]	6.09 (1.22)	7.47[a]	5.90 (1.42)	7.86[a]
Mean value of all tests		7.17 (4.79)	8.05 (1.58)	7.09 (4.75)	8.40 (1.89)	7.38 (5.85)	8.56 (1.95)

7-point ..... Seven point averaging method for the calculation of da/dN as described in ASTM E647 [42]

Full fit..... Fitting the full range of crack length data versus number of cycles with a second order power law fit

[a] ..... Only one valid specimen (R^2>0.95)

Figure 3.32 directly compares the results of SBT, CBT and MCC for one laboratory. The crack growth rates were calculated from visually observed crack lengths, crack lengths calculated via compliance calibration and crack lengths calculated via the effective crack length method. The different crack length calculation methods seem to agree quite well with respect to the resulting slope in the Paris plot, but the SBT data seem to be shifted in either da/dN or G_{Imax} relative to those from CBT or MCC. MCC and CBT, therefore, show more conservative values than SBT.

In the low delamination growth rate regime increasing scatter can be seen. In order to evaluate the source of this scatter, a load trace for Material A is plotted in Figure 3.33(a). It can be seen, that the loads rapidly decrease to below 30 N. In Figure 3.33(b) the influence of the da/dN averaging method on Paris plots of CFRPs with epoxy matrix is shown. Four types of da/dN calculation were compared. For the secant method (2 point method) da/dN was calculated from the slope of a line connecting two adjacent value pairs of crack length and number of cycles. With the 5-point and 7-point polynomial fitting method, respectively, da/dN was calculated by fitting a second order polynomial to sets of 5 and 7 successive data points [42]. The fourth type of da/dN calculation included a second order power law fit of the crack length data obtained from compliance calibration versus number of cycles and numerical differentiation of this fit function. It can be seen that the averaging technique has an effect on the values of da/dN and that the power law fit results in the smoothest curves.

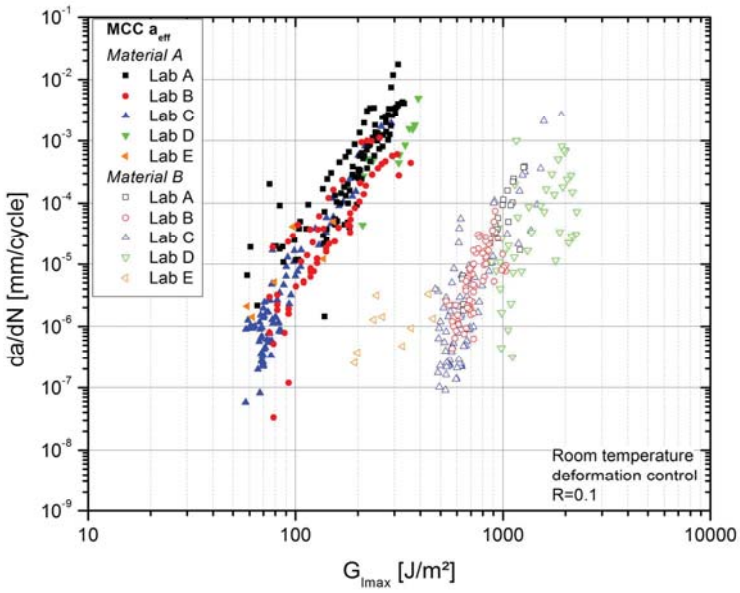

Figure 3.31: Paris plots. Crack growth rates calculated from effective crack lengths and G_{Imax} calculated via modified compliance calibration.

In Figure 3.34(a) crack lengths calculated from various approaches (see the section crack length detection) and the corresponding load signal are plotted versus number of cycles. Crack lengths calculated via compliance calibration seem to agree quite well with visually measured crack lengths.

The effective crack length approach yields lower values. This difference can possibly be explained by the use of the average E-modulus value rather than the individual modulus of the specimen used.

When da/dN is calculated from the compliance data calculated from this load signal via the 7-point method without prior data reduction, then a considerable amount of scatter in da/dN is received, see Figure 3.34(b). This scatter can be caused even by very little scatter in the load trace, since it is transferred to crack length data when calculating crack lengths via compliance. One way to reduce this scatter is deleting data that does not meet a minimum increment of 0.1 mm in crack length, see Figure 3.34(c). However, even with this filter, every spike in the compliance data can still lead to scatter in the da/dN data. When fitting the full range of load data with a second-order power law the least scatter in da/dN is received, see Figure 3.34(d).

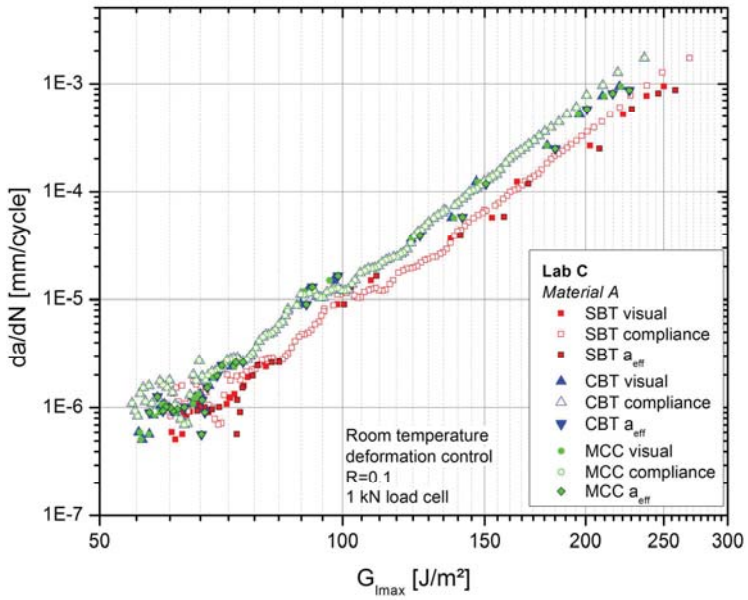

Figure 3.32: Influence of different G_{Imax} calculation methods on the Paris plots of materials A, B and C.

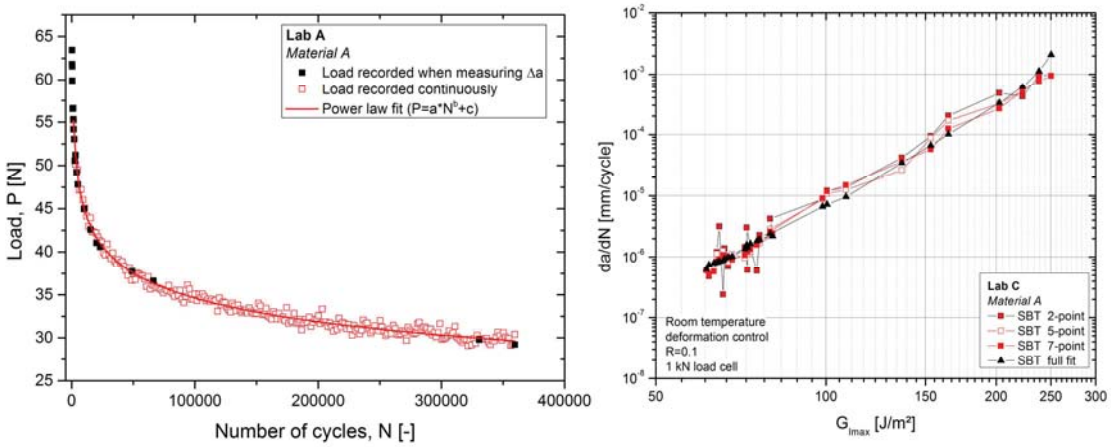

(a) (b)

Figure 3.33: (a) Load versus number of cycles.
(b) Influence of da/dN averaging method on the Paris plot.

Applying this power law fitting procedure to the calculation of the Paris plots yields Figure 3.35. The scatter for both materials is clearly reduced when compared to that from the other analysis methods including polynomial fitting and now amounts to much less than half a decade in G_{Imax} (or two decades or more in da/dN) seen in the raw data (compare Figs. 3.27, 3.29 and 3.31).

Assuming that (1) scatter in both, da/dN and G_{Imax} in the Paris-plots is caused by measurement errors in the respective quantities used for the calculations, (2) these measurements are independent, and (3) repeated measurements yield a normal (Gaussian) distribution, an error estimate can be calculated based on Gaussian error propagation. In the following, this error estimate is determined for the example of the data presented in Figs. 3.26 and 3.33. The error estimates for each measured quantity are determined at an arbitrarily selected number of 250'000 cycles and are compiled in Table 3.7.

The detailed discussion on scatter in da/dN presented in the sections above makes it clear that the major contribution for scatter in the delamination rate derives from the variation in load measurement, possibly with minor contributions from delamination length and displacement measurements.

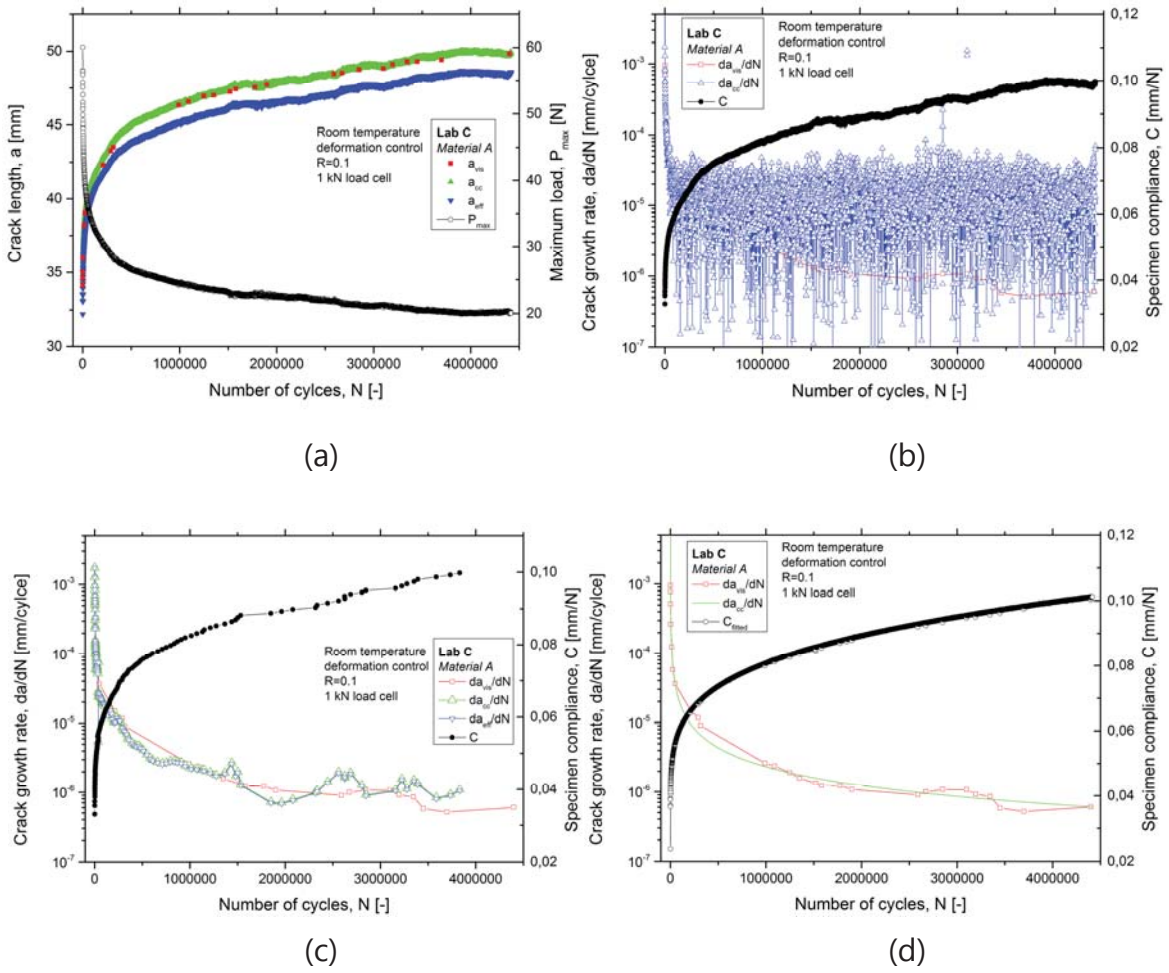

Figure 3.34: Influence of processing of compliance data on scatter in da/dN.

(a) Crack length and maximum Load, P_{max}, versus number of cycles.
a_{vis} visually measured crack length
a_{cc} crack length calculated via compliance calibration
a_{eff} effective crack length

(b) Specimen compliance, C, and crack growth rate, da/dN, versus number of cylces. All da/dN values calculated via 7-point method.

(c) Specimen compliance and da/dN values after eliminating all compliance data that do not meet the $\Delta a > 0.1$ mm criterion.

(d) Course of specimen compliance fitted with a second order polynomial and resulting da/dN curve.

The average value of G_{Imax} calculated from the data in Table 3.7 is 115 J/m^2 for the CBT and MCC methods, and 130 J/m^2 for the SBT method. This difference between SBT and the other methods (CBT and MCC) can possibly be attributed to the neglect of corrections in SBT which, e.g., underestimates the compliance of the specimens by assuming a perfectly built-in beam (rather than the load block and large displacement corrections which have been shown to be minor).

For the SBT method, Gaussian error propagation (i.e. average values of partial derivatives multiplied by the estimated error) yields an error of about 5 J/m^2, 0.3 J/m^2 and 1.3 J/m^2 for the contribution from load, displacement and delamination length measurement, respectively. This adds up to a total error around 6.8 J/m^2, i.e., a relative error (and hence possible scatter) of around 5 %. For the MCC method, the errors are around 6.2 J/m^2, 0.2 J/m^2 and 2.1 J/m^2 for the contribution from load, displacement and slope n, respectively.

This adds up to a total error around 8.4 J/m^2, i.e., a relative error around 7.3 %. For the CBT method, the errors are 4.6 J/m^2, 0.2 J/m^2 and 1.3 J/m^2 for the contribution from load, displacement and delamination length measurement, but around 18.2 J/m^2 for the contribution from the estimated error in the crack length correction Δ. This adds up to a total error estimate around 24.3 J/m^2 and a relative error around 21.2 %. The relatively large error derived for the crack length correction Δ can be explained by the fact that this quantity is determined from an extrapolation of a plot of the cube-root of compliance versus delamination length.

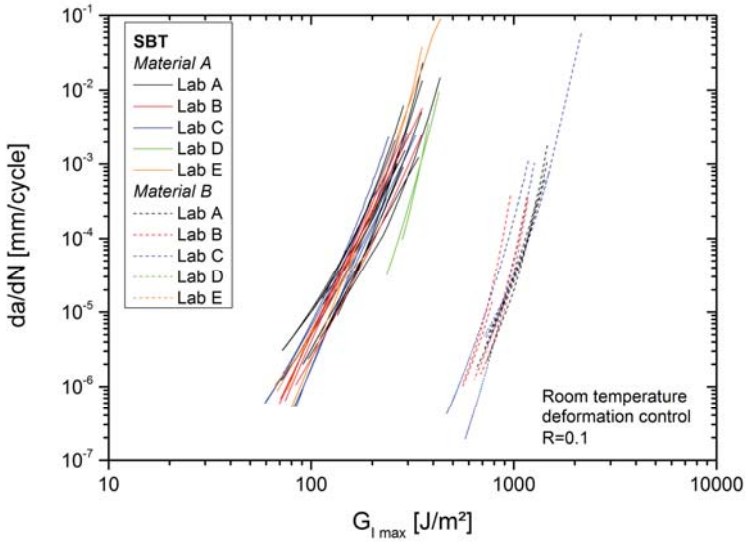

Figure 3.35: Paris plots of data calculated via the path described in Fig. 3.34(d).

Table 3.7: Average values and estimated errors for measured quantities at 250'000 cycles for material A tested at Lab A (from data shown in Figs. 3.26 and 3.33).

Quantity and units	Average value	Estimated error	Remarks
Load P [N]	31.25	1.25	From data graphic [a]
Displacement δ [m]	0.0024	0.000005	From data graphic [a]
Delamination length a [m]	0.0435	0.00045	From data graphic [a]
Delamination length correction Δ (CBT) [m]	0.0056	0.00058[b]	From extrapolation of linear regression $((C/N)^{1/3}$ vs. a)
Slope m (MCC) $[(m^2/N)^{1/3}]$	0.00085	0.000015[c]	From linear regression $((BC/N)^{1/3}$ vs. a/(2h))
Specimen thickness 2h [m]	0.0036	0.0000	Error not considered
Specimen width B [m]	0.020	0.000	Error not considered
Large displacement correction F [-]	1.0	0.0	Error not considered
Load block correction N [-]	1.0	0.0	Error not considered

[a] Not shown, the recorded machine data for δ, P and a were plotted as a function of cycle number, resulting in a scatter of about 5 μm.

[b] Standard error in slope of linear regression.

[c] Error due to standard error in slope of linear regression (extrapolation towards $(C/N)^{1/3}=0$).

This example shows that measurement errors can yield scatter on the order of about 5 to 21 % in G_{Imax}. These values may be higher in extreme cases, e.g., at low values of G_{Imax}. Looking at the contributions from the individual and independent measurements, again, as for da/dN, load stands out as a major source of scatter (even for the crack length correction Δ in the CBT-method, since compliance is calculated from load and displacement data). It can hence be concluded that efforts to reduce in-laboratory scatter have to look into load measurement and to attempt to reduce scatter there.

It can be questioned whether the fitting and numerical differentiation procedure for machine load data presented above as an alternative approach for improving Paris plots of mode I delamination fatigue (da/dN versus G_{Imax}) with respect to in- and inter-laboratory scatter will not mask incipient changes towards a threshold behavior with increasing number of fatigue cycles. In order to investigate this, a selected set of crack length versus number of cycles data were fitted within incremental ranges (20 %, 40 %, 60 %, 80 %) of the full data set and compared with the "full" fit of the complete recorded data (100 %). These incremental fits, extrapolated to the full number of tested cycles are shown in Figure 3.35(a). It can be seen that, at least in this example, the extrapolation of the fit of the first 20 % of the crack length data clearly over-estimates the effectively observed crack length (starting at less than 100'000 cycles). The other fits yield roughly comparable extrapolations. Figure 3.35(b) then shows the error in crack length for the different extrapolations compared with the "full" power law fit of all recorded data. In this case, the 60 %-fit does slightly over- and the 40 % and 80 %-fits do slightly under-estimate the crack length from the "full" fit. The errors in this case are on the order of 0.05 to 0.07 mm, i.e., about at the level of resolution required for delamination length measurements in [34]. This empirical analysis presented here at least supports the interpretation that it is unlikely that the "full" fit will "hide" clear trends towards a threshold behavior. The only source for an apparent threshold behavior in the round robin data identified so far, therefore, remains the scatter in recorded load data (when testing under displacement control) [38].

Since materials A and B, used in ESIS TC4 round robin 2, were stored for several years under laboratory conditions, the influence of the strain energy release rate calculation on the course of da/dN over G_{Imax} was additionally investigated with material C, which was a newly manufactured material tested in ESIS TC4 round robin 1 in 2008 and 2009. The results are compared with those of materials A and B in Figure 3.37. Again, the results generated by CBT and MCC show more conservative values than SBT. Nevertheless it has to be considered that MCC and

CBT can result in more scatter than SBT as shown in Figure 3.27. The combination of more conservative values and larger scatter will ultimately yield more conservative limits when using fracture mechanics based structural design.

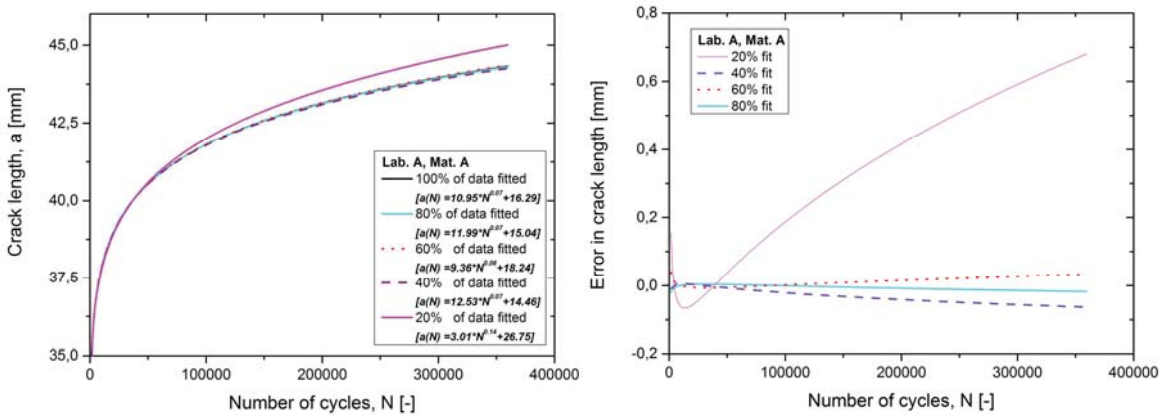

Figure 3.36: Influence of fitting range on quality of the fit.
(a) Fits of 20, 40, 60, 80 and 100 % of the full range of crack length data calculated from compliance.
(b) Error of extrapolated fits (20, 40, 60 and 80 % of full range data fitted) compared to a fit of the full range data.

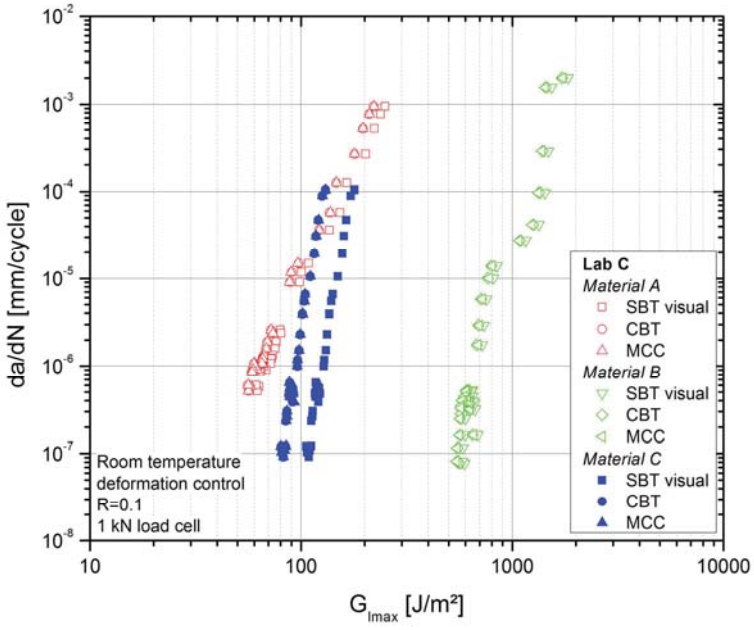

Figure 3.37: Comparison of different averaging methods for the calculation of the crack growth rate da/dN: (a) material A, (b) material B and (c) material C.

3.4.6 Conclusions

In this paper the results of a mode I fatigue delamination round robin with three carbon fiber-reinforced laminates performed at five different laboratories are compared.

The inter-laboratory scatter of the raw data is significant (amounting to more than two decades in delamination propagation da/dN for a given value of G_{Imax}) and up to 21 % (possibly more in extreme cases) in G_{Imax}. Scatter depends on the type of laminate (less for CF-Epoxy than for CF-PEEK). It may hence be questioned whether the latter data can be used in fracture mechanics based structural design. Detailed investigation has shown that even small scatter in the recorded load signal (when testing under displacement control) can yield significant in- and inter-laboratory scatter in da/dN (via compliance based crack length evaluation), but also yields the largest error contribution and hence scatter in G_{Imax} (directly via load, but also via delamination length again). Smoothing data with polynomial fitting according to [42] and/or using a load cell range with high resolution (0-500 N or 0-200 N) are shown to be less effective in reducing scatter than a second order power law fit and numerical differentiation of the load versus cycle number signal. Since fitting load data with a second order power law fit may mask load drops due to unstable crack growth during the test, it is mandatory to check the quality of the fit. In this paper an arbitrary limit for the coefficient of determination, R^2 of ≥0.95, was used to quantify “valid” fits for each specimen.

Introducing this quantitative, but arbitrary, criterion, combined with power law fitting of the load signal approach yielded in- and inter-laboratory scatter in the linear part of the Paris plots (da/dN versus G_{Imax}) on the order of one fifth of a decade in G_{Imax} for a given value of da/dN, or 1.5 decades in da/dN for a given value of G_{Imax} for material A, respectively and one fifth of a decade in G_{Imax}, or less than one decade in da/dN for material B, respectively. Alternatively, the scatter in average slope amounts to less than ±3 for material A and less than ±2 for material B. Detailed analysis of the slope “m” of the linear part of the Paris plot determined by linear fitting further seems to indicate that operator experience may affect the observed scatter as well. The range of materials, participating test laboratories and test machines used in the round robins makes it rather unlikely that further significant reductions in scatter will be feasible, unless other test procedures (e.g., operator-independent delamination length approach [39]) or more sophisticated data fitting algorithms are used.

Comparing different data analysis schemes (simple and corrected beam theory, modified compliance calibration) indicates that the latter two yield more conservative results than simple beam theory, but also somewhat higher scatter. In particular, for corrected beam theory, the delamination length correction Δ yields significant scatter (presumably due to the use of an extrapolated linear fit based on machine compliance data). Design rules considering scatter-based safety factors may hence result in more conservative designs, if data analysis uses corrected beam theory or modified compliance calibration.

The results obtained in the round robins, the range of test equipment, test parameters and composite materials explored so far as well as the elucidation of effects that contribute to scatter and how these are affected by different averaging procedures now provide a solid basis for drafting a standard test and analysis procedure for mode I fatigue delamination propagation.

3.4.7 Acknowledgments

The experimental technical assistance provided by Mr. Daniel Völki (Empa) and Dr. Joseph Mohan (UCD) and helpful discussions with Dr. James G. Ratcliffe and Dr. William M. Johnston (National Institute of Aerospace, USA) are gratefully acknowledged.

3.4.8 References

[1] Shue B, Moreira A, Flowers G. Review of recent developments in composite material for aerospace applications: Presented at 2009 ASME International Design Engineering Technical Conferences and Computers and Information in Engineering Conference, August 30 - September 2, 2009, San Diego, California USA. Proceedings of the ASME International Design Engineering Technical Conferences and Computers and Information in Engineering Conference 2009 2010:811–9.

[2] Gloria A, Ronca D, Russo T, D'Amora U, Chierchia M, Santis R de et al. Technical features and criteria in designing fiber-reinforced composite materials: from the aerospace and aeronautical field to biomedical applications. Journal of Applied Biomaterials and Biomechanics 2011;9(2):151–63.

[3] Gibson RF. A review of recent research on mechanics of multifunctional composite materials and structures. Composite Structures 2010;92(12):2793–810.

[4] Gorbatikh L, Lomov SV, Verpoest I. Nano-engineered composites: a multiscale approach for adding toughness to fibre reinforced composites. Procedia Engineering 2011;10:3252–8.

[5] Tay TE. Characterization and analysis of delamination fracture in composites: An overview of developments from 1990 to 2001. Applied Mechanics Reviews 2003;56:1–31.

[6] Brunner AJ, Blackman BRK, Davies P. A status report on delamination resistance testing of polymer–matrix composites. Engineering Fracture Mechanics 2008;75(9):2779–94.

[7] Williams JG. On the calculation of energy release rates for cracked laminates. International Journal of Fracture 1988;36:101–19.

[8] Williams JG. The fracture mechanics of delamination tests. Journal of Strain Analysis for Engineering Design 1989;24(4):207–14.

[9] Newaz GM, Ahmad J. A simple technique for measuring mode I delamination energy release rate in polymeric composites. Engineering Fracture Mechanics 1989;33(4):541–52.

[10] O'Brien TK, Roderick H. Martin. Round robin testing for mode I interlaminar fracture toughness of composite materials. Journal of Composites Technology & Research 1993;15(4):269–81.

[11] Hojo M, Kageyama K, Tanaka K. Prestandardization study on mode I interlaminar fracture toughness test for CFRP in Japan. Composites 1995;26:243–55.

[12] Martin R. Interlaminar Fracture Characterization. Key Engineering Materials) 1996;120-121:329–46.

[13] O'Brien TK. Interlaminar fracture toughness: the long and winding road to standardization. Composites Part B: Engineering 1998;29(1):57–62.

[14] Hojo M, Tanaka K, Gustafson CG, Hayashi R. Effect of stress ratio on near-threshold propagation of delamination fatigue cracks in unidirectional CFRP. Composites Science and Technology 1987;29:273–92.

[15] Adams DF, Zimmerman RS, Odom EM. Frequency and load ratio effects on critical strain energy release rate G_c thresholds of graphite/epoxy composites. In: Johnston NJ, editor. Toughened Composites:

ASTM STP 937. West Conshohocken, PA: American Society for Testing and Materials; 1987, p. 242–259.

[16] O'Brien TK. Fatigue delamination behavior of PEEK thermoplastic composite laminates. Journal of Reinforced Plastics and Composites 1988;7:341–59.

[17] Newaz GM, Mall S. Relaxation-Controlled Cyclic Delamination Growth in Advanced Thermoset and Thermoplastic Composites at Elevated Temperature. Journal of Composite Materials 1989;23(2):133–45.

[18] Martin RH, Murri GB. Characterization of mode I and mode II delamination growth and thresholds in AS4/PEEK composites. In: Garbo S, editor. Composite Materials: Testing and Design: ASTM STP 1059. West Conshohocken, PA: American Society for Testing and Materials; 1990, p. 251–270.

[19] Dahlen C, Springer GS. Delamination growth in composites under cyclic loads. Journal of Composite Materials 1994;28(8):732–81.

[20] Hojo M, Ochiai S. Effect of matrix resin on delamination fatigue crack growth in CFRP laminates. Engineering Fracture Mechanics 1994;49(1):35–47.

[21] Cvitkovich M. Polymer matrix effects on interlaminar crack growth in advanced composites under monotonic and fatigue mixed-mode I/II loading conditions. Ph.D. Thesis. Leoben; 1995.

[22] Martin RH. Delamination characterization of woven glass/polyester composites. Journal of Composites Technology & Research 1997;19(1):20–8.

[23] Asp LE, Sjorgen A, Greenhalgh ES. Delamination growth and thresholds in a carbon/epoxy composite under fatigue loading. Journal of Composites Technology & Research 2001;23(2):55–68.

[24] Hojo M, Ando T, Tanaka M, Adachi T, Ochiai S, Endo Y. Modes I and II interlaminar fracture toughness and fatigue delamination of CF/epoxy laminates with self-same epoxy interleaf. International Journal of Fatigue 2006;28(10):1154–65.

[25] Argüelles A, Viña J, Canteli AF, Bonhomme J. Fatigue delamination, initiation, and growth, under mode I and II of fracture in a carbon-fiber epoxy composite. Polym. Compos 2009:700–6.

[26] Martin RH. Incorporating interlaminar fracture mechanics into design. Proceedings of the Institution of Mechanical Engineers, Part L: Journal of Materials Design and Applications 2000;214(2):91–7.

[27] Murri GB, Schaff JR. Fatigue life methodology for tapered hybrid composite flexbeams. Composites Science and Technology 2006;66(3-4):499–508.

[28] Shivakumar K, Chen H, Abali F, Le D, Davis C. A total fatigue life model for mode I delaminated composite laminates. International Journal of Fatigue 2006;28(1):33–42.

[29] Wimmer G, Pettermann H. A semi-analytical model for the simulation of delamination in laminated composites. Composites Science and Technology 2008;68(12):2332–9.

[30] Wimmer G, Schuecker C, Pettermann H. Numerical simulation of delamination in laminated composite components – A combination of a strength criterion and fracture mechanics. Composites Part B: Engineering 2009;40(2):158–65.

[31] Chen J, Ravey E, Hallett S, Wisnom M, Grassi M. Prediction of delamination in braided composite T-piece specimens. Composites Science and Technology 2009;69(14):2363–7.

[32] JIS - Japanese Standards Association. JIS K 7086:1993 Testing methods for interlaminar fracture toughness of carbon fibre reinforced plastics(K 7086); 1993.

[33] ASTM - American Society for Testing and Materials. ASTM D5528:2001 - Standard test method for mode I interlaminar fracture toughness of unidirectional fiber-reinforced polymer matrix composites.

[34] ISO - International Organization for Standardization. ISO 15024:2001 - Fibre-reinforced plastic composites — Determination of mode I interlaminar fracture toughness, GIC, for unidirectionally reinforced materials.

[35] ASTM - American Society for Testing and Materials. ASTM D6115:1997 - Standard test method for mode I fatigue delamination growth onset of unidirectional fiber-reinforced polymer matrix composites.

[36] Brunner AJ, Murphy N, Pinter G. Development of a standardized procedure for the characterization of interlaminar delamination propagation in advanced composites under fatigue mode I loading conditions. Engineering Fracture Mechanics 2009;76(18):2678–89.

[37] Brunner AJ, Paris I, Pinter G. Fatigue propagation test development for polymer-matrix fibre-reinforced laminates. Proc. 12th Int. Conf. on Fracture ICF-12, paper No. 00371 2009;1-8 2009:1–8.

[38] Stelzer S, Brunner AJ, Argüelles A, Murphy N, Pinter G. Mode I delamination fatigue crack growth in unidirectional fiber reinforced composites: Development of a standardized test procedure. Composites Science and Technology 2012;72(10):1102–7.

[39] Brunner AJ, Blackman BRK, Williams JG. Calculating a damage parameter and bridging stress from GIC delamination tests on fibre composites. Composites Science and Technology 2006;66(6):785–95.

[40] ISO - International Organization for Standardization. ISO 178:2010 - Plastics - Determination of flexural properties.

[41] Bamber Blackman. (Imperial College London) private communication.

[42] ASTM - American Society for Testing and Materials. ASTM E647:2011 - Standard test method for measurement of fatigue crack growth rates; 2011.

[43] Williams JG. End corrections for orthotropic DCB specimens. Composites Science and Technology 1989;35:367–76.

[44] Kageyama K, Kobayashi T, Chou T. Analytical compliance method for mode I interlaminar fracture toughness testing of composites. Composites 1987;18(5):393–9.

3.5 PUBLICATION 4

MODE II FATIGUE DELAMINATION RESISTANCE OF ADVANCED FIBER-REINFORCED POLYMER-MATRIX LAMINATES: TOWARDS THE DEVELOPMENT OF A STANDARDIZED TEST PROCEDURE

3.5.1 Bibliographic Information

- Authors and their relevant contributions to the publication:
  - Andreas J. Brunner[1]
    Preparation of the manuscript, fracture mechanical tests in laboratory B and analysis of fracture mechanical tests in laboratory B.
  - Steffen Stelzer[2]
    Fracture mechanical tests in laboratory A and analysis of fracture mechanical tests in laboratory A.
  - Gerald Pinter[2,3]
    Academic supervision of the work carried out in laboratory A.
  - Giovanni P. Terrasi[1]
    Supervision of the work carried out in laboratory B.
- Affiliations:
  [1] EMPA, Swiss Federal Laboratories for Materials Science and Technology, CH-8600 Dübendorf, Switzerland
  [2] Institute of Materials Science and Testing of Polymers, Montanuniversitaet Leoben, Leoben, Austria
  [3] PCCL, Polymer Competence Center Leoben, Roseggerstrasse 12, A-8700 Leoben, Austria

- Periodical: International Journal of Fatigue
- DOI: 10.1016/j.ijfatigue.2012.02.021

Statement with regard to publication: The manuscript presented here is an adapted accepted manuscript in order to fit the formatting of the thesis and does not necessarily reflect the actually published version.

3.5.2 Abstract

Delamination resistance testing of fiber-reinforced polymer–matrix laminates under fatigue loads is important for materials development and structural design. Mode II in-plane shear fatigue test development using three-point bending end-notched flexure (3-ENF) and two-point bending end-loaded split (ELS) set-ups is performed in a round robin. Effects of specimen restraint observed earlier in ENF tests are confirmed and preliminary data indicate differences between the two set-ups, if simple beam theory or experimental compliance analyses are applied. Possible reasons for the observed disagreement are discussed.

3.5.3 Introduction

Research on delamination resistance testing under fatigue mode II (in-plane shear) loading of fiber-reinforced polymer–matrix (FRP) composites started in the late 1980s and continues today; see e.g., [1–14]. Most of these references deal with carbon-fiber reinforced polymers (CFRP), specifically different types of epoxy resins [1,3,5–9,12,13], two with thermoplastic poly-ether-ether-ketone (PEEK) [3,4] and a few with glass–fiber rein-forced polymers (GFRP), again using epoxy resins as matrix [2,11, 13]. With respect to test set-up or configuration, the three-point bending, so-called end-notched flexure test (ENF) is most widely used [1–5,9,11,12]. Other test configurations have been used as well, such as the four-point bending end-notched flexure (4-ENF) [13], the end-loaded split (ELS) [7], the similar end-notched canti-lever beam (ENCB) [6], or the central cut ply (CCP) specimen [14]. With the exception of [2,8] that investigate the formation and propagation of mode II fatigue delaminations by acoustic emission damage monitoring [2] and fractography on impact-damaged laminates after cyclic compression–compression loading [8], all others evaluate the delamination rate versus applied load (G_{IImax} or ΔG_{II}) and present the corresponding Paris plots. Beside experimental investigations, some groups have also tried to develop models for describing mode II fatigue delamination propagation and comparing previously published data, e.g., [10,14].

This research provides a basis for understanding the intricacies and problems of mode II fatigue delamination crack propagation that will be applied for the development of a standardized test procedure. Delamination resistance test method development (recently reviewed by, e.g., [15]) so far has yielded one standard on quasi-static mode II testing [16], two draft standards for quasi-static mode II [17,18] and plans for a joint international round robin on mode II fatigue

which, however, was never performed (see [15] for details). Drafting a standardized test method requires defining scope and aims, establishing a procedure and data analysis that is applicable in an industrial test environment. The draft procedure is then explored in round robin tests with a range of FRP laminates and modified or refined, if necessary. Aims for round robin tests are defining applicability and limitations, determining inter-laboratory reproducibility and scatter as well as validating the data analysis. Since the published mode II fatigue test data [1–14] were obtained from different types of laminates and under various test conditions, they do not provide information on inter-laboratory scatter and reproducibility. The present contribution reports first attempts at developing a standardized procedure for mode II fatigue delamination resistance. It mainly highlights the problems encountered so far and in concluding outlines further steps that are deemed necessary for achieving a test procedure that can be submitted for standardization. The main reasons for the long development times for a quasi-static procedure for mode II testing of FRP that started in the 1980s [15] are concerns about the interpretation of the data and potential friction effects (see, e.g., [19,20]), the large variety of pro-posed test set-ups and intrinsic difficulties in defining and measuring delamination lengths (see, e.g., [15,21] for details).

3.5.4 Experimental

Based on the analogous development of fatigue testing under mode I (tensile opening) delamination resistance [22,29] it is expected that the quasi-static test set-ups are a useful starting point for the development of the mode II fatigue loading procedure. Therefore, the so-called end-notched flexure (ENF) test based on a three-point bending set-up (sometimes labelled 3-ENF in order to distinguish it from the corresponding four-point bending ENF test, i.e., the 4-ENF), and the clamp-calibrated end-loaded split test based on a two point bending set-up of a beam specimen clamped on one side (C-ELS) have been selected [21]; Figs. 3.38 and 3.39 show photographs of each type of set-up. The C-ELS set-up can also be used for a fixed-ratio mixed mode I/II test with a mode I to mode I ratio of 4:3 by simply inverting the load application on the specimen [15].

Two CFRP epoxy laminates are used in the round robin tests. The first material is Celion G30-500 12k/Rigidite 5276 (courtesy of BASF Structural Materials, Charlotte, USA). Beam type specimens were prepared with a length of 145 mm, a width of 20 mm and a thickness of 3.1 mm. A poly-tetra-fluor-ethylene (PTFE) film (about 20 µm thick) at the laminate mid-plane provided the starter crack. This is larger than recommended for quasi-static testing [17,18]. Since in the round robin

tests, the fatigue delamination onset [4] is not investigated and quasi-static precracking in mode I or mode II is recommended the effect of the starter crack thickness is considered negligible. Also, if the delamination is propagated over sufficiently long increments, the starter crack thickness will affect only the initial part, even if no precracking is applied. Specimens had been stored under laboratory conditions (nominally +23 °C and 50 % relative humidity) for a long period before testing under the same conditions. The second is IM7/977-2 (courtesy of Cytec Inc., USA). Again, beam type specimens were prepared with a nominal length around 150 mm, a width of 20 mm and a thickness of 4.4 mm. A fluorinated ethylene–polyethylene (FEP) film with a thickness around 10 µm provides the starter crack. Mechanical properties of IM7/977-2 are summarized and reported by, e.g., [23,24]. The delamination resistance of this laminate has been extensively investigated already, quasi-static values under mode I, mode II and fixed-ratio mixed mode I/II loadings have been determined by [6,25–28] and fatigue behavior under mode I loading by [6,22,29].

The 3-ENF fatigue tests on Celion G30-500 12k/Rigidite 5276 have been performed at Laboratory A on an electro-dynamic test machine (type Bose 3450) at 5 Hz under displacement control with an R value of 0.1. The radius of the specimen support and loading rollers was 7.5 mm. When loading the specimens for the first time, the delamination became unstable and propagated to the area near or under the loading fin.

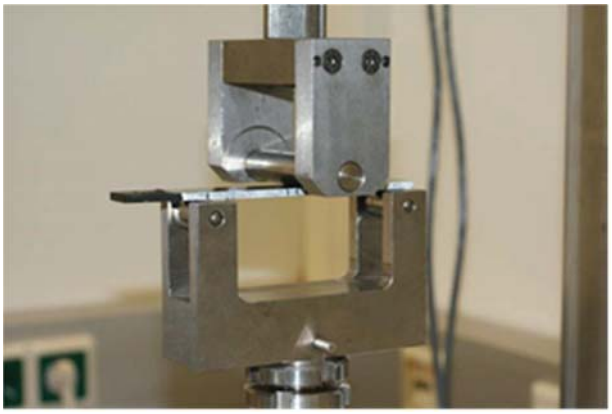

Figure 3.38: 3-ENF set-up without restraint used at Laboratory A, the CFRP specimen is 140 mm long, 20 mm wide and 3.1 mm thick, the diameter of the center loading fin is 15 mm and the free span between the outer supports is 100 mm, in the set-up shown, the deflection of the beam is applied by the center loading fin which is pushed downward by the action of the test machine.

Figure 3.39 C-ELS set-up used at Laboratory B, the CFRP specimen is 150 mm long, 20 mm wide and 4.4 mm thick, in the set-up shown, the load is applied through a load-block in top of the beam which is deflected downward by the action of the test machine.

Effectively, this corresponds to mode II precracking which is expected to eliminate any possibly negative effect from the insert starter film which was thicker than the 13 µm recommended for quasi-static delamination initiation.

The C-ELS and 3-ENF tests on IM7/977-2 were performed servo-hydraulic test machines (MTS type 831 in Laboratory A) or on a servo-hydraulic test machine (Instron type 1273 in Laboratory B) at 3 Hz and 5 Hz, respectively, under displacement control with a R-ratio of 0.1. The beam type specimens for the C-ELS test require one load-block which was adhesively bonded. Specimens were tested without precracking. Using the C-ELS set-up for mode II fatigue delamination resistance has the inherent disadvantage that a ratio of precrack or delamination length of 55 % or more of the free length is needed for obtaining stable delamination propagation in the quasi-static test [18]. In order to avoid possible unstable delamination growth, the same delamination length to free length ratio has been used for the cyclic mode II fatigue tests. Nevertheless, there were some tests that showed stick–slip behavior, i.e., occasional arrest of delamination propagation after brief unstable delamination growth. Considering that delamination resistance may also be affected once the tip reaches the area near the clamp (analogous to the potential effect discussed above for the clamped 3-ENF), there is a limited delamination length available for testing. Of course, the free length L can be increased after a first test and the same specimen tested again from the mode II fatigue precrack. If the initial applied displacement is

chosen too large, the test may have to be stopped before sufficiently low delamination rates are obtained.

Further, Double Cantilever Beam (DCB) mode I fatigue tests on Celion G30-500 12k/Rigidite 5276 have been performed at Laboratory A for a comparison with the mode II fatigue data. A servo-hydraulic test machine (MTS type 858) has been used and the test was performed as detailed in [22] for the mode I fatigue on IM7/977-2 laminates.

Earlier tests of mode II fatigue delamination resistance had al-ready pointed out a need for modifying the three-point flexure set-up used for the quasi-static three-point bending ENF test [30] with a specimen restraint, also discussed and shown in detail in [11]. Cyclic mode II fatigue loading without restraint typically resulted in a shifting of the beam specimen in the set-up during the test. Visual observation indicated that this shift can amount to as much as 20 mm.

The guidelines for the round robin initiated within Technical Committee 4 on Fracture of Polymers, Composites and Adhesives of the European Structural Integrity Society (ESIS) hence recommended using either the three-point bending ENF set-up with some type of specimen restraint (choice left to the participants) or the clamp-calibrated ELS set-up, or both. The R value was set at 0.1, the test frequency as high as possible, but not higher than 10 Hz (in order to limit hysteretic heating effects) and testing required under displacement (not load) control. Hence, the effects of shear reversal versus no shear reversal, as discussed by Dahlen and Springer [6] will not be investigated in this round robin. Whether specimens shall be tested from the insert or from a mode I or mode II precrack was again left to the participants, since for the ENF-test, quite likely, a mode II precrack seemed unavoidable. Peak machine loads and displacements shall be recorded every 500 or 1000 cycles and the delamination length periodically be checked by visual observation with the aid of a travelling microscope. The cyclic fatigue loading may be stopped for visual observation if necessary, but the specimen shall not be removed from the test rig. The test shall be run for at least 24 h or 400,000 cycles, and, if possible, longer. For the C-ELS set-up clamping conditions are crucial. It is recommended to use a defined, reproducible torque to tighten the screws and to check on that when the cyclic load is stopped for visual observation of the delamination length.

The data analysis is typically based on either beam theory for establishing the relation between delamination length and measured loads and displacements or

on an experimental compliance calibration scheme. Simple beam theory (SBT) uses the following equation (3.10) for calculating G_{IIC}:

$$G_{IIc} = \frac{9Pa^2\delta}{2b\left(\frac{1}{4}L^3+3a^3\right)} \text{ (for 3-ENF) and}$$

$$G_{IIc} = \frac{9P^2a^2\delta}{4b^2h^3E_1} \text{ (for C-ELS)} \quad (3.10)$$

with P the maximum load during the cycle, a the corresponding delamination length, d the corresponding flexural displacement (in the 3-ENF test), b the specimen width, h the specimen thickness, L the free length and E_1 the flexural modulus of the specimen. E_1 can be determined from the slope of a plot of the cube-root of the compliance versus free length L from a so-called clamp calibration test [21] by equation (3.11) or from an independent measurement of the flexural modulus of the laminate.

$$E_1 = \frac{1}{2b(hn)^3} \quad (3.11)$$

again with b the specimen width, h the specimen thickness and n the slope of the cube-root compliance plot versus free length L. The experimental compliance method (ECM) for calculating G_{IIC} is based on the following equation (3.12):

$$G_{IIc} = \frac{3mP^2a^2}{2b} \text{ (for 3-ENF and C-ELS)} \quad (3.12)$$

with m the slope of the linear regression of a plot of compliance C versus the cube of the delamination length a, P the maximum load during the cycle, a the corresponding delamination length and b the width of the specimen.

Finally, delamination rates (average delamination length increment per cycle) shall be plotted versus applied maximum load $G_{II\text{-}max}$ in a Paris plot representation for comparison of data. There is a further approach for data analysis that is based on compliance which allows to calculate so-called effective delamination lengths and the corresponding G_{IIC} values, eliminating the need for visual observation of delamination length which is difficult in mode II tests and hence a possible source of error [21]. This analysis will be applied to the round robin data, but has not been used in the preliminary analysis presented here.

3.5.5 Results and discussion

The data from the 3-ENF mode II fatigue tests on Celion G30-500 12k/Rigidite 5276 were analyzed using simple beam theory which neglects certain corrections. For comparative purposes, this does not matter, but when using the data for design of composite structures, a detailed analysis including corrections and appropriate safety factors may have to be used. Testing yields mode II delamination resistance data that can be evaluated in the form of Paris plots, i.e., delamination rate per cycle da/dN versus applied load G_{IImax}.

First, the effect of specimen restraint in the three-point bending 3-ENF test will be discussed. As shown in Fig. 3.40, the 3-ENF tests without specimen restraint on Celion G30-500 12k/Rigidite 5276 yield reproducible results with sufficiently small scatter, in spite of specimen shifting. However, as shown in the same Figure, specimen shifting will yield significantly lower values of delamination resistance than specimens that are restrained during the test. If the specimen is restrained, the Paris plot for mode II delamination resistance yields again consistent values with reasonable scatter.

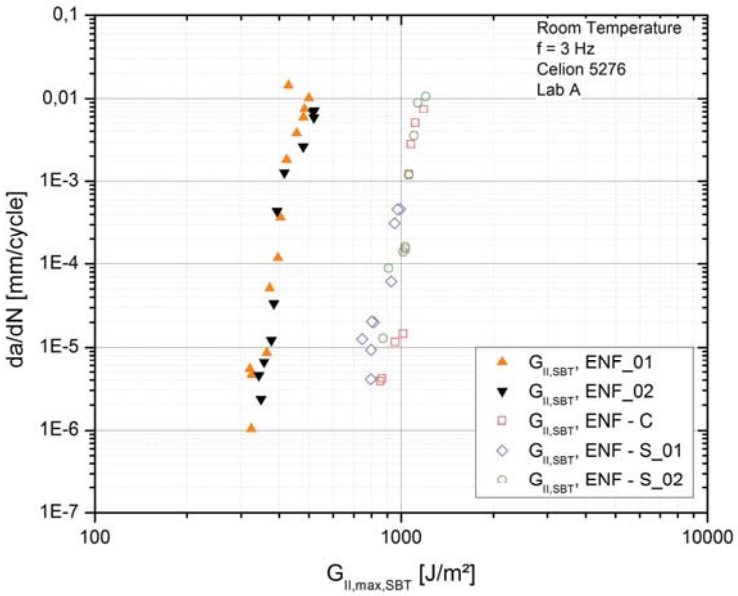

Figure 3.40: 3-ENF data on Celion R5276 with and without specimen restraint, each reproducible in spite of specimen shifting without restraint, specimen restraint C uses clamping at center loading fin (see [11,31]) and specimen restraint S uses a string between center fin and end support (see Fig. 3.41).

In the 3-ENF experiments, two different types of specimen restraint have been used for the beam specimens. A first, developed in the mid-1990s [30] uses a compression clamping device (data labelled ‘‘C’’) integrated into the loading fin at the center of the specimen as shown in [11]. This design has the disadvantage that it applies an additional compressive stress at the center of the specimen. This could potentially affect the delamination behavior, e.g., the delamination rate, since the delamination starts in that area after unstable quasi-static precracking. As an alternative, avoiding this problem, a second type used a string fixation (data la-belled ‘‘S’’) between loading fin and specimen end (Fig. 3.41). The string is attached to the intact end of the beam (without delamination), since observation had shown that the specimen shifted al-ways towards that side. The data in Fig. 3.40 shows no evidence for a dependence of the values on the type of specimen restraint (‘‘C’’ or ‘‘S’’).

Fig. 3.42 compares cyclic mode I fatigue delamination resistance for Celion G30-500 12k/Rigidite 5276 (tested according to the procedure described in [22]) with the values obtained from the 3-ENF mode II fatigue test with the string-type specimen restraint (S). For comparable delamination-rates da/dN, e.g., between 10^{-4} and 10^{-5} mm/cycle, mode II requires about a 5- to 10-fold higher applied load (G_{IImax}) than mode I (90–150 J/m^2 versus about 900–1050 J/m^2).

The slope for the mode I fatigue data does seem to be somewhat lower than for the mode II fatigue. However, considering the typical scatter for mode I data determined from round robin testing, see, e.g., [22,29], this difference in slope may be accidental. It can be noted that the mode II values determined for fatigue on the 3-ENF setup without specimen restraint are also higher than those found for mode I fatigue testing (comparing Figs. 3.40 and 3.42).

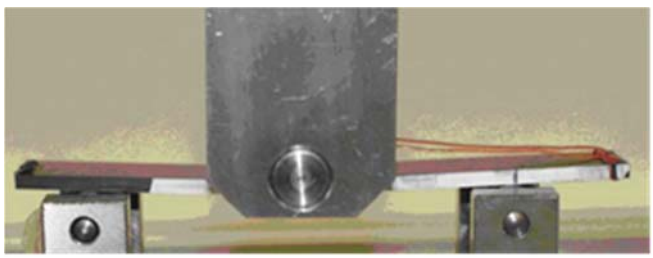

Figure 3.41: 3-ENF set-up with a string specimen restraint (type S) used at Laboratory A. The dimensions are as in Fig. 3.38.

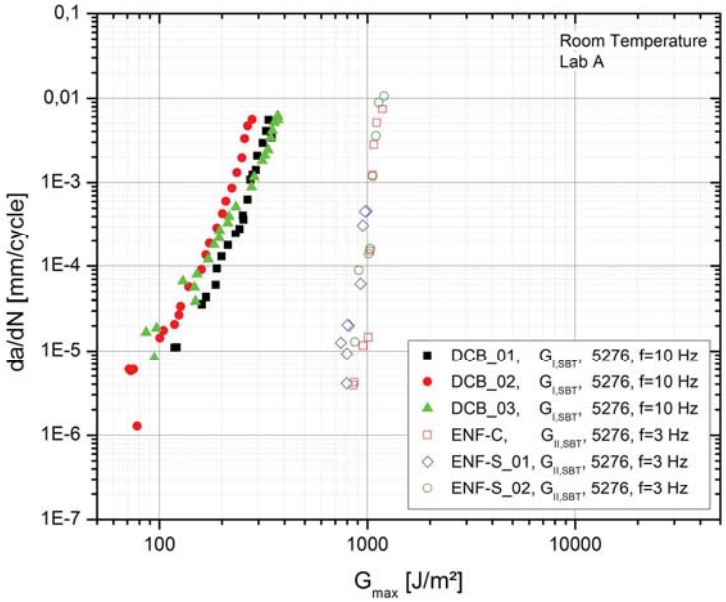

Figure 3.42: Data for DCB mode I and 3-ENF mode II with string type (S) specimen restraint on Celion R5276. Please note that 3-ENF data without restraint (Fig. 3.40) are higher than the mode I data).

Hence, a comparison with mode I fatigue data on the same laminate would not have revealed the effect of specimen shifting in 3-ENF mode II fatigue testing. It can be seen from Fig. 3.40 that the slopes of the two Paris plots for Celion G30-500 12k/Rigidite 5276 (without and with specimen restraint, respectively) do not differ much. In its central part, between about 10^{-3} and 10^{-5} mm/cycle, the slopes are very steep, i.e., showing a large increase in delamination-rate for a small increase in applied load (G_{IImax}). In addition it can be noted that quasi-static testing had yielded average values of G_{IC} and G_{IIC} (using the so-called direct beam theory analysis) of about 391 and 1375 J/m^2 for this material [30], i.e., an increase by a factor of about 3.5 for going from mode I to mode II.

In the following sections, first results from the round robin on IM7/977-2 laminates will be presented and discussed. Tests at Lab-oratory A have been performed with both, 3-ENF with string-type (S) specimen restraint and C-ELS, while Laboratory B has only used the C-ELS test. These results are preliminary, since only part of the test program has been completed yet.

Fig. 3.43 shows 3-ENF data with string (“S”) type specimen restraint for IM7/977-2 obtained at Laboratory A and C-ELS data for the same material obtained at Laboratories A and B. All data have been analyzed using simple beam theory. Fig. 3.43 shows that two tests each yield relatively low scatter, similar to that

observed for the Celion G30-500 12k/Rigidite 5276 laminate. As for the Celion G30-500 12k/Rigidite 5276 the 3-ENF test with string-type (S) restraint yields a rather steep slope of the linear part of the Paris plot. For higher delamination rates (above about 10^{-2} mm/cycle) the values are very close to the quasi-static value of about 1040 J/m^2 which is in good agreement with the quasi-static mode II value of 994 J/m^2 determined by [6].

The data shown in Fig. 3.43 from C-ELS tests at two laboratories (A and B) are fairly consistent and also indicate sufficiently low scat-ter. Testing two specimens in the 3-ENF test at different frequencies (3 Hz and 5 Hz) at Laboratory A also yielded consistent results with no indication of frequency dependence. The exponents of a power law fit of the Paris law curves are summarized on Table 3.8.

The location of the linear parts of the Paris curve in this case differ significantly from that obtained by the 3-ENF test (Fig. 3.43), and also the slopes are clearly less steep (as shown by the exponents in Table 3.8). This disagreement between the two test set-ups is, at first sight, rather surprising, e.g., when considering that a round robin on quasi-static mode II delamination testing had yielded some scatter between different test set-ups but not comparable disagreement for several CFRP laminates [31].

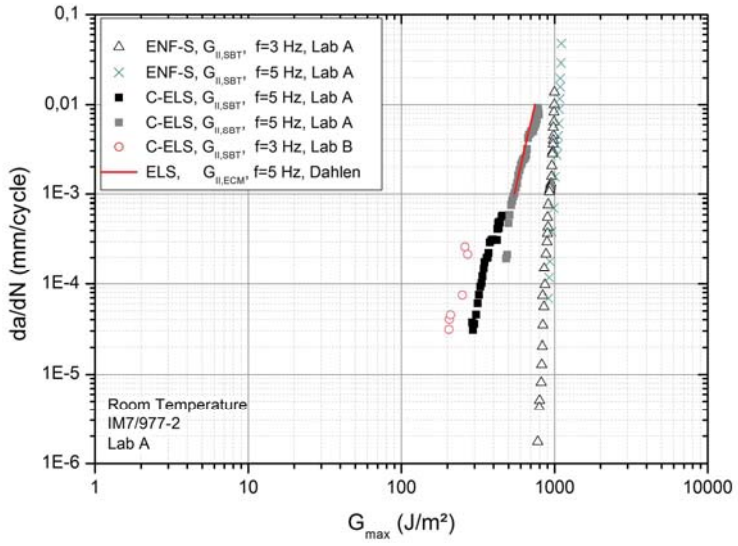

Figure 3.43: First round robin data from 3-ENF with string-type (S) specimen restraint and C-ELS for IM7/977-2 obtained at Laboratories A and B and a comparison with literature data for the same laminate from Dahlen and Springer [6].

The preliminary data from the robin test exercise hence indicate that the two types of test rig (3-ENF and C-ELS) do yield mode II fatigue delamination resistance data for identical laminates that clearly differ in position and slope of the Paris curve. However, both data sets (C-ELS and 3-ENF) yield Paris plots that are below the quasi-static mode II delamination resistance values and also above mode I fatigue test data for the same laminate [22,29]. The reasons for the discrepancy are currently not clear. For possible explanations, it can be speculated that the 3-ENF test rig may yield adverse compressive stresses in the region under and near the center loading pin that adversely affect delamination propagation, even if no compressive specimen restraint is used. Displacement control of mode II fatigue delamination propagation might thus yield lower effective loads for producing the observed delamination length increments and the recorded loads would shift the corresponding G_{IImax} to apparently higher values in the analysis. In order to further analyze this, observation of the position of the tip of the delamination with respect to the center loading fin of the ENF set-up will be necessary in the remaining round robin tests still to be performed. Presumably, a variation in counter-acting compressive loads as a function of delamination length would be required to yield the observed steep slope in the Paris lot for the ENF test. A detailed Finite Element Simulation of the 3-ENF set-up and its behavior under applied displacements might provide further information on the compressive load along the beam specimen due to the center loading pin.

In quasi-static mode II tests, it had been noted by some authors that the 3-ENF test would only yield initiation values but not allow for a determination of the so-called resistance curve, i.e., G_{IIC} versus delamination length, mainly because of the typical unstable crack growth following initiation [19,21]. Upon initiation, the crack tip was frequently observed to grow rapidly in an unstable manner and arrest at or near the center loading fin. In quasi-static mode I tests, unstable crack arrest and re-initiation of the delamination propagation are known to require higher loads than for continuous propagation [32]. Therefore, stick–slip phenomena producing arrest of the delamination tip may also contribute to apparent higher loads.

Another area that requires further investigation is data analysis. Simple beam theory neglects certain corrections (e.g., load block correction, large displacement correction), however, usually, these effects are considered to be small (on the order of a few percent). It will also be of interest to compare beam theory based analysis with the experimental compliance method.

The different C-ELS test rigs used at two laboratories yield roughly comparable results, i.e., similar slope and position of the Paris curves. The only literature data for IM7/977-2 using an ENCB test rig similar to the C-ELS but somewhat different test parameters [6] are also in rough agreement with the preliminary C-ELS data from the recent round robin. However, also in that case, more detailed data analysis will have to be performed, e.g., using the so-called effective crack length approach [21] which eliminates uncertainties of visual observation of delamination length.

As noted in the experimental part, reproducible and constant clamping is crucial for the C-ELS test. In preparation for the round robin, the reproducibility of clamping and the effect of different torques applied to the screws have been investigated at selected laboratories. These results will be analyzed in detail with the effective crack length approach which incorporates a correction for the clamping effect in the C-ELS test [21].

Clearly, at this stage it is too early to draft a standard procedure or to initiate the standardization process at this stage. Further re-search and comparative round robin testing will be required to re-solve the observed differences between the two test set-ups (3-ENF and C-ELS) and to establish test procedures and data analyses that yield reproducible values with sufficiently low scatter.

Table 3.8: Exponents of the Paris curves for the different test set-ups and materials, all data analyzed by simple beam theory.

Test Laboratory	Specimen label and material	Exponent of Paris curve from power law fit (–)	Remarks
A	ENF_01 Celion R 5276	15.4	No restraint
A	ENF_02 Celion R5276	12.5	No restraint
A	ENF_C Celion R 5276	23.5	Compressive restraint (C)
A	ENF_S_01 Celion R 5276	18.2	String restraint (S)
A	ENF_S_02 Celion R5276	16.8	String restraint (S)
A	ENF_S IM7/977-2	39.4	String restraint (S) 3 Hz
A	ENF_S IM7/977-2	38.1	String restraint (S) 5 Hz
A	C-ELS IM7/977-2	5.5	Black square symbols 5 Hz
A	C-ELS IM7/977-2	5.1	Gray square symbols 5 Hz
B	C-ELS IM7/977-2	7.3	3 Hz

3.5.6 Summary and conclusions

The data from preliminary mode II fatigue delamination resistance testing on two types of CFRP epoxy laminates show the significant effect of specimen restraint that had previously been noted by others [11,30], when the three-point bending ENF test rig is being used. Even though the slopes of the Paris plot are hardly affected by specimen shifting in the test rig (at least within the typical scatter for this type of experiment), specimens that are prevented from shifting yield clearly higher delamination resistance. This effect would have implications for fracture mechanics based design of composite structures. With or without specimen restraint, the mode II fatigue delamination resistance is higher than that determined from mode I loading (for identical laminates). Hence, mode I fatigue data could still be used as a lower limit for design.

First data from a current round robin test exercise indicate that the two types of test rig (3-ENF and C-ELS) do yield mode II fatigue delamination resistance data for identical laminates that clearly differ in position and slope of the Paris curve. The data obtained with different designs of C-ELS test rigs at two laboratories yield roughly comparable results, i.e., similar slope and position of the Paris curves. Both data sets (3-ENF and C-ELS) are below the respective quasi-static mode II delamination resistance values. The reasons for this discrepancy are currently not clear. It can be speculated that the 3-ENF test rig may yield adverse compressive stresses in the region under and near the center loading pin that affect delamination propagation resulting in apparently higher loads. For the C-ELS test, the effects of variation in clamping will have to be investigated which may produce some error. Another area that requires further investigation is the correlation between different types of data analysis and the effects of the different test parameters.

Once all data from the current round robin have been collected, detailed data analysis and evaluation will be undertaken in order to investigate the relation between C-ELS and 3-ENF test rig. Only if all the problems are resolved will it be time to draft a standard test procedure for mode II fatigue delamination testing.

3.5.7 Acknowledgments

Technical support and test monitoring by Mr. D. Völki at Empa, testing and data analysis by Mr. G. Singer within a M.Sc. project and discussions with Dr. D.D.R. Cartié (Cranfield University) are gratefully acknowledged.

3.5.8 References

[1] Russell AJ. Micromechanisms of interlaminar fracture and fatigue. Polym Compos 1987;8:342–51.

[2] Roy C, Elghorba M. Monitoring progression of mode-II delamination during fatigue loading through acoustic-emission in laminated glass–fiber composite. Polym Compos 1988;9:345–51.

[3] Threthewey BR, Gillespie JW, Carlsson LA. Mode II cyclic delamination growth. J Compos Mater 1988;22:459–83.

[4] Martin RH, Murri GB. Characterization of mode I and mode II delamination growth and thresholds in AS4/PEEK composites. In: Garbo SP, editor. Composite materials: testing and design. ASTM STP 1059, American Society for Testing and Materials; 1990. p. 251–70.

[5] Hwang JR, Lee AS. Thermal-damage effects on mode-II interlaminar fatigue crack propagation of graphite epoxy composites. Compos Struct 1994;27:389–93.

[6] Dahlen C, Springer GS. Delamination growth in composites under cyclic loads. J Compos Mater 1994;28:732–81.

[7] Gilchrist MD, Svensson N. A fractographic analysis of delamination within multidirectional carbon/epoxy laminates. Compos Sci Technol 1995;55:195–207.

[8] Heutling E, Franz HE, Friedrich K. Microfractographic analysis of delamination growth in fatigue loaded carbon fibre thermosetting matrix composites. Mat – Wiss Werkst 1998;29:239–53.

[9] Hojo M, Matsuda S, Ochiai S, Tsujioka N, Nakanishi Y, Maekawa Z, et al. Mode II interlaminar properties under static and fatigue loadings for CF/epoxy laminates with different fiber surface treatment. Adv Compos Mater 2001;10:237–46.

[10] Andersons J, Hojo M, Ochiai S. Empirical model for stress ratio effect on fatigue delamination growth rates in composite laminates. Int J Fatigue 2004;26:597–604.

[11] Matsubara G, Ono H, Tanaka K. Mode II fatigue crack growth from delamination in unidirectional tape and satin-woven fabric laminates of high strength GFRP. Int J Fatigue 2006;28:1177–86.

[12] Beghini M, Bertini L, Forte P. Experimental investigation on the influence of crack front to fiber orientation on fatigue delamination growth rate under mode II. Compos Sci Technol 2006;66:240–7.

[13] Shindo Y, Takeda T, Narita F, Saito N, Watanabe S, Sanada K. Delamination growth mechanisms in woven glass fiber reinforced polymer composites under mode II fatigue loading at cryogenic temperatures. Compos Sci Technol 2009;69:1904–11.

[14] Allegri G, Jones MI, Wisnom MR, Hallett SR. A new semi-empirical model for stress ratio effect on mode II fatigue delamination growth. Composites 2011;A42:733–40.

[15] Brunner AJ, Blackman BRK, Davies P. A status report on delamination resistance testing of polymer–matrix composites. Eng Fract Mech 2008;75:2779–94.

[16] JSA, Japanese Standards Association, Japanese Industrial Standard JIS K7086. Testing methods for interlaminar fracture toughness of carbon fibre reinforced plastics; 1993.

[17] ASTM, American Society for Testing and Materials International, Subcommittee D30.06 Interlaminar Properties, Work Item WK22949. Test method for determination of the mode II interlaminar fracture toughness of unidirectional fiber reinforced polymer matrix composites using the end-notched flexure (ENF) test; 2009.

[18] ISO, International Organisation for Standardization. Working draft ISO/WD 15114 fibre-reinforced plastic composites – determination of apparent mode II interlaminar fracture toughness for unidirectionally reinforced materials; 2010.

[19] O'Brien TK. Interlaminar fracture toughness: the long and winding road to standardisation. Compos Part B: Eng 1998;29B:57–62.

[20] Davidson BD, Sun XK, Vinciquerra AJ. Influence of friction, geometric nonlinearities and fixture compliance on experimentally observed toughnesses from three-and four-point bend end-notched flexure tests. J Compos Mater 2007;41:1177–96.

[21] Blackman BRK, Brunner AJ, Williams JG. Mode II fracture testing of composites: a new look at an old problem. Eng Fract Mech 2006;73:2443–55.

[22] Brunner AJ, Pinter G, Murphy N. Development of a standardized procedure for the characterization of interlaminar crack growth in advanced composites under fatigue mode I loading. Eng Fract Mech 2009;76:2678–89.

[23] Finn SR, He Y-F, Springer GS. Delaminations in composite plates under transverse impact loads – experimental results. Compos Struct 1993;23:191–204.

[24] Hoang NT, Gamby D, Lafarie-Frenot M-C. Predicting fatigue transverse crack growth in cross-ply carbon–epoxy laminates from quasi static strength tests by using iso-damage curves. Int J Fatigue 2010;32:166–73.

[25] Brunner AJ, Blackman BRK, Davies P. Mode I delamination. In: Moore DR, Pavan A, Williams JG, editors. Fracture mechanics test methods for polymers, adhesives, and composites. Elsevier; 2001. p. 277–305 [Chapter 4.1].

[26] Davies P, Blackman BRK, Brunner AJ. Mode II delamination. In: Moore DR, Pavan A, Williams JG, editors. Fracture mechanics test methods for polymers, adhesives, and composites. Elsevier; 2001. p. 307–33 [Chapter 4.2].

[27] Blackman BRK, Brunner AJ, Davies P. Delamination fracture of continuous fibre composites. Mixed-mode delamination. In: Moore DR, Pavan A, Williams JG, editors. Fracture mechanics test methods for polymers, adhesives and composites. Elsevier; 2001. p. 335–59 [Chapter 4.3].

[28] Brunner AJ. Experimental study of delamination in cross-ply composites, Chapt. 9. In: Sridharan S, editor. Delamination behaviour of composites. Woodhead Publ.; 2008. p. 281–309.

[29] Stelzer S, Brunner AJ, Argüelles A, Murphy N, Pinter G. Mode I delamination fatigue crack growth in unidirectional fiber reinforced composites. Development of a standardized test procedure, Compos Sci Technol; 2012. in press.

[30] Cvitkovich MK, Polymer matrix effects on interlaminar crack growth in advanced composites under monotonic and fatigue mixed mode I/II loading conditions. PhD thesis, Montanuniversität Leoben; 1995.

[31] Davies P, Sims GD, Blackman BRK, Brunner AJ, Kageyama K, Hojo M, et al. Comparison of test configurations for the determination of GIIc of

unidirectional carbon/epoxy composites, an international round robin. Plast Rubber Compos 1999;28:432–7.

[32] Brunner AJ. Experimental aspects of mode I and mode II fracture toughness testing of fibre-reinforced polymer–matrix composites. Comput Methods Appl Mech Eng 2000;185:161–72.

4 APPLICATION OF THE TEST PROCEDURE

4.1 INTRODUCTION

In **publications 2 and 3** it was shown that the mode I fatigue delamination test procedure developed within this thesis can be applied to various unidirectionally fiber reinforced polymer composites [1,2]. **Publication 1** [3] showed that it can also be applied to multiaxial, braided composites.

Several authors have investigated the effect of matrix properties on the delamination behavior of composite materials both under quasi-static and fatigue loads (e.g. [4–19]). Sela and Ishai [20] give a review of early works on interlaminar fracture toughness and toughening of laminated composite materials. Other research groups focused on studying the influence of fiber surface treatments and coatings (e.g. [21–30]) and of fiber volume content (e.g. [31]) on the quasi-static mode I delamination properties.

Cooper investigated the effect of flaws in fibers on the fracture mechanical properties of composite materials. He found decreasing fracture properties when the fibers were weakened. For these tests, however, the fibers were orientated perpendicular to the crack plane [32].

Jang et al. [33] addressed the influence of the prepreg manufacturing method on the interlaminar mode II fracture toughness of CFRP. For prepreg production, they used three different production methods to disperse thermoplastic particles as toughness modifier in an epoxy matrix resin. Mode II testing proved to be sensitive to changes in the production process. Other authors investigated the influence of multi-directional stacking sequences on the interlaminar fracture properties of composites [34,35].

This chapter aims at quantifying the influence of textile preforming on the fracture mechanical properties of composite materials. Standardized quasi-static delamination tests are carried out in mode I and mode II, as well as fatigue mode I delamination tests based on the test procedure introduced in chapter 3.

4.1.1 References

[1] Stelzer S, Brunner AJ, Argüelles A, Murphy N, Pinter G. Mode I delamination fatigue crack growth in unidirectional fiber reinforced composites: Development of a standardized test procedure. Composites Science and Technology 2012;72(10):1102–7.

[2] Stelzer S, Brunner A, Argüelles A, Murphy N, Cano G, Pinter G. Mode I delamination fatigue crack growth in unidirectional fiber reinforced composites: Results from ESIS TC4 round-robins. Engineering Fracture Mechanics 2014;116:92–107.

[3] Stelzer S, Schillfahrt C, Wolfahrt M, Pinter G, Noisternig J, Frieß S. Influence of fiber placement and architecture on fracture mechanical properties of carbon fiber reinforced composites. SAMPE 2012 Technical Conference Proceedings: Connecting the Advanced Materials Community, Baltimore, MD 2012;May 21-24:1–8.

[4] Altus E, Ishai O. The effect of soft interleaved layers on the combined transverse cracking/delamination mechanisms in composite laminates. Composites Science and Technology 1990;39:13–27.

[5] Álvarez V, Bernal CR, Frontini PM, Vázquez A. The influence of matrix chemical structure on the mode I and II interlaminar fracture toughness of glass-fiber/epoxy composites. Polymer Composites 2003;24(1):140–8.

[6] Arai M, Noro Y, Sugimoto K, Endo M. Mode I and mode II interlaminar fracture toughness of CFRP laminates toughened by carbon nanofiber interlayer. Composites Science and Technology 2008;68(2):516–25.

[7] Armstrong-Carroll E IBKIDT. The Influence of Interleaf Deformation Behavior and Film-Resin Adhesion on the Fracture Toughness of Interleaved Composites. In: Stinchcomb WW, Ashbaugh NE, editors. Composite Materials: Fatigue and Fracture: ASTM STP 1156. West Conshohocken, PA: American Society for Testing and Materials; 1993, p. 299–317.

[8] Armstrong-Carroll E CR. Improvement of Delamination Resistance with Carbon Nonwoven Mat Interleaves. In: Martin RH, editor. Composite Materials: Fatigue and Fracture: ASTM STP 1230, 5th ed. West Conshohocken, PA: American Society for Testing and Materials; 1995, p. 124–31.

[9] Chen SF, Jang BZ. Fracture behaviour of interleaved fiber-resin composites. Composites Science and Technology 1991;41:77–97.

[10] Compston P, Jar PB, Burchill PJ, Takahashi K. The effect of matrix toughness and loading rate on the mode-II interlaminar fracture toughness of glass-fibre/vinyl-ester composites. Composites Science and Technology 2001;61:321–33.

[11] Ishai O, Rosenthal H, Sela N, Drukker E. Effect of selective adhesive interleaving on interlaminar fracture toughness of graphite/epoxy composite laminates. Composites 1988;19(1):49–54.

[12] Jang J, Yang H. Toughness improvement of carbon-fibre/polybenzoxazine composites by rubber modification. Composites Science and Technology 2000;60:457–63.

[13] Kageyama K, Kimpara I, Suzuki T, Ohsawa I, Esaki K. Effect of Interleaf Thickness of Mode II Fatigue Delamination Growth of Interleaved Carbon/Epoxy. Key Engineering Materials 1998;137:187–94.

[14] Matsuda S, Hojo M, Ochiai S, Murakami A, Akimoto H, Ando M. Effect of ionomer thickness on mode I interlaminar fracture toughness for ionomer toughened CFRP. Composites Part A: Applied Science and Manufacturing 1999;30:1311–9.

[15] Sela N, Ishai O, Banks-Sills L. The effect of adhesive thickness on interlaminar fracture toughness of interleaved CFRP specimens. Composites 1989;20(3):257–64.

[16] Vickers PE, Boniface L, Pricket A, Watts J. F. The effect of siloxane-type molecules on the interlaminar toughness of CFRP. Composites Part A: Applied Science and Manufacturing 2000;31:559–69.

[17] Wang XR, Wu XQ, Liu ML. Experimental study on interlaminar fracture toughness of modified epoxy resin composites. Polymers & Polymer Composites 2012;20(1&2):161–3.

[18] van der Heijden, Sam, Daelemans L, Schoenmaker B de, Baere I de, Rahier H, van Paepegem W et al. Interlaminar toughening of resin transfer moulded glass fibre epoxy laminates by polycaprolactone electrospun nanofibres. Composites Science and Technology 2014;104:66–73.

[19] Sato N, Hojo M, Nishikawa M. Intralaminar fatigue crack growth properties of conventional and interlayer toughened CFRP laminate under mode I

loading. Composites Part A: Applied Science and Manufacturing 2015;68:202–11.

[20] Sela N, Ishai O. Interlaminar fracture toughness and toughening of laminated composite materials: a review. Composites 1989;20(5):423–35.

[21] Albertsen H, Ivens J, Peters P, Wevers M, Verpoest I. Interlaminar fracture toughness of CFRP influenced by fibre surface treatment: part I. experimental results. Composites Science and Technology 1995;54:135–45.

[22] Albertsen H, Peters PWM. The influence of fibre/matrix interface strength on interlaminar fracture toughness of CFRP. Proc. 11th International Conference on Interfacial Phenomena on Composite Materials 1991:247–8.

[23] Arrington M, Harris B. Some properties of mixed fibre cfrp. Composites 1978;9(3):149–52.

[24] Hinkley JA. Effect of fiber-matrix adhesion on interlaminar fracture toughness of graphite thermoplastic composites. In: Vigo TLKBJ, editor. Composite Applications: The Role of Matrix, Fiber and Interface. California: VCH; 1992, p. 267–76.

[25] Hu X, Mai Y. Mode I delamination and fibre bridging in carbon-fibre/epoxy composites with and without pval coating. Composites Science and Technology 1993;46:147–56.

[26] Ivens J, Albertsen H, Wevers M, Verpoest I, Peters P. Interlaminar fracture toughness of CFRP influenced by fiber surface treatment: part II. modelling of the interface effect. Composites Science and Technology 1995;54:147–59.

[27] Kim J, Mai Y. Fracture of CFRP containing impregnated fibre bundles. Composites Science and Technology 1993;49:51–60.

[28] Madhukar MS, Drzal LT. Fiber-Matrix Adhesion and Its Effect on Composite Mechanical Properties: IV. Mode I and Mode II Fracture Toughness of Graphite/Epoxy Composites. Journal of Composite Materials 1992;26(7):936–68.

[29] Suzuki Y, Maekawa Z, Hamada H, Kibune M, Hojo M, Ikuta N. Influence of adsorption behaviour of a silane coupling agent on interlaminar fracture in a glass fibre fabric-reinforced unsaturated polyester laminates. Journal of Materials Science (Journal of Materials Science) 1992;27:6782–90.

[30] Varelidis PC, McCullough RL, Papaspyrides CD. The effect on the mechanical properties of carbon/epoxy composites of polyamide coatings on the fibers. Composites Science and Technology 1999;59:1813–23.

[31] Chen JH, Schulz E, Bohse J, Hinrichsen G. Effect of fibre content on the interlaminar fracture toughness of unidirectional glass-fibre/polyamide composite. Composites Part A: Applied Science and Manufacturing 1999;30:747–55.

[32] Cooper GA. The fracture toughness of composites reinforced with weakened fibres. Journal of Materials Science (Journal of Materials Science) 1970;5:645–54.

[33] Jang K, Cho W, Ha C. Influence of processing method on the fracture toughness of thermoplastic-modified. carbon-fiber-reinforced epoxy composites. Composites Science and Technology 1999;59:995–1001.

[34] Zabala H, Aretxabaleta L, Castillo G, Aurrekoetxea J. Loading rate dependency on mode I interlaminar fracture toughness of unidirectional and woven carbon fibre epoxy composites. Composite Structures 2015;121:75–82.

[35] Alif N, Carlsson LA, Gillespie JW. Mode I, Mode II, and Mixed Mode Interlaminar Fracture of Woven Fabric Carbon/Epoxy. In: Hooper SJ, editor. Composite Materials: Testing and Design: ASTM STP 1242, 13th ed. West Conshohocken, PA: American Society for Testing and Materials; 1997, p. 82–106.

4.2 PUBLICATION 5

INFLUENCE OF FIBER PLACEMENT AND ARCHITECTURE ON FRACTURE MECHANICAL PROPERTIES OF CARBON FIBER REINFORCED COMPOSITES

4.2.1 Bibliographic Information

- Authors and their relevant contributions to the publication:
  - Steffen Stelzer[1]
    Preparation of the manuscript, fracture mechanical tests on multi-axial braidings, fractography/microscopy and analysis of all data.
  - Christian Schillfahrt[2]
    Fracture mechanical tests on unidirectional composites.
  - Markus Wolfahrt[2,3]
    Project co-ordination and co-supervision of the work.
  - Gerald Pinter[1,2]
    Academic supervision of the work carried out in this publication.
  - Johannes Noisternig[3]
    Organization of specimen production at FACC AG.
  - Sebastian Frieß[4]
    Organization of carbon fiber manufacturing and textile preforming at Toho Tenax Europe GmbH.
- Affiliations
  [1] Institute of Materials Science and Testing of Polymers, Montanuniversitaet Leoben, Leoben, Austria
  Relevant contributions to the publication:
  [2] PCCL, Polymer Competence Center Leoben, Roseggerstrasse 12, A-8700 Leoben, Austria
  [3] FACC AG, Ried im Innkreis, A-4910
  [4] Toho Tenax Europe GmbH, Wuppertal, D-42103
- Source: SAMPE 2012 Technical Conference Proceedings: Connecting the Advanced Materials Community, Baltimore, MD

Statement with regard to publication: The manuscript presented here is an adapted accepted manuscript in order to fit the formatting of the thesis and does not necessarily reflect the actually published version.

The Society for the Advancement of Material and Process Engineering (SAMPE) agrees that in response to your inquiry, and subject to the terms below, we will grant you permission to reprint from a SAMPE publication, the text, photographs and/or illustrations indicated in your request.

- This material is to be reprinted by you no later than one (1) year from the date of this agreement. No deletions from, additions to, or changes in the text or illustrations may be made without prior written approval.
- Permission is granted for the one-time use of the specified material only, for the sole purpose designated in your request. This permission is non-exclusive for the English language.
- Permitted use is limited to the reprint in the publication described below, and does not include the right to grant others permission to photocopy or reproduce this material.
- Appropriate credit to our publication and organization must appear on every copy of your reprint, either on the first page of the quoted text or in the figure legend. The following components must be included: Title, Author(s) and/or Editor(s), or Journal Title (if applicable). AReprinted by permission from the Society for the Advancement of Material and Process Engineering (SAMPE).
- One copy of the finished reprint should be sent to the SAMPE address given on this letterhead.

This permission does not extend to any copyrighted matter from any other sources that may be incorporated in the material. The rights hereby granted may not be assigned or transferred, and shall terminate in the event the use of the requested copies for the stated purpose is not made by the designated reprint date.

This permission is not final until you have notified us of your acceptance of its terms by signing and returning by mail or by facsimile, a copy of this letter.

Thank you for your interest in SAMPE and its publications.

Sincerely,
SAMPE

Sylvia A. Smith
Office Manager

Title of Reprint:
Optimized experimental methods and failure criteria for the description of the delamination and failure behavior of high performance composites and joints (PhD Thesis, Steffen Stelzer, Montanuniversitaet Leoben, AUT)

SAMPE Publication:
Influence of Fiber Placement and Architecture on fracture mechanical properties of carbon fiber reinforced composites (SAMPE 2012 Technical Conference Proceedings: Connecting the Advanced Materials Community, Baltimore, MD)

Name
Steffen Stelzer

Date
10/28/2014

Signature

Society for the Advancement of Material and Process Engineering
1161 Park View Drive, Suite 200, Covina, CA 91724-375

4.2.2 Abstract

Within this work an experimental investigation of the influence of different fiber placement techniques and fiber architecture on the interlaminar crack growth of carbon fiber reinforced composites under monotonic and fatigue loading conditions was carried out. Unidirectional laminate plates were manufactured based on braiding, filament winding and filament winding with additional bobbins to account for any damage induced by bobbins in the braiding process. Under mode I loading conditions a significant difference in delamination behavior of the investigated laminates could be found for both monotonically and cyclically loaded specimens. The same trends could be observed under mode II loading conditions. Furthermore the use of biaxial and triaxial braids led to increased interlaminar fracture toughnesses in both mode I and mode II when compared to the unidirectionally reinforced specimens. An investigation of the fracture surfaces of the specimens showed distinct differences in the micromechanical fracture behavior.

4.2.3 Introduction

Due to the possibility of an automated fabrication of large structures with complex shape and high production rates, braided textile composites produced via liquid resin infusion are increasingly considered for structural commercial aircraft components. Furthermore through their use the impact and delamination resistance can be improved [1,2]. Biaxial braids consist of two yarns located at an angle of ±θ to the longitudinal direction along the mandrel axis. Through adding fibers in the longitudinal (0°) direction a triaxial braid can be achieved [3]. Since the braid geometry has an influence on the mechanical properties of a part it is imperative to evaluate the differences in the performance of different braid geometries [4]. This report will focus only on fracture mechanical properties, other properties will be reported elsewhere [4]. Fiber reinforced polymer composites (FRP) are susceptible to delaminations and delaminations in FRP can grow to a critical size when subjected to cyclic loads, even below the static strength of the material and can thus trigger the failure of a structure. Therefore it is essential to create key figures to describe the growth and the initiation of delaminations in FRPs. These figures can be used in the design phase of structures in order to prohibit failure by delamination [5,6,7,8]. The most critical loading cases for the growth of delaminations are mode I and mode II loading. The mode I load is a tensile crack opening load and the mode II load a shear load in the crack plane.

The out of plane mode III load is of less practical importance. All three loading cases are depicted schematically in Figure 4.1 [8,9,10].

4.2.4 Experimental

The textile composites examined in this report were produced via braiding and filament winding and were made of epoxy resin reinforced with carbon fibers from Toho Tenax Europe GmbH (Wuppertal, D). The carbon fibers were processed to braided preforms at the Institute of Aircraft Design, University of Stuttgart (Stuttgart, D). Therefore the carbon fibers were braided onto a rectangular core with a length of 1000 mm, a width of 200 mm and a thickness of 15 mm. Unidirectional (UD) preforms, biaxial preforms and triaxial preforms were braided. To be able to braid the UD-samples thermoplastic auxiliary yarns were used in one braiding direction instead of carbon fibers in order to stabilize the UD preform. These thermoplastic yarns had a low melting temperature so that they did not affect the infiltration process. After braiding the yarns over a cylindrical mandrel the braids were removed from the mandrel, slit along the 0° direction, flattened and placed in a mold. At the Technical University in Munich (Munich, D), Institute of Carbon Composites, all preforms were infiltrated with resin using a resin infusion technique. Additional UD preforms were produced via circumferential filament winding at Carbon Großteile GmbH (Wallerstein, D). Therefore the dry yarns were wound onto rectangular plates with a length of 450 mm, a width of 400 mm and a thickness of 4.5 mm.

After the winding process the dry preforms were infiltrated with resin and cured. The UD-specimens were cut out of the cured plates. To be able to further assess the influence of bobbins, which are mainly used in the braiding process, on the fracture mechanical performance of fiber composites, another set of preforms was produced in filament winding after rewinding the yarns from the original spool onto a bobbin.

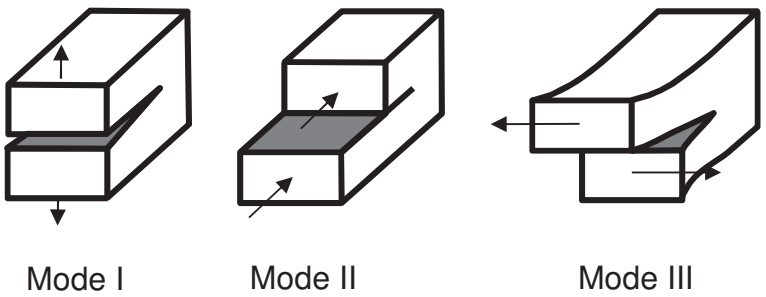

Figure 4.1: Relevant fracture mechanical loading cases.

For the examination of the delamination behavior under mode I loading conditions, double cantilever beam specimens according to AITM 1-0005 and for mode II end notched flexure specimens according to AITM 1-0006 were manufactured [11,12]. All tests under mode I loading conditions were carried out on a servo hydraulic test machine from MTS Systems Corporation (Eden Prairie, USA). The mode II tests were done on a testing machine from Zwick Roell (Ulm, D) using a three point bending setup. While the monotonic mode I and mode II tests were analyzed using AITM 1-0005 and AITM 1-0006 respectively, the mode I fatigue tests were interpreted using modified compliance calibration (MCC) by Kageyama [13,14]. In order to avoid an influence of facial interference on the results of the measurements G_{Imax} was used instead of ΔG_I [15].

4.2.5 Results

4.2.5.1 Fracture mechanical measurements

The monotonic and cyclic mode I strain energy release rate values, G_{IC} and G_{Imax}, of the UD laminates show that the thermoplastic yarns, which were necessary for manufacturing the braided UD samples, greatly increased the mode I delamination resistance when compared to the filament wound UD specimens. The same trend could be found for the monotonic mode II values. The use of an additional bobbin in filament winding led to a moderate increase of both the G_{IC} and G_{IIC} values. The results of the monotonic mode I and mode II tests on UD laminates can be seen in Figure 4.2.

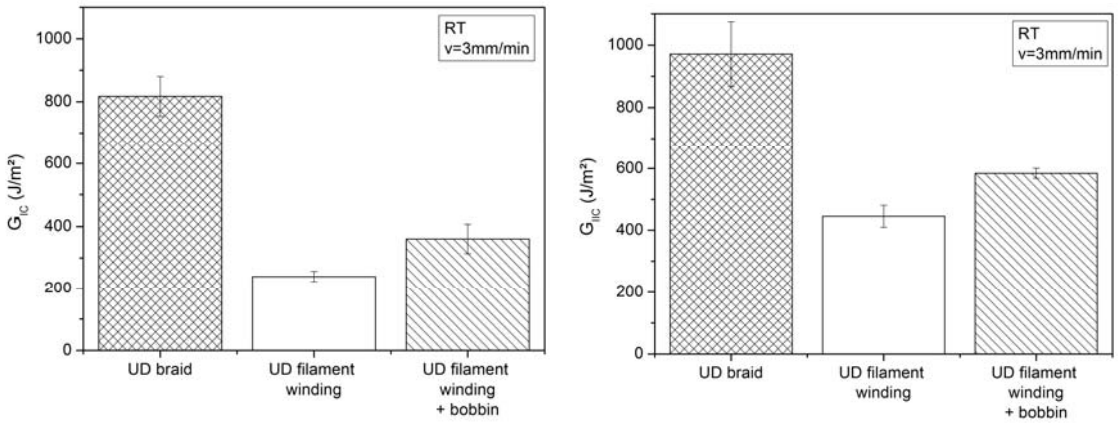

(a) (b)

Figure 4.2: (a) Influence of the manufacturing process on G_{IC} values.
(b) Influence of the manufacturing process on G_{IIC} values.

The cause for the influence of the bobbin in the filament winding process on the delamination properties can be seen in Figure 4.3.This figure shows a detail of the preforms after the filament winding process. The preforms that are produced via a filament winding process have well aligned fibers. When the carbon fiber rovings are rewound onto a bobbin before they are deposited on the mandrel a non-uniform fiber distribution, which is reflected in higher G_{IC} and G_{IIC} values, is achieved.

The results of the cyclic mode I delamination measurements are shown in Figure 4.4. Again the braided UD composites show the highest G_I values for all crack growth rates due to the thermoplastic yarns used for the stabilization of the textile preform.

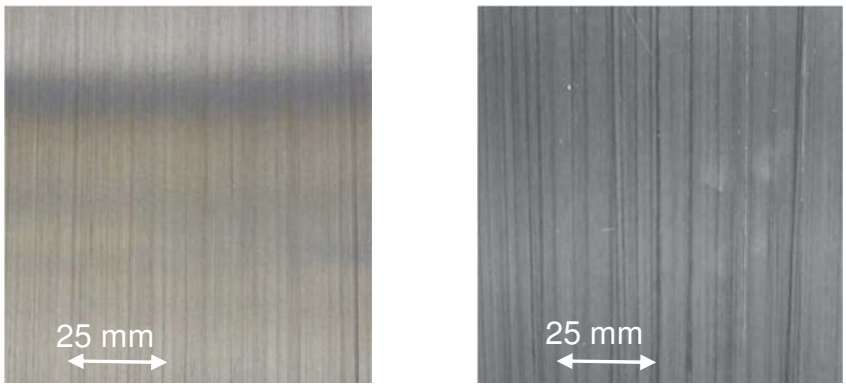

Figure 4.3: (a) Detail of uniform fiber distribution in UD preform produced via filament winding. (b) Detail of non-uniform fiber distribution in UD preform produced via filament winding using additional bobbin.

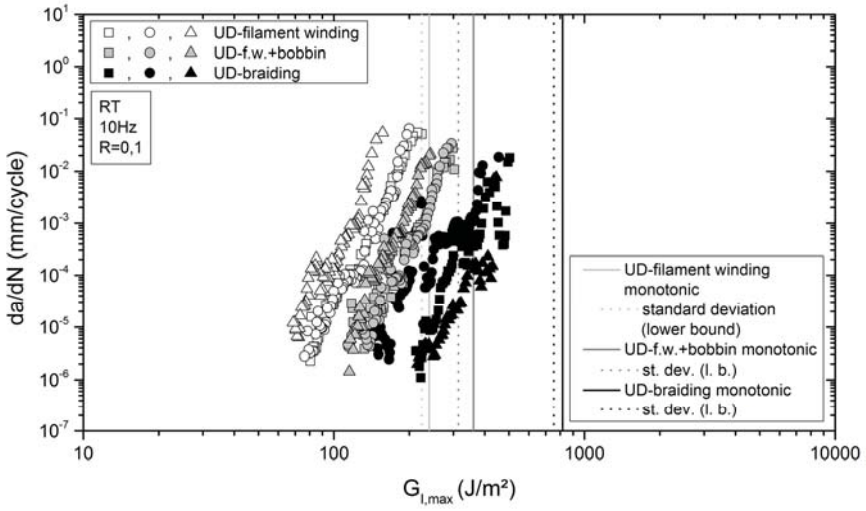

Figure 4.4: Crack growth curves of UD reinforced composites after braiding, filament winding and filament winding over additional bobbin.

Also the positive influence of the use of a bobbin in the filament winding process on the mode I strain energy release rate values could be reproduced in fatigue delamination measurements.

The bi- and triaxial (multidirectional) braids showed increased G_{IC} and G_{IIC} values compared to the UD laminates, see Figure 4.5. This is because fibers which are not aligned in the 0° direction deflect the growing crack and thereby lead to higher strain energy release rate values. In mode II this effect was even more pronounced than in mode I, especially in the case of the triaxial braid tested in transversal direction. There the G_{IIC} values showed a big amount of scatter due to the interaction of the crack tip with the yarns located perpendicular to the crack growth direction. In Figure 4.6 the fatigue crack growth behavior of the multidirectional braids is depicted as log da/dN versus log G_{Imax} diagram.

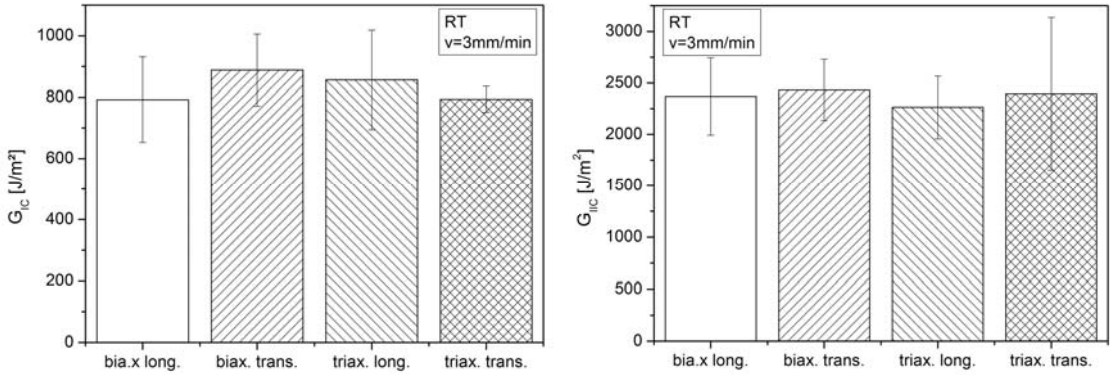

Figure 4.5: (a) G_{IC} values of the biaxially and triaxially braided composites.
(b) G_{IIC} values of the biaxially and triaxially braided composites.

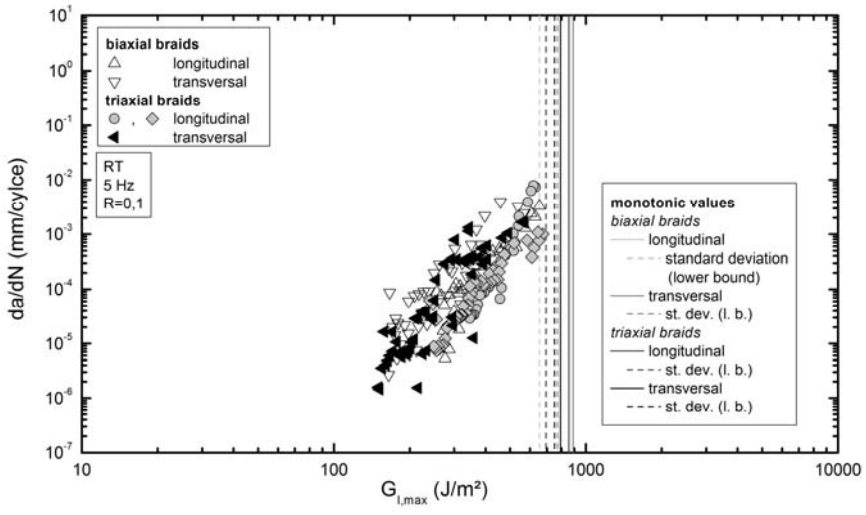

Figure 4.6: Crack growth curves of biaxially and triaxially braided composites.

The triaxial braids which were tested in longitudinal direction showed less scatter than the biaxial braids and the triaxial braids that were tested in transversal direction. The scatter can be ascribed to two mechanisms.

On the one hand, the crack growth is stopped at fibers that are not aligned in the 0° direction and the crack is deflected from its nominal growth plane ('crack deflection'). On the other hand, a second crack plane is created in some cases ('crack branching'). In Figure 4.7 these mechanisms are shown in a picture taken during the measurements on a biaxial braid. It has to be mentioned that the results shown here were calculated based on equations that require the ideal case of one single and even crack plane [16]. Hence the results are not fully valid. Yet, Morais et al. analyzed the fracture behavior of cross ply laminates. They concluded that compliance based data reduction schemes are insensitive to the type of crack propagation and remain applicable, even when the crack is periodically deflected to a neighboring layer [17].

4.2.5.2 Microscopy

Figure 4.8 and Figure 4.9 show scanning electron microscopy pictures of the fracture surfaces of one UD laminate and one multidirectionally braided textile composite respectively, after mode I and mode II loading. In both cases 'hackle pattern' morphologies were observed on the fracture surfaces after mode II loading [18,19]. For the mode I loading situation a significantly smoother fracture surface was found and a faint 'river pattern' morphology could be observed.

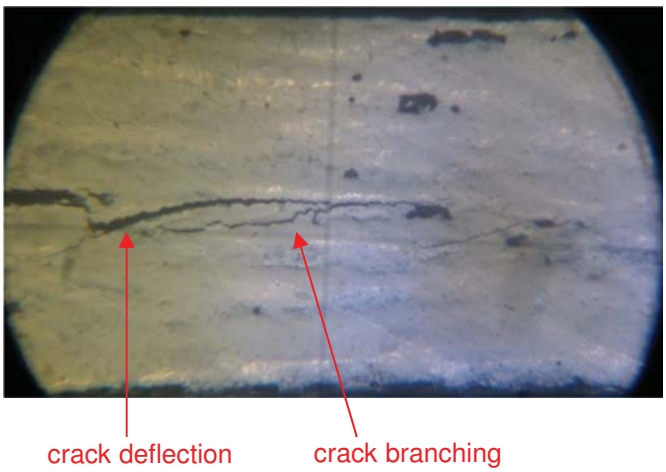

Figure 4.7: Crack deflection and crack branching in the biaxial braid.

In contrast to the mode I interlaminar fracture surfaces of the UD laminates, the fracture surfaces of the multidirectional braids showed a combination of 'river patterns', which are known to occur after mode I loading, and 'hackle patterns', the predominant fracture surface morphology after mode II loading. According to Liu et al. delaminations grow faster alongside fibers than perpendicular to them [20]. This may be the cause for the inhomogeneous fracture surface of the multidirectionally braided textile composites after global mode I loading.

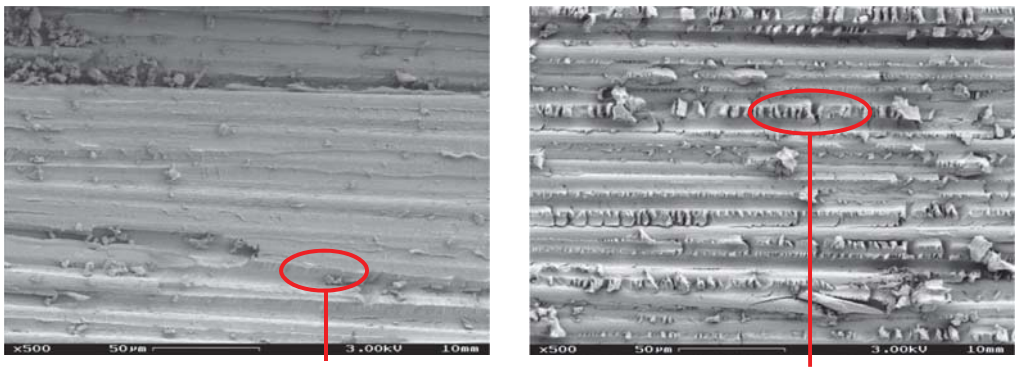

(a) (b)

Figure 4.8: SEM pictures of a UD reinforced braided composite.
(a) Fracture surface after mode I loading. 500 x magnification.
(b) Fracture surface after mode II loading. 500 x magnification.

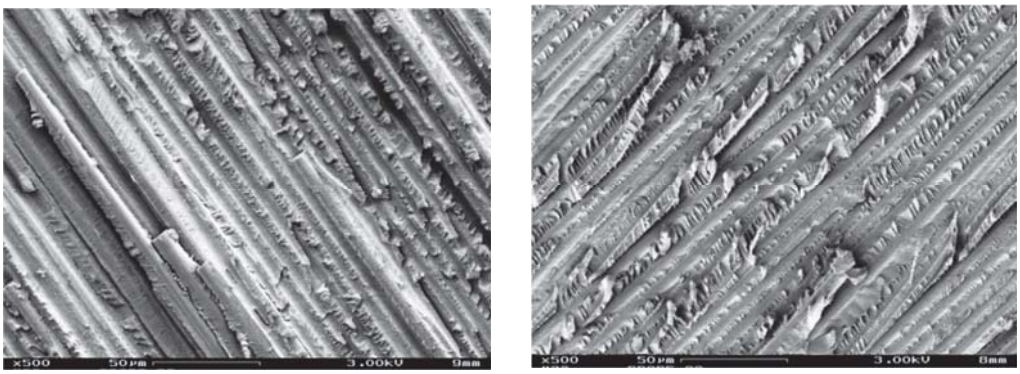

(a) (b)

Figure 4.9: SEM picture of a triaxially braided composite.
(a) Fracture surface after mode I loading. 500 x magnification.
(b) Fracture surface after mode II loading. 500 x magnification.

4.2.6 Conclusions

The results of monotonic and cyclic delamination tests on specimens produced via a braiding and filament winding process show that both the thermoplastic thread, which is needed for braiding unidirectional textiles, and an additional bobbin have a positive impact on the delamination resistance. The biggest increase in G_I and G_{II} could be achieved by using bi- and triaxially (multidirectionally) braided textile composites. The monotonic and cyclic fracture mechanical tests on multi-directionally braided textile composites show that no significant improvement can be achieved by using triaxial instead of biaxial braids. Both mode I and mode II tests on these multidirectional composites yielded similar strain energy release rate values.

Compared to the unidirectionally reinforced laminates however, the bi- and triaxial laminates showed significantly higher G_{IIC} values. The big scatter of the mode II values of the triaxially braided composites that were loaded in transversal direction can be ascribed to the deviation of the crack when it reaches a yarn that is oriented perpendicular to the crack growth direction. The crack grows through the low strength thermoset matrix instead of growing through the carbon fiber. Fatigue crack growth measurements on multidirectionally braided composites under mode I loading conditions yielded reproducible results. While the crack in the biaxially braided composites and the triaxially braided composites loaded in transversal direction showed ‘Stop and Go’ behavior (discontinuous crack growth), the triaxially braided composites that were loaded in longitudinal direction yielded continuous crack growth.

Scanning electron microscopy of the interlaminar fracture surfaces showed that the predominant fractographic features of UD laminates are ‘river patterns’ after mode I loading and ‘hackle patterns’ after mode II loading. Multidirectional laminates however seem to locally fail in a mixed mode, which is indicated by a mix of ‘river’ and ‘hackle pattern’ morphologies on the fracture surface.

4.2.7 Acknowledgement

The research work was performed at the Polymer Competence Center Leoben GmbH (PCCL, Austria) within the framework of the COMET-program of the Austrian Ministry of Traffic, Innovation and Technology with contributions by University of Leoben (Chair of Materials Science and Testing of Plastics), Munich University of Technology (Institute of Carbon Composites), FACC AG and Toho

Tenax Europe. The PCCL is funded by the Austrian Government and the State Governments of Styria and Upper Austria.

4.2.8 References

[1] Masters, J.E. & Ifju, P.G. “A phenomenological study of triaxially braided textile composites loaded in tension” *Composites Science and Technology* 56 (1996) 347-358

[2] Smith, L.V. & Swanson, S.R. “Strength design with 2-D triaxial braid textile composites” *Composites Science and Technology* 56 (1996) 359-365

[3] Avranci, C. & Carey J. “2D braided composites: A review for stiffness critical applications” *Composite Structures* 85 (2008) 43,58

[4] Wolfahrt, M.; Pinter, G.; Zaremba, S.; von Reden, T. & Ebel C., “Effect of preform architecture on the mechanical and fatigue behavior of braided composites for generating design allowables”. *SAMPE Europe*, Paris, 2009, Vol. 30, 277-282

[5] Stelzer, S.; Brunner, A.J.; Argüelles, A.; Murphy, N. & Pinter, G. “Mode I delamination fatigue crack growth in unidirectional fiber reinforced composites: Development of a standardized test procedure” *Composite Science and Technology* DOI: 10.1016/j.compscitech.2011.11.033 (2011) In Press

[6] Stelzer. S.; Wolfahrt, M.; Pinter, G.; von Reden, T. & Noisternig, J. “Damage Tolerance and interlaminar crack growth of braided composites” *14th European Conference on Composite Materials*, Budapest, 2010, Paper ID: 519-ECCM14

[7] Sierakowski, R.L. & Newaz, G.M. *Damage tolerance in advanced composites*, Boca Raton, FL: CRC Press, 1995

[8] Cvitkovich M. “Polymer matrix effects on interlaminar crack growth in advanced composites under monotonic and fatigue mixed mode I/II loading conditions” *PhD Thesis*, Montanuniversitaet Leoben, Austria (1995)

[9] Brunner, A.J.; Stelzer, S.; Pinter, G. & Terrasi, G.P. “Mode II fatigue delamination resistance of advanced fiber-reinforced polymer-matrix laminates: Towards the development of a standardized test procedure” *International Journal of Fatigue* 50 (2013) 57-62

[10] Brunner A.J.; Blackman, B.R.K. & Davies, P. “A status report on delamination resistance testing of polymer-matrix composites” *Engineering Fracture Mechanics* 75 (2008) 2779-2794

[11] AITM Standard 1-0005, 1994, “Determination of interlaminar fracture toughness energy – Mode I” Airbus Industrie, 31700 Blagnac Cedex, France

[12] AITM Standard 1-0006, 1994, “Determination of interlaminar fracture toughness energy – Mode II” Airbus Industrie, 31700 Blagnac Cedex, France

[13] Kageyama, K. & Hojo, M. Proc. 5th Japan-US Conference on Composite Materials, Kokon-shoin (1990) 227-234

[14] Kageyama, K.; Kobayashi, T. & Chou, T.W. “Analytical compliance method for Mode I interlaminar fracture toughness testing of composites” *Composites* 18(5) (1987) 393-399

[15] Martin, R.H. & Murri, G.B. “Characterization of mode I and mode II delamination growth and thresholds in graphite/peek composites” *NASA technical memorandum* 100577, (1988): 1-52.

[16] Williams, Gordon., “On the calculation of energy release rates for cracked laminates” *International Journal of Fracture* 36 (1988) 101-119

[17] Morais AB de, Moura MF de, Marques AT, Castro PT de. Mode-I interlaminar fracture of carbon/epoxy cross-ply composites. Composites Science and Technology 2002;62:679–86.

[18] Bonhomme, J.; Argüelles, A. Vina J. & Vina, I. “Fractography and failure mechanisms in static mode I and mode II delamination testing of unidirectional carbon reinforced composites” *Polymer Testing* 28 (2009) 612-617

[19] Asp, L.E.; Sjögren, A. & Greenhalgh, E.S. “Delamination growth and thresholds in a carbon/epoxy composite under fatigue loading” *Jounal of Composite Technology and Research* 23 (2001) 55-68

[20] Liu, S.; Kutlu, Z.; Chang, F.-K. *Composite Materials, Fatigue and Fracture*, Ed. Stinchcomb, W.W., Ashbaugh, N.E., Vol. 4, Philadelphia: ASTM Publications, 1993, 86-101

5 DESIGN BASED ON FATIGUE DELAMINATION GROWTH IN COMPOSITES

5.1 INTRODUCTION TO DESIGN BASED ON FATIGUE DELAMINATION GROWTH IN COMPOSITES

Publication 2 [1] and **publication 3** [2] as well as research work carried out in literature [3–5] show that the measurement of the delamination growth in composite materials yields high values of the exponent in the Paris law. These large exponents mean that a small change in the applied load will cause a large change in the predicted delamination growth rates. Thus, it is difficult to design composite structures for finite life against delamination failure. A much shorter life than the design value can be caused by minor design alterations or small analysis errors [4,5].

A viable alternative would be design for infinite life. For this purpose, the delamination threshold would be an important material property [5]. But as shown in **publication 3** [2], the determination of the delamination threshold is limited by measurement resolution and testing time. Also, publications [6,7] have shown that thresholds for sub-millimeter defects in metallic structural elements under operational load become very low and that crack growth can be assumed to commence on day one. It has yet to be investigated whether this also applies to composite materials.

The so-called ‘small crack effect’ for metals is included in ASTM E647 [8]. It is addressed in chapter X3 of [8] and crack sizes are classified in Table X3.1. Implementing similar short cracks of a few micrometers at a defined location in the CFRP composite fatigue test specimens is difficult. Starter cracks for CFRP composites are usually manufactured by inserting thin, polymer films (thickness less than 13 micrometer is recommended [9–11]) extending over the full width of the specimen and 40 to 60 millimeters from the load line along the beam at the mid-thickness of the laminates. Frequently, composite laminates, and specifically CFRP epoxy composites, already contain micro-pores or micro-cracks from manufacturing, e.g., caused by relaxation of residual stresses. These, as well as specifically manufactured micro-cracks for investigating short crack growth in CFRP composites are further quite likely subject to a complex, multi-axial stress field on the micro-scale even if the globally applied fatigue load is mode I or mode

II. Fatigue loading a CFRP composite specimen without defined macroscopic starter crack (e.g., from laminated thin polymer films) may, therefore, initiate crack growth from several short cracks already present after manufacturing at different locations simultaneously.

Small or short cracks in composites could, e.g., be defined as below or comparable to the fracture process zone size, i.e., up to a few millimeter at most [12], if the criterion of plastic zone size for small cracks in metals from Appendix X3 of [8] is adapted analogously for composites. Therefore, the only information on the behavior of small and short cracks in composites could currently be drawn from testing structural elements or components and comparing the observed fatigue crack growth behavior with models based on a Paris type law and the associated threshold. Instances in which failure in a high-performance CFRP composite component may have been due to short cracks developing to critical size under fatigue loading are presented and discussed in references [13–18].

Martin [19] and Attia et al. [20] have shown that designs can be based on delamination growth data, despite the above mentioned limitations. A global/local modelling approach is necessary to incorporate fracture mechanics into design. Stiffness and strength requirements are checked in a global analysis based on 2D shell elements. In a next step, areas of concern have to be identified[3] and analyzed in a local FE model that represents the through-thickness properties properly [19,20]. The local models can be accompanied by local tests of these areas. In the subsequent damage tolerance design phase, fracture analyses are carried out. If a delamination is predicted to initiate, then it must be determined how far it will grow and if this amount of growth is critical, leading to component failure [19].

Yet, the aforementioned uncertainties from large exponents of a Paris law data representation remain. In order to overcome the problems arising from large exponents, it is essential to provide designers with data presentations for fatigue crack growth, which give low values of exponent.

In 1970 Hartman and Schijve [21] suggested that da/dN should be dependent on the amount by which ΔK exceeds the fatigue threshold ΔK_{th} (i.e. on $\Delta K - \Delta K_{th}$). In

[3] This is done by engineering judgment, because global FE models invariably use 2D shell models that do not identify areas of high interlaminar stress [19].

2004 Andersons et al. [22] derived an equation, similar to the Hartman-Schijve approach, that could represent delamination growth in composites:

$$\frac{da}{dN} = C' \left(\frac{\Delta K - \Delta K_{th}}{K_c - K_m} \right)^{\propto} \tag{5.1}$$

where C' and α are constants, K_m is the mean applied stress intensity factor and ΔK_{th} ist the threshold stress intensity factor range. This equation was later adapted by Jones et al. [7]:

$$\frac{da}{dN} = D \left(\frac{\Delta\sqrt{G} - \Delta\sqrt{G_{thr}}}{\sqrt{1 - \sqrt{G_{max}}/\sqrt{G_{cy}}}} \right)^{ß} \tag{5.2}$$

Where D and ß are again constants of the power law and $\Delta\sqrt{G_{th}}$ and $\sqrt{G_{cy}}$ are a threshold like parameter and a toughness like parameter, respectively.

In a first paper, Jones et al. showed that by using equation (5.2), the exponent is approximately 2 for a big variety of materials, including composites, and is thus considerably lower than the exponent in Paris law representations [7]. Further, the results become independent of the stress ratio (R value) and thus reveal that R value effects can be accounted for by merely accounting for a change in threshold.

This chapter addresses the use of a modified Hartman-Schijve equation for the prediction of composite delamination under fatigue load and discusses its impact on the design of composites.

5.1.1 References

[1] Stelzer S, Brunner AJ, Argüelles A, Murphy N, Pinter G. Mode I delamination fatigue crack growth in unidirectional fiber reinforced composites: Development of a standardized test procedure. Composites Science and Technology 2012;72(10):1102–7.

[2] Stelzer S, Brunner A, Argüelles A, Murphy N, Cano G, Pinter G. Mode I delamination fatigue crack growth in unidirectional fiber reinforced composites: Results from ESIS TC4 round-robins. Engineering Fracture Mechanics 2014;116:92–107.

[3] Tay TE. Characterization and analysis of delamination fracture in composites: An overview of developments from 1990 to 2001. Applied Mechanics Reviews 2003;56:1–31.

[4] Asp LE, Sjögren A, Greenhalgh ES. Delamination Growth and Thresholds in a Carbon/Epoxy Composite under Fatigue Loading. Journal of Composites Technology & Research 2001;23(2):55–68.

[5] Mall S, Yun KT, Kochhar NK. Characterization of Matrix Toughness Effect on Cyclic Delamination Growth in Graphite Fiber Composites. In: Lagace PA, editor. Composite Materials: Fatigue and Fracture: ASTM STP 1012. West Conshohocken, PA: American Society for Testing and Materials; 1989, p. 296–310.

[6] Stelzer S, Jones R, Brunner AJ. Interlaminar fatigue crack growth in carbon fiber reinforced composites. In: Hoa SV, Hubert P, editors. Proceedings of the 19th International Conference on Composite Materials: Canadian Association for Composite Structures and Materials; 2013, p. 1689–97.

[7] Jones R, Pitt S, Brunner A, Hui D. Application of the Hartman–Schijve equation to represent mode I and mode II fatigue delamination growth in composites. Composite Structures 2012;94(4):1343–51.

[8] ASTM - American Society for Testing and Materials. E647:2013 - Standard test method for measurement of fatigue crack growth rates(E647:2013).

[9] ASTM - American Society for Testing and Materials. D5528:2001 - Standard test method for mode I interlaminar fracture toughness of unidirectional fiber-reinforced polymer matrix composites(D5528:2001).

[10] ISO - International Organization for Standardization. ISO 15024 - Fibre-reinforced plastic composites — Determination of mode I interlaminar fracture toughness, GIC, for unidirectionally reinforced materials(15024); 2001.

[11] ISO - International Organization for Standardization. ISO 15114 - Fibre-reinforced plastic composites — The determination of the Mode II fracture resistance, GIIC, for unidirectionally reinforced materials using the calibrated end loaded split (C-ELS) test and an effective crack length approach(15114); 2011.

[12] Brunner AJ, Blackman BRK, Williams JG. Calculating a damage parameter and bridging stress from GIC delamination tests on fibre composites. Composites Science and Technology 2006;66(6):785–95.

[13] Savage G. Sub-critical crack growth in highly stressed Formula 1 race car composite suspension components. Engineering Failure Analysis 2009;16(2):608–17.

[14] Chalkley P, Geddes R. Service history of the F-111 wing pivot fitting upper surface boron/epoxy doublers: DSTO-TN-0168. Department of Defence, September 1998.

[15] Raizenne D. Case history: CF116 upper wing skin fatigue enhancement boron doubler. In: Baker A, Rose L, Jones R, editors. Advances in the bonded composite repair of metallic aircraft structure: Volume 1, 1st ed. Amsterdam: Elsevier; 2002.

[16] Seneviratne W, Tomblin J, Kittur M. Durability and residual strength of adhesively-bonded composite joints: the case of F/A-18 A-D wing root stepped-lap joint. In: Vassilopoulos AP, editor. Fatigue and fracture of adhesively-bonded composite joints. Cambridge: Woodhead Publishing; 2015, p. 289–320.

[17] Schön J, Nyman T, Blom A, Ansell H. A numerical and experimental investigation of delamination behaviour in the DCB specimen. Composites Science and Technology 2000;60(2):173–84.

[18] Greenhalgh ES. Delamination growth in carbon-fibre composite structures. Composite Structures 1993;23(2):165–75.

[19] Martin RH. Incorporating interlaminar fracture mechanics into design. Proceedings of the Institution of Mechanical Engineers, Part L: Journal of Materials Design and Applications 2000;214(2):91–7.

[20] Attia O, Kinloch AJ, Matthews FL. Modelling the fatigue life of polymer–matrix fibre-composite components. Composites Science and Technology 2001;61(15):2273–83.

[21] Hartman A, Schijve J. The effects of environment and load frequency on the crack propagation law for macro fatigue crack growth in aluminium alloys. Engineering Fracture Mechanics 1970;1(4):615–31.

[22] Andersons J, Hojo M, Ochiai S. Empirical model for stress ratio effect on fatigue delamination growth rate in composite laminates. International Journal of Fatigue 2004;26(6):597–604.

5.2 PUBLICATION 6

MODE I, II AND MIXED MODE I/II DELAMINATION GROWTH IN COMPOSITES

5.2.1 Bibliographic Information

- Authors and their relevant contributions to the publication:
  - Rhys Jones[1]
    Preparation and submission of the manuscript. Derivation of the modified Hartman-Schijve equation for the application to composite materials.
  - Steffen Stelzer[1]
    Analysis of all data and preparation of all graphs. Mode I and mode II measurements for Figure 5.11.
  - Andreas J. Brunner[3]
    Mixed mode I/II measurements for Figure 5.11.
- Affiliations:
  [1] Centre of Expertise in Structural Mechanics, Department of Mechanical and Aerospace Engineering, Monash University, Australia
  [2] Institute of Materials Science and Testing of Polymers, Montanuniversitaet Leoben, Leoben, Austria
  [3] Empa, Swiss Federal Laboratories for Materials Science and Technology, Dübendorf, Switzerland
- Periodical: Composite Structures
- DOI: 10.1016/j.compstruct.2013.12.009

Statement with regard to publication: The manuscript presented here is an adapted accepted manuscript in order to fit the formatting of the thesis and does not necessarily reflect the actually published version.

5.2.2 Abstract

This paper presents an approach for computing the growth of Mode I, II and Mixed Mode I/II delaminations in carbon fiber reinforced polymer composites (CFRP) using a modified Hartman–Schijve equation. Unlike other equations it does not involve splitting the energy release rate into its various components. One advantage of this formulation is that the exponent of the associated power law appears to be independent of the mode as is the constant of proportionality. This formulation is shown to accurately compute the delamination growth rates associated with a range of Mode I, II and Mixed Mode I/II data available in the open literature. The potential for this approach to be used to overcome the no growth philosophy associated with current composite designs is also discussed.

5.2.3 Introduction

Composite materials are now widely used in aircraft structural components. For example the Boeing 787 passenger aircraft has approximately 50 % (by weight) composite parts on its major components whilst the F/A-18 has approximately 39 % (by weight) of its external wetted surface fabricated from advanced composites. In the Joint Strike Fighter (JSF), a ‘‘next generation’’ aircraft, advanced composites make up approximately 35 % of the aircraft’s weight.

However, the primary structural members in these aircraft are still metallic. A similar situation arises in the civilian sphere where skins, stabilizers, fins, control surfaces, etc., where the strain levels in these components are low, now make extensive use of CFRP composites. For certification purposes current designs are such that any delamination will not grow. This approach places an artificial limit on the use of composite materials and the components that can be lightened through their use. However, reference [1] presented a number of examples, viz: in F-111, A-320, F/A-18 and Canadian CF-5 aircraft, which illustrated that, despite this limit, fleet data and data obtained from full scale fatigue tests reveal that small sub mm initial delaminations can grow when subjected to operational flight loads. The delamination seen in the F/A-18 fatigue test [2,3] is perhaps the first known example of this phenomenon, see Figure 5.1.

In this instance small sub mm initial defects, typically less than 0.1 mm arose at the last step in titanium joint in the AS4 3501-6 graphite epoxy composite to the Ti–6Al–4V titanium end fitting, see Figure 5.2. The geometry and details of the ply configuration of the step lap joint are given in Figure 5.2 and [2]. This delamination grew during the (room temperature) fatigue test to a size of approximately 150 by

300 mm, see Figure 5.1.The test was performed at room temperature and prior to the test the wing was not subjected to environmental conditioning.

If we are to move away from the current strain level restrictions imposed by this no growth design philosophy we need to allow for a limited amount of growth. As such the challenge is to develop a methodology capable of predicting the growth of delaminations and in particular small naturally occurring initial delaminations growing in operational airframes.

The problem of delamination growth in aircraft structures generally involves complex stress states, the delamination in the F/A-18 step lap joint is a good example of this, with the potential for a delamination to grow in Modes I, II, III and/or any combination of these Modes. Unfortunately, there is no generally accepted equation to cover Mixed Mode delamination growth. Consequently the present paper will address the potential for a single equation to represent Modes I, II and Mixed Mode I/II delamination growth. The importance of using a crack growth curve that is an amalgam of the short and long crack growth curves was stressed in [4,5].

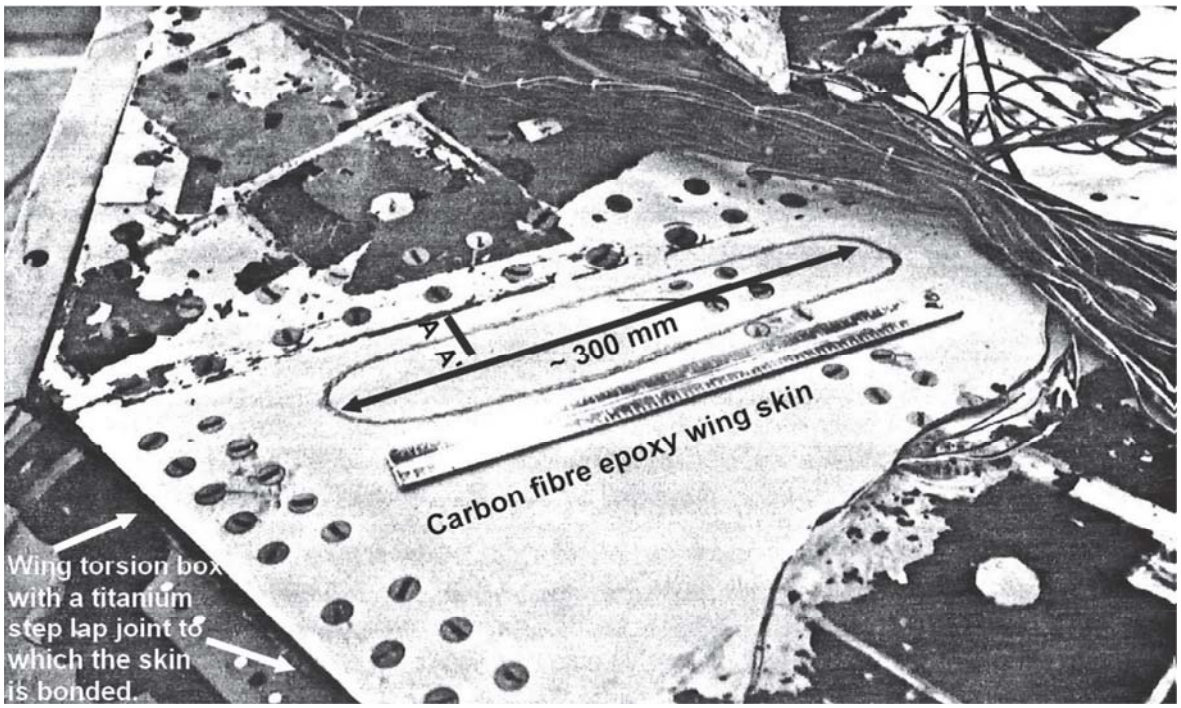

Figure 5.1: A large delamination seen in an early F/A-18 fatigue test at 1633 simulated flight hours, from [3]. The location of section A–A_0 shown in Figure 5.2 is also given.

(a)

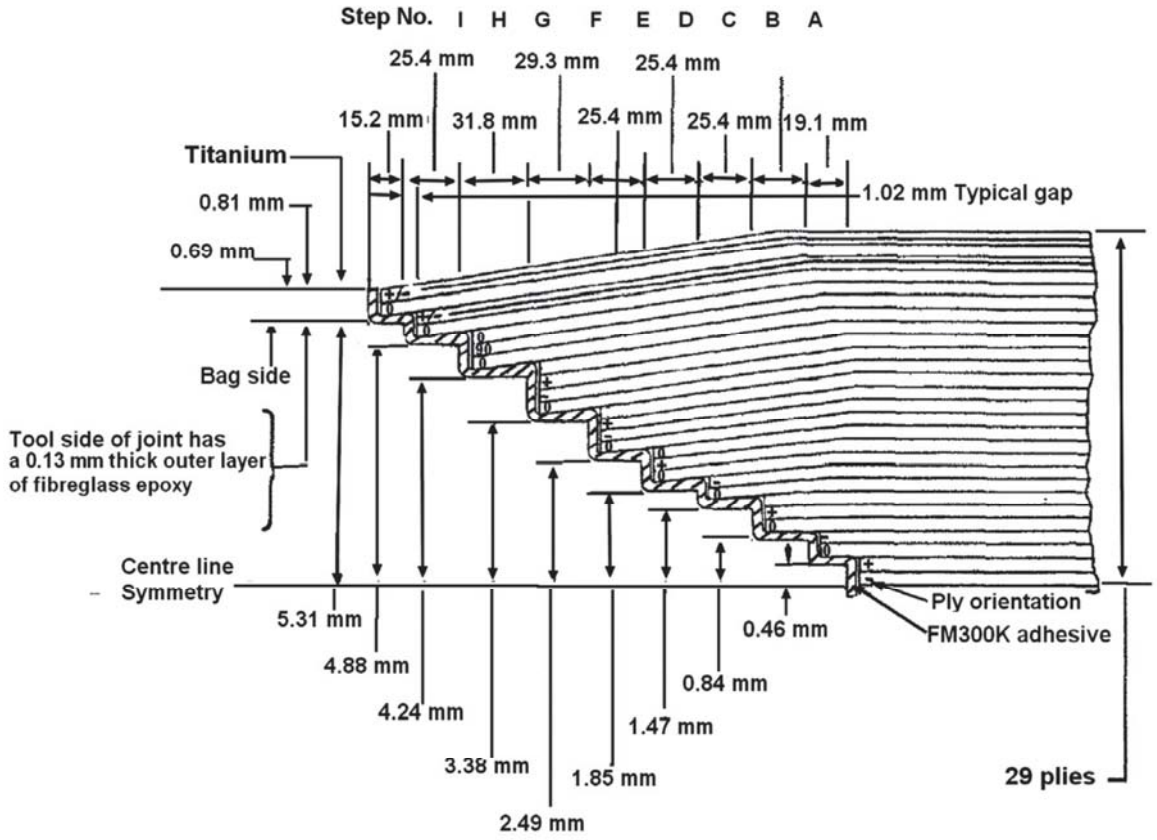

(b)

Figure 5.2: (a) Crossection A–A' of the step lap joint showing the location of the initial flaw and (b) details of the ply configuration.

In this context the USAF and Boeing evaluation of crack growth in F-15 aircraft [4] stated for Equivalent Initial Flaw Size (EIFS) that:

> *"Fig. 3 shows the short-crack correction to the long-crack data for both aluminum and titanium that McDonnell used for this study. The inclusion of the short-crack effect was key to the success of the program. The inclusion of the short-crack effect enabled McDonnell to pool the coupon test EIFSs derived from constant amplitude tests with the random flight-by-flight loaded test aircraft EIFSs. This is a significant finding in that earlier use of the long-crack threshold for crack growth made it appear that the equivalent initial flaws in the structure were spectrum dependent."*

Thus any analysis of the fatigue behavior of naturally occurring cracks in metal structures in operational aircraft requires an assessment of short crack behavior. Given that, as outlined above, small delaminations arise and grow in composites in operational aircraft this suggests that a means for assessing/computing the growth of delaminations from small naturally occurring material discontinuities in composite airframes is also important. In metals, as shown in [1,5–7], this behaviour can, as a first approximation, be determined from long crack data via Eq. (5.1) with the variability in the crack length versus cycles history being controlled by the parameter ΔK_{thr}.

$$\frac{da}{dN} = D\left(\frac{\Delta K - \Delta K_{thr}}{1 - K_{max}/K_{cy}}\right)^{\beta} \tag{5.1}$$

where D and K_{cy} are constants and the exponent β is approximately 2[4]. The question thus arises can this formulation be extended so as to apply to the Mixed Mode growth of delamination damage in composites?

The review paper [9] noted that there are several possible formulae in the literature, see [10–16], that have been used to relate da/dN to the energy release rates[5] some of which can be expressed in the form, viz:

$$\frac{da}{dN} = C\frac{G_{max}{}^{m}}{1 - G_{max}/G_C}; \tag{5.2}$$

$$\frac{da}{dN} = C_1\frac{G_{Imax}{}^{m}}{1 - G_{Imax}/G_{IC}} + C_2\frac{G_{IImax}{}^{n}}{1 - G_{IImax}/G_{IIC}} + C_3\frac{G_{IIImax}{}^{p}}{1 - G_{IIImax}/G_{IIIC}}; \tag{5.3}$$

$$\frac{da}{dN} = C_1\left(\sqrt{G_{Imax}} - \sqrt{G_{Imin}}\right)^{q}; \tag{5.4}$$

etc.

as well as variants that include various mode interaction terms [14].

---

[4] As such this formulation represents a variant of the Nasgro's Forman-Mettu crack growth equation [8], see Appendix A.

[5] With the exception of a standard test method for fatigue delamination growth onset under Mode I (tensile opening) load issued by the American Society for Testing and Materials (ASTM) [17], there are no standardized test methods for fatigue delamination growth in CFRP composites available yet. Both, Technical Committee 4 on Polymers, Composites and Adhesives of the European Structural Integrity Society (ESIS) and Subcommittee D30.06 on interlaminar properties of composites of ASTM have started round robin testing towards development of a Mode I fatigue delamination growth standard. These are essentially based on the existing quasi-static test procedures which are then adapted for fatigue loading. Preliminary results for Mode I fatigue [1, 18] and for Mode II fatigue [19] have been published.

Here the terms G_{Imax}, G_{IImax}, G_{IIImax} and G_{max} are the maximum values of the Mode I, II, and III components and the maximum value of the total energy release rate G in a given cycle respectively, G_{Imin} is the minimum values of the Mode I energy release rate, G_{Ic}, G_{IIc} and G_{IIIc} are the apparent toughness, and C, C_1, C_2, C_3, m, n, p and q are constants. Other variants of this equation have the term $(G_{max})^m$ replaced with $(\Delta G)^m$ etc. Unfortunately the exponents m, n, p and q in these various relationships tend to be large, see [1,10–16], and as a result [11] concluded:

> *"For composites, the exponents for relating propagation rate to strain energy release rate have been shown to be high especially in Mode I. With large exponents, small uncertainties in the applied loads will lead to large uncertainties (at least one order of magnitude) in the predicted delamination growth rate. This makes the derived power law relationships unsuitable for design purposes."*

In this context [1,20,21] have shown that there are a number of cases where as an extension to the Hartman and Schijve [22] hypothesis that the crack growth rate (da/dN) in metals is a function of $\Delta K – \Delta K_{thr}$, where ΔK_{thr} is related to the fatigue threshold for the material, and the work presented in [15,16] the delamination growth rate (da/dN) can be expressed as a function of $(\sqrt{G_{max}} – \sqrt{G_{thr}})^{\beta}$, viz:

$$\frac{da}{dN} = D\left(\frac{\sqrt{G_{max}}-\sqrt{G_{thr}}}{\sqrt{1-\sqrt{G_{max}/A}}}\right)^{\beta} \tag{5.5}$$

and/or variants based on $\Delta\sqrt{G}$ rather than $\sqrt{G}$. Here

$$\Delta\sqrt{G} = \sqrt{G_{max}}-\sqrt{G_{min}} \tag{5.6}$$

and G_{max} and G_{min} are the maximum and minimum values respectively of the total energy release rate G in a given cycle, A and G_{thr} can be thought of as a toughness like parameter and a threshold like respectively, which are chosen such that Eq. (5.5) best represents the experimental data, and the exponent ß is approximately 2 both for Mode I and Mode II delamination, see [1,20]. A similar formulation is presented in [23].

This begs the question: Is it possible to express delamination growth as a single function of G_{max} or ΔG with the same constant of proportionality and exponent regardless of the level of mode mixity?

This question needs to be answered before we attempt to address the earlier question as to the ability of this approach to use long delamination data to generate data that can approximate the behavior of small naturally occurring delaminations. To this end the present paper examines a number of cases that suggest that Eq. (5.5), with a value of b of approximately 2, is a reasonable first approximation for both Modes I and II as well as for Mixed Mode I/II delamination growth.

We have previously noted that researchers at NASA [11] have concluded that, because of the large exponents, Paris like power law relationships are unsuitable for design purposes. Furthermore, the exponents generally vary depending on the level of mode mixity. One advantage of this particular variant of the Nasgro equation, i.e. Eq. (5.5), is that it would appear that, for the examples studied, the value of the exponent is not large and is independent of the level of mode mixity. If it could be shown that this formulation also held for the growth of delaminations from small naturally occurring defects then this would raise the possibility that the time for a delamination to grow from a small naturally occurring defect to an observable size could be conservatively estimated using a simple Paris growth law with an exponent of approximately two. As such this would remove the design limitation suggested in [11] and, repeated above, that results when using more traditional Paris type representations.

5.2.4 Mode I and Mode II delamination growth

To examine this hypothesis we first examined the Mode I and Mode II delamination data given in [11,21] for a unidirectional AS4/PEEK laminate[6], see Figure 5.3. In each case we used equation (5.5) to compute the delamination growth rate. Here D was fixed at 7.0×10^{-10} and ß = 2 and we merely changed the threshold and the value of A, see Table 5.1. As can be seen this ‘‘unified’’ formulation (reasonably) accurately reproduces both of the measured Mode I and Mode II responses.

To further examine this hypothesis we analyzed the Mode I and Mode II delamination data given in [24] for T800/3631. In this case [24] expressed da/dN in terms of the stress intensity factor K, and not G. We therefore computed the

[6] Unless otherwise stated all of the examples studied are unidirectional laminates and the initial delamination lengths are large, i.e. greater than 20 mm.

growth rate using equation (5.1) where the terms ΔK, ΔK_{thr}, K_{max} and K_{cy} are the associated Mode I or Mode II values depending on the problem set being analyzed.

When computing the crack growth rates we used the values of $\beta = 2$ and $D = 7.0 \times 10^{-8}$ for both modes. The values of ΔK_{thr} were varied and were dependent on whether it was Mode I or Mode II growth and also on R, the ratio between minimum and maximum load, see Table 5.2.

For a given Mode the value of K_{cy} was kept fixed (independent of R). However, different K_{cy} values were used for Modes I and II. The complete list of values used in the analysis is given in Table 5.2.

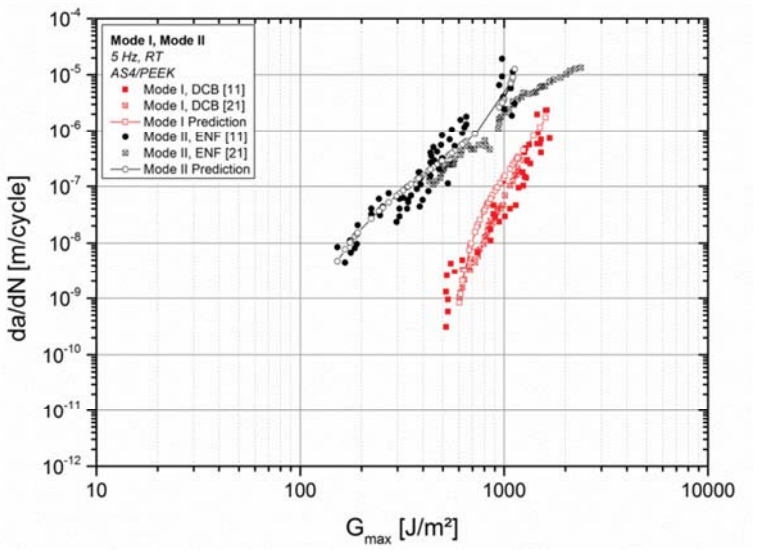

Figure 5.3: Computed and measured Modes I and II delamination in AS4/Peek [11,21].

Table 5.1: Values used in computing da/dN in Figure 5.3.

D	$7.0\ 10^{-10}$
β	2.0
Mode I Threshold	
G_{thr} (J/m^2)	570
A (J/m^2)	1700
Mode II Threshold	
G_{thr} (J/m^2)	105
A (J/m^2)	1200

The resultant measured and computed da/dN versus ΔK curves are shown in Figure 5.5 where it can be seen that this approach gave computed delamination growth curves that were (again) in quite good agreement with the measured data.

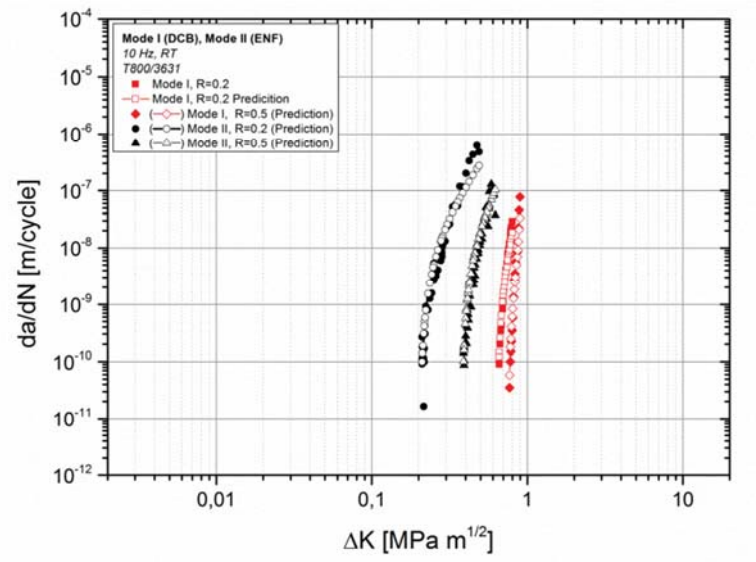

Figure 5.4: Measured and computed delamination rates for Mode I and Mode II delamination growth data, from [24].

Table 5.2: Values used in computing da/dN in Figure 5.4.

D	7.0×10^{-8}
β	2.0
Mode II K_{cy} (MPa √m)	6.2
Mode I K_{cy} (MPa √m)	1.4
Mode II Thresholds	
ΔK_{thr}, R = 0.2, (MPa √m)	1.01
ΔK_{thr}, R = 0.5, (MPa √m)	1.175
Mode I Thresholds	
ΔK_{thr}, R = 0.2, (MPa √m)	0.716
ΔK_{thr}, R = 0.5, (MPa √m)	0.525

To continue this study we examined the Mode I and Mode II data presented in [25] for T300/#3100 and the measured and computed delamination data are presented in Figure 5.5 where we again see reasonably good agreement. In each case D was fixed at 2.0 x 10^{-9} and β = 2. The values of the thresholds and the values of A used are given in Table 5.3.

We next examined the Mode I and Mode II data presented in [25] for 3 mm thick unidirectional (CFRP) Toho UT500/111 laminates. The measured and computed delamination data for Modes I and II at R = 0.1 and R = 0.5 are presented in Figure 5.6 where we again see reasonably good agreement. In each case D was fixed at 4.0 x 10^{-9} and β = 2. The values of the thresholds and the values of A used are given in Table 5.4.

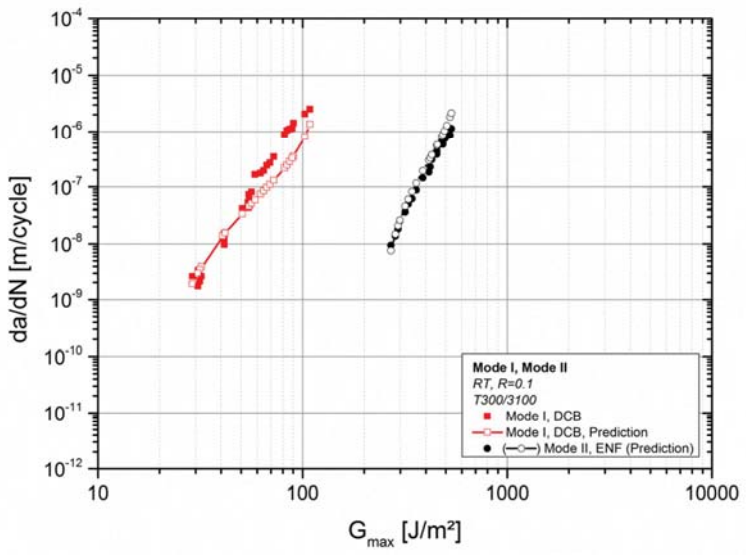

Figure 5.5: Measured and computed growth rates for the various test data given in [25].

Table 5.3: Values used in computing da/dN in Figure 5.5.

D	2.0 x 10^{-9}
β	2.0
Mode I	
G_{thr} (J/m^2)	235
A (J/m^2)	600
Mode 2	
G_{thr} (J/m^2)	22
A (J/m^2)	120

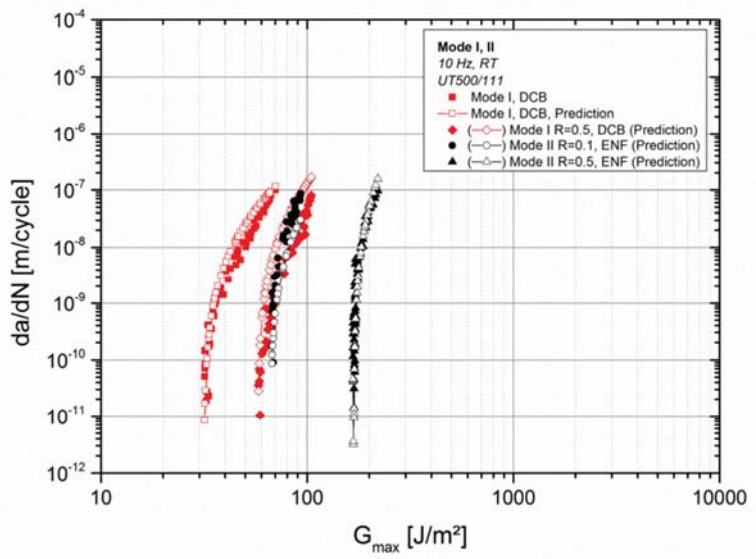

Figure 5.6: Measured and computed delamination rates for Mode I and Mode II delamination growth data, from [26].

Table 5.4: Values used in computing da/dN in Figure 5.6.

D	4×10^{-9}
β	2.0
Mode I	
G_{thr} (J/m^2) R = 0.5	57.3
G_{thr} (J/m^2) R = 0.1	31.5
A (J/m^2)	300
Mode I	
G_{thr} (J/m^2) R = 0.5	168
G_{thr} (J/m^2) R = 0.1	66
A (J/m^2)	450

5.2.5 Mixed mode I/II delamination growth

To continue this study we next examined the Mode I and Mixed Mode I/II delamination growth data presented in [27] for T300/5208. The Mode I delamination data was generated via DCB tests on $[(0_2/\pm45)_3/0]_s$ laminates whilst the Mixed Mode I/II data was obtained via cracked lap shear tests (CLS) on $[(0_2/\pm45_2/0_2]_s$ laminates where the ends of the specimens were not constrained against lateral movement. The CLS was such that the ratio G_{II}/G_{Total} was

approximately 80 %. The resultant computed and measured delamination data are shown in Figure 5.7.

In each case D was fixed at 4.0 x 10^{-8} and ß = 2. The corresponding values of the thresholds and the values of A used are given in Table 5.5. Given the scatter in the experimental data it again appears that this ‘‘unified’’ formulation reasonably accurately reproduces both the measured Mode I and Mode II response.

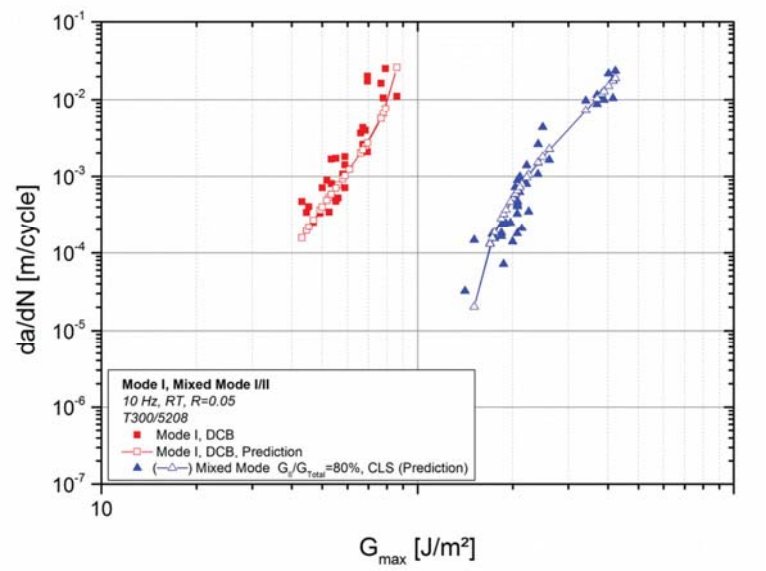

Figure 5.7: Measured and computed growth rates for the various test data given in [27].

Table 5.5: Values used in computing da/dN in Figure 5.7.

D	4.0 x 10^{-8}
β	2.0
Mode I	
G_{thr} (J/m^2)	30
A (J/m^2)	90
CLS	
G_{thr} (J/m^2)	139
A (J/m^2)	600

We next evaluated the room temperature (RT) Mixed Mode I/II da/dN versus G_{max}/G_{II} curves for various values of the ratio G_{II}/G_{Total}, viz: 0 (Mode I), 0.5, a mixed mode failure (MMF), and 1 (Mode II), presented in [28] for HTA/6376C carbon fibre/epoxy laminates. The resultant computed and measured curves are presented in Figure 5.8 where we again see a reasonable agreement. The values of A, which was taken from [28], and D used are given in Table 5.6.

Ref. [28] also presented the da/dN versus G_{max} curve for the case $G_{II}/G_{max} = 0.5$ tested at +100 °C. In this instance the da/dN versus G_{max} curve can be reasonably well computed using the room temperature value of D, together with the value of A given in [28] for this temperature and merely lowering the value of G_{th}, see Table 5.6 and Figure 5.9.

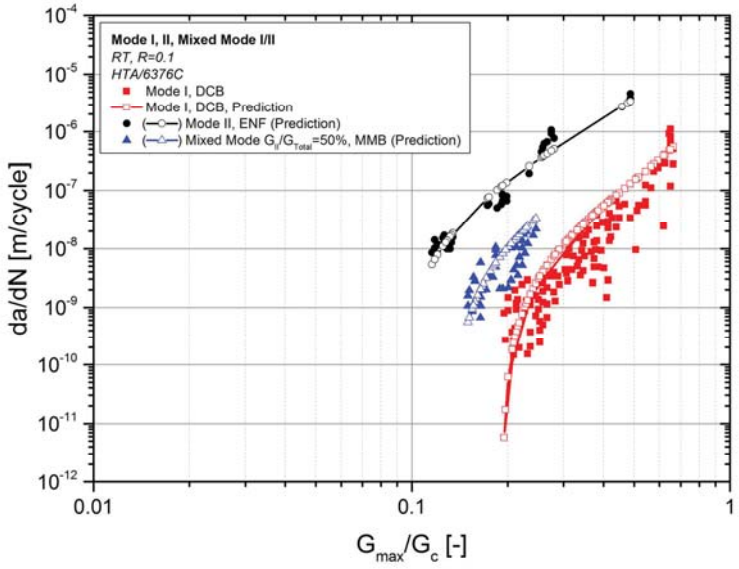

Figure 5.8: Measured and computed growth rates for the various test data given in [28].

The analysis was then repeated on the data sets presented in [29] where the measured growth rates, da/dN, were correlated with ΔG_{Total} (the total energy release rate) for various percentages of the ratio G_{II}/G_{Total}, viz: 82 %, 50 % and 28 % in a 52 % (vol) of E-glass fibre, 5 % of which were woven perpendicularly to hold the parallel fibers together with a Ml0 epoxy resin (VICOTEX) tested at R = 0.1. The measured and computed da/dN-versus-ΔG_{Total} relationships are shown in Figure 5.10 where we again see reasonably good agreement. The values of the constants used in this analysis are given in Table 5.7. Note that as previously D and ß (=2) are fixed for each Mode.

Table 5.6: Values used in computing da/dN in Figure 5.8 and Figure 5.9.

D	$6.7\ 10^{-12}$
β	2.0
Mode I	
G_{thr} (J/m^2)	50
A (J/m^2)	260
MMF	
G_{thr} (J/m^2)	60
A (J/m^2)	447
MMF (100°C)	
G_{thr} (J/m^2)	37
A (J/m^2)	535
Mode II	
G_{thr} (J/m^2)	93
A (J/m^2)	1002

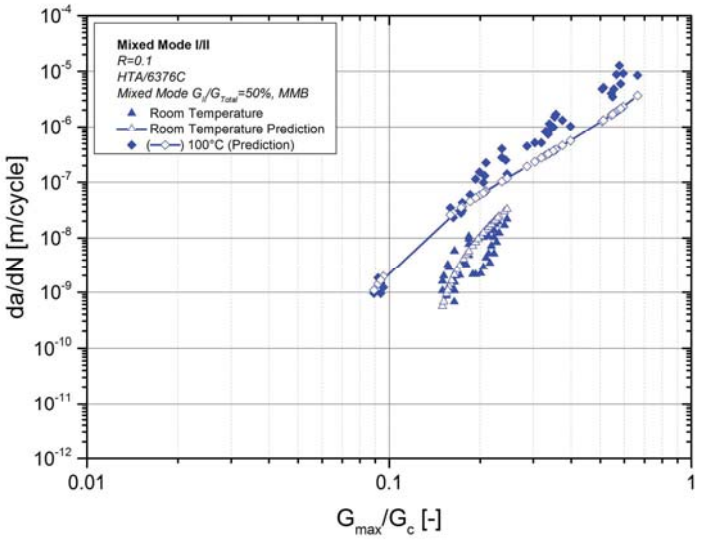

Figure 5.9: Measured and computed growth rates for the MMF test at room temperature and +100 °C [28].

We then evaluated the Mixed Mode I/II (fixed ratio 4:3) data for IM7/977-2 presented in [30]. The measured and computed results, using the constants presented in Table 5.8, are shown in Figure 5.11. The fixed-ratio Mixed Mode I/II prediction (finely dotted line) calculated from the pure Mode I and Mode II data (represented in Figure 5.11 by the coarser and finer dashed lines, respectively) is the weighted average in a ratio of 4:3 (Mode I to Mode II) of the highest and lowest G_{max} value of each pure Mode I and II, respectively.

The examples presented suggest that, as previously postulated, it is possible to express Mode I, Mode II and Mixed Mode I/II delamination growth as a single function of G_{max} or ΔG with the same constant of proportionality and exponent regardless of the level of mode mixity.

However, it should be stressed that the present formulation is empirical and that, due to lack of data, Mode III delamination growth has not been studied. Indeed, further work is also required to establish if this approach can be used to represent the variability seen in Mode I and Mode II delamination tests. The implications of this finding for the growth of delaminations from small naturally occurring material discontinuities will be discussed in the next section.

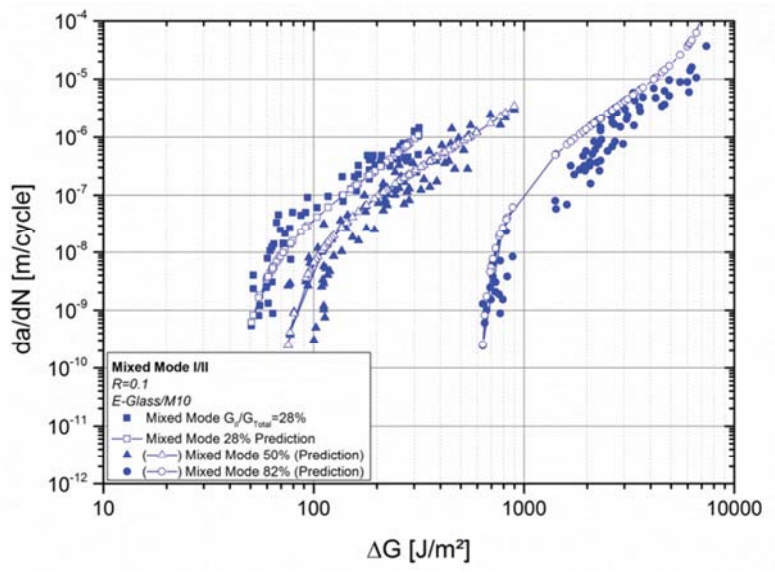

Figure 5.10: Measured and computed growth rates for the various test data given in [29].

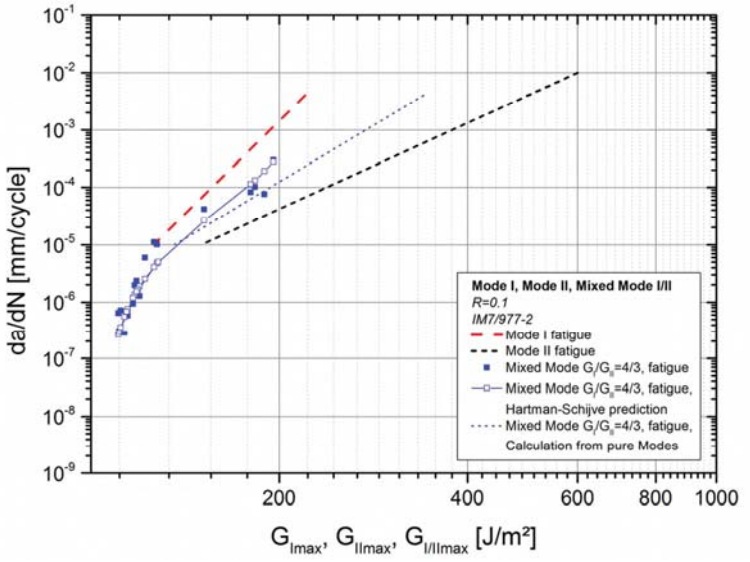

Figure 5.11: Mode I, Mode II and Mixed Mode I/II (fixed ratio 4:3) data for IM7/977-2 [30].

Table 5.7: Values used in computing da/dN in Figure 5.10.

D	1.8×10^{-9}
β	2.0
28 %	
ΔG_{thr} (J/m^2)	44
A (J/m^2)	555
50 %	
ΔG_{thr} (J/m^2)	70
A (J/m^2)	1754
82 %	
ΔG_{thr} (J/m^2)	622
A (J/m^2)	8888

Table 5.8: Values used in computing da/dN in Figure 5.11.

D	1.0×10^{-6}
β	2.0
G_{thr} (J/m^2)	105
A (J/m^2)	217

5.2.6 Naturally occurring delaminations

At the moment the strain limits imposed on composite structures are to a large extent the result of the requirement that there should be no delamination growth. To remove these somewhat artificial limits and allow for limited growth we need to be able to predict the Region I delamination growth, i.e. slow growth, associated with small naturally occurring defects in composites under arbitrary Mixed Mode conditions. As previously noted [1,3] have presented instances where there has been delamination growth associated with small naturally occurring material discontinuities in either operational aircraft or in full scale fatigue tests. Since the magnitude of the energy release rate is (in general) a function of the size/length of the delamination this suggests that for small naturally occurring defects in composites it would be reasonable to hypothesize that, as for metals (discussed in [4,5,31–34]), the Mode I, II and III thresholds for such small delaminations are very small. If true and if Eq. (5.5) could be shown to also hold for the growth of delaminations from small naturally occurring defects then conservative estimates for the initial delamination growth rates could be obtained by simplifying Eq. (5.5) and then ignoring threshold effects. Furthermore, since we are predominantly interested in the Region I growth of small naturally occurring delaminations it is reasonable to expect that, in this region, as a first approximation the term G_{max} should be small in comparison to the toughness A so that the term $(1-\sqrt{(G_{max}/A)})$ in Eq. (5.5) can also be neglected. With these assumptions Eq. (5.5) simplifies to:

$$da/dN = D\ (\sqrt{G_{max}})^{\beta} \tag{5.7}$$

or an equivalent equation based upon $\Delta\sqrt{G}$ so that a single equation could be used to compute delamination growth regardless of the delamination mode. In this approach the constant D and ß could be obtained from large delamination DCB tests with the values derived using Eq. (5.5) to represent the measured da/dN versus $\sqrt{G_{max}}$ (or ($\Delta\sqrt{G}$) curve. This would then provide a simple tool for determining a conservative estimate for the time for a small naturally occurring delamination to grow to a size where it would become detectable[7]. As such it is clear that, to validate this hypothesis, there is a need for experimental data associated with the growth of delaminations from small naturally occurring defects in composite structures.

[7] In the case of composite repairs to metallic structures [35] it is possible to routinely detect 6–10 mm long delaminations using either infra-red thermography or C-scans.

5.2.7 Conclusions

In the examples presented in this paper we see that the proposed variant of the Hartman-Schijve formulation appears to hold reasonably well for Mode I, Mode II and Mixed Mode I/II delamination growth. It also removes the large values of the exponent seen in Paris like formulation.

As such the examples presented in this paper reveal a potential for this approach, and therefore for the Nasgro equation, to be used to:

(a) Unify and simplify the description and analysis of Mixed Mode delamination growth;
(b) Allow the current no growth requirement associated with delamination damage in composite airframe designs to be relaxed.

This raises the following questions:

i. Does this mean that, if we know the threshold and toughness for Modes II and III, we can, as a first approximation, use the growth equation determined from Mode I DCB tests to describe Modes II and III delamination growth?

ii. Will this formulation also hold for the growth of delaminations that arise from small naturally occurring defects in composite airframes?

Whilst there is, as yet, insufficient data to answer these questions the various examples considered in this paper suggest that this approach is worthy of further investigation.

5.2.8 Appendix A. A generalisation of the Nasgro equation

The Nasgro crack growth equation [8], which is used in both Nasgro and AFGROW, can be written in the form:

$$da/dN = D\,\Delta K_{eff}^{(m-p)}\,(\Delta K_{eff} - \Delta K_{eff,thr})^{p}/(1-K_{max}/A)^{q} \qquad (5.A1)$$

where D is a constant, and ΔK_{eff} is the effective stress intensity factor[8], which as first explained by Elber [32], can be expressed in terms of a function U(R), viz:

$$\Delta K_{eff} = U(R)\,\Delta K \qquad (5.A2)$$

[8] The purpose of introducing the term ΔK_{eff} was to collapse the various R ratio da/dN versus ΔK curves onto a single da/dN versus ΔK_{eff} curve.

We can generalize this equation so as to apply to delamination growth in composites by replacing the term ΔK by $\Delta\sqrt{G}$ so that equation (5.A1) can be expressed as:

$$da/dN = D\ \Delta\sqrt{G_{eff}}^{(m-p)}\ (\Delta\sqrt{G_{eff}} - \Delta\sqrt{G_{thr,eff}})^p/(1-\sqrt{G_{max}}/A)^q \quad (5.A3)$$

or an equivalent version based on $\sqrt{G_{max}}$, viz:

$$da/dN = D\ \sqrt{G_{max,eff}}^{(m-p)}\ (\sqrt{G_{max,eff}} - \sqrt{G_{max,eff,thr}})^p/(1-\sqrt{G_{max}}/A)^q \quad (5.A4)$$

where as before we assume that there exists a function U(R) such that by defining

$$\Delta\sqrt{G_{eff}} = U(R)\ \Delta\sqrt{G} \quad (5.A5)$$

the various R ratio dependent da/dN versus $\Delta\sqrt{G}$ (or $\sqrt{G_{max}}$) curves reduce to a single da/dN versus $\Delta\sqrt{G_{eff}}$ (or $\sqrt{G_{max,eff}}$) curve which is (essentially) coincident with the high R ratio da/dN versus $\Delta\sqrt{G}$ (or $\sqrt{G_{max}}$) curve(s) for the material, see [1].

This equation contains the Hartman-Schijve-McEvily crack growth equation(s), viz:

$$da/dN = D\ (\Delta\sqrt{G_{eff}} - \Delta\sqrt{G_{thr,eff}})^p/(1-\sqrt{G_{max}}/A)^{p/2} \quad (5.A6)$$

or an equivalent version based on $\sqrt{G_{max}}$, viz:

$$da/dN = D\ (\sqrt{G_{max,eff}} - \sqrt{G_{max,eff,thr}})^p/(1-\sqrt{G_{max}}/A)^{p/2} \quad (5.A7)$$

as a special case, i.e. m = p and q = p/2.

If, as for metals [5,33,34], there is little crack tip shielding associated with delaminations that grow from small naturally occurring material discontinuities then for such small defects $\Delta\sqrt{G_{eff}}$ and $G_{max,eff}$ can be approximated by $\Delta\sqrt{G}$ and G_{max} respectively so that equations (5.A6) and (5.A7) become

$$da/dN = D\ (\Delta\sqrt{G} - \Delta\sqrt{G_{thr}})^p/(1-\sqrt{G_{max}}/A)^{p/2} \quad (5.A8)$$

and

$$da/dN = D\ (\sqrt{G_{max}} - \sqrt{G_{max,thr}})^p/(1-\sqrt{G_{max}}/A)^{p/2} \quad (5.A9)$$

respectively. However, this hypothesis, i.e. the vanishing of crack (delamination) tip shielding effects associated with small naturally occurring material discontinuities in composites, has yet to be substantiated.

5.2.9 References

[1] Jones R, Pitt S, Brunner AJ, Hui D. Application of the Hartman–Schijve equation to represent Mode I and Mode II fatigue delamination growth in composites. Compos Struct 2012;94(4):1343–51.

[2] van Blaricum TJ, Bates P, Jones R. An experimental investigation into the effect of impact damage on the compressive strength of step lap joints. Eng Fracture Mech 1989;32(5):667–74.

[3] MACAIR Report, LMA03.02-002R. Final report F/A-18 inner wing torque box assembly (PTOI).

[4] Lincoln JW, Melliere RA. Economic life determination for a military aircraft. AIAA J Aircraft 1999;36(5):737–42.

[5] Jones R, Tamboli D. Implications of the lead crack philosophy and the role of short cracks in combat aircraft. Eng Failure Anal 2013;29:149–66.

[6] Jones R, Molent L, Walker K. Fatigue crack growth in a diverse range of materials. Int J Fatigue 2012;40:43–50.

[7] Jones R, Molent L, Barter SA. Calculating crack growth from small discontinuities in 7050–T7451 under combat aircraft spectra. Int J Fatigue 2013;55:178–82.

[8] Forman RG, Mettu SR. Behavior of surface and corner cracks subjected to tensile and bending loads in Ti–6Al–4V Alloy. In: Ernst HA, Saxena A, McDowell DL, editors. Fracture mechanics 22nd symposium, ASTM STP 1131, Vol. 1. Philadelphia: American Society for Testing and Materials; 1992.

[9] Pascoe JA, Alderliesten RC, Benedictus R. Methods for the prediction of fatigue delamination growth in composites and adhesive bonds – a critical review. Eng Fracture Mech 2013;112–113:72–96.

[10] Ramkumar RL, Whitcomb JD. Characterization of Mode I and Mixed-Mode delamination growth in T300/5208 graphite epoxy. In: Johnson WS. (Ed.), Delamination and debonding of materials, ASTM STP 876; 1985, pp. 315–35.

[11] Martin RH, Murri GB. Characterization of mode I and mode II delamination growth and thresholds in AS4/PEEK composites. In: Garbo PS. (Ed.), ASTM STP 1059; 1990, pp. 251–70.

[12] Dahlen C, Springer GS. Delamination growth in composites under cyclic loads. J Compos Mater 1994;28(8):732–81.

[13] Tay TE, Williams JF, Jones R. Characterisation of pure and mixed mode fracture in composite laminates. Theor Appl Fracture Mechan 1987;7(2):115–23.

[14] Allegri G, Wisnom MR, Hallett SR. A new semi-empirical law for variable stress-ratio and mixed-mode fatigue delamination growth. Compos: Part A 2013;48:192–200.

[15] Khan R, Rans CD, Benedictus R. Effect of stress ratio on delamination growth behavior in unidirectional Carbon/Epoxy under mode I fatigue loading. In: Proceedings ICCM-17, Edinburgh; 2009.

[16] Alderliesten RC. Damage tolerance of bonded aircraft structures. Int J Fatigue 2009;31(6):1024–30.

[17] ASTM – American Society for Testing and Materials. ASTM D6115:1997 - Standard test method for mode I fatigue delamination growth onset of unidirectional fiber-reinforced polymer matrix composites.

[18] Brunner AJ, Murphy N, Pinter G. Development of a standardized procedure for the characterization of interlaminar delamination propagation in advanced composites under fatigue mode I loading conditions. Eng Fracture Mech 2009;76(18):2678–89.

[19] Brunner AJ, Stelzer S, Pinter G, Terrasi GP. Mode II fatigue delamination resistance of advanced fiber-reinforced polymer–matrix laminates: towards the development of a standardized test procedure. Int J Fatigue 2013;50:57–62.

[20] Jones R, Pitt S, Brunner AJ, Hui D. Fatigue crack growth in nano-composites. Compos Struct 2013;99:375–9.

[21] Stelzer S, Jones R, Brunner AJ. Interlaminar fatigue crack growth in carbon fiber reinforced composites. In: Hoa SV, Hubert P. (Eds.), Proceedings 19th international conference on composite materials. Canada; 2013, pp. 1689–1697.

[22] Hartman A, Schijve J. The effects of environment and load frequency on the crack propagation law for macro fatigue crack growth in aluminium alloys. Eng Fracture Mechan 1970;1(4):615–31.

[23] Xiang Y, Liu R, Peng T, Liu Y. A novel subcycle composite delamination growth model under fatigue cyclic loadings. Compos Struct 2014;108:31–40.

[24] Andersons J, Hojo M, Ochiai S. Empirical model for stress ratio effect on fatigue delamination growth rate in composite laminates. Int J Fatigue 2004;26(6):597–604.

[25] Mall S, Yun KT, Kochhar NK. Characterization of matrix toughness effect on cyclic delamination growth in graphite fiber composites. In: Lagace PA. (Ed.), Composite materials: fatigue and fracture, ASTM-STP 1012, vol. 2; 1989, pp. 296–310.

[26] Hojo M, Ando T, Tanaka M, Adachi T, Ochiai S, Yoshihiro E. Modes I and II interlaminar fracture toughness and fatigue delamination of CF/epoxy laminates with self-same epoxy interleaf. Int J Fatigue 2006;28:1154–65.

[27] Ramkumar RL. Performance of a quantitative study of instability-related delamination growth, NASA Contractor Report 166046. 1983

[28] Sjogren A, Asp LE. Effects of temperature on delamination growth in a carbon/epoxy composite under fatigue loading. Int J Fatigue 2002;24:179–84.

[29] Kenane M, Benzeggagh ML. Characterization of mixed mode delamination growth and thresholds. In: Boukharouba T et al., editors. Damage and fracture mechanics: failure analysis of engineering materials and structures. Springer Science+Business Media B.V; 2009. p. 523–30.

[30] Brunner AJ. Fracture mechanics of polymer composites in aerospace. In: Irving PE, Soutis C, editors. Polymer composites in the aerospace industry. Woodhead Publishing; 2014 [chapter 10].

[31] Wanhill RJH. Characteristic stress intensity factor correlations of fatigue crack growth in high strength alloys: reviews and completion of NLR investigations 1985–1990. NLR-TP-2009-256; 2009

[32] Elber W. The significance of fatigue crack closure, damage tolerance in aircraft structures, ASTM STP 486. Am Soc Test Mater 1971:230–42.

[33] Ritchie RO, Yu W, Blom AF, Holm DK. An analysis of crack tip shielding in aluminium alloy 2124: a comparison of large, small through-crack and surface fatigue cracks. Fatigue Fracture Eng Mater Struct 1987;10(5):343–63.

[34] McEvily AJ, Eifler D, Macherauch E. An analysis of the growth of short fatigue cracks. Eng Fracture Mechan 1991;40:571–84.

[35] Baker A, Jones R. Bonded repair of aircraft structure. The Hague: Martinus Nijhoff Publishers; 1988 (Book).

6 CONCLUSIONS TO PART II

Composite materials are increasingly used for structural applications in lightweight design due to their outstanding specific mechanical properties (e.g. ratio between stiffness and density). Yet, their application is limited because of their susceptibility to delamination. Under cyclic loading conditions delaminations can grow to a critical size at loads far below the static strength of the material. This will subsequently lead to failure of the composite structure, when damage is not monitored and repaired.

To date, there are no standardized test methods available for the determination of fatigue delamination growth in fiber reinforced polymer (FRP) composites. This is despite various reports on fatigue crack growth in composite structures [1–6]. In this thesis, fatigue delamination growth was examined in detail and pre-standardization tests were carried out with the aim to subsequently create a test procedure that allows to reproducibly measure and evaluate delamination growth in composite materials. Pre-standardization parameter studies on carbon FRP (CFRP) composites indicate that parameters which are governed by the test machine, such as test frequency (when kept below 10 Hz), control mode and type of test machine, show no significant influence on the test results. When specimen parameters (initial crack length and thickness) are varied, however, the results show the need for guidelines concerning these parameters.

Based on these preliminary findings, round robin testing towards the development of a mode I fatigue delamination growth standard was carried out within both, Technical Committee 4 on Polymers, Composites and Adhesives of the European Structural Integrity Society (ESIS) and Subcommittee D30.06 on interlaminar properties of composites of the American Society for Testing and Materials (ASTM). Two types of CFRP composites have been studied in the ESIS round robin tests, one thermoplastic poly-ether-ether-ketone (PEEK) matrix polymer reinforced with AS4 fibers and one thermoset epoxy polymer (R5276) reinforced with G30-600 fibers. The ASTM round robin covered two types of carbon fiber (IM7/977-3 and G40-800/5276-1) and one glass fiber (S2/5216) reinforced epoxy polymer. In spite of some scatter (in- and inter-laboratory), the slopes (exponents of the Paris law) of these materials could be clearly distinguished. Comparing materials based on slope values seems feasible and slope values could, in

principle, be used for design of composite structures. However, beside the scatter noted above, the slopes of fatigue delamination growth curves for composites turn out to be rather steep and show a large change in da/dN (sometimes more than one decade) even for a small change in applied load (G_{max}). Also, a comparison of composites solely based on slope values is not sufficient for describing the fatigue delamination growth behavior. Publication 2 additionally gives a comparison of strain energy release rates at a fixed value of crack growth rate. Although, in this case, this comparison of strain energy release rates coincides with the relative ranking from quasi-static tests, it does not give information on the behavior at other crack growth rates. Therefore, the determination of the threshold value would be beneficial. It is a material property that is influenced only by the applied load ratio, environmental effects (e.g. humidity), test temperature and intrinsic material properties (e.g. chemical structure, physical microstructure).

Detailed analysis of selected mode I fatigue crack propagation data from ESIS TC4 round robin tests and from literature indicate that an apparent, threshold-like behavior can be mimicked by limited resolution of the load measurements in displacement-controlled fatigue tests at da/dN values as high as 10^{-5} to 10^{-6} mm/cycle. Polynomial smoothing applied to the data analogous to the procedure for metals fatigue (ASTM E 647) does not seem to reduce the scatter sufficiently for eliminating this apparent threshold in all cases. Further, performing delamination growth tests at low delamination rates da/dN, e.g., 10^{-7} to 10^{-8} mm/cycle, will require high numbers of cycles to achieve measurable delamination growth (e.g., 5 million cycles at 10^{-8} mm/cycle for 50 micrometer growth). Therefore, verification of the existence of a threshold with virtually no delamination growth will require correspondingly longer test durations.

Data from preliminary mode II fatigue delamination resistance testing on two types of CFRP epoxy laminates show a significant effect of specimen restraint, when the three-point bending end-notched flexure test rig is being used. Without specimen restraint, the measured crack growth rate can deviate from the crack growth rate present in the specimen, when the specimen moves in the test set-up. With or without specimen restraint, the mode II fatigue delamination resistance for the composite material tested in this part of the thesis is higher than that determined from mode I loading for identical laminates. Hence, mode I fatigue data could still be used as a lower limit for design.

The applicability of the mode I fatigue delamination test to complex fracture problems, despite the problems encountered in round robin testing, is shown in

publication 5. Delamination tests on specimens produced via braiding and filament winding show that both monotonic and cyclic delamination testing is sensitive to changes in the fiber architecture of these materials. Both the thermoplastic stabilizer thread used for braiding unidirectional textiles and small changes in fiber alignment lead to increases in the fatigue delamination resistance. Even bigger increases in G_I and G_{II} can be achieved by the use of multi-directionally braided textiles in the CFRP laminate. This is caused by local changes in the loading mode. When the delamination is deflected from its original crack plane, mode II loading is locally imposed on the CFRP. This increases the fatigue delamination resistance and is indicated by hackle patterns on the fracture surface.

Further, it is shown in this part of the thesis that design based on the delamination fatigue properties is complex and erroneous when based on Paris type data representations. Applying data analysis schemes based on a modified Hartman-Schijve equation to the presentation of fatigue crack propagation data for FRP composites under mode I, mode II and mixed mode I/II loads yields suitable predictions for fatigue crack growth. The exponent value ß in this type of data representation amounts to around 2 within a margin of about 10 %. Further, the results become independent of the stress ratio (R value) and hence indicate that the R value affects only the threshold. Neither fiber bridging, nor closure need to be considered to obtain one single master curve. These results were later proved by Khan et al. [7], who related their research to publication 6 [8] and investigated the effects of crack closure and fiber bridging on delamination growth in composites. Detailed investigations will have to be carried out on other types of composite materials to prove these findings.

Experimentally, at present, a safe approach for fracture mechanics based FRP composite structural design would have to be based on laboratory fatigue tests on structural elements considering the load spectra from the intended application and implementing a sufficient safety factor in the number of cycles tested, while simultaneously monitoring delamination crack propagation or damage accumulation. Use of a ‘no growth’ approach with respect to cracks in CFRP composites design requires the existence of a threshold and/or the absence of anomalous short crack behavior. Even if a threshold can be shown to exist at some value of G_{max}, defining a safe value taking the inherent scatter in the experimental data into account could then result in very low values (possibly a few tens of J/m^2 or even lower) which effectively may exclude structural designs using that approach.

6.1 REFERENCES

[1] G. Savage, Sub-critical crack growth in highly stressed Formula 1 race car composite suspension components, Engineering Failure Analysis 16 (2009) 608–617.

[2] W. Seneviratne, J. Tomblin, T. Cravens, Durability and residual strength assessment of F/A-18 A-D wing-root stepped-lap joint, Proc. 11th AIAA ATIO Conference, AIAA Centennial of Naval Aviation Forum (2011).

[3] J. Schön, T. Nyman, A. Blom, H. Ansell, A numerical and experimental investigation of delamination behaviour in the DCB specimen, Composites Science and Technology 60 (2000) 173–184.

[4] E.S. Greenhalgh, Delamination growth in carbon-fibre composite structures, Composite Structures 23 (1993) 165–175.

[5] P. Chalkley, R. Geddes, Service history of the F-111 wing pivot fitting upper surface boron/epoxy doublers: DSTO-TN-0168. Department of Defence, September (1998).

[6] D.S. Cairns, T. Riddle, J. Nelson, Wind Turbine Composite Blade Manufacturing: The Need for Understanding Defect Origins, Prevalence, Implications and Reliability, Sandia Report 1094 (2011).

[7] R. Khan, R. Alderliesten, L. Yao, R. Benedictus, Crack closure and fibre bridging during delamination growth in carbon fibre/epoxy laminates under mode I fatigue loading, Composites Part A: Applied Science and Manufacturing 67 (2014) 201–211.

[8] R. Jones, S. Stelzer, A.J. Brunner, Mode I, II and Mixed Mode I/II delamination growth in composites, Composite Structures 110 (2014) 317–324.

Part III:

Delamination Suppression and joining

7 INTRODUCTION TO DELAMINATION SUPPRESSION AND JOINING

As shown in **publication 6** [1] delaminations can occur in structures under operational load, despite current no growth design philosophies. In the example given there, a delamination initiated at the last step of a titanium step lap joint in the AS4/3501-6 CFRP and grew during fatigue loading. Additional information can be found in [2]. Various other publications show that either interlaminar stresses, or manufacturing defects, or a combination of both can lead to the initiation of delaminations in composite structures during service [3–9].

Figure 7.1 gives examples for locations, where delaminations tend to initiate. Interlaminar stresses (caused e.g. by the geometry of the structure) exhibit the interlaminar strength of the composite (or the adhesive in adhesively bonded joints) and thus lead to the formation of cracks in this area [7,9–11]. With the exception of manufacturing defects (blisters, voids) [6] at least one of the sources for interlaminar stresses shown in Figure 7.1 is commonly present in composite joints and may lead to the initiation of delamination. Cairns et al. [6] even stated:

> *"…suppressing damage and delamination in-service emanating from ply drops is not possible, though in most cases there is a threshold loading under which little growth after initiation was noted…"*

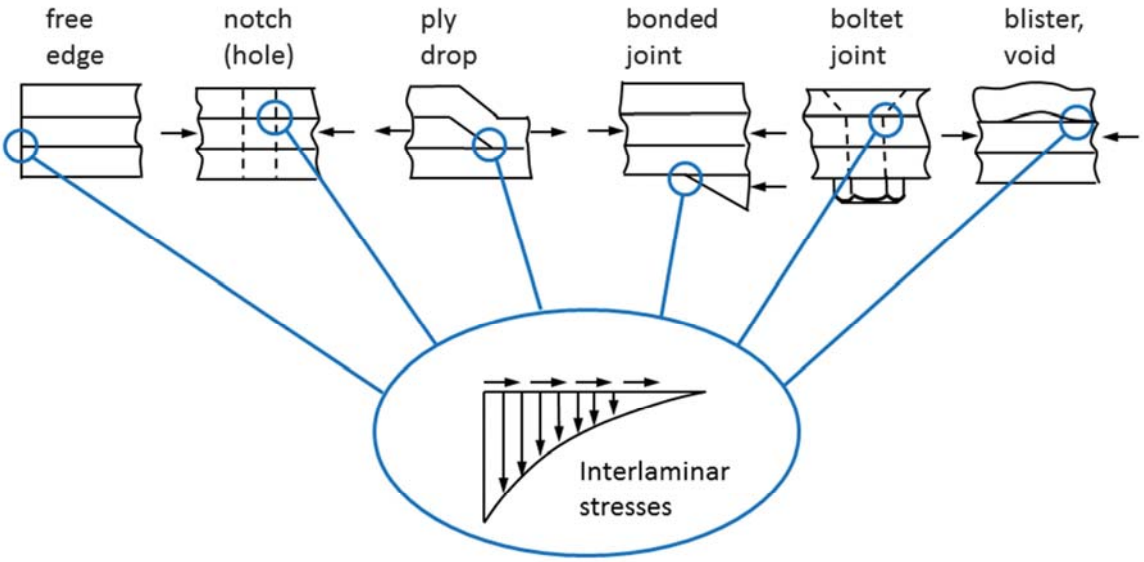

Figure 7.1: Interlaminar stresses in composites (adapted from [7,10–12]).

Although composite technology offers the advantage of reducing the need of structural coupling as a result of integral design and special manufacturing techniques, composite structures still show joined areas due to size, design, technological and logistic limitations. Other reasons are repair, maintenance and handling requirements [13].

7.1 CONVENTIONAL JOINING TECHNOLOGIES FOR COMPOSITES

Currently, composite structures are either joined by adhesive bonding or mechanical fastening. Adhesive bonding gives low weight joints and it is not necessary to cut fibers (e.g. by drilling holes). But bolt-free connections are sensitive to through-the-thickness or peel stresses, which can initiate delaminations in the bond line. Growth of these delaminations can lead to the subsequent failure of the composite structure [14]. Additionally they are sensitive to initial surface preparation and hot/wet environment. Together with the possibility of sudden catastrophic failure, these factors tend to lead to a conservative design approach (e.g. high safety factors, “chicken” rivets) [13,15].

In bolted joints cracks can initiate in fatigue loading due to stress concentrations and free edge effects at fastener holes (see Figure 7.1) [7,16]. Crack growth subsequently occurs in the joined laminates [14,17]. However, due to certification issues, bolts and rivets are commonly used in composite-composite joints in order to provide alternative load paths (multi load path design; load path redundancy) in case of failure of the adhesive bond [13].

But then again bolting and riveting have the mandatory need of drilling the composite and therefore cutting continuous fibers in the composite which are essential for the load transfer [18,19]. Moreover, the cross-section gets reduced, stress concentrations can appear around the holes and there is an imminent danger of delamination with drilling of composite materials [19–22].

It is thus an imperative goal in the design of composite structures to avoid interlaminar stresses and minimize the amount of joints in order to avoid the problems mentioned above. In cases, where this is not possible, it would be beneficial for designers to be provided with low weight, fiber-friendly alternatives to bolts and rivets.

7.2 THROUGH-THE-THICKNESS REINFORCEMENTS FOR CFRP

There are various approaches to reduce delamination by increasing the local shear strength and reducing interlaminar normal stresses in 2D composite materials. In recent years, research groups focused on incorporating fibers, fabrics and metallic rods in the through-the-thickness direction of laminates [14,23–26].

Such through-the-thickness reinforcement methods can be used to either establish a mechanical link between different plies of a laminate (structural reinforcement), or between two adhesively bonded laminates (joining reinforcement) [27]. Various authors have shown that z-pinning [28,29], tufting [26,30], as well as stitching [23,24,29,31–33] can increase the delamination resistance of FRPs. While tufting and stitching are textile techniques, where needles carry a thread through-the-thickness of a preform [23,26,31], z-pinning involves the insertion of pre-cured CFRP pins [14,26,34–39] or metallic rods [13,15,25,40–42] into the composite prior to curing.

Cox and Sridar [43] investigated the failure mechanisms of through-the-thickness reinforcements in CFRP-CFRP joints. In detailed microscopic observations they found that during failure (1) these reinforcements debond from the laminate and their pull out is resisted by friction, (2) axial tension develops in the rods during pull out, (3) the through thickness reinforcements shear through large strains and (4) the reinforcements plough through the laminate.

Based on this work, Cartié et al. [25] tested CFRP-CFRP joints which were reinforced with titanium and composite rods. When subjected to tensile loading (pull out from the matrix), the CFRP and titanium rods yielded similar load-displacement behavior. But when loaded in shear, the CFRP rods showed brittle failure, while the titanium rods deformed plastically. Consequently CFRP reinforced with titanium rods showed higher peak failure loads and higher ultimate displacement values than CFRP reinforced with CFRP rods.

Additionally, Cartié et al. [25] found a correlation between the insertion angle of the rods and the measured peak load in shear tests. Angles that favored rod failure gave higher loads than angles resulting in rod pull out. When rod failure was the dominant mechanism and opening of the specimen was constrained, titanium rod reinforced composites gave the highest peak loads.

Two conclusions can be drawn from these literature results: (1) Titanium (metallic) reinforcements allow for plastic deformation and can therefore add to the damage tolerance of a composite-composite joint. (2) Constraining opening displacements

in joints reinforced with titanium (metallic) rods gives the highest peak loads and ultimate displacement values.

While Cartié et al. [25] used constraining guides in their test rig to constrain opening displacements, these opening displacements may also be constrained locally, by introducing a form fit into the connection.

Different authors have investigated the effect of 3D shaped metallic reinforcements on the failure behavior of metal-composite joints [40,44–47].

Most of these authors based the formation of 3D shaped metal reinforcements on additive layer manufacturing (ALM) techniques [40,44,48]. This technology shows a low technology readiness level, but yields promising results regarding strength and damage tolerance [40,48]. Graham et al. [40] stated:

> *"For research purposes these techniques[9] are in many respects ideal, but they remain a costly option for industry. Cold metal transfer (CMT) is a relatively modern technique that allows droplets of molten metal wire to be deposited onto a substrate in progressive layers… This adapted additive layer technique effectively deposits the full length of the pin in a single action, and subsequently forms the head geometry as part of the breakoff process. It is generally possible to perform each of these processes on a range of metals including steel, aluminium and titanium."*

Ucsnik et al. [45] presented the CMT technique in 2008 with the aim to reinforce metal-composite joints in the through-the-thickness direction. This technology was later adapted by Stelzer et al. [49] to allow for joining composites to composites.

7.2.1 Cold metal transfer welded reinforcements for CFRP

The modified cold metal transfer welding process (CMT pin) is based on the CMT process by FRONIUS International [50]. The CMT process is a low-energy arc-welding process which allows the energy efficient welding of thin metal sheets in a material gentle manner. The adjustment of the welding control, welding current, voltage, and the wire movement are key issues for the modified CMT-pin process.

[9] Author's remark: Additive layer manufacturing

It consists of the following steps:

1. Warm up and filler wire deposit phase

   The filler wire is moved towards the weld-pool until a short cut ignites an electric arc between filler wire and metal sheet. The electric arc melts the metal surface and the filler wire. The end of the molten wire is moved towards the metal and is dipped into the weld-pool on the surface.

2. Cooling phase

   Energy input is stopped. The molten weld-pool and attached filler-wire cool down.

3. Pin sculpturing phase

   Shaping of the welding agent is carried out through introduction of a combination of electric current and tensile force. This leads to tearing off the wire at a certain height with a specific pin geometry.

Possible pin shapes are cylinder pins with a flat ending, spike pins with a tipped ending, and ballhead pins with a spherical ending [46]. The combination of a ballhead pin with a small spike pin on top results in a ballhead spike pin. The ballhead with its spherical undercut supports the load transfer. The tipped ending on top enhances the draping of dry or pre-impregnated fibers onto arrays of such pins.

When fiber-textiles are placed onto arrays of pins, the pins penetrate the single layers. They push aside the fibers and build up a loose form with only little influences on the fibers. After the curing process the pins form a through-the-thickness reinforcement with the composite [46].

In order to be able to join composites to composites, arrays of pins are disposed on thin metal sheets, see Figure 7.2. These thin sheets are then inserted into the bond area of a CFRP-CFRP joint. The metal sheets are fixed in the mold to provide reproducible pin alignment and positioning, see **publication 7** [51].

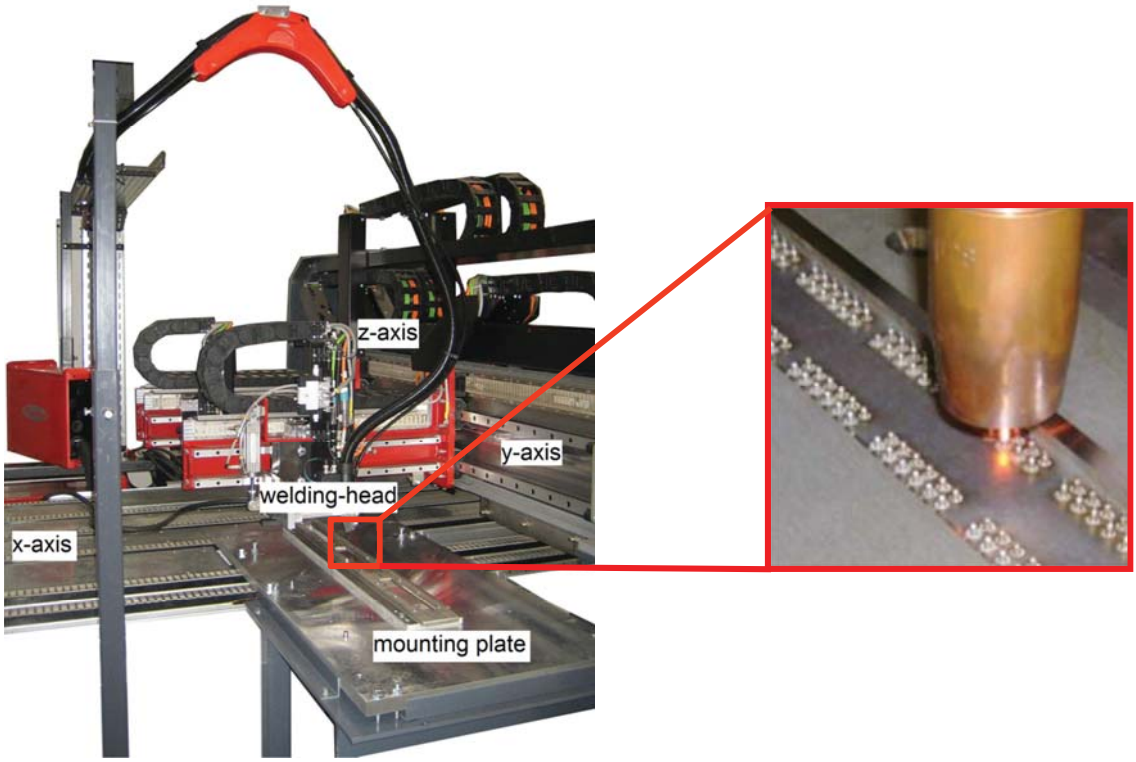

Figure 7.2: Welding of CMT pins onto thin metal sheets including a detail of the welding head during the welding process.

7.3 REFERENCES

[1] Jones R, Stelzer S, Brunner AJ. Mode I, II and Mixed Mode I/II delamination growth in composites. Composite Structures 2014;110(1):317–24.

[2] Baker AA, Dutton S, Kelly D. Composite materials for aircraft structures. 2nd ed. Reston, VA: American Institute of Aeronautics and Astronautics; 2004.

[3] Savage G. Sub-critical crack growth in highly stressed Formula 1 race car composite suspension components. Engineering Failure Analysis 2009;16(2):608–17.

[4] Schön J, Nyman T, Blom A, Ansell H. A numerical and experimental investigation of delamination behaviour in the DCB specimen. Composites Science and Technology 2000;60(2):173–84.

[5] Chalkley P, Geddes R. Service history of the F-111 wing pivot fitting upper surface boron/epoxy doublers: DSTO-TN-0168. Department of Defence, September 1998.

[6] Cairns DS, Riddle T, Nelson J. Wind Turbine Composite Blade Manufacturing: The Need for Understanding Defect Origins, Prevalence, Implications and Reliability. Sandia Report 2011;1094.

[7] Sierakowski RL, Newaz GM. Damage tolerance in advanced composites. Basel: Technomic Publishing AG; 1995.

[8] Dharan CKH. Delamination-based approach toward fracture control of composite spacecraft structures. Journal of Spacecraft and Rockets 1989;26(4):229–33.

[9] Martin RH. Incorporating interlaminar fracture mechanics into design. Proceedings of the Institution of Mechanical Engineers, Part L: Journal of Materials Design and Applications 2000;214(2):91–7.

[10] Flemming M, Roth S. Faserverbundbauweisen: Eigenschaften - Mechanische, konstruktive, thermische, elektrische, ökologische, wirtschaftliche Aspeke. Berlin: Springer; 2003.

[11] Sela N, Ishai O. Interlaminar fracture toughness and toughening of laminated composite materials: a review. Composites 1989;20(5):423–35.

[12] Garg AC. Delamination - a damage mode in composite structures. Engineering Fracture Mechanics 1988;29(5):557–84.

[13] Löbel T, Kolesnikov B, Scheffler S, Stahl A, Hühne C. Enhanced tensile strength of composite joints by using staple-like pins: Working principles and experimental validation. Composite Structures 2013;106:453–60.

[14] Allegri G, Zhang X. On the delamination and debond suppression in structural joints by Z-fibre pinning. Composites Part A: Applied Science and Manufacturing 2007;38(4):1107–15.

[15] Graham D, Rezai A, Baker D, Smith PA, Watts JF. A hybrid joining scheme for high strength multi-material joints. In: Proceedings of the 18th International Conference on Composite Materials. Jeju, South Corea; 2011.

[16] Saunders DS, Galea SC, Deirmendjian GK. The development of fatigue damage around fastener holes in thick graphite/epoxy composite laminates. Composites 1993;24(4):309–21.

[17] Fernlund G, Spelt JK. Mixed-mode fracture characterization of adhesive joints. Composites Science and Technology 1994;50(4):441–9.

[18] Andrews SD, Ochoa OO, Owens SD, Andrews SD, Ochoa OO, Owens SD. The Effects of Fastener Hole Defects. Journal of Composite Materials 1993;27(1):2–20.

[19] Suemasu H, Takahashi H, Ishikawa T. On failure mechanisms of composite laminates with an open hole subjected to compressive load. Composites Science and Technology 2006;66(5):634–41.

[20] Khashaba U. Delamination in drilling GFR-thermoset composites. Composite Structures 2004;63(3-4):313–27.

[21] Chen W. Some experimental investigations in the drilling of carbon fiber-reinforced plastics (CFRP) composite laminates. International Journal for Machining Tools and Manufacture 1997;37(8):1097–108.

[22] Davim JP, Reis P. Study of delamination in drilling carbon fiber reinforced plastics (CFRP) using design experiments. Composites Structures 2009;59:481–7.

[23] Aymerich F, Priolo P, Sun C. Static and fatigue behaviour of stitched graphite/epoxy composite laminates. Composites Science and Technology 2003;63(6):907–17.

[24] Mouritz A, Leong K, Herszberg I. A review of the effect of stitching on the in-plane mechanical properties of fibre-reinforced polymer composites. Composites Part A: Applied Science and Manufacturing 1997;28:979–91.

[25] Cartié D, Cox B, Fleck NA. Mechanisms of crack bridging by composite and metallic rods. Composites Part A: Applied Science and Manufacturing 2004;35(11):1325–36.

[26] Cartié DD, Dell'Anno G, Poulin E, Partridge IK. 3D reinforcement of stiffener-to-skin T-joints by Z-pinning and tufting. Engineering Fracture Mechanics 2006;73(16):2532–40.

[27] Noguiera AC, Drechsler K, Hombergsmeier E. Properties and failure mechanisms of a 3D-reinforced joint. JEC Composites Magazine 2011:39–44.

[28] Grassi M, Zhang X, Meo M. Prediction of stiffness and stresses in z-fibre reinforced composite laminates. Composites Part A: Applied Science and Manufacturing 2002;33(12):1653–64.

[29] Dickinson LC, Farley GL, Hinders MK. Translaminar Reinforced Composites: A Review. Journal of Composites Technology & Research 1999;21(1):3–15.

[30] Dell'Anno G, Cartié DD, Partridge IK, Rezai A. Exploring mechanical property balance in tufted carbon fabric/epoxy composites. Composites Part A: Applied Science and Manufacturing 2007;38(11):2366–73.

[31] Dransfield K, Baillie C, Mai Y. Improving the delamination resistance of CFRP by stitching—a review. Composites Science and Technology 1994;50(3):305–17.

[32] Sharma SK, Sankar BV. Effect of through-the-thickness stitching on impact and interlaminar fracture properties of textile graphite/epoxy laminates. NASA Contractor Report 1995;195042:1–140.

[33] Hinders M, Dickinson L. Trans-laminar-reinforced (TLR) composites. NASA GRANT 1997;1-1647:1–226.

[34] Cartié D, Partridge IK. Delamination behaviour of z-pinned laminates. European Structural Integrity Society 2000;27:27–36.

[35] Cartié DD, Troulis M, Partridge IK. Delamination of z-pinned carbon fibre reinforced laminates. Composites Science and Technology 2006;66(6):855–61.

[36] Lenzi F, Riccio A, Clarke A, Creemers R. Coupon Tests on z-Pinned and Unpinned Composite Samples for Damage Resistant Applications. Macromolecular Symposia 2007;247(1):230–7.

[37] Li R, Huong N, Crosky A, Mouritz A, Kelly D, Chang P. Improving bearing performance of composite bolted joints using z-pins. Composites Science and Technology 2009;69(7-8):883–9.

[38] Rugg KI, Cox BN, Massabò R. Mixed mode delamination of polymer composite laminates reinforced through the thickness by z-fibers. Composites Part A: Applied Science and Manufacturing 2002;33:170–90.

[39] Steeves CA, Fleck NA. In-plane properties of composite laminates with through-thickness pin reinforcement.

[40] Graham DP, Rezai A, Baker D, Smith PA, Watts JF. The development and scalability of a high strength, damage tolerant, hybrid joining scheme for

composite–metal structures. Composites Part A: Applied Science and Manufacturing 2014;64:11–24.

[41] Rugg KL, Cox BN, Ward KE, Sherrick GO. Damage mechanisms for angled through-thickness rod reinforcement in carbon–epoxy laminates. Composites Part A: Applied Science and Manufacturing 1998;29(12):1603–13.

[42] Son H, Park Y, Kweon J, Choi J. Fatigue behaviour of metal pin-reinforced composite single-lap joints in a hygrothermal environment. Composite Structures 2014;108:151–60.

[43] Cox BN, Sridhar N. A Traction Law for Inclined Fiber Tows Bridging Mixed-Mode Cracks. Mechanics of Advanced Materials and Structures 2002;9(4):299–331.

[44] Parkes PN, Butler R, Meyer J, Oliveira A de. Static strength of metal-composite joints with penetrative reinforcement. Composite Structures 2014;118:250–6.

[45] Ucsnik S, Pahr D. Investigation of novel composite-metal-joints. Proc. 11th Japanese-European Symposium on Composite Materials 2008.

[46] Ucsnik S, Scheerer M, Zaremba S, Pahr D. Experimental investigation of a novel hybrid metal–composite joining technology. Composites Part A: Applied Science and Manufacturing 2010;41(3):369–74.

[47] Ucsnik S, Tauchner J, Fleischmann M, Waldhör A. Mischbau-Fügetechnik für Metall-Composite-Lasteinleitungen. lightweightdesign 2013.

[48] Parkes PN, Butler R, Almond DP. Growth of damage in additively manufactured metal-composite joints. Proc. 15th European Conference on Composite Materials 2012:1–8.

[49] Stelzer S, Ucsnik S, Tauchner J, Unger T, Pinter G. Novel composite-composite joining technology with through the thickness reinforcement for enhanced damage tolerance. In: Hoa SV, Hubert P, editors. Proceedings of the 19th International Conference on Composite Materials: Canadian Association for Composite Structures and Materials; 2013, p. 4645–53.

[50] Schierl A. The CMT process, a revolution in welding technology. Welding in the world 2005;49:38.

[51] Stelzer S, Ucsnik S, Fuchs P, Pinter G. Mechanical characterization of a novel compositecomposite joining technology with through the thickness reinforcement for enhanced damage tolerance. Composite Science and Technology:submitted on 09/23/2014.

8 QUASI-STATIC TESTING OF COMPOSITE-COMPOSITE JOINTS

8.1 INTRODUCTION TO QUASI-STATIC TESTING OF THROUGH-THE-THICKNESS REINFORCED COMPOSITE-COMPOSITE JOINTS

Quasi-static tensile tests on composite-composite joints are commonly carried out on single lap shear (SLS) [1–3] or double lap shear (DLS) [4,5] specimens. Various authors analyzed the stress distributions in adhesively bonded lap joints under tensile loads. Early works by Adams and Peppiatt and by Hart-Smith showed that shear stress concentrations occur at the ends of the overlap region of SLS specimens [3,6–8].

The distribution of shear stresses in the bond line of adhesively bonded joints is governed by several factors such as (1) mechanical properties (stiffness, strength and plasticity) of the adhesive and the adherend [3], (2) thickness of the adhesive layer [7] and (3) length and width of the bond line [3].

While DLS specimens are loaded in a symmetrical manner with no bending moment in the loading arms, there is an eccentricity in the load path in SLS specimens. This eccentricity induces peel stresses at the ends of the overlap region [3,8]. Peel stresses act on the adhesive and, in the case of composite materials, can even lead to the interlaminar failure of the adherend, see Figure 7.1.

In structural applications it is thus essential to avoid load path eccentricity and resulting peel stresses in composite-composite joints. This can be achieved by using scarfed [9–13] or stepped joints [10,13]. Further, if load path eccentricity cannot be avoided, tapering the ends of the adherend will reduce the peel stresses in the joint. Scarfed and step-lap joints, when correctly designed, develop negligible peel stresses. As shown in Figure 7.2, this markedly increases the strength of the joint [13–17].

Grassi et al. showed in numerical simulations that z-pinning is another way to significantly reduce the interlaminar stresses at free edges. Z-Pins placed in the immediate vicinity of the free edge pick up the free edge stresses and hence reduce the maximum interlaminar peel stresses [18].

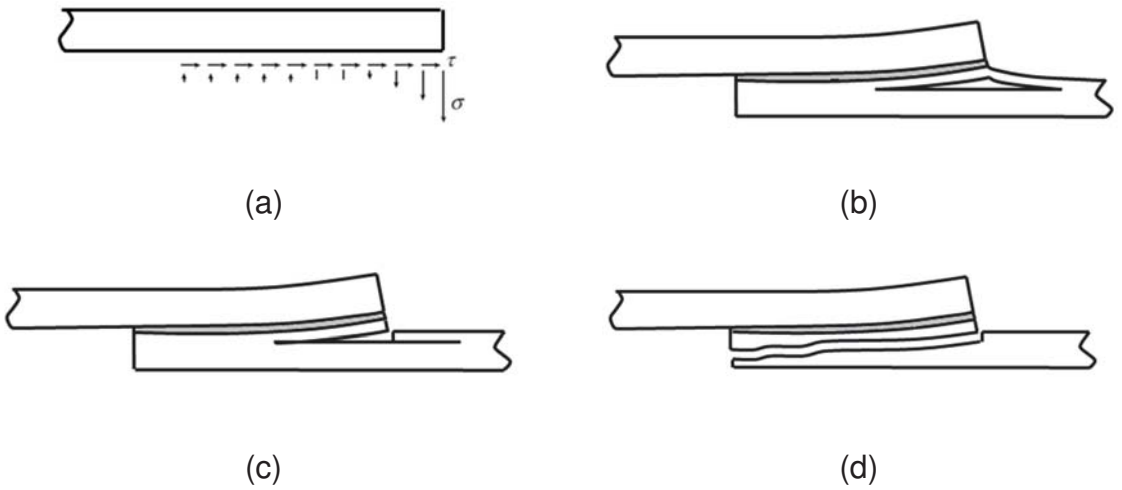

Figure 7.1: Schematic illustrations of interlaminar stresses in adhesive joints and subsequent failure of the composite adherend (adapted from [3,8]): (a) stress distribution in the bond line of the adherend, (b) delamination of the composite laminate, (c) interlaminar failure and breakage of the top ply (plies) of the composite laminate and (d) failure of the composite adherend.

Several authors have studied the effect of z-pinning on the fracture mechanical properties of composites (structural reinforcement) and composite-composite joints (joining reinforcement). Tests in mode I opening load were carried out on z-pin reinforced [19–28] and stitched [29–34] composites using DCB specimens. Tests in mode II shear loading were mainly done using 3ENF specimens. Examples are given for z-pinned [35–37] and stitched [20,32,33,38–40] composites. In all cases, energy absorption during failure was governed by pull-out of the through-the-thickness reinforcements.

Since CMT pins establish a form fit connection between the composite and the metal reinforcement, pull-out of the pins is prevented and instead of delamination growth in a defined plane within the specimen, there are numerous complex failure mechanisms that increase energy absorption during failure. Thus, fracture mechanical approaches towards the evaluation of the fracture behavior of CMT pin reinforced joints are not feasible.

In literature either SLS/DLS specimens [41–49] or T-joint specimens [50] are used to test the mechanical properties of joints with 3D reinforcements. Both test configurations have in common that they cause elevated peel stresses at the ends of the bond line [13]. Figure 7.2 shows the influence of adherend thickness and adherend geometry on the joint strength. Un-tapered SLS joints with thick adherends give the lowest joint strength, due to elevated peel stresses caused by

the geometry of the joint and by bending of the adherends due to the eccentric load path.

In order to investigate the worst case (lowest joint strength due to joint design, see Figure 7.2), un-tapered SLS specimens with thick adherends are used in this chapter to investigate the mechanical properties of CMT pin reinforced joints under quasi-static loading.

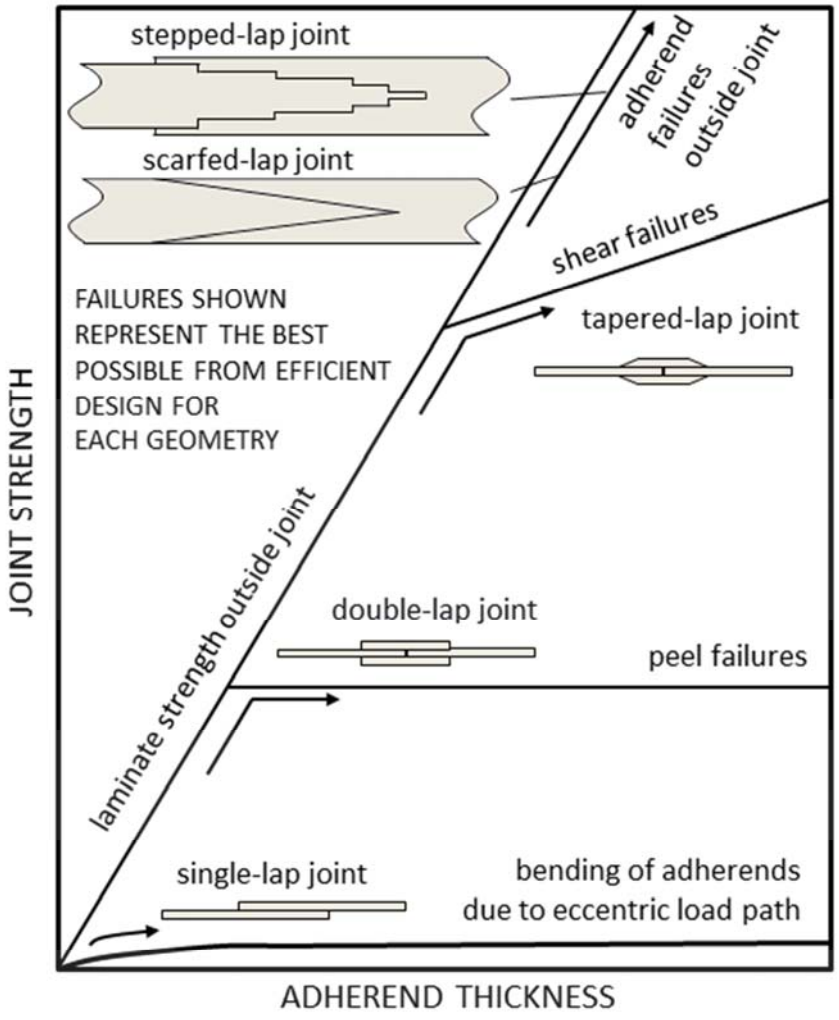

Figure 7.2: Schematic illustrations of load carrying capacity of adhesive joints (adapted from [13]).

8.1.1 References

[1] ASTM - American Society for Testing and Materials. D5868:01 - Standard test method for lap shear adhesion of fiber reinforced plastic bonding(D5868:01).

[2] ASTM - American Society for Testing and Materials. D3163:01 - Standard test method for determining strength of adhesively bonded rigid plastic lap-shear joints in shear by tension loading(D3163-01); 2012.

[3] Hart-Smith LJ. Adhesive-bonded single-lap joints: CR 112236: NASA Technical Report; 1973.

[4] ASTM - American Society for Testing and Materials. D3528:96 - Standard Test Method for Strength Properties of Double Lap Shear Adhesive Joints by Tension Loading.

[5] Hart-Smith LJ. Adhesive-bonded double-lap joints: CR-112235: NASA Technical Report; 1973.

[6] Adams RD, Peppiatt NA. Effect of poisson's ratio strains in adherends on stresses of an idealized lap joint. The Journal of Strain Analysis for Engineering Design 1973;8(2):134–9.

[7] Adams RD, Peppiatt NA. Stress analysis of adhesive-bonded lap joints. The Journal of Strain Analysis for Engineering Design 1974;9(3):185–96.

[8] da Silva L, Campilho R. Design of adhesively-bonded composite joints. In: Vassilopoulos AP, editor. Fatigue and fracture of adhesively-bonded composite joints. Cambridge: Woodhead Publishing; 2015, p. 43–71.

[9] Campilho, R. D. S. G., de Moura, M. F. S. F., Domingues, J. J. M. S. Stress and failure analyses of scarf repaired CFRP laminates using a cohesive damage model. Journal of Adhesion Science and Technology 2007;21(9):855–70.

[10] Ahn S, Springer GS. Repair of Composite Laminates; 2000.

[11] Adkins DW, Byron Pipes R. End effects in scarf joints. Composites Science and Technology 1985;22(3):209–21.

[12] Wang CH, Gunnion AJ. Optimum shapes of scarf repairs. Composites Part A: Applied Science and Manufacturing 2009;40(9):1407–18.

[13] Baker AA, Dutton S, Kelly D. Composite materials for aircraft structures. 2nd ed. Reston, VA: American Institute of Aeronautics and Astronautics; 2004.

[14] Cherry BW, Harrison NL. Note: The Optimum Profile for a Lap Joint. The Journal of Adhesion 1970;2(2):125–8.

[15] Adams RD, Atkins RW, Harris JA, Kinloch AJ. Stress Analysis and Failure Properties of Carbon-Fibre-Reinforced-Plastic/Steel Double-Lap Joints. The Journal of Adhesion 1986;20(1):29–53.

[16] Rispler AR, Tong L, P. Steven G, Wisnom MR. Shape optimisation of adhesive fillets. International Journal of Adhesion and Adhesives 2000;20(3):221–31.

[17] Hart-Smith LJ. Designing to minimize peel stresses in adhesive-bonded joints. In: Johnson WS, editor. Delamination and debonding of materials: ASTM STP 876. West Conshohocken, PA: American Society for Testing and Materials; 1985, p. 238–66.

[18] Grassi M, Zhang X, Meo M. Prediction of stiffness and stresses in z-fibre reinforced composite laminates. Composites Part A: Applied Science and Manufacturing 2002;33(12):1653–64.

[19] Chen L, Sankar BV, Ifju PG. A new mode I fracture test for composites with translaminar reinforcements. Composites Science and Technology 2002;62:1407–14.

[20] Chengye Fan, Ben Jar P, Cheng JR, Davies P. Mode II Delamination Toughness in Glass Fiber-Reinforced Polymers with Bridging Fibers and Stitching Threads. Journal of Reinforced Plastics and Composites 2009;28(14):1689–703.

[21] Dantuluri V, Maiti S, Geubelle PH, Patel R, Kilic H. Cohesive modeling of delamination in Z-pin reinforced composite laminates. Composites Science and Technology 2007;67(3-4):616–31.

[22] Dransfield KA, Jain LK, Mai Y. On the effects of stitching in CFRPs - I. Mode I delamination toughness. Composites Science and Technology 1998;58:815–27.

[23] Grassi M, Zhang X. Finite element analyses of mode I interlaminar delamination in z-fibre reinforced composite laminates. Composites Science and Technology 2003;63(12):1815–32.

[24] Iwahori Y, Nakane K, Watanabe N. DCB test simulation of stitched CFRP laminates using interlaminar tension test results. Composites Science and Technology 2009;69(14):2315–22.

[25] Jain LK, Dransfield KA, Mai Y. Effect of Reinforcing Tabs on the Mode I Delamination Toughness of Stitched CFRPs. Journal of Composite Materials 1998;32(22):2016–41.

[26] Jain LK, Mai YW. Mode I delamination toughness of laminated composites with through-thickness reinforcement. Applied Composite Materials 1994;1:1–17.

[27] Partridge IK, Cartié DD. Delamination resistant laminates by Z-Fiber® pinning: Part I manufacture and fracture performance. Composites Part A: Applied Science and Manufacturing 2005;36(1):55–64.

[28] Sridhar N, Massabò R, Cox BN, Beyerlein IJ. Delamination dynamics in through-thickness reinforced laminates with application to DCB specimen. International Journal of Fracture 2002;118:119–44.

[29] Aymerich F, Priolo P, Sun C. Static and fatigue behaviour of stitched graphite/epoxy composite laminates. Composites Science and Technology 2003;63(6):907–17.

[30] Jain LK, Mai YW. On the effect of stitching on mode I delamination toughness of laminated composites. Composites Science and Technology 1994;51:331–45.

[31] Mouritz AP, Baini C, Herszberg I. Mode I interlaminar toughness properties of advanced textile fibreglass composites. Composites Part A: Applied Science and Manufacturing 1999;30:859–70.

[32] Mouritz AP, Jain LK. Further validation of the Jain and Mai models for interlaminar fracture of stitched composites. Composites Science and Technology 1999;59:1653–62.

[33] Plain KP, Tong L. An experimental study on mode I and II fracture toughness of laminates stitched with a one-sided stitching technique. Composites Part A: Applied Science and Manufacturing 2011;42(2):203–10.

[34] Velmurugan R, Solaimurugan S. Improvements in Mode I interlaminar fracture toughness and in-plane mechanical properties of stitched glass/polyester composites. Composites Science and Technology 2007;67(1):61–9.

[35] Bianchi F, Zhang X. Predicting mode-II delamination suppression in z-pinned laminates. Composites Science and Technology 2012;72(8):924–32.

[36] Cox BN, Sridhar N. A Traction Law for Inclined Fiber Tows Bridging Mixed-Mode Cracks. Mechanics of Advanced Materials and Structures 2002;9(4):299–331.

[37] Jain LK, Dransfield KA, Mai Y. On the effects of stitching in CFRPs - II. Mode II delamination toughness. Composites Science and Technology 1998;58:829–37.

[38] Jain LK, Mai YW. Determination of mode II delamination toughness of stitched laminated composites. Composites Science and Technology 1995;55:241–53.

[39] Massabò R, Mumm DR, Cox BN. Characterizing mode II delamination cracks in stitched composites. International Journal of Fracture 1998;92:1–38.

[40] Sankar BV, Sharma SK. Mode II delamination toughness of stitched graphite/epoxy textile composites. Composites Science and Technology 1997;57:729–37.

[41] Noguiera AC, Drechsler K, Hombergsmeier E. Analysis of the Static and Fatigue Strength of a Damage Tolerant 3D-Reinforced Joining Technology on Composite Single Lap Joints. In: Ouwehand L, editor. Proc. 12th European Conference on Spacecraft Structures, Materials and Environmental Testing; 2012.

[42] Noguiera AC, Drechsler K, Hombergsmeier E, Furfari D, Pacchione M. Investigation of a hybrid 3D-reinforced joining technology for lightweight structures. In: Ferreira (Hg.) 2011 – 16th International Conference on Composite Materials.

[43] Graham D, Rezai A, Baker D, Smith PA, Watts JF. A hybrid joining scheme for high strength multi-material joints. In: Proceedings of the 18th International Conference on Composite Materials. Jeju, South Corea; 2011.

[44] Graham DP, Rezai A, Baker D, Smith PA, Watts JF. The development and scalability of a high strength, damage tolerant, hybrid joining scheme for composite–metal structures. Composites Part A: Applied Science and Manufacturing 2014;64:11–24.

[45] Ucsnik S, Gradinger R. Evaluation of a Novel Lightweight Metal-Composite-Joint Technology. Proc. 14th European Conference on Composite Materials 2010(paper ID 311-ECCM14).

[46] Ucsnik S, Pahr D. Investigation of novel composite-metal-joints. Proc. 11th Japanese-European Symposium on Composite Materials 2008.

[47] Ucsnik S, Scheerer M, Zaremba S, Pahr D. Experimental investigation of a novel hybrid metal–composite joining technology. Composites Part A: Applied Science and Manufacturing 2010;41(3):369–74.

[48] Parkes PN, Butler R, Almond DP. Growth of damage in additively manufactured metal-composite joints. Proc. 15th European Conference on Composite Materials 2012:1–8.

[49] Parkes PN, Butler R, Meyer J, Oliveira A de. Static strength of metal-composite joints with penetrative reinforcement. Composite Structures 2014;118:250–6.

[50] Heimbs S, Nogueira A, Hombergsmeier E, May M, Wolfrum J. Failure behaviour of composite T-joints with novel metallic arrow-pin reinforcement. Composite Structures 2014;110:16–28.

8.2 PUBLICATION 7

MECHANICAL CHARACTERIZATION OF A NOVEL COMPOSITE-COMPOSITE JOINING TECHNOLOGY WITH THROUGH-THE-THICKNESS REINFORCEMENT FOR ENHANCED DAMAGE TOLERANCE

8.2.1 Bibliographic Information

- Authors and their relevant contributions to the publication:
  - Steffen Stelzer[1]
    Preparation and submission of the manuscript, execution of all experimental tests, calculation and analysis of all test results.
  - Stephan Ucsnik[2]
    Project co-ordination and expert knowledge on cold metal transfer welding.
  - Peter Fuchs[3]
    Numerical simulations and analysis.
  - Gerald Pinter[1]
    Academic supervision of the work carried out in this publication.
- Affiliations:
  [1] Institute of Materials Science and Testing of Polymers, Montanuniversitaet Leoben, Leoben, Austria
  [2] Leichtmetallkompetenzzentrum Ranshofen GmbH, Austrian Institute of Technology, Lamprechtshausenerstraße Postfach 26, A-5282 Ranshofen, Austria
  [3] PCCL, Polymer Competence Center Leoben GmbH, Roseggerstrasse 12, A-8700 Leoben, Austria
- Periodical: submitted to Composites Science and Technology
- Manuscript number: CSTE-D-14-01150R1

Statement with regard to publication: The manuscript presented here is an adapted accepted manuscript in order to fit the formatting of the thesis and does not necessarily reflect the actually published version.

8.2.2 Abstract

A novel composite-composite joining technology based on metal pins oriented in through thickness direction of the composites is presented. A defined pin geometry, which is capable of establishing a through-thickness form-fit connection between composites and the metal reinforcement, is created on thin metal sheets in an automated pin production process. Based on numerical simulations of the fracture of unreinforced single lap shear (SLS) composite specimens, optimum locations for the pin reinforcement were found. Tests on reinforced SLS specimens proved that an enhanced damage tolerance can be achieved by the use of cold metal transfer welded pins (CMT pins) as through-the-thickness reinforcement for the joint area. This paper investigates the mechanisms responsible for the load transfer and failure of such through-the-thickness reinforced composite-composite joints during monotonic loading.

8.2.3 Introduction

Along with the growing use of carbon fiber reinforced polymers (CFRP) for structural applications comes the demand for advanced joining technologies which rise up to the potential such a material possesses. Special care has to be taken of fiber alignment and out-of-plane stresses because of the anisotropic behavior of single CFRP sheets and the laminar structure of composites. There are areas in the CFRP that are especially prone to out-of-plane loads. These are e.g. free edges, notches (holes) and ply drops [1].

Conventional bonding technologies like adhesive bonding, bolting and riveting only partly meet the challenges imposed on the joint by the properties of the CFRP. Bolting and riveting for example have a mandatory need for drilling the CFRP and therefore cutting the continuous fibers in the CFRP, which are essential for the load transfer [2–5]. Moreover, the laminate's cross-section gets reduced, stress concentrations appear around the holes and there is an imminent danger of delamination with drilling of fiber reinforced polymers [5–7]. Adhesive bonding on the other hand can transfer out-of-plane or peel stresses only to a limited extent, it possesses low bonding strength and requires wide joining areas [8].

Various 3D reinforcement methods have been studied over the recent years with the goal to establish either a mechanical link between the different plies of the laminate (structural reinforcement), or between two adhesively bonded laminates (joining reinforcement). Tufting [9,10], stitching [11–15] and z-pinning [9,16–20] are examples of structural reinforcement methods. These methods typically use

dry polymeric yarns, or pre-cured carbon fiber rods as through-the-thickness reinforcement. Another approach is the use of metallic reinforcements, which combine high strength with the ability for plastic deformation and therefore increase energy absorption and damage tolerance of the joints [21–27].

Cartié et al. [25] showed that for composite-composite joining titanium z-pins can be superior to composite z-pins due to plastic deformation, especially when pull-out of the z-pins is suppressed. Recently, research groups made use of 3D shaped metallic through-the-thickness reinforcements for composite-composite joining [22,28–30].

The herein presented novel joining technology for CFRP to CFRP joints aims at combining the joining mechanisms form-fit and adhesive-bonding, with an integrative, metallic joint approach [31–33]. Arrays of vertical elevations (pins) are disposed on thin metal sheets through the modified cold metal transfer welding process (CMT pin) [34]. These metal sheets are later placed in the stacking sequence of the composite.

The underlying CMT process is a low-energy arc-welding process which allows the energy efficient welding of thin metal sheets in a material gentle manner. The adjustment of the welding control, welding current, voltage, and the wire movement are key parameters, when welding pins on metal sheets through CMT pinning [31,34].

Possible pin shapes are cylinder pins with a flat ending, spike pins with a tipped ending, and ballhead pins with a spherical ending [32]. The combination of a ballhead pin with a small spike pin on top results in a ballhead spike pin. The spherical undercut of the ballhead ending supports the form-fit and the load transfer. A tipped ending on top of the pin facilitates the draping of dry or pre-impregnated fibers onto arrays of such pins. When fiber-textiles are placed onto arrays of CMT pins, the CMT pins penetrate the single layers. They push aside the fibers and build up a loose form fit with the fibers. After the curing process the CMT pins form a through-the-thickness reinforcement with the composite [32,35].

Ucsnik et al. [36] investigated the capability of CMT pins for joining metal to CFRP on sub-component level. Tests on Double Lap Shear (DLS) specimens and parts for serial production (Figure 8.3) showed that CMT pins can compete with Hi-Lok® joints at significantly lower weight. DLS specimens reinforced with CMT pins reached 50.6 % higher failure loads than Hi-Lok® riveted specimens at the same level of applied mass.

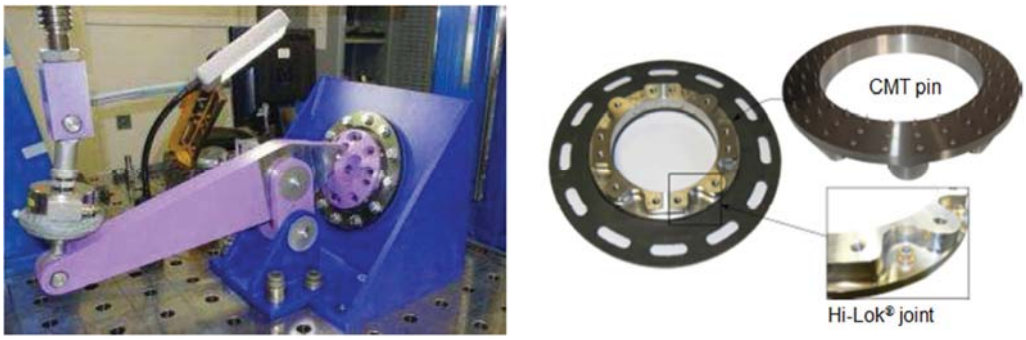

(a) (b)

Figure 8.3: Subcomponent-tests with a 2D load on a representative support ring fixation assembly of a flap trade fairing (Ucsnik et al. 2013 [36]): (a) test set-up, (b) metal to CFRP ring connection, one with CMT pins, one with Hi-Lok® rivets. Reprinted with permission from [36].

Subcomponents reinforced with CMT pins could carry about 80% of the loads of subcomponents that were riveted with 8 Hi-Lok® joints. Thereby, the mass of the CMT pins was 93 % lower than the mass of the Hi-Lok® joints, without any secondary mass savings being taken into account. Various other authors have investigated the applicability of different pin shaping technologies to metal-composite joining [37–39].

For this paper, the CMT joining technology used by Ucsnik et al. is adapted, so that it allows to join composites to composites. It focuses on the investigation of mechanisms, which are actively involved in the load transfer and failure behavior of CFRP to CFRP joints, which are reinforced with CMT pins in the out-of-plane direction.

8.2.4 Experimental

8.2.4.1 Composite material and specimen geometries

The CFRP used in this work consisted of epoxy resin from Hexcel Composites (Hexflow® RTM6) reinforced with high tenacity, standard modulus carbon fibers from Toho Tenax (Tenax® HTS, Saertex® biaxial non-crimp fabric (NCF), 540 g/m² areal weight).

SLS specimens were used for the characterization of the joints' mechanical properties. They had overall dimensions of 190 x 25 x 10 mm (Figure 8.5) based on ASTM D5868 [40] and a joining area of 25 x 30 mm². An increased lap

thicknesses of 5 mm was chosen so that the through thickness reinforcements were completely covered with CFRP.

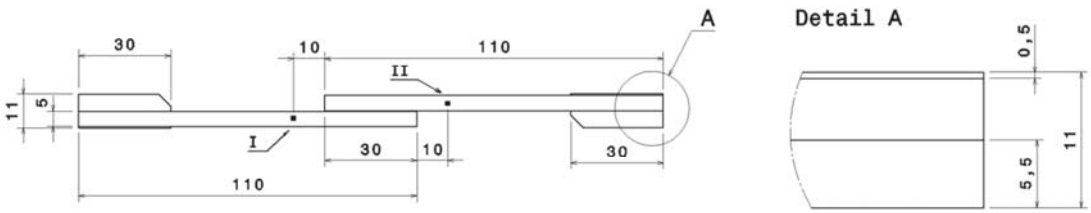

(a)

(b)

Figure 8.4: SLS specimen: (a) sectional view of the specimen, (b) final SLS joint specimen.

The two ends of the SLS specimens' overlap regoin were not tapered in order to maximize out-of-plane stresses.

For the determination of the CFRP's basic mechanical properties (e.g. Young's Moduli E_{11}, E_{22}, $E_{45°}$, shear modulus G_{12} and Poisson's ratio ν_{12}), specimens based on ISO 527-4 [41] were produced. The specimens had overall dimensions of 280 x 25 x 5 mm and were cut out of a representative CFRP panel with quasi-isotropic stacking in 0°, 45° and 90° direction.

8.2.4.2 Manufacturing of SLS specimens and CMT pins

CFRP panels, comprising 12 SLS specimens each, were produced via a liquid resin infusion process. GFRP tabs were bonded onto the ends of the CFRP specimen-panels to ensure both a symmetric clamping of the specimens within the test system and an axially aligned joining interface. The final SLS specimens were cut out of the panel by waterjet cutting.

CMT pin material

The metallic reinforcement inserts used in this study were made of stainless steel type AISI 316L. They consisted of ballhead spike pins, which were welded onto stainless steel sheets, type AISI 304, with a thickness of t = 0.6 mm.

Positioning of CMT pins

Numerical simulations of tensile tests on co-cured SLS specimens were carried out in order to get a basic understanding of the fracture behavior of unreinforced SLS specimens and to find optimum locations for through-the-thickness reinforcements in SLS specimens with the above mentioned geometry. The model was analyzed using the FE-solver Abaqus 6.13-2 (Dassault Systèmes Simulia Corp., Providence, RI, USA). Using a mesh size of 0.5 mm in the overlap region, the model contained a total number of 83464 elements (Abaqus types C3D20). The specimen geometry (see Figure 8.4) and boundary conditions were specified according to the experimental set-up. A defined displacement was applied to the outer surfaces of the specimens tabs. Figure 8.5 gives a detail of the model in the overlap region. The material properties used for the numerical simulations are listed in Table 8.1.

Figures 8.6 (a) and (b) show that elevated peel and shear stresses, respectively, are present at the very ends of the bond line during loading of the SLS specimen. This is in good agreement with results from literature [8] and shows the size of the highly stressed region for SLS specimens with the above mentioned geometry. The elevated stresses occur in the joined area up to approximately 5 mm from both ends of the bond line (see Figure 8.6 (c) for a 2D plot of the stress distribution at mid-width). Thus, through-the-thickness reinforcements are most effective within 5 mm from both ends of the bond line. Accordingly, 2 x 6 pins were positioned at each end of the overlap region to counteract the elevated stresses.

The CMT pin arrays were manufactured with an automated, computer controlled welding machine [31]. The CMT welding head was attached to a three axes moving portal. Blank metal inserts were fixed in mounting plates.

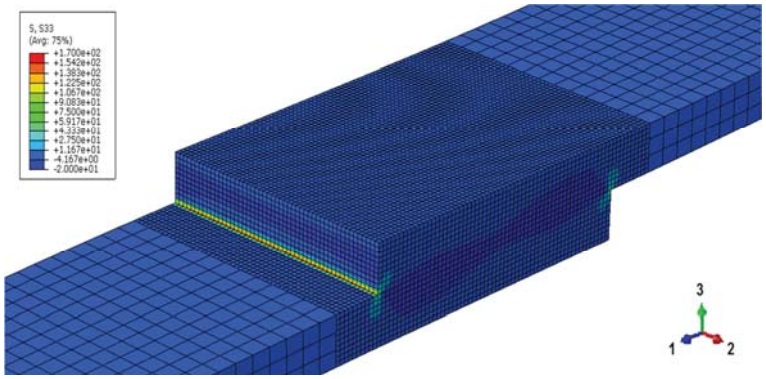

Figure 8.5: Detail of the numerical simulation at 14 MPa average shear stress (load per joining area). The mesh size was set to 0.5 mm in the overlap region.

Table 8.1: Material properties used in the finite element model.

Laminate properties		
E_{11} = 52.9 ± 1.4* GPa	E_{22} = 51.9 ± 1.1* GPa	E_{33} = 10.6** GPa
G_{12} = 21.3 ± 0.3* GPa	G_{13} = 4.2** GPa	G_{23} = 4.2** GPa
ν_{12} = 0.26 ± 0.02*	ν_{13} = 0.25**	ν_{23} = 0.25**

* measured via the test procedure given in chapter 8.2.4.3.

** from 3D periodic unit cells based on homogenization of single layers [43]

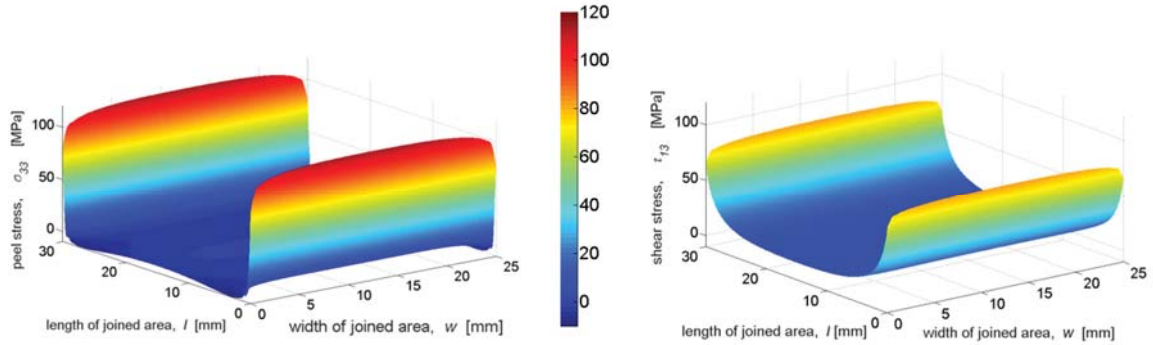

(a) (b)

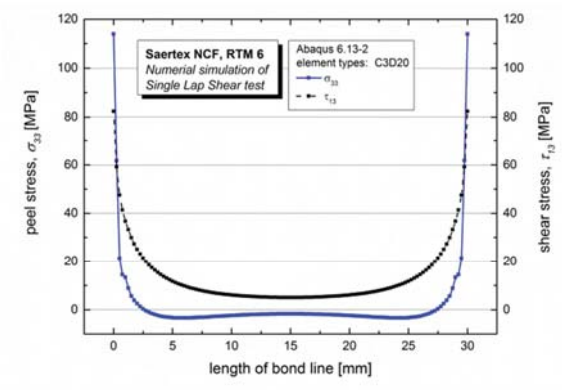

(c)

Figure 8.6: Distribution of (a) peel stresses and (b) shear stresses across the joint area of co-cured SLS specimens at 14 MPa average shear stress (load per joining area). (c) shows the distributions of peel and shear stresses along the bond line at 12.5 mm in width direction of the overlap.

These mounting plates were attached to the machine frame and were responsible for suppressing waviness of the metal sheets due to thermally induced distortions and for accurate and reproducible positioning of the blank metal inserts during CMT pin welding. One metal insert carried six 4 x 6 CMT pin arrays for six SLS specimens (Figure 8.7 (a)). The pin step in lateral direction was 4.2 mm. The outer two rows of 6 pins were 1.5 mm away from the free edges of the metal insert and the inner two rows 3.0 mm away from the outer two rows of pins.

Prior to the draping process the metal sheets and CMT pins were surface treated by cleaning and sandblasting in order to remove contaminations such as grease and welding tinder. At the same time sandblasting increased the roughness of the metallic surface and therefore increased the adhesion between the metal and the epoxy resin. In a final step the inserts were cleaned with an organic solvent. Figure 8.7 (b) shows a CAD drawing of CMT pins on top and bottom of a metal sheet. Figure 8.7 (c) shows a metal sheet carrying six arrays of 4 x 6 CMT pins. It was accurately and reproducibly fixed in a mold prior to draping the NCF textiles on top of them. Each of the SLS specimens' laps had a quasi-isotropic stacking.

Co-cured SLS specimens

Co-cured specimens were produced for the characterization of the failure behavior of unreinforced SLS specimens. They were manufactured by simultaneously infusing two separate quasi-isotropic stacks of NCFs with resin. The resin infiltrated the joint region and acted as an adhesive between the two SLS specimen's laps.

SLS specimens carrying metal sheet without CMT pins

In this study, a thin metal sheet carrying CMT pins was placed in the SLS joint's overlap region. The metal sheet was left within the joining area for manufacturing reasons and unused parts were, yet, not removed. In order to investigate the effect of the metal sheet on the joint's mechanical properties, a metal sheet carrying no pin reinforcements was placed in the stacking sequence.

SLS specimens carrying CMT pins treated with mold release agent

For a better understanding of the load transfer and reinforcement effect of the CMT pin reinforced joints during loading and failure, the outer surface of one CMT pin carrying metal sheet was treated with mold release agent prior to draping the carbon fibers. This was done to avoid adhesion between the CFRP and the metal reinforcement insert.

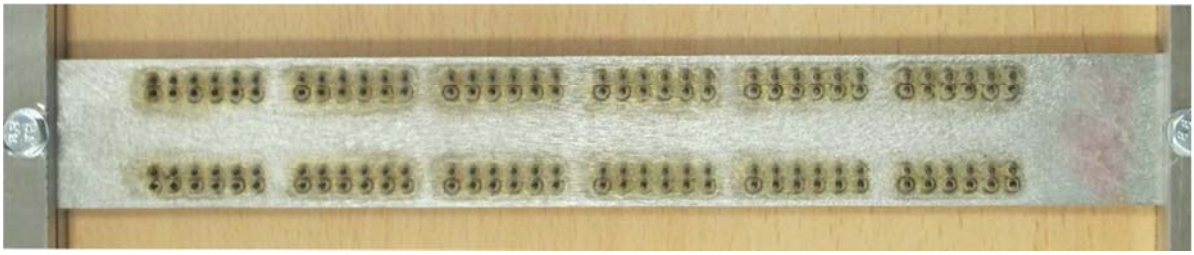

(a)

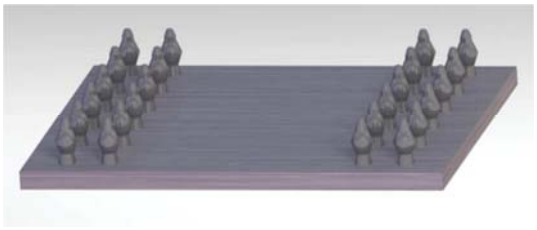

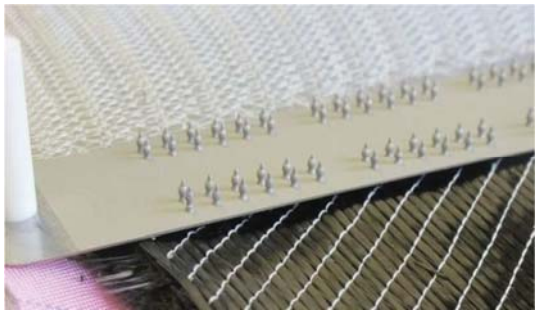

(b) (c)

Figure 8.7: Metal sheet carrying arrays of CMT pins: (a) top view of insert carrying reinforcements for six SLS specimens with 4 x 6 CMT pins after the welding process, (b) CAD schematic of 25 x 30 mm overlap section and (c) metal sheet positioned in mold carrying double-side CMT pins, with single-side integration in dry CFRP stack.

8.2.4.3 Test procedure

Tensile tests on CFRP coupons and SLS specimens were carried out on a servo-hydraulic test system, MTS 322 (MTS Systems Corp., Minneapolis, USA), with a load range of 250 kN (±0.1%). In both cases the specimens were loaded in a displacement controlled manner at a crosshead velocity of 2 mm/min [34,35]. The digital image correlation system GOM 'Aramis' (GOM GmbH, Braunschweig, Germany) was used in order to get full field strain (FFS) information of the tested specimens (front of the tensile and side of the SLS specimens).

In case of the tensile coupon tests this allowed to compute the mean values of strains (ε_1, ε_2 with 1 being the loading direction and 2 being the lateral direction) and Poisson's ratio (ν_{12}) based on the strains of the specimens' faces. In the case of SLS specimens, FFS-measurements gave information about highly strained areas in the overlap region of the joint. Additionally, joint expansions were measured by evaluating the distance of two defined points. These were positioned

10 mm outside of the 30 mm long joint area (see Figure 8.4 (a), I-II). The relation of the axial joint expansion to the original distance of the two points (L_0=|I-II|=50 mm) gave the joint strain ε.

The values of the shear modulus G_{12}, which were needed for the numerical simulations, were calculated using the following equation [42]:

$$G_{12} = \frac{E_{45°} E_{11} E_{22}}{4E_{11}E_{22} - E_{45°}[E_{22} - 2\nu_{12}E_{22} - E_{11}]} \quad (8.1)$$

with $E_{45°}$ being the Young's modulus from specimens cut out of the CFRP panel in 45° direction. The missing values (e.g. G_{13}, G_{23}, ν_{13}, ν_{23}) were chosen based on numerical work carried out by Ucsnik [43]. In his thesis, the out-of-plane material properties were determined via a stiffness homogenization approach of single 0°-CFRP layers and by means of a 3D periodic unit cell model.

All tests were carried out at a laboratory atmosphere of 23 ± 1 °C and 50 ± 10 % relative humidity. Specimens were preconditioned at laboratory conditions for at least 24 hours. Micrographs were taken with an optical stereo microscope type Olympus SZX12.

8.2.5 Results

The CMT pin reinforced SLS specimens show a load transfer behavior (Figure 8.8), that consists of two phases. First, the load rises linearly until a first distinct peak is reached. This first load peak in the stress-strain curve is called first failure stress (τ_{FF}) by the authors and is indicated in Figure 8.8. τ_{FF} values amounted to 14.1 ± 1.3 N/mm² at local joint strains of 1.1 ± 0.3 %. After a small load drop and another distinct peak the second phase begins. The stress-strain curve shows a nonlinear behavior until ultimate failure is reached at high joint strains. The highest stresses in this second phase are referred to as τ_{UF} by the authors. τ_{UF} values amounted to 14.7 ± 0.7 N/mm² at joint strains of 3.0 ± 0.5 % for the CMT pin reinforced samples.

Figure 8.9 shows micrographs of pins after tensile testing. The pins were predominantly sheared off (Figure 8.9 (a)) leaving metal residua behind (Figure 8.9 (b)). Some of the CMT pins were pulled out of the CFRP (Figure 8.9 (c)). The pins which remained in the CFRP were bent (Figure 8.9 (d)) until the pins failed on the opposite side of the metal insert.

Figure 8.10 (a) shows the distribution of major strains on the lateral surface of the specimen at the first distinct shear stress peak (τ_{FF}).

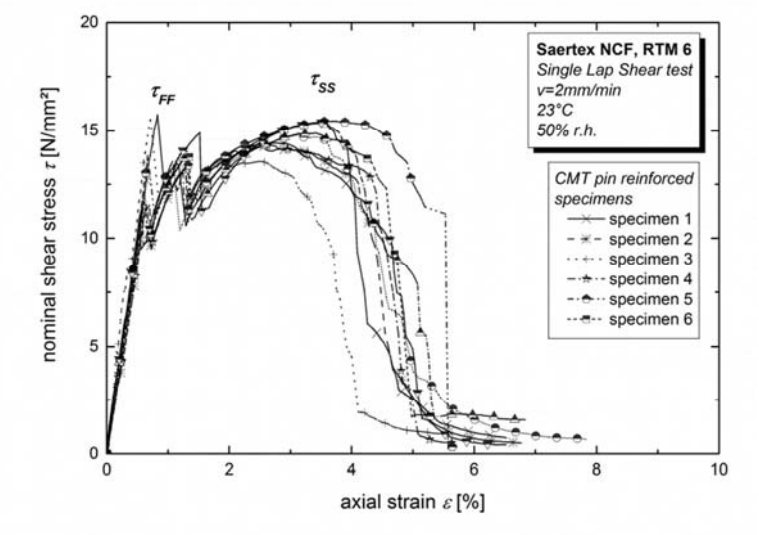

Figure 8.8: Shear stress versus local joint strain for SLS specimens reinforced with stainless steel inserts with CMT pins.

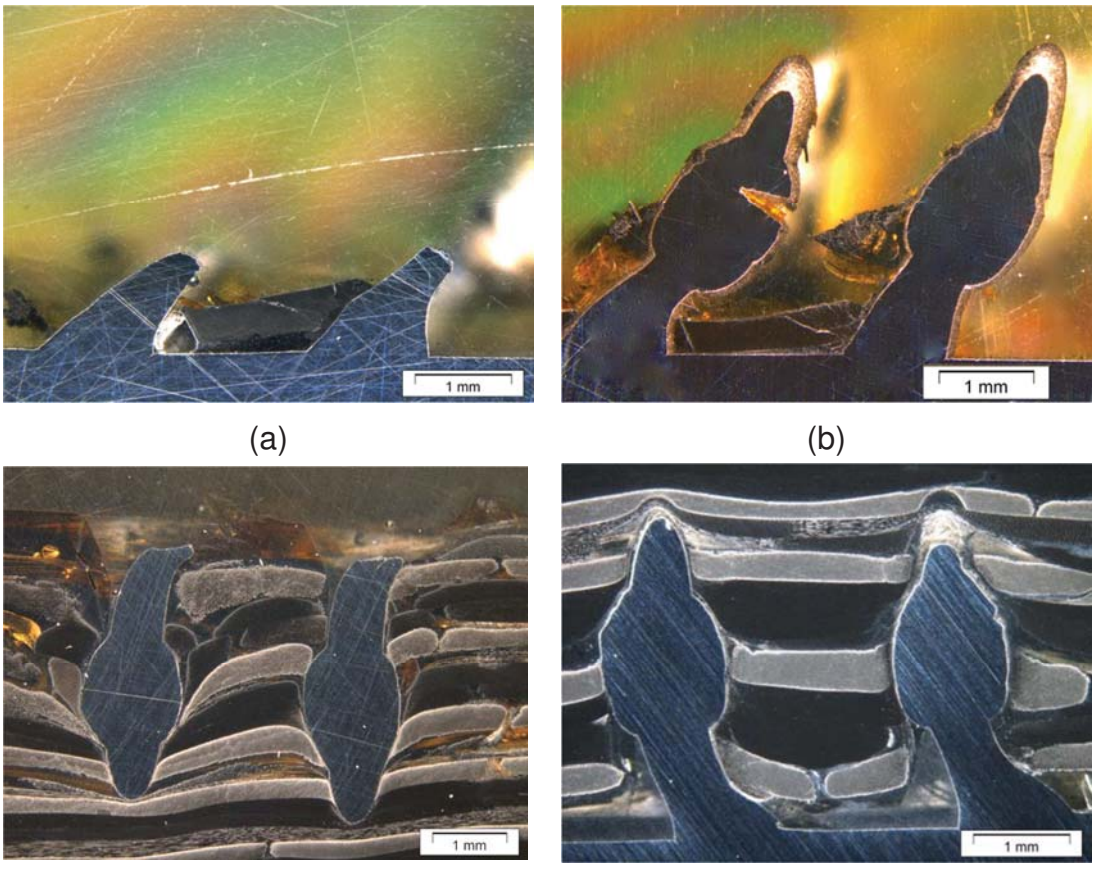

(a) (b)

(c) (d)

Figure 8.9: Micrographs of pins after final failure: (a) metal residua of sheared off pins (b) pulled out pins (c) sheared off pins (d) bent pins.

The highest local strains appear in the area of the joint interface leading to delamination of the bond line before reaching τ_{FF}. When phase two in the stress-strain curve is reached, the joint interface has already failed, see Figure 8.10 (b).

High local strains, evident in the area of the CMT pin reinforcement indicate cracks that form around the pins and grow towards the surface of the specimen. Before ultimate failure, the cracks reach the surface and extensive damage forms in the area of the pin reinforcement. Despite this extensive damage, the joint is able to carry 60 % of τ_{UF} (see Figure 8.10 (c)).

Additional tests were carried out to get a better understanding of the failure mechanisms in CMT pin reinforced specimens. Figure 8.11 shows stress-strain curves of co-cured SLS specimens and SLS specimens carrying steel sheets with and without CMT pins in the overlap region of SLS joints.

The co-cured SLS specimens reached shear strengths (τ_{SS}) of 14.6 ± 1.1 N/mm² at joint strains of 0.51 ± 0.03 %. Thus, co-cured specimens reached a similar level of stress as the steel CMT pin reinforced SLS joints, but at half and one sixth of the strain compared to strains at τ_{FF} and τ_{UF}, respectively. SLS specimens carrying metal sheets with no CMT pins reached shear strengths of 9.4 ± 0.6 N/mm² at joint strains of 0.42 ± 0.05 %. This corresponds to a loss of 35.6 % of shear strength compared to co-cured samples.

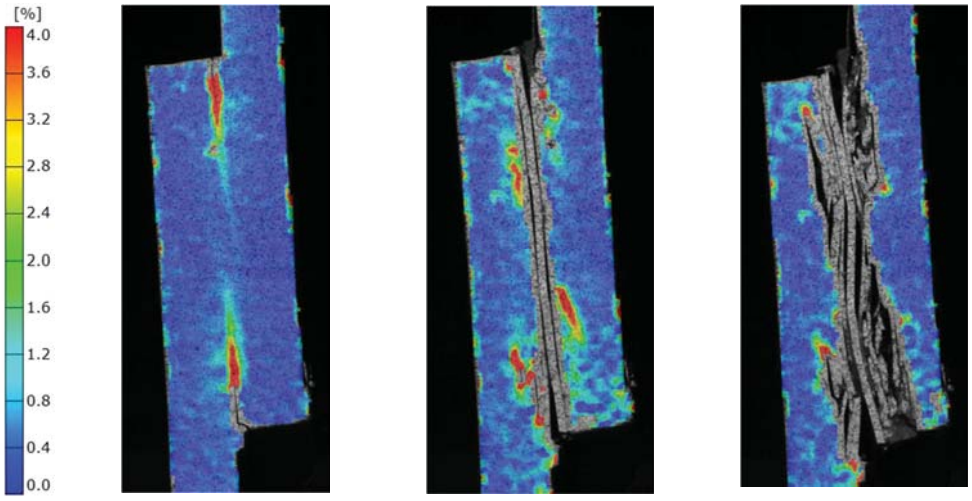

Figure 8.10: Distribution of major (axial/total) strains on the lateral SLS specimen's surface: (a) at first failure stress (τ_{FF}). (b) at ultimate failure stress (τ_{UF}), (c) at 60% of τ_{UF} after ultimate failure.

The failure behavior of SLS specimens that were reinforced with CMT pins covered with mold release agent (Figure 8.11) differed significantly from the untreated CMT pin reinforced specimens (Figure 8.8). No distinct load peaks are evident before reaching the nonlinear stress-strain behavior at high local joint strains. These load peaks can therefore be ascribed to adhesive failure of the interface between the metal reinforcement and the CFRP. The following nonlinear stress-strain behavior is assumed to be caused by plastic deformation of the CMT pins (see Figure 8.9) and by the formation of cracks in the matrix resin surrounding the metal reinforcements. Both mechanisms contribute to the damage tolerance of the joint by increasing the energy dissipation during loading.

The comparison of stress-strain curves (Figure 8.12) shows that CMT pin reinforced specimens combine the strength and stiffness of the co-cured, unreinforced specimens with the high deformation capability of the metal reinforcement. The failure mechanism evolution for CMT pin reinforced SLS specimens (Figure 8.13) is derived based on microscopy (Figure 8.9), digital image correlation measurements (Figure 8.10) and measurements on SLS specimens reinforced with mold release agent treated CMT pins (Figure 8.11). The first two distinct stress peaks in the stress-strain curves of the SLS tensile tests are caused by interfacial failure of the adhesive connection between the CFRP and the steel reinforcements. The following non-linear stress-strain behavior is assumed to be caused by bending of the CMT pin and initiation of cracks in the vicinity of the CMT pins. Final failure of the joint is caused by extensive crack growth in the CFRP (Figure 8.10(c)) accompanied by shear failure or rather pull-out of the CMT pins (Figure 8.9).

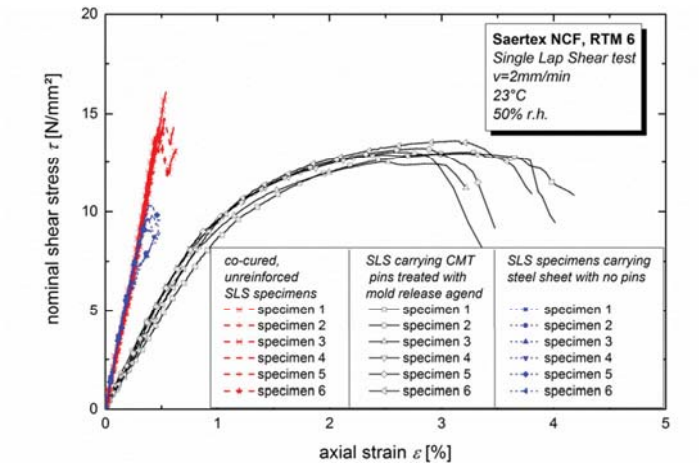

Figure 8.11: Shear stress versus local joint strain for co-cured SLS specimens, SLS specimens carrying steel sheets without CMT pins and SLS specimens reinforced with mold release agent treated steel CMT pins.

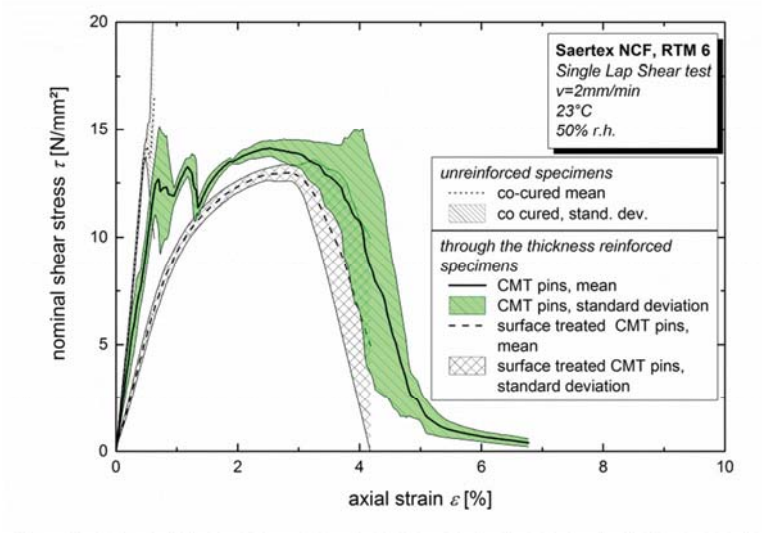

Figure 8.12: Mean shear stress and standard deviation versus local joint strain for all tested SLS specimens.

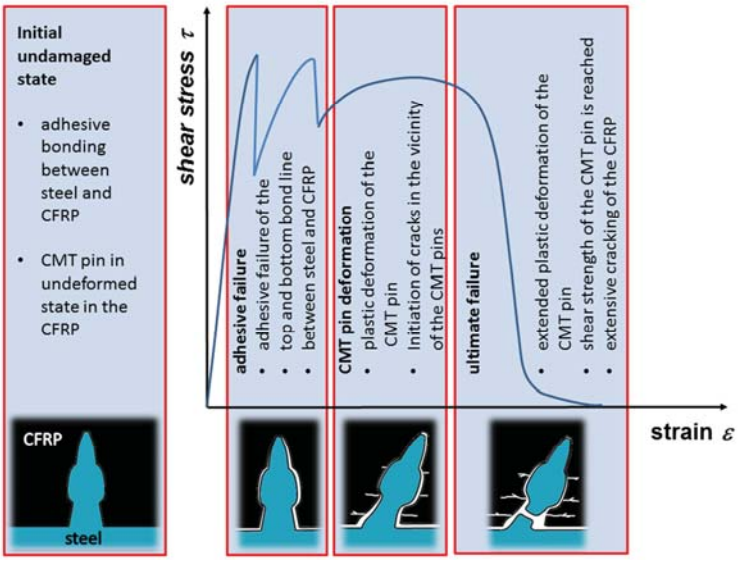

Figure 8.13: Schematic of failure development and progress for CMT pin reinforced SLS samples.

8.2.6 Conclusions and Outlook

In this paper, tensile tests are carried out on CFRP to CFRP joints. Numerical simulations of tests on co-cured, unreinforced SLS specimens helped to understand the stress distribution in composite-composite joint specimens and to find suitable reinforcement locations. The locations facing increased peel and shear stresses were reinforced with CMT pins.

CMT pin reinforced specimens gave significantly higher strains and hence damage tolerance than co-cured specimens at similar levels of stress. Detailed investigations of the failure behavior of CMT pin reinforced specimens show that after initial failure of the bond line at τ_{FF}, the pins carry loads up to high values of strain until ultimate failure is reached at τ_{UF}. Extensive damage of the CFRP in the vicinity of the CMT pins and shear failure of the CMT pins themselves leads to final failure of the specimen.

Stainless steel was used as reinforcement in this first phase to get an insight into the failure mechanisms and the mechanical behavior of CMT pin reinforced SLS specimens. In further investigations, this knowledge will be extended towards inserts and pins made of titanium.

8.2.7 Acknowledgements

The funding of the Austrian Research Promotion Agency for project 830384 “Composite+composite Joints with Enhanced damage toleranCe (CoJEC)” is gratefully acknowledged as well as the support of the involved project partners FACC AG, Fronius International GmbH, Rübig GmbH & Co KG, Fill GmbH, RECENDT GmbH and LKR Leichtmetall Kompetenzzentrum Ranshofen.

8.2.8 References

[1] Sierakowski RL, Newaz GM. Damage tolerance in advanced composites. Basel: Technomic Publishing AG; 1995.

[2] Olmedo Á, Santiuste C. On the prediction of bolted single-lap composite joints. Composite Structures 2012;94(6):2110–7.

[3] Riccio A. Effects of geometrical and material features on damage onset and propagation in single-lap bolted composite joints under tensile load: Part II - Numerical studies. Journal of Composite Materials 2005;39(23):2091–112.

[4] Andrews SD, Ochoa OO, Owens SD, Andrews SD, Ochoa OO, Owens SD. The Effects of Fastener Hole Defects. Journal of Composite Materials 1993;27(1):2–20.

[5] Suemasu H, Takahashi H, Ishikawa T. On failure mechanisms of composite laminates with an open hole subjected to compressive load. Composites Science and Technology 2006;66(5):634–41.

[6] Chen W. Some experimental investigations in the drilling of carbon fiber-reinforced plastics (CFRP) composite laminates. International Journal for Machining Tools and Manufacture 1997;37(8):1097–108.

[7] Davim JP, Reis P. Study of delamination in drilling carbon fiber reinforced plastics (CFRP) using design experiments. Composites Structures 2009;59:481–7.

[8] Hart-Smith LJ. Designing to minimize peel stresses in adhesive-bonded joints. In: Johnson WS, editor. Delamination and debonding of materials: ASTM STP 876. West Conshohocken, PA: American Society for Testing and Materials; 1985, p. 238–66.

[9] Cartié DD, Dell'Anno G, Poulin E, Partridge IK. 3D reinforcement of stiffener-to-skin T-joints by Z-pinning and tufting. Engineering Fracture Mechanics 2006;73(16):2532–40.

[10] Dell'Anno G, Cartié DD, Partridge IK, Rezai A. Exploring mechanical property balance in tufted carbon fabric/epoxy composites. Composites Part A: Applied Science and Manufacturing 2007;38(11):2366–73.

[11] Aymerich F, Priolo P, Sun C. Static and fatigue behaviour of stitched graphite/epoxy composite laminates. Composites Science and Technology 2003;63(6):907–17.

[12] Aymerich F. Experimental investigation into the effect of edge stitching on the tensile strength and fatigue life of co-cured joints between cross-ply adherends. Advanced Composites Letters 2004;13(3):151–61.

[13] Mouritz AP, Jain LK. Further validation of the Jain and Mai models for interlaminar fracture of stitched composites. Composites Science and Technology 1999;59:1653–62.

[14] Dransfield KA, Baillie C, Mai YW. Improving the delamination resistance of CFRP by stitching - a review. Composite Science and Technology 1994;50:305–17.

[15] Jain LK, Mai YW. On the effect of stitching on mode I delamination toughness of laminated composites. Composites Science and Technology 1994;51:331–45.

[16] Cartié D, Partridge IK. Delamination behaviour of z-pinned laminates. European Structural Integrity Society 2000;27:27–36.

[17] Cartié DD, Troulis M, Partridge IK. Delamination of z-pinned carbon fibre reinforced laminates. Composites Science and Technology 2006;66(6):855–61.

[18] Partridge IK, Cartié DD. Delamination resistant laminates by Z-Fiber® pinning: Part I manufacture and fracture performance. Composites Part A: Applied Science and Manufacturing 2005;36(1):55–64.

[19] Allegri G, Zhang X. On the delamination and debond suppression in structural joints by Z-fibre pinning. Composites Part A: Applied Science and Manufacturing 2007;38(4):1107–15.

[20] Pingkarawat K, Mouritz A. Improving the mode I delamination fatigue resistance of composites using z-pins. Composites Science and Technology 2014;92:70–6.

[21] Löbel T, Kolesnikov B, Scheffler S, Stahl A, Hühne C. Enhanced tensile strength of composite joints by using staple-like pins: Working principles and experimental validation. Composite Structures 2013;106:453–60.

[22] Heimbs S, Nogueira A, Hombergsmeier E, May M, Wolfrum J. Failure behaviour of composite T-joints with novel metallic arrow-pin reinforcement. Composite Structures 2014;110:16–28.

[23] Graham D, Rezai A, Baker D, Smith PA, Watts JF. A hybrid joining scheme for high strength multi-material joints. In: Proceedings of the 18th International Conference on Composite Materials. Jeju, South Corea; 2011.

[24] Pegoretti A, Cristelli I, Migliaresi C. Experimental optimization of the impact energy absorption of epoxy–carbon laminates through controlled delamination. Composites Science and Technology 2008;68(13):2653–62.

[25] Cartié D, Cox B, Fleck NA. Mechanisms of crack bridging by composite and metallic rods. Composites Part A: Applied Science and Manufacturing 2004;35(11):1325–36.

[26] Rugg KI, Cox BN, Massabò R. Mixed mode delamination of polymer composite laminates reinforced through the thickness by z-fibers. Composites Part A: Applied Science and Manufacturing 2002;33:170–90.

[27] Ji H, Kweon J, Choi J. Fatigue characteristics of stainless steel pin-reinforced composite hat joints. Composite Structures 2014;108:49–56.

[28] Jürgens M, Noguiera AC, Lang H, Hombergsmeier E, Drechsler K. Influence of an optimized 3D-reinforcement layout on the structural mechanics of co-bonded CFRP joints. In: Proceedings of the 16th European Conference on Composite Materials, 22.06. - 26.06.2014.

[29] Noguiera AC, Drechsler K, Hombergsmeier E. Analysis of the Static and Fatigue Strength of a Damage Tolerant 3D-Reinforced Joining Technology on Composite Single Lap Joints. In: Ouwehand L, editor. Proc. 12th European Conference on Spacecraft Structures, Materials and Environmental Testing; 2012.

[30] Noguiera AC, Drechsler K, Hombergsmeier E, Furfari D, Pacchione M. Investigation of a hybrid 3D-reinforced joining technology for lightweight structures. In: Ferreira (Hg.) 2011 – 16th International Conference on Composite Materials.

[31] Stelzer S, Ucsnik S, Tauchner J, Unger T, Pinter G. Novel composite-composite joining technology with through the thickness reinforcement for enhanced damage tolerance. In: Hoa SV, Hubert P, editors. Proceedings of the 19th International Conference on Composite Materials: Canadian Association for Composite Structures and Materials; 2013, p. 4645–53.

[32] Ucsnik S, Scheerer M, Zaremba S, Pahr D. Experimental investigation of a novel hybrid metal–composite joining technology. Composites Part A: Applied Science and Manufacturing 2010;41(3):369–74.

[33] Ucsnik S, Pahr D. Investigation of novel composite-metal-joints. Proc. 11th Japanese-European Symposium on Composite Materials 2008.

[34] Schierl A. The CMT process, a revolution in welding technology. Welding in the world 2005;49:38.

[35] Korya C, Sanderson T. Method of forming a joint(US 2011/0240200 A1); 2011.

[36] Ucsnik S, Tauchner J, Fleischmann M. Vergleich von Mischbau-Fügetechniken am Beispiel einer Metall-CFK-Lasteinleitung aus der Luftfahrt. In: Proceedings of the 7th Ranshofener Leichtmetalltage, Gmunden, Austria, 07.11. - 08.11.2012.

[37] Graham DP, Rezai A, Baker D, Smith PA, Watts JF. The development and scalability of a high strength, damage tolerant, hybrid joining scheme for

composite–metal structures. Composites Part A: Applied Science and Manufacturing 2014;64:11–24.

[38] Parkes PN, Butler R, Almond DP. Growth of damage in additively manufactured metal-composite joints. Proc. 15th European Conference on Composite Materials 2012:1–8.

[39] Parkes PN, Butler R, Meyer J, Oliveira A de. Static strength of metal-composite joints with penetrative reinforcement. Composite Structures 2014;118:250–6.

[40] ASTM - American Society for Testing and Materials. D5868:01 - Standard test method for lap shear adhesion of fiber reinforced plastic bonding(D5868:01).

[41] ISO - International Organization for Standardization. ISO 527-4 - Plastics - Determination of tensile properties - Part 4: Test conditioning for isotropic and orthotropic fibre-reinforced plastic composites(ISO 527-4).

[42] Tuttle ME. Structural Analysis of Polymeric Composite Materials. New York: Marcel Dekker Inc; 2005.

[43] Ucsnik S. Development, Experimental and Numerical Investigations of a Novel Metal to Composite Joint Technology. PhD Thesis. Vienna; 2013.

8.3 PUBLICATION 8

STRENGTH AND DAMAGE TOLERANCE OF COMPOSITE-COMPOSITE JOINTS WITH METALLIC THROUGH-THE-THICKNESS REINFORCEMENTS

8.3.1 Bibliographic Information

- Authors and their relevant contributions to the publication:
  - Steffen Stelzer[1]
    Preparation and submission of the manuscript, execution of all tests, calculation and analysis of all test results.
  - Stephan Ucsnik[2]
    Project co-ordination and expert knowledge on cold metal transfer welding.
  - Gerald Pinter[1]
    Academic supervision of the work carried out in this publication
- Affiliations:
  [1] Institute of Materials Science and Testing of Polymers, Montanuniversitaet Leoben, Leoben, Austria
  [2] Leichtmetallkompetenzzentrum Ranshofen GmbH, Austrian Institute of Technology, Lamprechtshausenerstraße Postfach 26, A-5282 Ranshofen, Austria

- Periodical: submitted to Composites Part A
- Manuscript number: JCOMA-14-1356R1

Statement with regard to publication: The manuscript presented here is an adapted accepted manuscript in order to fit the formatting of the thesis and does not necessarily reflect the actually published version.

8.3.2 Abstract

Today´s aeronautic, automotive and marine industry is in demand of fiber-friendly, low weight alternatives for composite-composite joints which combine the advantages of low weight input of adhesively bonded joints and high damage tolerance of through-the-thickness bolted joints. In the present work, composite-composite joints are reinforced through-the-thickness by thin metal inserts carrying cold metal transfer welded pins (CMT pins). The influence of pin alignment and type of pin on the damage tolerance of single lap shear (SLS) composite-composite joints is investigated. The use of titanium reinforcements is evaluated and compared to stainless steel reinforced, adhesively bonded and co-cured specimens. A detailed analysis of the stress-strain behavior is given and the stiffness and energy absorption of the SLS joints during tensile loading is assessed. The results show that joints reinforced with CMT pins absorb significantly higher amounts of energy, when compared to adhesively bonded and co-cured joints.

8.3.3 Introduction

Joining and through-the-thickness reinforcement of carbon fiber reinforced composites (CFRP) have been topics of increasing interest in recent years. This increasing interest originates from disadvantages of state-of-the-art joining technologies. Such disadvantages can be the reduction of substrate cross-section due to boreholes, stress concentrations around boreholes, cutting of continuous fibers due to drilling, or additional weight input due to joining elements and additional safety elements. This leads to a reduced degree of material utilization in state-of-the-art composite joints [1–3].

Adhesive bonding, a bolt-free alternative for composite joints, provides joints at a very low weight input without the requirement to cut fibers. However, adhesively bonded joints are sensitive to out-of-plane and peel stresses. At present, adhesively bonded joints are not considered for use in primary composite aircraft structures due to difficult quality control and certification issues. Rivets and bolts are commonly used to provide a load path redundancy in adhesively bonded joints. On the one hand, this increases the joint weight. On the other hand this weakens the composite material [4].

Fiber-friendly, low weight alternatives for composite joints, which combine the advantages of low weight of adhesively bonded joints and high damage tolerance of through-the-thickness bolted joints are thus in demand. Many researchers have

investigated the capability of carbon fibers [5–12], polymeric yarns [13–16], and glass fibers [9,17] for the through thickness reinforcement for CFRP laminates. They concluded that polymeric yarns, carbon fibers and glass fibers add to the damage tolerance of the laminate predominantly by crack bridging and energy absorption during pullout of the fibers from the matrix resin [5–13]. Investigations on metal reinforcements [4,12,18–24] have shown that such elements can additionally add to the damage tolerance by plastic deformation of the metal reinforcement [22–24].

The applicability of metal reinforcements to composite-composite joining was investigated by various research groups. Rugg et al. carried out SLS tests on composite-composite joints, which were reinforced with metallic rods. These rods were angled nominally at 45° to the plane of the laminate. In tensile loading, all of the rods were pulled out, regardless of rod orientation (+45° or -45°). This pull out happened at relatively low loads and had little effect on the damage tolerance of the SLS joint [25].

Cartié et al. studied the influence of the insertion angle of both carbon and titanium rods on the fracture mechanical behavior of through-the-thickness reinforced CFRP. They concluded that failure mechanisms are dominated by the following effects: (1) debonding and subsequent pull-out (2) rod/substrate friction, (3) deformation of the rods, and (4) ploughing of the rod through the matrix material. In shear loading, these mechanisms depend on the insertion angle of the rods, giving a transition from pull-out dominated failure mechanisms to rod dominated failure. Rod failure led to the highest failure loads. In shear loading, titanium rod reinforced samples gave higher peak loads and ultimate deformation values than carbon rod reinforced samples. In tensile (pull out) loading, titanium and composite rods yielded a similar load displacement behavior [26].

Metallic through thickness reinforcements can add to the damage tolerance of composite-composite joints. Due to higher shear strength properties compared to carbon composites they can even surpass the reinforcement effect of carbon rod reinforced composite-composite joints. To further increase the joint strength and the damage tolerance of through thickness reinforced composite joints, pull out of through thickness reinforcements needs to be suppressed.

Research groups at Airbus Groups Innovation [22,23,27–29] use the so-called RHEA (redundant high efficiency assembly) technology to reinforce composite-composite joints in the through thickness direction. RHEA is based on the use of thin metallic sheets, where the pin geometry is laser-cut and bent to obtain

reinforcement sheets with staggered pins and hooks on top and bottom surfaces. The pins provide a form fit connection between the metal reinforcement inserts and the surrounding CFRP.

Tests on T-joints led to increased residual forces after delamination initiation at the spar-skin interface [22]. This resulted from a crack bridging zone formed by the metallic pins at the debonded interface.

The metal inserts technology, used in the RHEA technology [22,23,27–29], does not provide the possibility for coaxially aligned pins on the top and bottom side of the insert surface. The pins are not co-axially aligned and thus do not provide a straight load path from top to bottom side in the joined composites. Furthermore, the staggered arrangement leads to a reduced material utilization of the metal reinforcement sheet.

Graham et al. as well as Parkes et al. produced metallic pins with a 3D geometry on solid metal parts by additive layer manufacturing (ALM) [19,30,31]. They then joined the metal part to a CFRP part and observed significant increases in strength and damage tolerance. In a more recent work, Graham et al. replaced ALM by stud welding due to manufacturing cost and time reasons. Again significant increases in strength (+80 %) and energy absorption (+1000 %) were achieved [30].

Ucsnik et al. [32–35] carried out thorough investigations in the fields of metal to CFRP joining by using the cold metal transfer (CMT) welding process by Fronius for surface shaping. This knowledge was transferred to the “surface treatment” of thin metal sheets with 3-dimensional pins on the top and bottom surface. Similar to RHEA, such metal inserts can be used to join and reinforce CFRP to CFRP joints (Stelzer et al. [18,36]). In contrast to RHEA inserts, CMT shaped inserts do provide the possibility for coaxially aligned pins. These in turn allow for a direct, non-staggered load transfer from top to bottom composite part through the metal pins.

The present work deals with the determination of the mechanical properties of CMT pin insert reinforced CFRP to CFRP joints. The focus is put onto SLS joints which are reinforced with steel or titanium inserts that carry arrays of 3D shaped, co-axially aligned pins on top and bottom side.

8.3.4 Experimental

8.3.4.1 Materials and specimens

All composite joint specimens were made of high tenacity, standard modulus carbon fibers from Toho Tenax (Tenax® HTS, Saertex® non-crimp fabric, 540 g/m² areal weight) and epoxy resin from Hexcel Composites (Hexflow® RTM6). The metal reinforcements were made of either stainless steel or titanium. In the case of stainless steel, inserts type AISI 304 with a sheet thickness of t = 0.6 mm were used. These carried arrays of ballhead spike pins, a combination of a ballhead pin with a small spike pin on top of it. They were made by cold metal transfer (CMT) welding a filler wire type AISI 316L with a diameter of 0.8 mm (see [21] for details). The titanium inserts and pins were made of Ti6Al4V. The titanium sheets had a thickness of 0.4 mm and the filler wire a diameter of 0.8 mm.

SLS specimens of a first test campaign were reinforced with steel inserts which had three different arrangements of 4 x 6 ballhead spike CMT pins co-axially aligned on top and bottom surface (Figure 8.14). Array 1 had an equal distance arrangement (Figure 8.14 (a)). Four rows, each with six CMT pins, were equally distributed with a pitch of p_x = 7.0 mm, starting 3.0 mm away from the free edges of the metal insert (x being the axial loading direction). The CMT pins had a lateral pitch of p_y = 4.2 mm (with y indicating the lateral direction).

For array 2, the CMT pins were primarily arranged at the end positions of the inserts. The outer two rows of 6 CMT pins were positioned each 1.5 mm away from the free edges of the metal insert with a pitch of p_x = 3.0 mm to the second rows (Figure 8.14 (b)). For array 3 the CMT pins were clustered at the four corners of the insert in a triangular shape (Figure 8.14 (c)). The pins had an equal pitch of $p_x = p_y$ = 3.0 mm.

Figure 8.15 shows a stainless steel insert with pin array type 1 after the CMT pin welding process. The CMT pins had an overall height of about 3.3 mm and a tapered shaft with a diameter of about 1.2 mm at the bottom and 0.8 mm below the ballhead.

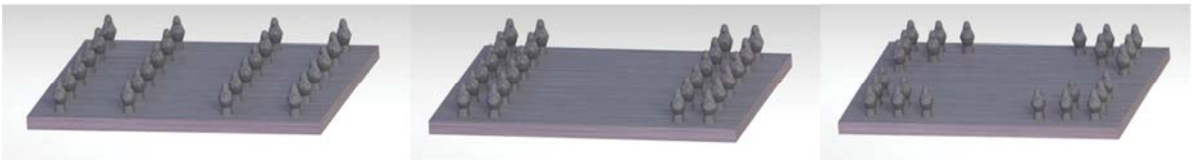

(a) (b) (c)

Figure 8.14: CAD schematics of the three types of pin arrays on metal inserts: (a) pin array 1, (b) pin array 2, (c) pin array 3.

Titanium inserts had the same arrangement of pins as the steel inserts of pin array type 2 (Figure 8.14 (b)). For comparison reasons, two types of titanium inserts were produced with pieces of titanium rods as vertical reinforcement elements (Ti z-pin) in addition to CMT welded titanium pin inserts (Ti CMT pin). The rods had diameters of 0.76 mm and 1.14 mm. These pins were press fitted into predrilled titanium sheets.

Prior to the draping process all inserts were surface treated by cleaning and sandblasting. This helped to remove contaminations such as grease and welding tinder and to increase the roughness of the metallic surface. This led to an increase in adhesion between the metal and the epoxy resin. In a final step the inserts were cleaned with an organic solvent.

For the preforming process, the metal sheets were reproducibly fixed in a metal mold. A set of dry CFRP textile layers was draped onto the top and bottom pin arrays in a symmetrical manner (Figure 8.16), so that quasi-isotropic laminate properties were achieved. CFRP specimen-panels were produced via a liquid resin infusion process.

Stepped CFRP panels were manufactured in a mold. Out of these panels, batches of six single SLS joint specimens were cut by waterjet cutting (see Figure 8.17). The final joint specimens had a width of 25 mm and a joining area of 750 mm² (see Figure 8.18 (a)). Before waterjet cutting, GFRP tabs were bonded onto both ends of the CFRP specimen-panels. This ensured both symmetric clamping of the SLS joint specimens in the test system and an axially aligned joining interface (see Figure 8.18 (b)).

Figure 8.15: Detail of a pinned interface (pin array 1) prior to sandblasting and cleaning.

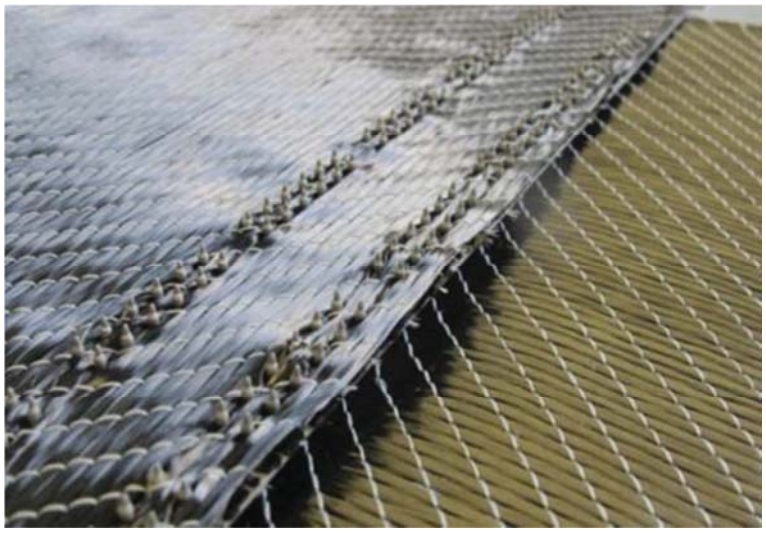

Figure 8.16: Draping of carbon fiber textiles onto metal insert with pin array 2.

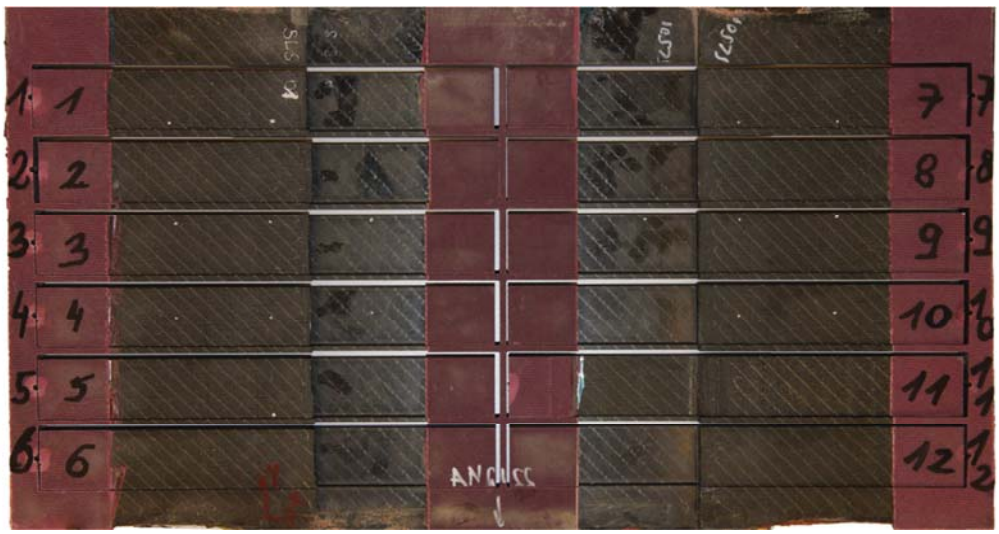

Figure 8.17: CFRP specimen-panel.

Adhesive-bonded and co-cured specimens with equal geometry, but without metal inserts, were chosen as reference. For the adhesive-bonded specimens, two separate CFRP panels with a quasi-isotropic stacking were adhesive-bonded with 3M Scotch-Weld adhesive film type AF 163-2L.

For the co-cured specimens, the textiles of the two CFRP panels were put in the metal mold, infused with resin and cured. The bonding between the two panels was realized through the cured resin.

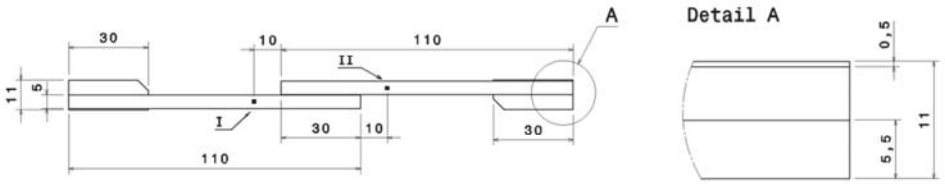

(a)

(b)

Figure 8.18: SLS specimen geometry: (a) sectional view of the specimen, (b) final SLS joint specimen.

8.3.4.2 Test methods and data reduction

Tensile tests of SLS specimens were executed on a servo-hydraulic test system, MTS 322 (MTS Systems Corp., Minneapolis, USA), with a load range of 250 kN (±0.1 %). The specimens were loaded in a displacement controlled manner at a crosshead velocity of 2 mm/min. Axial local joint strains were measured via full field strain analysis GOM 'Aramis' (GOM GmbH, Braunschweig, Germany) at ± 10 mm from the overlap region (see points I and II in Figure 8.18 (a), $L_0 = 50$ mm gage length).

The SLS joint's stiffness was calculated by relating the applied load to the deformation in the strain range between 0.05 % and 0.25 % (8.2):

$$k_{SLS} = \frac{P_{0.25\%} - P_{0.05\%}}{L_{0.25\%} - L_{0.05\%}} \tag{8.2}$$

where P is the axial load (N) and L the axial deformation (mm).

The amount of energy dissipated during deformation of the SLS joints in quasi-static loading, W, was calculated by equation (8.3):

$$W_x = \int_0^{L_x} P \, dL \tag{8.3}$$

where x indicates the different stages of the test, with FF being first failure, UF ultimate failure and SS shear strength. Integrating the entire load-displacement curve gives the total deformation energy, W_{total}.

All tests were carried out at a laboratory atmosphere of 23 ± 1 °C room temperature and 50 ± 10 % relative humidity. Specimens were preconditioned at laboratory conditions for at least 24 hours.

8.3.5 Results and Discussion

8.3.5.1 Steel CMT pin reinforced SLS joints

Figure 8.19 shows the load transfer behavior of the SLS specimens reinforced with the three types of steel inserts. The mean values and deviation bands of the shear stresses are plotted versus local joint strains. Regardless of the pin array in use the graphs follow similar load paths. At start, the curves rise until a first distinct load peak sets in, the so called “first failure stress” (τ_{FF}). This is followed by a load drop and by a second load peak-load drop combination. This is then followed by a non-linear loading behavior until the maximum, the “ultimate failure stress” (τ_{UF}), is reached. Depending on the metal insert version, τ_{UF} occurs at high local joint strains between 2.5 - 4.0 %. After τ_{UF} the stresses drop and the specimens fail.

Values of τ_{FF} of SLS specimens reinforced with pin array type 1 (equal distance distribution) reached 13.4 ± 0.5 MPa. This is within the standard deviation range of pin array type 2. Pin array type 2 (ending edge distribution) reached the highest τFF values of 14.1 ± 1.3 MPa.

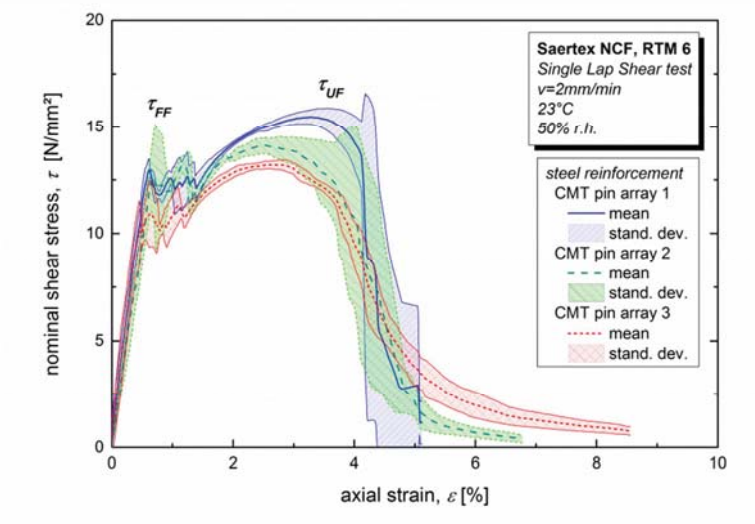

Figure 8.19: Mean shear stresses versus local joint strains and respective deviation bands for tensile tested SLS specimens reinforced by steel CMT pins.

SLS joints with insert type 3 (triangular pin distribution) reached τ_{FF} values of 12.3 ± 0.5 MPa. This is - 8.2 % and - 12.8 %, respectively, less than the first two versions.

Pin array type 1 reached τ_{UF} values of 15.5 ± 0.3 MPa. This shows an increase of + 5.5 % and + 16.7 % compared to pin array type 2 (14.7 ± 0.7 MPa) and pin array type 3 (13.3 ± 0.2 MPa), respectively. In contrast to τ_{FF}, τ_{UF} for pin array 1 is slightly higher than for pin array 2.

The amount of sheared off pins was counted and related to the overall number (24 – one side) of applied CMT pins for each batch of pin-reinforced SLS joints (see Figure 8.20 (a-c)). This allowed for the correlation between the pin arrangements, the resulting modes of failure and strength values. In the case of joints with pin array type 1, 77 ± 13 % of the pins were sheared off, whereas 51 ± 19 % of pins were sheared off in the case of pin array 2. In the case of pin array 3 most of the pins were pulled out of the CFRP. Only 17 ± 19 % of the pins were sheared off.

Figure 8.20 (a) shows the failed joint section of a SLS joint which was reinforced with pin array type 1. The first row of pins (left) was pulled out of the CFRP. Three rows of pins (right) were sheared off with small metal residua left on top of the metal insert. The metal insert still upholds the connection to the bottom CFRP. But the extent of deformation of the bottom pins is unknown.

Figure 8.20 (b) and Figure 8.20 (c) show pictures of failed joint sections that were reinforced with CMT pin arrays type 2 and 3, respectively. In case of pin array type 2 the majority of pins was sheared off. Pin array type 3 mainly showed pins that were pulled out from the CFRP.

(a) (b) (c)

Figure 8.20: Failed joint sections SLS specimens with (a) CMT pin array 1, (b) CMT pin array 2, (c) CMT pin array 3.

8.3.5.2 Titanium pin reinforced joints

Ti CMT pins

Stress-strain curves of titanium CMT pin reinforced specimens are depicted in Figure 8.21. These specimens reached values of τ_{FF} of 10.2 ± 0.03 MPa at local joint strains of 0.4 ± 0.1 % and values of τ_{UF} of 9.5 ± 1.3 MPa at local joint strains of 0.9 ± 0.1 %. The relatively high standard deviation in τ_{UF} compared to the steel pin reinforced joints can be attributed to a not yet fully optimized welding process and to a suboptimum shape of the Ti CMT pins. This led to difficulties in draping the carbon fibers around the Ti CMT pins. The pins did not possess a distinct undercut towards the titanium sheet. Thus, there was an increased amount of resin present around the pins. In many cases the parent titanium sheets broke during loading due to the inhomogeneous microstructure of the heat affected zone of the welded material (Figure 8.22 (a)).

Ti z-pins (d = 0.76 mm)

The titanium z-pins had cylindrical shape and a diameter of 0.76 mm. Stress-strain curves for this kind of reinforcement are shown in Figure 8.21. Only one of these specimens showed a distinct drop in shear stress before reaching τUF. The first failure stress amounted to 5 MPa at local joint strains of 0.4 %.

The SLS specimens reached τ_{UF} values of 8.0 ± 0.4 MPa at local joint strains of 1.8 ± 0.1 %. Compared to Ti CMT pins the local joint strains at τ_{UF} could be significantly increased at a similar level of stress.

Additionally the scatter in τ_{UF} could be reduced. Most of the z-pins, 83.3 ± 27.6 %, were sheared off, due to the small diameter of these pins. In Figure 8.22 (b) a failed joint section of a specimen reinforced with 0.76 mm thick titanium z-pins is shown.

Ti z-pins (d = 1.14 mm)

Figure 8.21 shows the stress-strain behavior of SLS specimens reinforced with Ti z-pins with a diameter of 1.14 mm. By increasing the diameter of the titanium rods τ_{FF} values of 5.7 ± 1.0 MPa at local joint strains of 0.35 ± 0.03 % and τ_{UF} values of 15.2 ± 0.7 MPa at local joint strains of 2.4 ± 0.1 % could be reached. The majority of these titanium pins was pulled out of the CFRP laps, 45.8 ± 42.5 % of pins were sheared off, see Figure 8.22 (c).

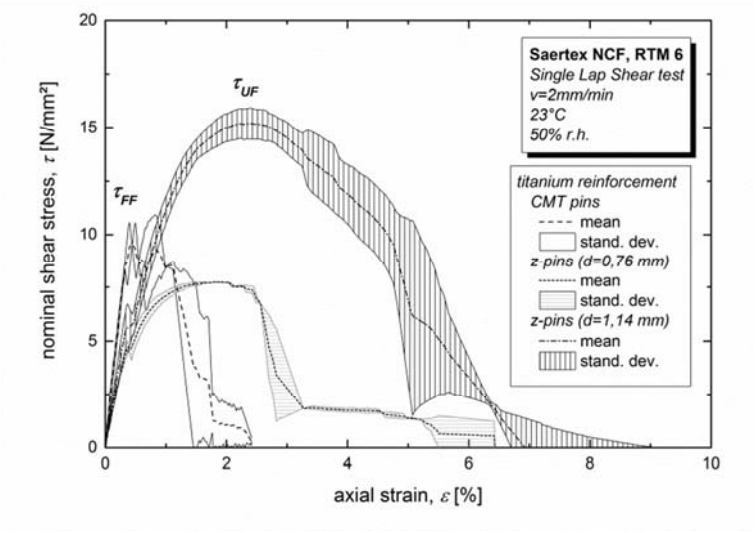

Figure 8.21: Mean shear stresses versus local joint strains and respective deviation bands for tensile tested SLS specimens reinforced with titanium pins.

(a) (b) (c)

Figure 8.22: Failed joint sections of specimen reinforced with (a) titanium CMT pins, (b) titanium z-pins (d=0.76 mm), (c) titanium z-pins (d=1.14 mm).

8.3.5.3 Co-cured reference joints

The loading behavior of co-cured SLS specimens is shown in Figure 8.23. They reached τss values of 14.6 ± 1.1 MPa at local joint strains of 0.51 ± 0.03 %. After τss the specimens failed in a spontaneous manner. Figure 8.24 (a) shows the fracture surface of a co-cured specimen after testing.

8.3.5.4 Adhesive-bonded reference joints

The loading behavior of adhesive-bonded reference specimens can be seen in Figure 8.23. The mean value of shear strength, τ_{ss}, amounts to 7.9 ± 1.6 MPa at local joint strains of 0.32 ± 0.06 %. Spontaneous failure sets in after maximum joint strains of around 0.75 % are reached. These strains are much lower than strains at τ_{UF} of > 4 % in the case of SLS specimens with steel inserts. Figure 8.24 (b)

shows the fracture surface of the joint section of an adhesive-bonded SLS specimen.

8.3.6 Comparison

Figure 8.25 shows a comparison of τ_{FF} values (Figure 8.25 (a)) and τ_{UF} values (Figure 8.25 (b)), reached by through-the-thickness reinforced SLS specimens in comparison to unreinforced SLS specimens (Figure 8.25 (c)). Pin array 2, the alignment of pins close to the outer ends of the overlap region of the SLS specimen, yields the highest τ_{FF} values. The outer ends of the overlap region are the areas with the highest peel stresses [21]. These areas are reinforced by the 2 x 6 pins in the out-of-plane direction at each end of the overlap region.

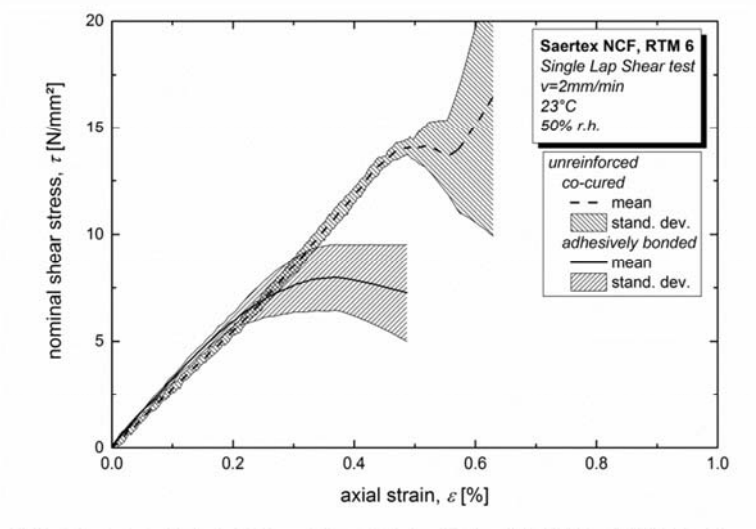

Figure 8.23: Mean shear stresses versus local joint strains and respective deviation bands for tensile tested co-cured and adhesively bonded SLS specimens.

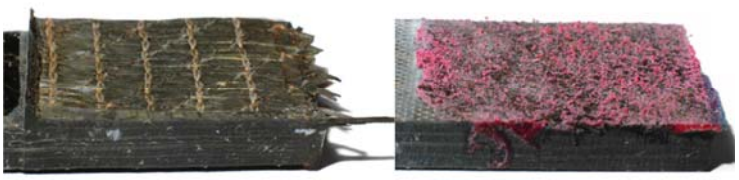

(a) (b)

Figure 8.24: Pictures of the failed joint sections of unreinforced SLS specimens: (a) co-cured specimen, (b) adhesive-bonded specimen.

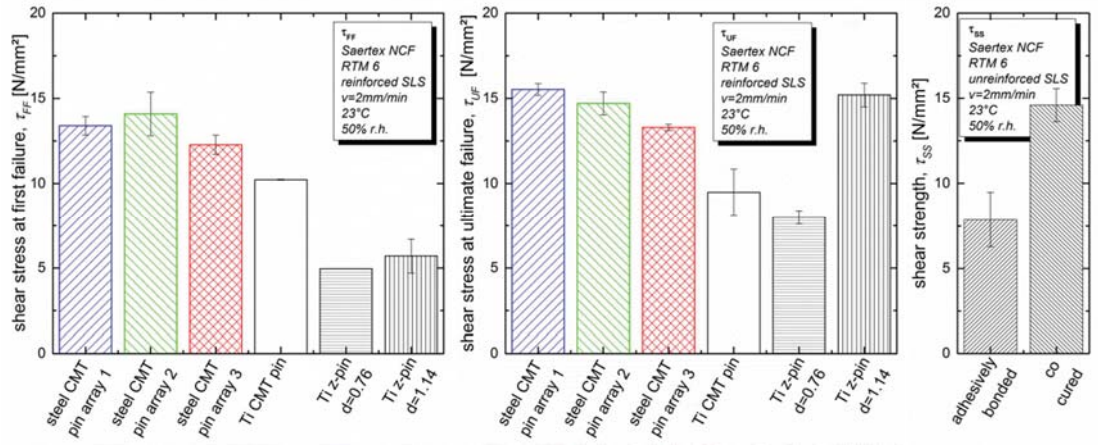

Figure 8.25: (a) First failure stresses, τ_{FF}, and (b) ultimate failure stresses, τ_{UF} compared to (c) shear strength, τ_{ss}, of adhesive-bonded and co-cured specimens.

τ_{FF} values of through-the-thickness reinforced SLS joints are related to adhesive failure of the interface between the metal reinforcement and the CFRP [21]. Therefore, they are compared to τ_{ss} values of co-cured SLS joints. Steel CMT pin reinforced specimens of type 1, 2 and 3 reached - 8.5 %, - 3.8 % and – 16.2 % lower values respectively. Compared to adhesively bonded reference joints, stainless steel pin reinforced SLS joints type 1, 2 and 3 show + 70.2 %, + 79.0 % and + 56.0 % increased failure stresses respectively. The improvements are related to the reinforcing pins and their positions.

τ_{FF} values of the Ti z-pin reinforced samples are significantly lower than those of the steel CMT pin reinforced SLS specimens. Compared to τ_{ss} values of co-cured SLS specimens the τ_{FF} values of samples reinforced with Ti z-pins are – 66.2 % (d = 0.76 mm) and – 60.8 % (d = 1.14 mm) lower.

This may be attributed to the absence of a form fit connection between the z-pins and the CFRP. An increase in the values of τ_{FF} can be reached by realizing a form fit in the connection between the CFRP and the titanium z-pins. Ti CMT pin reinforced SLS specimens show increased τ_{FF} values compared to the Ti z-pin reinforced samples. Compared to co-cured SLS specimens the values are – 30.2 % lower. For a further increase in τ_{FF} an improvement of the CMT welding process for thin titanium sheets is required.

Figure 8.25 (b) shows the comparison of τ_{UF} values of through-the-thickness reinforced SLS joints. Ultimate failure occurs at high local joint strains, see Figure 8.26 (b). Compared to τ_{ss} values of co-cured SLS specimens τ_{UF} values of

specimens reinforced with steel CMT pin array type 1 and type 2 were + 6.0 % and + 0.4 % higher, respectively. Thus, the joints are able to maintain the level of stress reached at τ_{FF} up to values of strain above 2.5 % present at τ_{UF}. Specimens reinforced with pin array type 3 showed – 9.2 % lower values.

The local joint strains at τ_{UF} of the SLS specimens reinforced with steel CMT pin arrays 1, 2 and 3 were + 567.9 %, + 498.9 % and + 402.1 % higher, respectively, than the local joints strains at τ_{ss} of the co-cured SLS specimens (Figure 8.26 (b) and (c)).

This underlines the envisaged enhancement of the damage tolerance by such reinforcement inserts. In the case of the titanium pin reinforced samples only z-pins with a diameter of 1.14 mm were able to reach similar strain values. The local joint strains at τ_{UF} were + 369.7 % higher than the local joints strains of the co-cured SLS specimens. Ti z-pins with d = 0.76 mm and Ti CMT pins yielded increases in strain of + 254.9 % and + 82.6 %, but at significantly lower values of stress (see Figure 8.25 and Figure 8.26).

Deformation energies for different stages of the test are depicted in Figure 8.27. Deformation energies of through-the-thickness reinforced samples at ultimate failure (Figure 8.27 (a)) are significantly higher than both, deformation energies of through-the-thickness reinforced samples at first failure (Figure 8.27 (b)) and unreinforced samples at shear strength (Figure 8.27 (c)).

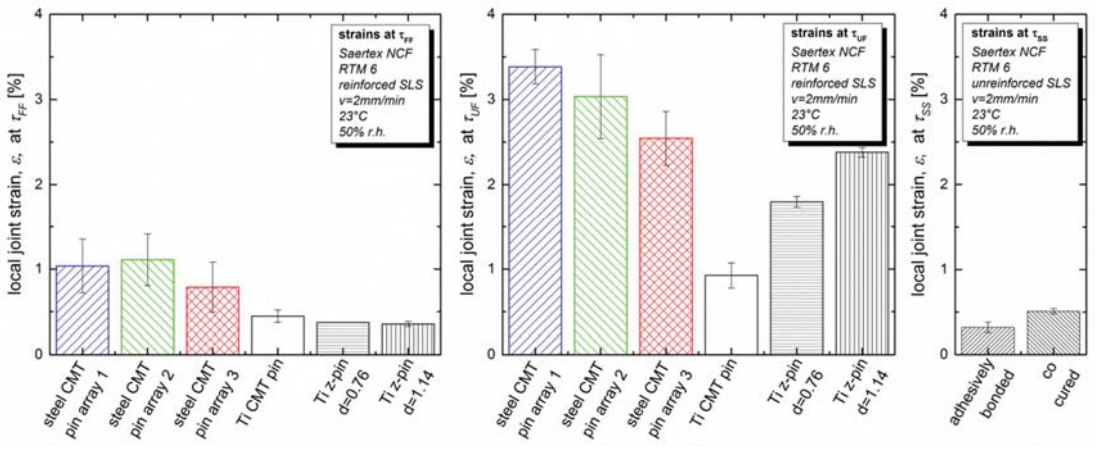

Figure 8.26: Local joint strains reached at (a) first failure stresses and (b) ultimate failure stresses compared to (c) local joint strains at shear strength reached by the adhesive-bonded and co-cured specimens.

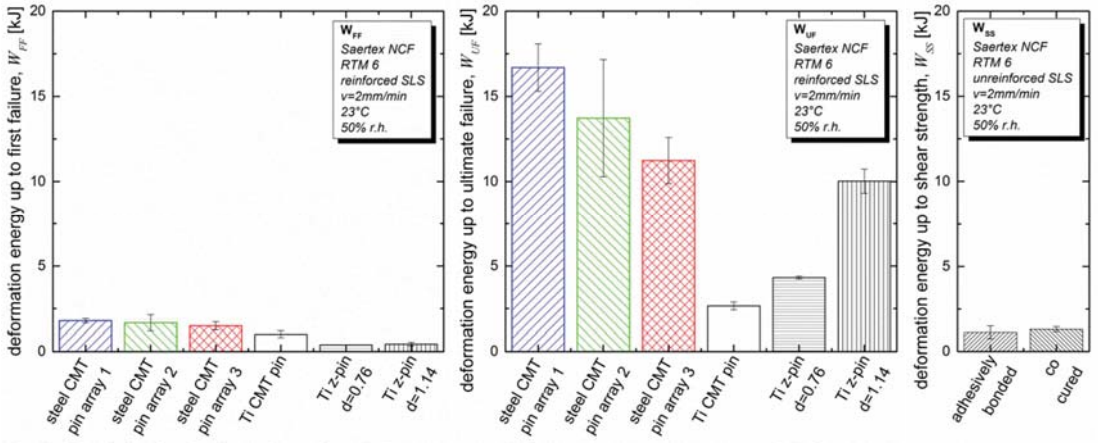

Figure 8.27: Deformation energies up to (a) first failure stress and (b) ultimate failure stress compared to (c) deformation energies up to shear strength of adhesive-bonded and co-cured specimens.

In Figure 8.28 the total deformation energies sustained by the through-the-thickness reinforced and unreinforced reference SLS specimens are compared. The three steel CMT pin reinforced SLS joint versions could bear total deformation energies of 22.3 ± 1.7 kJ, 23.0 ± 2.5 kJ and 22.1 ± 1.3 kJ, respectively. These values are approximately 14 times higher compared to the co-cured reference joints, which reached 1.6 ± 0.3 kJ. Thus, deformation energies can be significantly increased by the use of metal pins as through-the-thickness reinforcement.

The SLS specimens reinforced with thick Ti z-pins (d = 1.14 mm), thin Ti z-pins (d = 0.76 mm) and Ti CMT pins reached total deformation energies of 23.9 ± 3.5 kJ, 9.9 ± 1.2 kJ and 4.7 ± 1.0 kJ, respectively.

Figure 8.29 shows a comparison between the SLS specimens' relative stiffness values. All values are related to the adhesively bonded specimens. These yield the highest stiffness values. The use of metal pins as through-the-thickness reinforcement leads to a stiffness reduction of 18.3 % for Ti CMT pin reinforced samples, going up to 57.8 % in the case of samples reinforced with thin Ti z-pins.

The comparison of τ_{FF}, τ_{UF} and total deformation energies of the tested SLS joints shows, that the damage tolerance can be increased significantly by the use of CMT pins as through-the-thickness reinforcement compared to unreinforced specimens.

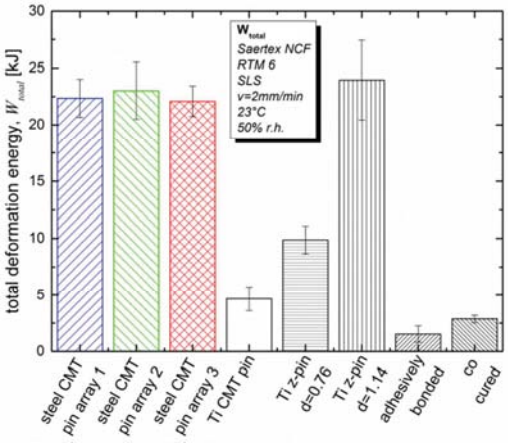

Figure 8.28: Total deformation energies of SLS specimens with pin reinforced interfaces compared to adhesive-bonded and co-cured reference joints.

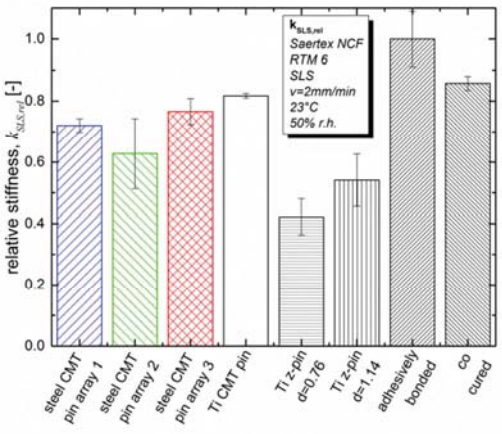

Figure 8.29: Relative stiffnesses (stiffnesses related to stiffness of adhesively bonded joint) of SLS specimens reinforced with different through-the-thickness reinforcements compared to adhesive-bonded and co-cured specimens.

8.3.7 Conclusions and outlook

The present work shows that 3D shaped stainless steel pins with small dimensions can be produced on thin stainless steel sheets via a modified cold metal transfer process. The use of ballhead pins with a spike on top improves both the drapability and the reinforcement of joining areas in CFRP to CFRP SLS joints. The use of pins in the joining area leads to a form-fit connection within the joint. This improves the load transfer performance and hence joint properties.

The use of reinforcing pins increases failure stresses and changes damage tolerance distinctively compared to adhesively bonded or co-cured specimens. This is reached without the need to cut fibers or drill holes and without a significant increase of structural weight.

The arrangement of steel CMT pins near the outer edges of the metal inserts leads to higher first failure stresses. The alignment of pins close to the center leads to higher ultimate failure stresses. The arrangement of pins has no distinct influence on the level of total deformation energy.

The reinforcement concept does work for titanium in principle. But for further enhancement of the mechanical properties of titanium pin reinforced joints, it is necessary to improve the CMT welding process. One approach is the utilization of a laser beam for stabilizing the welding arc.

In the present study, the metal sheets acted as carriage elements for coaxially aligned pins. The carriage elements were left within the joining area for manufacturing reasons. Future work will focus on the enhancement of the thin reinforcement inserts and on a further enhancement of such through-the-thickness reinforced CFRP to CFRP joints. Removing the sheet, or unused parts of the sheet, will give additional cutouts for resin bonding which will increase the mechanical properties of the joints.

8.3.8 Acknowledgements

The funding of the Austrian Research Promotion Agency for project 830384 “Composite+composite Joints with Enhanced damage toleranCe (CoJEC)” is gratefully acknowledged as well as the support of the involved project partners FACC AG, Fronius International GmbH, Rübig GmbH & Co KG, Fill GmbH, RECENDT GmbH and LKR Leichtmetall Kompetenzzentrum Ranshofen GmbH. Installation of the welding robot by Martin Schickbauer at Fill GmbH, calibration of the welding machine by Andreas Waldhoer from FRONIUS International GmbH and production of the press fitted titanium pins by Gerhard Sieglhuber from Fill GmbH are gratefully acknowledged.

8.3.9 References

[1] Pingkarawat K, Mouritz A. Improving the mode I delamination fatigue resistance of composites using z-pins. Composites Science and Technology 2014;92:70–6.

[2] Maurin R, Baley C, Cartié DDR, Davies P. Influence of Through-Thickness Pinning on Composite Shear Properties. Applied Composite Materials 2012;19(6):853–64.

[3] Cartié DD, Laffaille J, Partridge IK, Brunner AJ. Fatigue delamination behaviour of unidirectional carbon fibre/epoxy laminates reinforced by Z-Fiber® pinning. Engineering Fracture Mechanics 2009;76(18):2834–45.

[4] Lenzi F, Riccio A, Clarke A, Creemers R. Coupon Tests on z-Pinned and Unpinned Composite Samples for Damage Resistant Applications. Macromolecular Symposia 2007;247(1):230–7.

[5] Cartié DD, Dell'Anno G, Poulin E, Partridge IK. 3D reinforcement of stiffener-to-skin T-joints by Z-pinning and tufting. Engineering Fracture Mechanics 2006;73(16):2532–40.

[6] Cartié DD, Troulis M, Partridge IK. Delamination of Z-pinned carbon fibre reinforced laminates. Composites Science and Technology 2006;66(6):855–61.

[7] Partridge IK, Cartié DD. Delamination resistant laminates by Z-Fiber® pinning: Part I manufacture and fracture performance. Composites Part A: Applied Science and Manufacturing 2005;36(1):55–64.

[8] Rugg KI, Cox BN, Massabò R. Mixed mode delamination of polymer composite laminates reinforced through the thickness by z-fibers. Composites Part A: Applied Science and Manufacturing 2002;33:170–90.

[9] Plain KP, Tong L. An experimental study on mode I and II fracture toughness of laminates stitched with a one-sided stitching technique. Composites Part A: Applied Science and Manufacturing 2011;42(2):203–10.

[10] Rys T, Sankar BV, Ifju PG. Investigation of fracture toughness of laminated stitched composites subjected to mixed mode loading. Journal of Reinforced Plastics and Composites 2010;29(3):422–30.

[11] Aymerich F. Experimental investigation into the effect of edge stitching on the tensile strength and fatigue life of co-cured joints between cross-ply adherends. Advanced Composites Letters 2004;13(3):151–61.

[12] Aymerich F, Priolo P, Sun C. Static and fatigue behaviour of stitched graphite/epoxy composite laminates. Composites Science and Technology 2003;63(6):907–17.

[13] Dell'Anno G, Cartié DD, Partridge IK, Rezai A. Exploring mechanical property balance in tufted carbon fabric/epoxy composites. Composites Part A: Applied Science and Manufacturing 2007;38(11):2366–73.

[14] Stelzer S, Ucsnik S, Tauchner J, Unger T, Pinter G. Novel composite-composite joining technology with through the thickness reinforcement for enhanced damage tolerance. In: Hoa SV, Hubert P, editors. Proceedings of the 19th International Conference on Composite Materials: Canadian Association for Composite Structures and Materials; 2013, p. 4645–53.

[15] Löbel T, Kolesnikov B, Scheffler S, Stahl A, Hühne C. Enhanced tensile strength of composite joints by using staple-like pins: Working principles and experimental validation. Composite Structures 2013;106:453–60.

[16] Graham D, Rezai A, Baker D, Smith PA, Watts JF. A hybrid joining scheme for high strength multi-material joints. In: Proceedings of the 18th International Conference on Composite Materials. Jeju, South Corea; 2011.

[17] Ji H, Kweon J, Choi J. Fatigue characteristics of stainless steel pin-reinforced composite hat joints. Composite Structures 2014;108:49–56.

[18] Son H, Park Y, Kweon J, Choi J. Fatigue behaviour of metal pin-reinforced composite single-lap joints in a hygrothermal environment. Composite Structures 2014;108:151–60.

[19] Heimbs S, Nogueira A, Hombergsmeier E, May M, Wolfrum J. Failure behaviour of composite T-joints with novel metallic arrow-pin reinforcement. Composite Structures 2014;110:16–28.

[20] Noguiera AC, Drechsler K, Hombergsmeier E. Analysis of the Static and Fatigue Strength of a Damage Tolerant 3D-Reinforced Joining Technology on Composite Single Lap Joints. In: Ouwehand L, editor. Proc. 12th European Conference on Spacecraft Structures, Materials and Environmental Testing; 2012.

[21] Stelzer S, Ucsnik S, Fuchs P, Pinter G. Mechanical characterization of a novel compositecomposite joining technology with through the thickness reinforcement for enhanced damage tolerance. Composite Science and Technology:submitted on 09/23/2014.

9 FATIGUE TESTING OF COMPOSITE-COMPOSITE JOINTS

9.1 INTRODUCTION COMPOSITE-COMPOSITE JOINTS UNDER FATIGUE LOADS

Fatigue verification of joints is usually carried out on critical joints to demonstrate that the joint can carry the ultimate load through its design life. Therefore, representative service conditions of stress, temperature and humidity are applied. Principally, the same limitations as for quasi-static testing of joints apply to fatigue testing of joints. To date the influence of aspects such as scale, spectrum loading and service environment on joint performance cannot be inferred from test data on coupons. Fatigue tests on simple specimen and model joints, such as the SLS joint, are often undertaken at an early stage to screen candidate adhesives and provide preliminary design data [1].

So far, ASTM D3166 [2] is the only standard dealing with fatigue properties of bonded joints. Although it specifies fatigue testing of metal-metal joints, it can be assumed that this procedure also applies to composite-composite joints. It basically specifies positioning of SLS specimens in a fatigue test rig and the range of anticipated load cycles. The number of cycles to failure and the location of failure shall be recorded and the applied load shall be calculated in megapascals (load per overlap area). Since test geometries in ASTM D3166 refer to metal-metal joints, ASTM D5868 needs to be considered for geometries of composite-composite SLS specimens [3].

ASTM D3479 [4] deals with the determination of tension-tension fatigue properties of polymer matrix composite materials. It states that for preliminary fatigue testing of polymer matrix composite materials, a minimum number of six specimens should be tested to obtain preliminary and exploratory S-N curves. For research and development purposes, 12 specimens are recommended.

Fatigue testing on adhesively bonded joints was carried out extensively in literature [5–16]. Several authors presented classical S-N curves for adhesively bonded SLS and DLS joints [5–16] and some illustrated the stress-strain behavior [6] and the stiffness evolution [15] of adhesively bonded SLS joints under fatigue loading. It was also shown in literature that fracture mechanics can be applied to analyze and predict the fracture behavior of adhesively bonded joints [5,8,12,17–19]. Campilho and da Silva [19] correlated results from **publication 2** [20] with S-N curves and concluded that based on the fracture mechanical data from [20] it is

possible to predict the fatigue strength of joints of the same material. Yet, as shown by Bernasconi et al. [18], delamination initiation plays an important role in joint fatigue and can cause scatter in the predicted results. Thus, Bernasconi et al. correlated S-N curves on joints with fracture mechanics solely after the initiation of a delamination in the joint.

The initiation of cracks is significantly influenced by the geometry of the joint, as shown in chapter 6 of this thesis, and by the presence of through-the-thickness reinforcements. Fatigue testing of through-the-thickness reinforced joints was carried out by various authors. The majority used SLS specimens for the characterization of the fatigue properties of through-the-thickness reinforced joints [21–23], but in some cases tests on composite hat joints [24] and fracture mechanics tests [25] were also utilized. Fracture mechanics tests showed that through-the-thickness reinforcements rapidly decrease the crack growth leading to an apparent threshold behavior. This decrease in crack growth rate appears independent of applied load. Since the crack length does not increase significantly, the strain energy release rate is mainly controlled by the applied load [25]. Thus, fracture mechanical approaches towards the determination of the fatigue behavior of through-the-thickness reinforced joints are not feasible.

In this chapter, fatigue tests on SLS joints that are reinforced in the through-the-thickness direction, with either CMT or z-pins, are carried out and compared to the fatigue behavior of co-cured SLS specimens. A detailed investigation of the failure behavior is carried out by applying high resolution digital image correlation techniques to fatigue tests on composite-composite joints.

9.1.1 References

[1] Baker AA, Dutton S, Kelly D. Composite materials for aircraft structures. 2nd ed. Reston, VA: American Institute of Aeronautics and Astronautics; 2004.

[2] ASTM - American Society for Testing and Materials. D3166:99 - Standard test method for fatigue properties of adhesives in shear by tension loading (metal/metal)(D3166).

[3] ASTM - American Society for Testing and Materials. D5868:01 - Standard test method for lap shear adhesion of fiber reinforced plastic bonding(D5868:01).

[4] ASTM - American Society for Testing and Materials. D3479/D3479M:96 - Standard Test Method for Tension-Tension Fatigue of Polymer Matrix Composite Materials(D3479/D3479M:96); 1996 (2007).

[5] Abdel Wahab M, Ashcroft I, Crocombe A, Smith P. Finite element prediction of fatigue crack propagation lifetime in composite bonded joints. Composites Part A: Applied Science and Manufacturing 2004;35(2):213–22.

[6] Krenk S, Jönsson J, Hansen L. Fatigue analysis and testing of adhesive joints. Engineering Fracture Mechanics 1996;53(6):859–72.

[7] Wahab M, Ashcroft I, Crocombe A, Smith PA. Numerical prediction of fatigue crack propagation lifetime in adhesively bonded structures. International Journal of Fatigue 2002;24(6):705–9.

[8] Curley AJ, Hadavinia H, Kinloch AJ, Taylor AC. Predicting the service-life of adhesively-bonded joints. International Journal of Fracture 2000;103(1):41–69.

[9] Crocombe AD, Ong CY, Chan CM, Wahab, M. M. Abdel, Ashcroft IA. Investigating Fatigue Damage Evolution In Adhesively Bonded Structures Using Backface Strain Measurement. The Journal of Adhesion 2002;78(9):745–76.

[10] Meneghetti G, Quaresimin M, Ricotta M. Damage mechanisms in composite bonded joints under fatigue loading. Composites Part B: Engineering 2012;43(2):210–20.

[11] Sarfaraz R, Vassilopoulos AP, Keller T. Modeling the constant amplitude fatigue behavior of adhesively bonded pultruded GFRP joints. Journal of Adhesion Science and Technology 2013;27(8):855–78.

[12] Sarfaraz R, Vassilopoulos AP, Keller T. Experimental investigation of the fatigue behavior of adhesively-bonded pultruded GFRP joints under different load ratios. International Journal of Fatigue 2011;33(11):1451–60.

[13] Sarfaraz R, Vassilopoulos AP, Keller T. Experimental investigation and modeling of mean load effect on fatigue behavior of adhesively-bonded pultruded GFRP joints. International Journal of Fatigue 2012;44:245–52.

[14] Sarfaraz R, Vassilopoulos AP, Keller T. A hybrid S–N formulation for fatigue life modeling of composite materials and structures. Composites Part A: Applied Science and Manufacturing 2012;43(3):445–53.

[15] Zhang Y, Vassilopoulos AP, Keller T. Stiffness degradation and fatigue life prediction of adhesively-bonded joints for fiber-reinforced polymer composites. International Journal of Fatigue 2008;30(10-11):1813–20.

[16] Wang DY. Influence of stress distribution on fatigue strength of adhesive-bonded joints. Experimental Mechanics 1964;4(6):173–81.

[17] Abou-Hamda M, Megahed M, Hammouda M. Fatigue crack growth in double cantilever beam specimen with an adhesive layer. Engineering Fracture Mechanics 1998;60(5-6):605–14.

[18] Bernasconi A, Jamil A, Moroni F, Pirondi A. A study on fatigue crack propagation in thick composite adhesively bonded joints. International Journal of Fatigue 2013;50:18–25.

[19] Campilho R, da Silva L. Mode I fatigue and fracture behaviour of adhesively-bonded carbon fibre-reinforced polymer (CFRP) composite joints. In: Vassilopoulos AP, editor. Fatigue and fracture of adhesively-bonded composite joints. Cambridge: Woodhead Publishing; 2015, p. 93–120.

[20] Stelzer S, Brunner AJ, Argüelles A, Murphy N, Pinter G. Mode I delamination fatigue crack growth in unidirectional fiber reinforced composites: Development of a standardized test procedure. Composites Science and Technology 2012;72(10):1102–7.

[21] Aymerich F. Experimental investigation into the effect of edge stitching on the tensile strength and fatigue life of co-cured joints between cross-ply adherends. Advanced Composites Letters 2004;13(3):151–61.

[22] Chang P, Mouritz A, Cox B. Properties and failure mechanisms of pinned composite lap joints in monotonic and cyclic tension. Composites Science and Technology 2006;66(13):2163–76.

[23] Son H, Park Y, Kweon J, Choi J. Fatigue behaviour of metal pin-reinforced composite single-lap joints in a hygrothermal environment. Composite Structures 2014;108:151–60.

[24] Ji H, Kweon J, Choi J. Fatigue characteristics of stainless steel pin-reinforced composite hat joints. Composite Structures 2014;108:49–56.

[25] Cartié DD, Laffaille J, Partridge IK, Brunner AJ. Fatigue delamination behaviour of unidirectional carbon fibre/epoxy laminates reinforced by Z-Fiber® pinning. Engineering Fracture Mechanics 2009;76(18):2834–45.

9.2 PUBLICATION 9

FATIGUE BEHAVIOR OF CMT PIN REINFORCED COMPOSITE-COMPOSITE JOINTS

9.2.1 Bibliographic Information

- Authors and their relevant contributions to the publication:
  - Steffen Stelzer[1]
    Preparation and submission of the manuscript, execution of all tests, calculation and analysis of all test results.
  - Stephan Ucsnik[2]
    Project co-ordination and expert knowledge on cold metal transfer welding.
  - Gerald Pinter[1]
    Academic supervision of the work carried out in this publication.
- Affiliations:
  [1] Institute of Materials Science and Testing of Polymers, Montanuniversitaet Leoben, Leoben, Austria
  [2] Leichtmetallkompetenzzentrum Ranshofen GmbH, Austrian Institute of Technology, Lamprechtshausenerstraße Postfach 26, A-5282 Ranshofen, Austria
- Periodical: submitted to International Journal of Fatigue
- Manuscript number: IJFATIGUE-D-14-00475

Statement with regard to publication: The manuscript presented here is an adapted accepted manuscript in order to fit the formatting of the thesis and does not necessarily reflect the actually published version.

9.2.2 Abstract

In this paper the fatigue properties of through-the-thickness reinforced joints are studied in detail. Unreinforced specimens, specimens reinforced with cold metal transfer welded titanium and steel pins and specimens reinforced with titanium z-pins are investigated. Besides classical S-N diagrams, hysteresis curves and stiffness based approaches are applied to improve the understanding of the mechanical behavior of the joints in the progress of their fatigue life. Furthermore full field strain analysis gives information about damage initiation and growth in the joint section.

9.2.3 Introduction

Joining and through-the-thickness reinforcement of carbon fiber reinforced composites (CFRP) have been topics of increasing interest in recent years. The application of joints is important in areas, where integral design cannot be applied. These are areas, where limitations (coming from e.g. design, logistics or size) and requirements concerning e.g. repair, maintenance or handling are given [1,2]. Adhesive bonding provides low weight joints that do not require the cutting of fibers. However, bolt-free bonded joints are sensitive to peel and through thickness stresses. Thus, their use of for primary composite aircraft structures is still a certification issue. Rivets and bolts are commonly used to provide load path redundancy but increase the weight and weaken the composite material due to cut fibers [2].

Fiber-friendly, low weight alternatives for rivets and bolts may give additional options for designers to counteract peel stresses in composite-composite joints. Many researchers have investigated the capability of carbon fibers [3–10], polymeric yarns [11–14], glass fibers [7,15] and metal pins [2,10,16–22] as through-the-thickness reinforcement for CFRP laminates. They concluded that polymeric yarns, carbon fibers and glass fibers add to the damage tolerance of the laminate predominantly by crack bridging and energy absorption due to pullout of the fibers from the matrix resin [3–11]. Metal reinforcements can additionally add to the damage tolerance by plastic deformation of the metal reinforcement [20–22].

The applicability of metal reinforcements for composite-composite joining was investigated by various research groups in the past. Cartié et al. for example studied the influence of metallic rods on the fracture mechanical behavior of through-the-thickness reinforced CFRP. They concluded that failure mechanisms are dominated by debonding, rod/substrate friction and deformation of the rods.

These mechanisms depend on the insertion angle of the rods, giving a transition from pull-out dominated failure mechanisms to rod dominated failure. With rod failure giving the highest failure loads [23].

Rugg et al. carried out SLS tests on composite-composite joints which were reinforced with angled metallic rods. In tensile loading, all of the rods were pulled out, regardless of rod orientation. This pull out happened at relatively low loads and had thus little effect on the damage tolerance of the SLS joint [24]. Hence, in order to increase the damage tolerance of through thickness reinforced joints, the pull out of the through thickness reinforcements needs to be suppressed.

Research groups at EADS Innovation works [20,21,25–27] used sheet metal forming to reinforce composite-composite joints in the through thickness direction. The so-called RHEA (redundant high efficiency assembly) technology is based on the use of thin metallic sheets, where the pin geometry is laser-cut and bent to obtain reinforcement sheets with pins on both sides. Tests on T-joints gave increased residual forces after delamination initiation at the spar-skin interface. This is due to a crack bridging zone formed by the metallic pins at the debond interface [20]. However, pins based on the RHEA technology are not co-axially aligned and thus do not provide a straight load path between the joined composites.

Graham et al. produced metallic pins with a 3D geometry on laboratory scale by additive layer manufacturing (ALM). They joined metal to CFRP and observed significant increases in strength and damage tolerance [17,28]. In a more recent work, they replaced ALM by CMT welded pinning due to manufacturing cost and time reasons. Again significant increases in strength (+80 %) and energy absorption (+1000 %) were achieved [28].

The production of CMT pins on metal substrates was introduced by Ucsnik et al. and was used for the joining of meetal to CFRP [29–32]. The knowledge gained in the joining of metal to CFRP was later transferred to joining CFRP to CFRP (Stelzer et al. [16,33]). Reference [22] investigates the main failure mechanisms in CMT pin reinforced CFRP to CFRP joints.

This work deals with the determination of the mechanical properties of CFRP to CFRP joints that are reinforced with CMT pins. The focus is put on single lap shear (SLS) CFRP to CFRP specimens which are reinforced with thin steel or titanium sheets. These sheets carry arrays of 3D shaped pins co-axially aligned on top and bottom side.

9.2.4 Experimental

9.2.4.1 Materials and specimens

All SLS specimens tested in this study were made of epoxy resin from Hexcel Composites (Hexflow® RTM6) reinforced with high tenacity, standard modulus carbon fibers from Toho Tenax (Tenax® HTS, Saertex® non-crimp fabric, 540 g/m² areal weight). All laminates possessed a quasi-isotropic stacking sequence.

Metal reinforcements were made of stainless steel on the one hand and titanium on the other hand. Stainless steel inserts, see Figure 9.1, were of type AISI 304 with a sheet thickness of t = 0.6 mm. Ballhead spike pins, a combination of a ballhead pin with a small spike pin on top of it, were welded onto the steel sheets in a fully automated cold metal transfer welding process (steel CMT pin, see [22] for details). Steel CMT pins were made of filler wire type AISI 316L with a diameter of 0.8 mm. Titanium inserts were made of Ti6Al4V (Ti CMT pin). The titanium sheets had a thickness of 0.4 mm and the filler wire a diameter of 0.8 mm.

All metal inserts, both steel and titanium, carried coaxially aligned arrays of 4 x 6 pins on top and bottom side. The pins were arranged at the end positions of the inserts (see [22,34] for details).

Steel CMT pins had an overall height of about 3.3 mm and a tapered shaft with a diameter of about 1.2 mm at the bottom and 0.8 mm below the ballhead. Prior to the draping process the thin metal sheets and CMT pins were surface treated by cleaning and sandblasting in order to remove contaminations such as grease and welding tinder. At the same time sandblasting increased the roughness of the metallic surface and therefore increased the adhesion between the metal and the epoxy resin. In a final step the inserts were cleaned with an organic solvent.

Two types of titanium z-pin (Ti z-pin) reinforced specimens were additionally produced for comparison reasons. Type one carried with rods with a diameter of 0.76 mm and type two with rods with a diameter of 1.14 mm. In contrast to the Ti CMT pins, these pins were press fitted into predrilled titanium sheets (see [34] for details).

For the preforming process, the metal inserts were fixed in a metal mold (Figure 9.1). A set of dry CFRP textile layers was draped onto the pin arrays in a symmetrical manner on the top and bottom side of the insert, so that a stacking sequence for quasi-isotropic material properties was achieved. CFRP specimen panels were produced via a liquid resin infusion process.

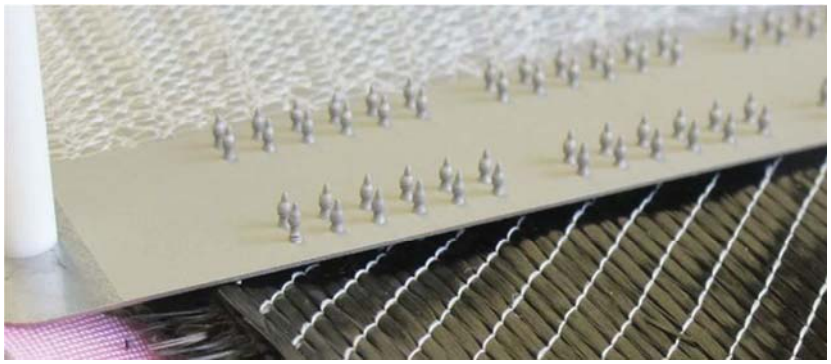

Figure 9.1: Metal insert carrying CMT pins fixed in a mold.

The final SLS specimens were cut out of the CFRP specimen-panels by waterjet cutting. Before waterjet cutting GFRP tabs were bonded onto both ends of the CFRP specimen-panels. This ensured both a symmetric clamping of the SLS joint specimens within the test system and an axially aligned joining interface. The final joint specimens had a width of 25 mm and a joining area of 750 mm² (Figure 9.2).

Co-cured specimens with equal geometry, but without metal inserts, were chosen as reference. To produce these specimens, the textiles for the two CFRP panels were put in the metal mold, infused with resin and cured simultaneously. The two CFRP panels were thus bonded by the cured resin.

9.2.4.2 Test methods

Fatigue tests were carried out on a servo-hydraulic test machine, type MTS 322 (MTS Systems Corp., Minneapolis, USA), with a 250 kN (±0.1%) load range. The frequency of the fatigue tests was fixed to 10 Hz in order to prevent hysteretic heating in the CFRP laps. The stress ratio, amounted to R = 0.1 for all tests. The tests were run until failure of the SLS specimens occurred or until a maximum number of cycles $N = 10^6$ was reached. S-N curves were analyzed based on ASTM E 739-98 [35].

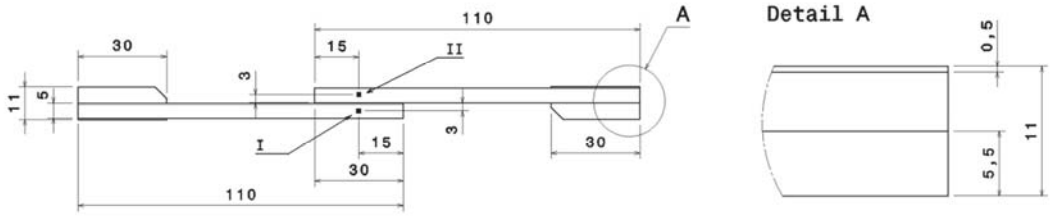

Figure 9.2: SLS specimen geometry.

All tests were carried out at a laboratory atmosphere of 23 ± 1 °C room temperature and 50 ± 10 % relative humidity. Specimens were preconditioned at laboratory conditions for at least 24 hours.

The digital image correlation (DIC) system Aramis (GOM GmbH, Braunschweig, Germany) was used to get information about local strains and displacements on the specimen's lateral surface. It was used to get information about damage initiation and growth in the joint section of the SLS specimens. Shear strains were measured using DIC. It was not feasible to calculate average shear strains from DIC, as strains showed a pronounced gradient in the bonding line. Therefore, two points were tracked at ± 3 mm from the joint interface in thickness direction (see points I, II in Figure 9.2). During fatigue tests, the distances in loading direction, L, and thickness direction, h, between these points was evaluated. Nominal shear strains, tan(γ), were calculated according to equation (9.1):

$$\tan(\gamma) = \Delta L/h \tag{9.1}$$

Local shear stresses were calculated by relating the load P to the initial joining area A_0:

$$\tau = P/A_0 \tag{9.2}$$

Local hysteresis data were gathered at every n^{th} cycle. Since DIC allowed for saving only a limited number of pictures to its memory, n had to be adapted for every load case. The change in hysteresis curves of polymer composites in fatigue tests can be ascribed to creep effects and material damage. While creep, caused e.g. by visco-eastic effects, leads to a horizontal shift of the hysteresis curve to higher strains at equal slope, material damage leads to a decrease in slope of the hysteresis. The dynamic shear modulus, G_{dyn}, describes the slope of the stress-strain hysteresis and can therefore be related to material damage [36]:

$$G_{dyn} = \left| \frac{\tau_{max} - \tau_{min}}{\tan(\gamma)_{max} - \tan(\gamma)_{min}} \right| \tag{9.3}$$

9.2.5 Results and Discussion

9.2.5.1 Co-cured reference joints

Co-cured specimens, carrying no reinforcements, were investigated under fatigue loading to get reference fatigue properties of unreinforced CFRP-CFRP SLS joints. An S-N diagram of co-cured specimens is shown in Figure 9.3. The nominal

maximum shear stress at N = 10^6 cycles ($\tau_{max,\ 10^6}$) amounts to 3.5 N/mm². The diagram shows limited scatter, $1/T_N$ = 4.2, and a slope value of k = 11.0.

For the assessment of the failure behavior of these joints, hysteresis curves at various numbers of cycles (Figure 9.4) and the corresponding DIC pictures (Figure 9.5) were recorded. The co-cured SLS specimens show hysteresis curves with a progressively declining slope and a rightwards shift. This is an indication of damage development in the specimen from cycle to cycle and visco-elastic effects in the polymer, respectively. Figure 9.5 (a-d) show DIC images at maximum stresses during these cycles. After N = 500 cycles (~50 % of the joint's lifetime) a crack has initiated at one end of the SLS specimens' joint area (Figure 9.5 (b)). With the progressing fatigue test, this crack grows (Figure 9.5 a and Figure 9.5 d) and leads to final failure of the specimen after N = 1180 cycles.

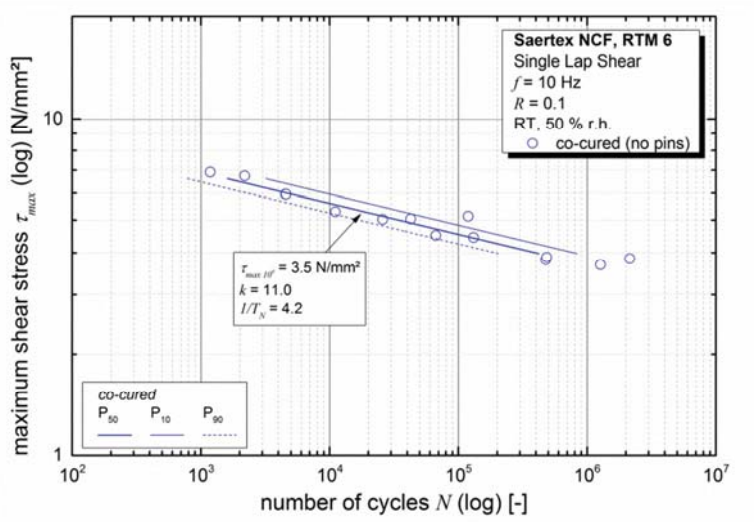

Figure 9.3: S-N curve for co-cured SLS specimens.

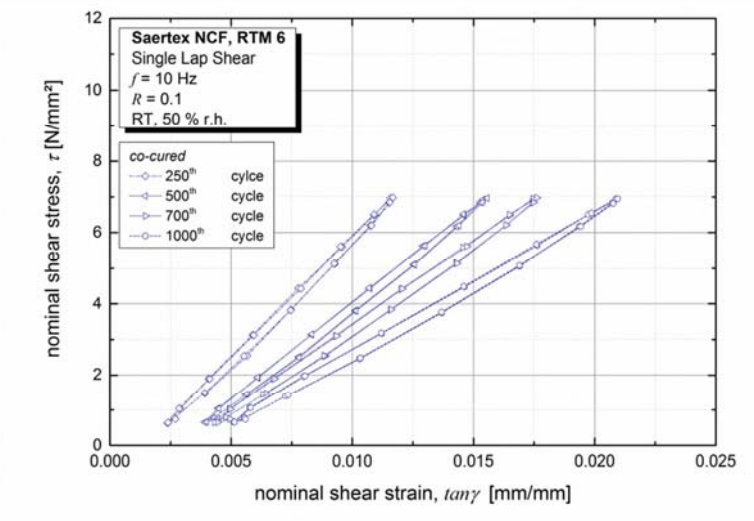

Figure 9.4: Stress-strain curves for a co-cured SLS specimen. Failure occurred after 1180 cycles.

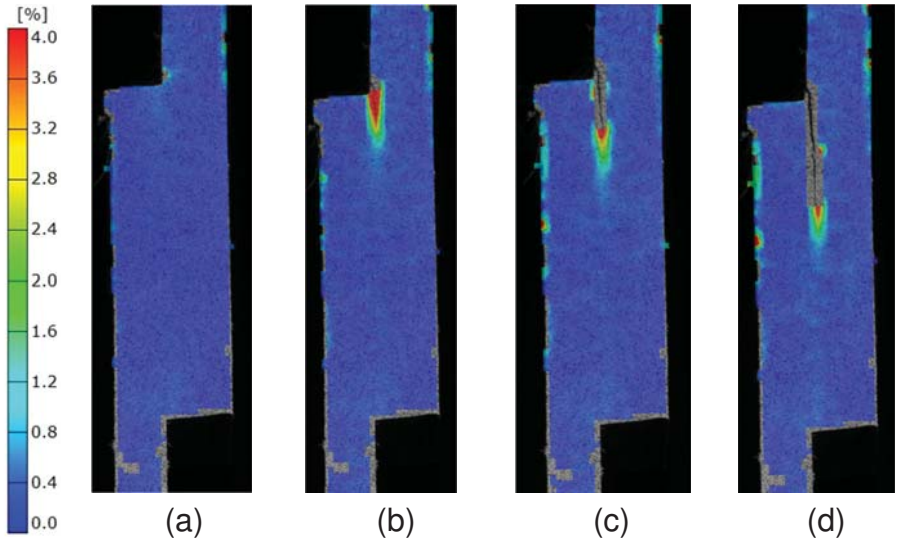

Figure 9.5: Distribution of major (axial/total) strains of a co-cured specimen at maximum load in fatigue after (a) 250 cycles, (b) 500 cycles, (c) 700 cycles and (d) 1000 cycles (failure occurred after 1180 cycles).

9.2.5.2 CMT pin reinforced SLS joints

Figure 9.6 shows S-N curves for both steel CMT pin reinforced SLS specimens (red lines) and Ti CMT pin reinforced SLS specimens (black lines). Steel CMT pin reinforced SLS joints reach higher shear stress levels of $\tau_{max,\,10^6} = 4.6$ N/mm² than Ti CMT pin reinforced samples with $\tau_{max,\,10^6} = 3.4$ N/mm². An increase in the amount of scatter, is quantified by $1/T_N$. For steel CMT pin reinforced SLS specimens $1/T_N = 5.8$ compared to Ti CMT pin reinforced samples $1/T_N = 78.5$ for Ti CMT pin reinforced samples.

Hysteresis curves at different numbers of cycles are shown in Figure 9.7. At equal level of applied shear stress, steel CMT pin reinforced SLS specimens sustain a significantly larger number of cycles (N = 62747 cycles) than the Ti CMT pin reinforced samples (N = 907 cycles). Steel CMT pin reinforced SLS specimens gave hysteresis curves with small decreases in slope and pronounced creep (see Figure 9.7 left).

For the Ti CMT pin reinforced samples on the other hand, a significant decrease in slope of the hysteresis curves and a horizontal shift of the curves is visible. The drop in dynamic stiffness is caused by damage initiation and propagation. A possible cause for the horizontal shifts of the hysteresis curves of both types of

CMT pin reinforced specimens is plastic deformation of the pin in combination with visco-elastic creep of the CFRP.

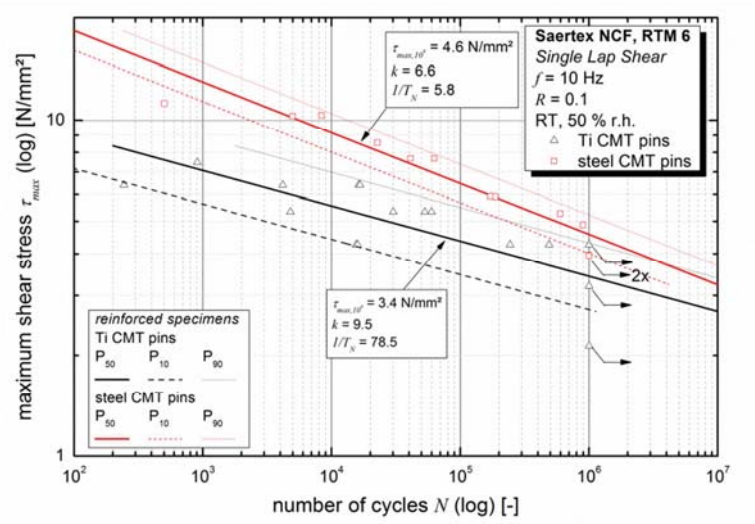

Figure 9.6: S-N curve for SLS specimens reinforced with CMT welded stainless steel (steel CMT pin, red lines) and titanium pins (Ti CMT pins, black lines).

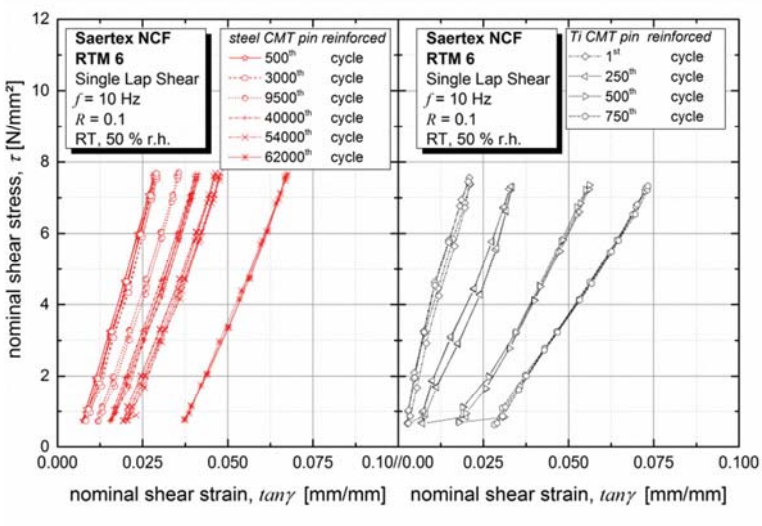

Figure 9.7: Left: Stress-strain curves for a SLS specimen reinforced with steel CMT pins. Failure occurred after 62747 cycles. Right: Stress-strain curves for a SLS specimen reinforced with Ti CMT pins (failure after 907 cycles).

DIC pictures of the steel CMT pin reinforced SLS specimens (Figure 9.8 (a-d)) show a highly strained interface region at the beginning of the test. Strain concentrations occur at the start and end of the connecting interface. In a progressed stage of the fatigue tests, in this case after about one third of the fatigue life of the specimen (N = 9500 cycles), cracks occur in the interface region (Figure 9.8 (b)) and steadily grow through the interface. Subsequently the

adhesive bonding fails. In contrast to unreinforced specimens, these specimens are still able to carry loads until a maximum of ~ 63000 cycles is reached. This is due to the reinforcing pins and their load carrying capability.

In the case of the Ti CMT pin reinforced samples, cracks initiate during the first cycle of fatigue testing (see Figure 9.9 (a)). In the progress of the test, the adhesive bond line fails and cracks grow within the CFRP laps (Figure 9.9 (b) and (c)).

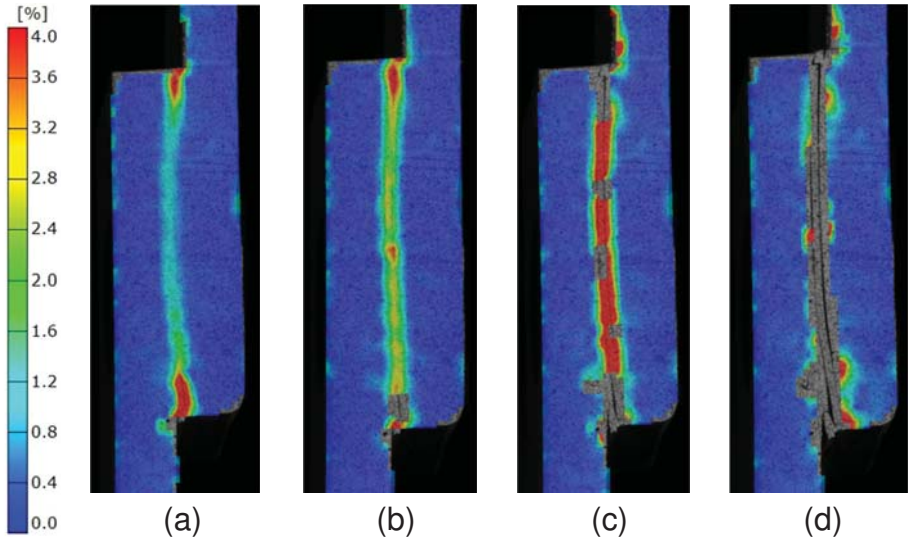

Figure 9.8: Distribution of major (axial/total) strains of steel CMT pin reinforced specimen at maximum load in fatigue after (a) 500 cycles, (b) 9500 cycles, (c) 54000 cycles and (d) 62000 cycles (failure occurred after 62747 cycles).

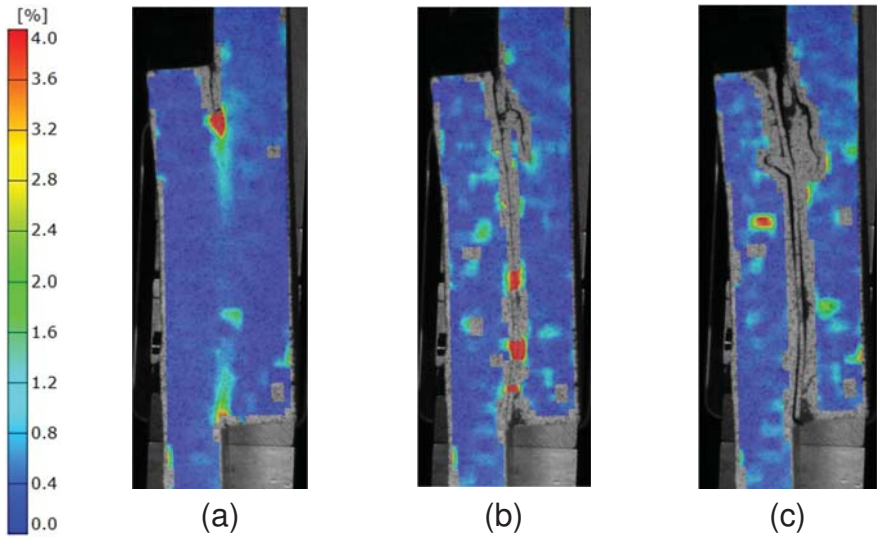

Figure 9.9: Distribution of major (axial/total) strains of Ti CMT pin reinforced specimens at maximum load in fatigue after (a) 1st cycle, (b) 250 cycles and (c) 750 cycles (failure occurred after 907 cycles).

A premature failure of the CFRP rather than progressive failure of the bond line and the pins indicates that Ti CMT pins act as an imperfection in the CFRP. The CMT welding process for titanium has yet to be improved.

9.2.5.3 z-pin reinforced joints

Figure 9.10 shows S-N curves of Ti z-pin reinforced SLS joints. There is a significant difference between the fatigue properties of SLS joints reinforced with thin (d = 0.76 mm) and thick (d = 1.14 mm) Ti z-pins. Samples reinforced with thin Ti z-pins sustain less cycles when fatigued at a certain level of stress.

$\tau_{max,\,10^6}$ amounts to 4.3 N/mm² for SLS specimens reinforced with thin Ti z-pins and 5.4 N/mm² for SLS specimens reinforced with thick Ti z-pins. This is reasonable due to the fact that an increased cross sectional area of the metal reinforcements leads to an enhanced load carrying capability of the same.

The slopes of the two S-N curves differ significantly with k = 13.9 for the thin Ti z-pins and k = 8.4 for the ones with 1.14 mm diameter. These results show that Ti z-pins are able to effectively contribute to the fatigue properties of the joint, but only above a certain pin diameter.

Figure 9.11 shows the stress-strain behavior of both types of Ti z-pin reinforced SLS specimens. SLS specimens reinforced with thin Ti z-pins (pink lines) show a pronounced creep behavior (shift of hysteresis) with significantly increasing strains at higher cycle numbers. This effect can be primarily ascribed to the subsequent loosening and pull out of the thin Ti z-pins from the CFRP.

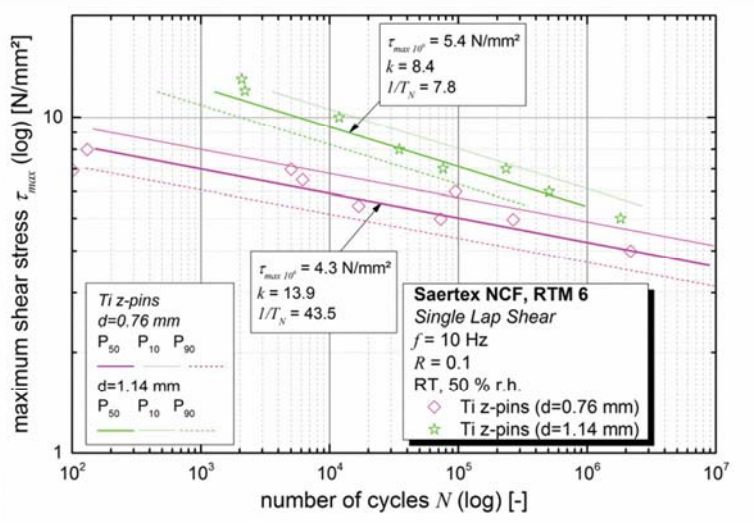

Figure 9.10: S-N curve for SLS specimens reinforced with Ti z-pins with 0.76 mm diameter (pink lines) and 1.14 mm diameter (green lines).

Figure 9.12 shows DIC images for both types of Ti z-pin reinforced SLS specimens. In both cases strains are predominantly occurring in the interface of the CFRP-CFRP joint.

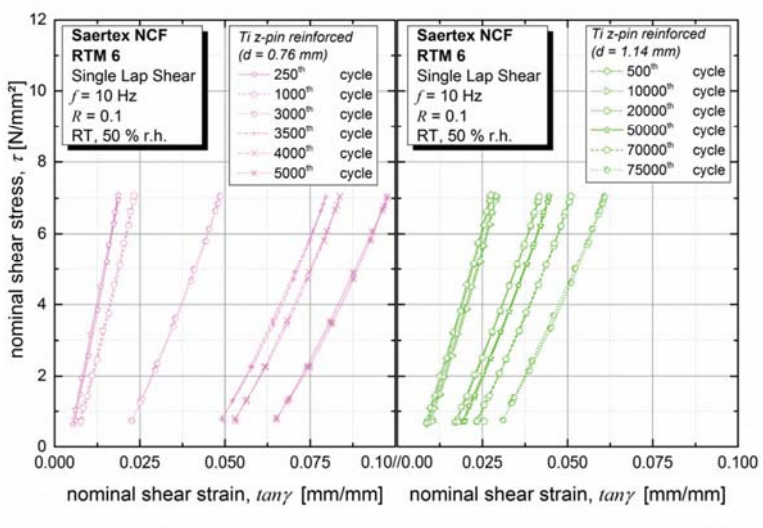

Figure 9.11: Left: Stress-strain curves for SLS specimens reinforced with Ti z-pins (d=0.76 mm). Failure occurred after 5025 cycles. Right: Stress-strain curves for a SLS specimen reinforced with Ti z-pins (d=1.14 mm). Failure occurred after 75963 cycles.

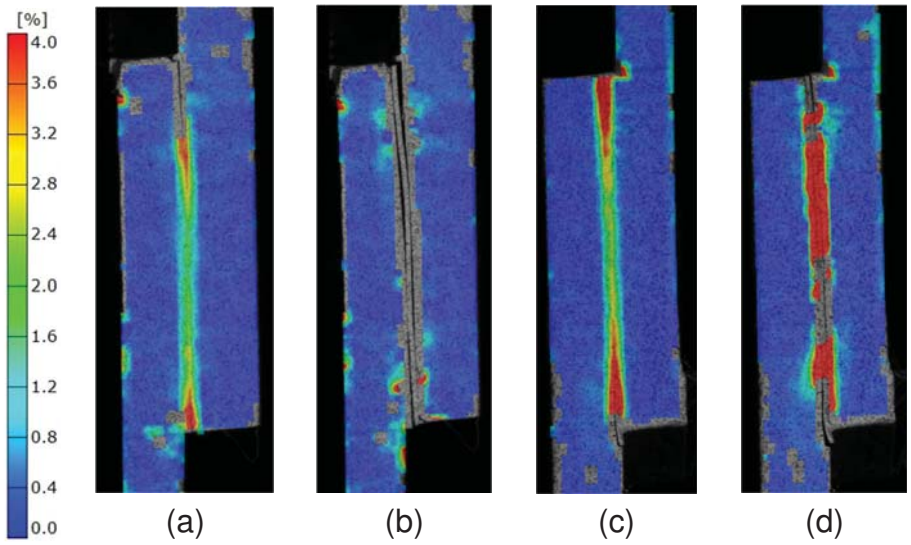

Figure 9.12: Distribution of major (axial/total) strains of Ti z-pin reinforced specimens at maximum load in fatigue: (a) $d_{z\text{-}pin}$ = 0.76 mm after 500 cycles,
(b) $d_{z\text{-}pin}$ = 0.76 mm after 5000 cycles (failure occurred after 5025 cycles),
(c) $d_{z\text{-}pin}$ = 1.14 mm after 500 cycles and
(d) $d_{z\text{-}pin}$ = 1.14 mm after 75000 cycles (failure occurred after 75963 cycles).

9.2.6 Comparison

Figure 9.13 gives a comparison of the 50 % probability of failure curves, P_{50}, of all tested SLS joints. SLS joints reinforced with either steel CMT pins or thick Ti z-pins (d = 1.14 mm) show superior fatigue behavior to co-cured SLS joints, SLS joints reinforced with Ti CMT Pins and SLS joints reinforced with thin Ti z-pins (d = 0.76 mm). The fatigue behavior of SLS specimens reinforced with thin Ti z-pin is very similar to co-cured SLS specimens. But increasing the z-pins' diameter to 1.14 mm leads to a fatigue behavior that is similar to SLS specimens reinforced with steel CMT pins.

Figure 9.14 shows post failure micrographs of the joint areas of SLS specimens reinforced with the four different types of metallic pins: (a) steel CMT pins, (b) Ti CMT pins, (c) thin Ti z-pins and (d) thick Ti z-pins. Steel CMT pins (Figure 9.14 (a)) and thick Ti z-pins (Figure 9.14 (d)) remain in the CFRP until failure of the joint. Cracks grew around the Ti CMT pins in the surrounding CFRP (Figure 9.14 (b)) because of suboptimum quality of those pins. The carbon fibers show areas of increased undulation, which indicates problems with draping. Thin Ti z-pins on the other hand were pulled out of the CFRP (Figure 9.14 (c)).

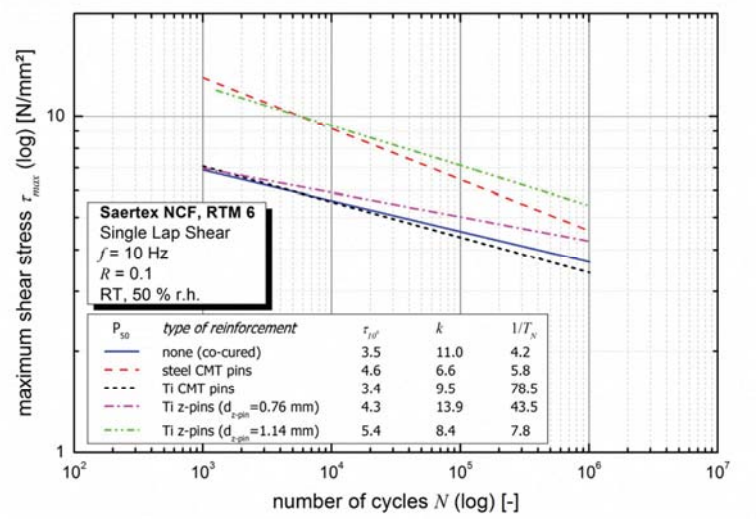

Figure 9.13: S-N curves of reinforced and unreinforced specimens versus number of cycles.

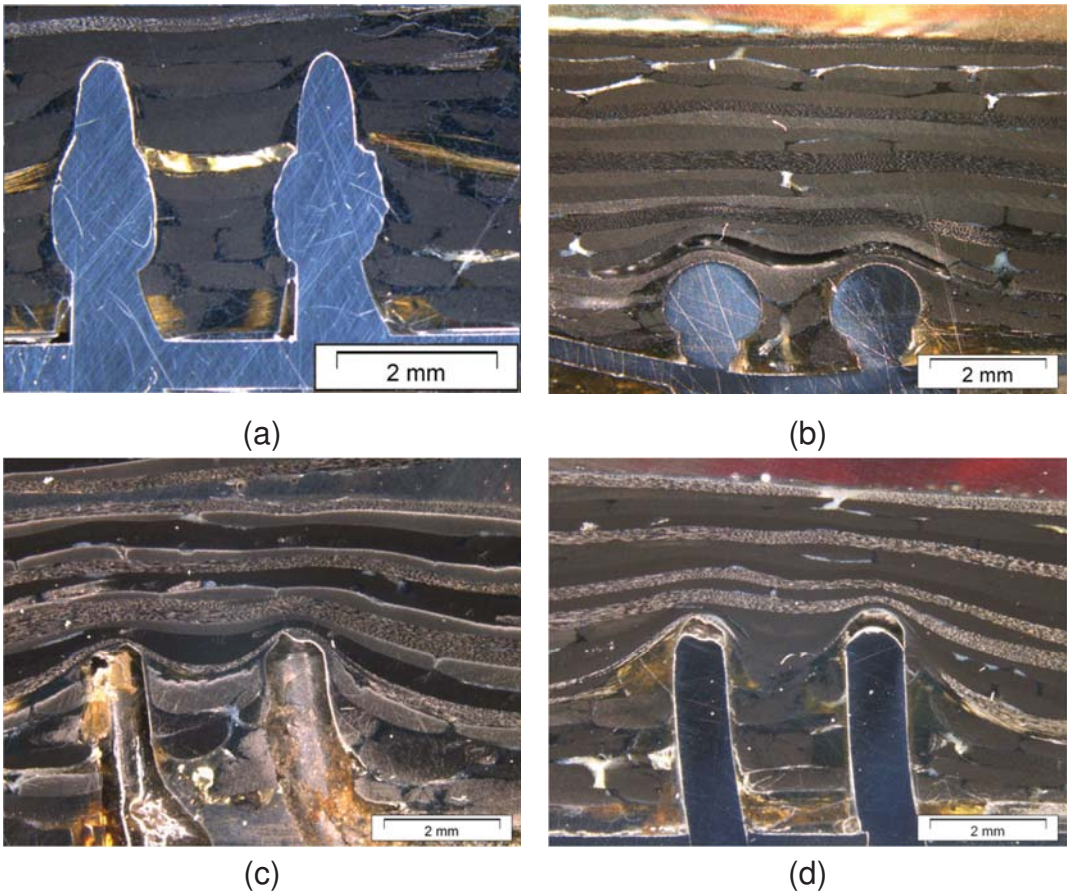

Figure 9.14: Micrographs of failed joint sections of SLS specimens reinforced with (a) steel CMT pins, (b) Ti CMT pins, (c) Ti z-pins (d = 0.76 mm) and (d) Ti z-pins (d = 1.14 mm).

The comparison of the failure behavior of the steel CMT pin reinforced SLS specimens (Figure 9.7 left) and Ti CMT pin reinforced specimens (Figure 9.7 right) shows that Ti CMT pin reinforced joints undergo significant losses in joint stiffness in their fatigue life. After failure of the adhesive bond line between the metal insert and the CFRP, the Ti CMT pin reinforced SLS joints are not able to maintain their stiffness. Cracks grow into the CFRP and deteriorate the joint and its properties (Figure 9.9).

The courses of relative dynamic shear moduli, G/G_0, with G_0 being the initial shear modulus, of SLS joints tested at τ_{max} = 5 N/mm² and τ_{max} = 7 N/mm² are shown in Figure 9.15 (for quasi-static strength values please see [34]). This allows the comparison of stiffness evolution of all tested SLS joints in fatigue. At start of fatigue tests, the relative dynamic shear modulus results to 1.0. With increasing cycle number, the relative stiffness decreases as damage grows. At failure, G/G_0 drops towards 0. All SLS joint specimens face losses in relative dynamic modulus

with increasing numbers of cycles. SLS specimens reinforced with either steel CMT pins (green line) or thick Ti z-pins (red dashed line) maintain the dynamic stiffness for a larger number of cycles. SLS specimens reinforced with Ti CMT pins, or thin Ti z-pins and co-cured SLS specimens face a much earlier drop of G/G_0.

One method to account for this loss in stiffness in the S-N curves is to define failure by a specific decrease in dynamic modulus [37]. Thus, in this study an arbitrary value of - 10 % loss in dynamic stiffness, as indicated in Figure 9.15, was chosen as failure criterion. Figure 9.16 shows the resulting S-N curves. The slope values k decrease by - 55 %, - 20 % and - 46 % for the co-cured and both CMT pin (steel and Ti) reinforced SLS specimens, respectively. In all three cases k amounts to around 5, when considering a - 10 % loss in stiffness as failure. Hence the curves are steeper than the fatigue strength based S-N curves.

$\tau_{max,\,10^6}$ values decrease by - 53 %, - 28 % and - 47 % for the co-cured, steel CMT pin and Ti CMT pin reinforced SLS specimens, respectively. Thus, the steel CMT pin reinforcements are able to maintain most of the SLS joint's stiffness during fatigue. The Ti CMT pin reinforced and co-cured SLS specimens on the other hand undergo significant decreases in dynamic modulus.

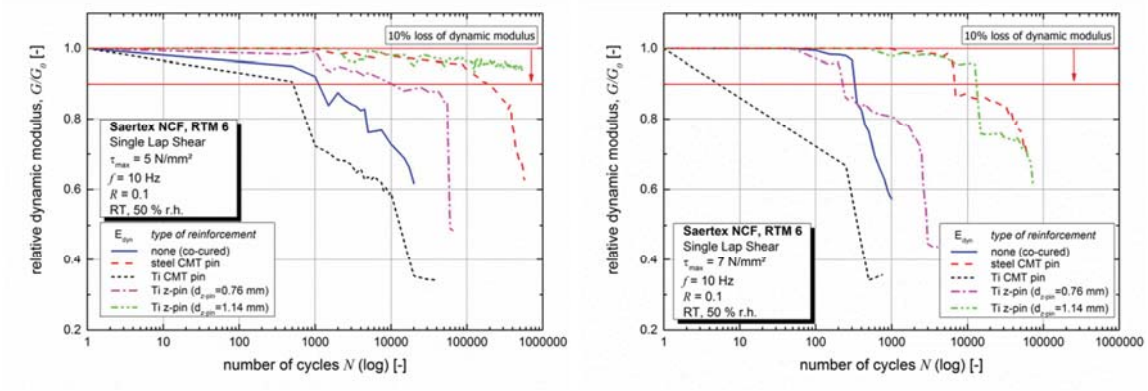

Figure 9.15: Dynamic stiffnesses of reinforced and unreinforced specimens versus number of cycles. The specimens were fatigued in load control at a maximum shear stress of (a) 5 N/mm² and (b) 7 N/mm².

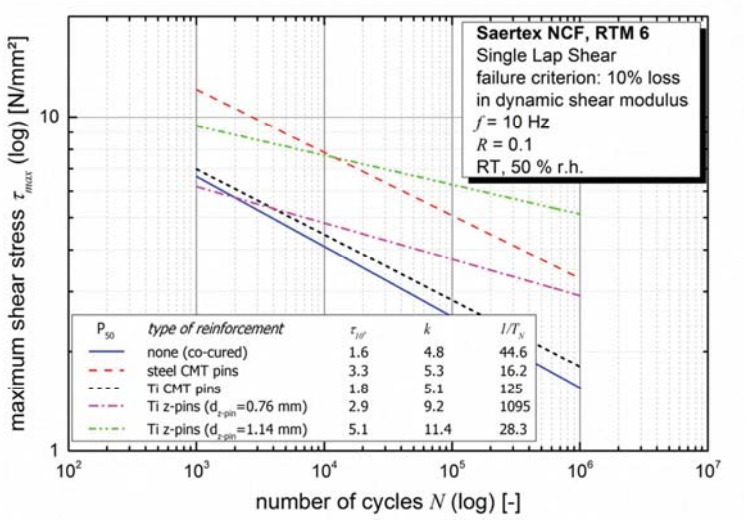

Figure 9.16: S-N curves of reinforced and unreinforced specimens versus number of cycles. 10% loss of dynamic stiffness was considered as failure of the SLS joint connection.

The $\tau_{max,\,10^6}$ values of SLS specimens reinforced with thin and thick Ti z-pins decrease by - 51 % and - 11 %, respectively.

While the value of k decreases by - 45 % for SLS specimens reinforced with thin Ti z-pins, they increase by + 11 % for SLS specimens reinforced with thick Ti z-pins. Thus, SLS specimens reinforced with thick Ti z-pins face higher losses in stiffness at high stress amplitudes than in the high cycle fatigue regime.

9.2.7 Conclusions and Outlook

Cold metal transfer welded steel pins proved to be an effective means for reinforcing CFRP-CFRP SLS joints in the through thickness direction. After failure of the bond line between the two CFRP laps, pins carry the loads and maintain the joint's stiffness until final failure.

CMT welded titanium pins on the other hand turned out to be less effective for reinforcing CFRP-CFRP joints. This can be partly ascribed to the lack of a pronounced ballhead-spike geometry for Ti CMT pins. Welding process improvements for thin titanium sheets are necessary for an increased fatigue performance.

Tests on reference titanium z-pin reinforced specimens show that titanium pins can be effective for reinforcing SLS joints. Nevertheless, thin Ti z-pins are pulled out of the CFRP and the capability of reinforcing the joint is lost. A form fit

connection between the CFRP and the Ti z-pins would prevent pull out of the z-pins from the CFRP.

The herein presented test routine gives comprehensive information on the fatigue behavior of SLS joints. Measurements of the strain distributions on the surface of the specimens via DIC turned out to be a powerful tool for assessing crack initiation, crack growth and the failure behavior. It gives information about damage initiation, interface failure and subsequent damage mechanisms related to the pin reinforcement. Hysteresis curves and derived dynamic modulus allow for information about the creep behavior of the joint and about damage evolution in the joint.

9.2.8 Acknowledgements

The funding of the Austrian Research Promotion Agency for project 830384 “Composite+composite Joints with Enhanced damage toleranCe (CoJEC)” is gratefully acknowledged as well as the support of the involved project partners FACC AG, Fronius International GmbH, Rübig GmbH & Co KG, Fill GmbH, RECENDT GmbH and Austrian Institute of Technology GmbH. Installation of the welding robot by Martin Schickbauer at Fill GmbH, calibration of the welding machine by Andreas Waldhoer from FRONIUS International GmbH and support in testing by Jürgen Grosser at the Montanuniversität Leoben are gratefully acknowledged.

9.2.9 References

[1] Baker AA, Dutton S, Kelly D. Composite materials for aircraft structures. 2nd ed. Reston, VA: American Institute of Aeronautics and Astronautics; 2004.

[2] Löbel T, Kolesnikov B, Scheffler S, Stahl A, Hühne C. Enhanced tensile strength of composite joints by using staple-like pins: Working principles and experimental validation. Composite Structures 2013;106:453–60.

[3] Pingkarawat K, Mouritz A. Improving the mode I delamination fatigue resistance of composites using z-pins. Composites Science and Technology 2014;92:70–6.

[4] Maurin R, Baley C, Cartié DDR, Davies P. Influence of Through-Thickness Pinning on Composite Shear Properties. Applied Composite Materials 2012;19(6):853–64.

[5] Cartié DD, Laffaille J, Partridge IK, Brunner AJ. Fatigue delamination behaviour of unidirectional carbon fibre/epoxy laminates reinforced by Z-Fiber® pinning. Engineering Fracture Mechanics 2009;76(18):2834–45.

[6] Lenzi F, Riccio A, Clarke A, Creemers R. Coupon Tests on z-Pinned and Unpinned Composite Samples for Damage Resistant Applications. Macromolecular Symposia 2007;247(1):230–7.

[7] Cartié DD, Dell'Anno G, Poulin E, Partridge IK. 3D reinforcement of stiffener-to-skin T-joints by Z-pinning and tufting. Engineering Fracture Mechanics 2006;73(16):2532–40.

[8] Cartié DD, Troulis M, Partridge IK. Delamination of Z-pinned carbon fibre reinforced laminates. Composites Science and Technology 2006;66(6):855–61.

[9] Partridge IK, Cartié DD. Delamination resistant laminates by Z-Fiber® pinning: Part I manufacture and fracture performance. Composites Part A: Applied Science and Manufacturing 2005;36(1):55–64.

[10] Rugg KI, Cox BN, Massabò R. Mixed mode delamination of polymer composite laminates reinforced through the thickness by z-fibers. Composites Part A: Applied Science and Manufacturing 2002;33:170–90.

[11] Plain KP, Tong L. An experimental study on mode I and II fracture toughness of laminates stitched with a one-sided stitching technique. Composites Part A: Applied Science and Manufacturing 2011;42(2):203–10.

[12] Rys T, Sankar BV, Ifju PG. Investigation of fracture toughness of laminated stitched composites subjected to mixed mode loading. Journal of Reinforced Plastics and Composites 2010;29(3):422–30.

[13] Aymerich F. Experimental investigation into the effect of edge stitching on the tensile strength and fatigue life of co-cured joints between cross-ply adherends. Advanced Composites Letters 2004;13(3):151–61.

[14] Aymerich F, Priolo P, Sun C. Static and fatigue behaviour of stitched graphite/epoxy composite laminates. Composites Science and Technology 2003;63(6):907–17.

[15] Dell'Anno G, Cartié DD, Partridge IK, Rezai A. Exploring mechanical property balance in tufted carbon fabric/epoxy composites. Composites Part A: Applied Science and Manufacturing 2007;38(11):2366–73.

[16] Stelzer S, Ucsnik S, Tauchner J, Unger T, Pinter G. Novel composite-composite joining technology with through the thickness reinforcement for enhanced damage tolerance. In: Hoa SV, Hubert P, editors. Proceedings of the 19th International Conference on Composite Materials: Canadian Association for Composite Structures and Materials; 2013, p. 4645–53.

[17] Graham D, Rezai A, Baker D, Smith PA, Watts JF. A hybrid joining scheme for high strength multi-material joints. In: Proceedings of the 18th International Conference on Composite Materials. Jeju, South Corea; 2011.

[18] Ji H, Kweon J, Choi J. Fatigue characteristics of stainless steel pin-reinforced composite hat joints. Composite Structures 2014;108:49–56.

[19] Son H, Park Y, Kweon J, Choi J. Fatigue behaviour of metal pin-reinforced composite single-lap joints in a hygrothermal environment. Composite Structures 2014;108:151–60.

[20] Heimbs S, Nogueira A, Hombergsmeier E, May M, Wolfrum J. Failure behaviour of composite T-joints with novel metallic arrow-pin reinforcement. Composite Structures 2014;110:16–28.

[21] Noguiera AC, Drechsler K, Hombergsmeier E. Analysis of the Static and Fatigue Strength of a Damage Tolerant 3D-Reinforced Joining Technology on Composite Single Lap Joints. In: Ouwehand L, editor. Proc. 12th European Conference on Spacecraft Structures, Materials and Environmental Testing; 2012.

[22] Stelzer S, Ucsnik S, Fuchs P, Pinter G. Mechanical characterization of a novel compositecomposite joining technology with through the thickness reinforcement for enhanced damage tolerance. Composite Science and Technology:submitted on 09/23/2014.

[23] Cartié D, Cox B, Fleck NA. Mechanisms of crack bridging by composite and metallic rods. Composites Part A: Applied Science and Manufacturing 2004;35(11):1325–36.

[24] Rugg KL, Cox BN, Ward KE, Sherrick GO. Damage mechanisms for angled through-thickness rod reinforcement in carbon–epoxy laminates. Composites Part A: Applied Science and Manufacturing 1998;29(12):1603–13.

[25] Jürgens M, Noguiera AC, Lang H, Hombergsmeier E, Drechsler K. Influence of an optimized 3D-reinforcement layout on the structural

mechanics of co-bonded CFRP joints. In: Proceedings of the 16th European Conference on Composite Materials, 22.06. - 26.06.2014.

[26] Noguiera AC, Drechsler K, Hombergsmeier E, Furfari D, Pacchione M. Investigation of a hybrid 3D-reinforced joining technology for lightweight structures. In: Ferreira A, editor. 16th International Conference on Composite Structures ICCS16; 2011.

[27] Noguiera AC, Drechsler K, Hombergsmeier E. Properties and failure mechanisms of a 3D-reinforced joint. JEC Composites Magazine 2011:39–44.

[28] Graham DP, Rezai A, Baker D, Smith PA, Watts JF. The development and scalability of a high strength, damage tolerant, hybrid joining scheme for composite–metal structures. Composites Part A: Applied Science and Manufacturing 2014;64:11–24.

[29] Ucsnik S, Gradinger R. Evaluation of a Novel Lightweight Metal-Composite-Joint Technology. Proc. 14th European Conference on Composite Materials 2010(paper ID 311-ECCM14).

[30] Ucsnik S, Pahr D. Investigation of novel composite-metal-joints. Proc. 11th Japanese-European Symposium on Composite Materials 2008.

[31] Ucsnik S, Scheerer M, Zaremba S, Pahr D. Experimental investigation of a novel hybrid metal–composite joining technology. Composites Part A: Applied Science and Manufacturing 2010;41(3):369–74.

[32] Ucsnik S, Tauchner J, Fleischmann M. Vergleich von Mischbau-Fügetechniken am Beispiel einer Metall-CFK-Lasteinleitung aus der Luftfahrt. In: Proceedings of the 7th Ranshofener Leichtmetalltage, Gmunden, Austria, 07.11. - 08.11.2012.

[33] Stelzer S, Ucsnik S, Sehrschön H, Tauchner J, Pinter G. Fatigue behavior of through the thickness reinforced joints. In: Proceedings of the 16th European Conference on Composite Materials, 22.06. - 26.06.2014.

[34] Stelzer S, Ucsnik S, Pinter G. Composite-composite joints with metallic through the thickness reinforcements. Composites Part A: Applied Science and Manufacturing:submitted on 10/27/2014.

[35] ASTM - American Society for Testing and Materials. ASTM E 739 - 98 - Standard Practice for Statistical Analysis of Linear or Linearized Stress-Life (S-N) and Strain-Life (e-N) Fatigue Data(E739 - 98).

[36] Pinter G, Ladstätter E, Billinger W, Lang R. Characterisation of the tensile fatigue behaviour of RTM-laminates by isocyclic stress–strain-diagrams. International Journal of Fatigue 2006;28(10):1277–83.

[37] ASTM - American Society for Testing and Materials. D3479/D3479M:96 - Standard Test Method for Tension-Tension Fatigue of Polymer Matrix Composite Materials(D3479/D3479M:96); 1996 (2007).

10 CONCLUSIONS TO PART III

Results from laboratory fatigue tests on structural elements presented in literature [1–5] and in publication 6 of this thesis show that delaminations can initiate in composite structures, despite current design philosophies for composites. This is mainly due to stress gradients acting out-of-plane at geometric flaws (e.g. ply drops, bonded joints) and boundaries (e.g. free edges, holes) in the composite structure. Locally increasing the interlaminar strength of the composite at these critical locations will delay the initiation of delaminations. In this thesis, a novel composite-composite joining technology is evaluated in quasi-static and fatigue loading. This technology is based on cold metal transfer (CMT) welded pins that are placed out-of-plane in the joint area of the composite. The CMT pins provide a three dimensional shape that offers a form fit, non-detachable connection between the pin and the surrounding composite. A thin metal sheet acted as a carrier element for the CMT pins in this thesis. It eased the positioning of the pins in the joined area, but on the other hand acted as imperfection avoiding cohesive resin bonding in the joint.

Nevertheless, this approach proved to be effective towards improving the damage tolerance of composite-composite joints without significantly increasing the structural weight. In a first step, optimum pin reinforcement locations in single lap shear (SLS) specimens were investigated using numerical simulations and tests on unreinforced specimens. Subsequent tests on CMT pin reinforced SLS specimens under quasi-static loading indicated that strains at failure and damage tolerance can be increased substantially compared to unreinforced (co-cured or adhesively bonded) SLS specimens.

Detailed investigations of the failure mechanisms of steel CMT pin reinforced SLS specimens were carried out. Micrographs of failed specimens, digital image correlation and quasi-static tests on pretreated SLS specimens led to a schematic that describes the different stages of failure in the CMT pin reinforced SLS joint.

A first attempt to use CMT welded titanium pins instead of steel CMT pins as through-the-thickness reinforcement for composite joints illustrated the need for process improvements in the CMT pin sculpturing stage for titanium. Sub optimum titanium CMT pin shapes yield mechanical properties that are below the properties of titanium z-pin and steel CMT pin reinforced samples. This affects both, the

quasi-static and fatigue properties of the joint. When subjected to fatigue loads, unreinforced, co-cured specimens show a common failure behavior consisting of crack initiation and crack growth resulting in catastrophic failure of the joint. Through-the-thickness reinforced specimens on the other hand are able to carry loads even after the adhesive failure of the bond line. This is due to the reinforcing pins and their load carrying capability.

10.1 REFERENCES

[1] G. Savage, Sub-critical crack growth in highly stressed Formula 1 race car composite suspension components, Engineering Failure Analysis 16 (2009) 608–617.

[2] W. Seneviratne, J. Tomblin, T. Cravens, Durability and residual strength assessment of F/A-18 A-D wing-root stepped-lap joint, Proc. 11th AIAA ATIO Conference, AIAA Centennial of Naval Aviation Forum (2011).

[3] E.S. Greenhalgh, Delamination growth in carbon-fibre composite structures, Composite Structures 23 (1993) 165–175.

[4] P. Chalkley, R. Geddes, Service history of the F-111 wing pivot fitting upper surface boron/epoxy doublers: DSTO-TN-0168. Department of Defence, September (1998).

[5] D.S. Cairns, T. Riddle, J. Nelson, Wind Turbine Composite Blade Manufacturing: The Need for Understanding Defect Origins, Prevalence, Implications and Reliability, Sandia Report 1094 (2011).

[6] C. Soutis, F. Smith, F. Matthews, Predicting the compressive engineering performance of carbon fibre-reinforced plastics, Composites Part A: Applied Science and Manufacturing 31 (2000) 531–536.

[7] C. Liljedahl, M.E. Fitzpatrick, L. Edwards, Residual stresses in structures reinforced with adhesively bonded straps designed to retard fatigue crack growth, Composite Structures 86 (2008) 344–355.

Part IV:

Summary and Outlook

11 SUMMARY AND OUTLOOK

In this thesis, delamination fatigue tests were carried out on various endless fiber reinforced polymer (FRP) composites. It was shown that different materials yield distinguishable slope values (Paris law's exponents of the delamination growth curve) and that these values can, in principle, be used for design of composite structures. However, up to now, composites show a delamination growth behavior with large slope values. This fact makes it hard to correctly predict the delamination growth in composite structures based on the Paris law relationship.

The large scatter seen in round robins on delamination fatigue testing of composite materials limits the applicability of this kind of test for design. The sources of this scatter have to be investigated in detail and solutions have to be found to reduce the scatter, before fatigue delamination tests can be applied in the design of composite structures. One option might be the calculation of expected numbers of cycles to failure from crack growth kinetics and comparing this data with the results from fatigue tests. Correct Paris law representations will yield similar numbers of cycle to failure as the experiment and will provide reliable data for fatigue life predictions (see e.g. Frank [1] for lifetime prediction of polyolefin pipes).

Additionally, the effect of slope value on the fatigue life will have to be studied extensively. It is debatable whether a composite with a low slope value will be preferable since such a laminate may yield higher delamination rates at relatively low applied loads. Composite structures are designed in a way that the composite has to carry low loads and faster crack growth at these low loads may be detrimental for service life.

Delamination fatigue measurements on braided and filament wound carbon FRPs carried out in this thesis show that delamination fatigue tests can be sensitive to small changes in the structure of the material, despite the problems encountered in the round robin tests. Both monotonic and cyclic delamination tests picked up changes in the delamination resistance due to differences in the fiber architecture or the use of a thermoplastic stabilizer thread in the braiding process.

Preliminary fatigue delamination testing in mode II loading gave differences between two types of test rig (end notched flexure and end loaded split). Adverse compressive stresses under and near the center loading pin may affect the

delamination propagation in the end-notched flexure set-up and thus yield apparently higher loads. Ongoing round robin testing for mode II fatigue delamination will investigate this topic and additionally address the influence of test parameters and data reduction on the results of mode II fatigue delamination tests. Only if all the problems are resolved, will it be time to draft a standard test procedure for mode II fatigue delamination testing.

The testing routines presented in this thesis, in principle, allow to measure threshold values. However, the measurement of the threshold is a very complex and sensitive topic due to (1) large in- and inter-laboratory scatter, (2) the sensitivity of delamination tests to load range resolution and (3) possible influences of fiber-bridging on the threshold value. Further, testing at very low delamination growth rates requires high numbers of cycle for small increments in delamination length. Together with the need to test at low frequencies to avoid hysteretic heating in composites, this leads to very long test durations.

Data analysis schemes that address some of the problems encountered during round robin testing are presented in chapter 5 of this thesis. A modified Hartman-Schijve approach yields power law representations of delamination fatigue growth curves with exponents that amount to around 2. Further, the results become independent of stress ratio and resemble the crack growth behavior of metals. The analogy or similarity in the power law describing the fatigue crack growth for different classes of materials (metals and composites) with the Hartman-Schijve equation may, in principle, imply possible analogies in the fatigue crack growth behavior, specifically at low values of strain energy release rate [2]. Since fracture mechanics was first developed for metals, it is worthwhile to investigate whether effects observed for that class of materials also apply to FRP composites.

Foremost, there remains the question whether the fatigue threshold for small or short cracks (e.g., millimeter or sub-millimeter size) in composite materials or structural elements becomes ‘very small’. This would constitute a composite analogy to the so-called ‘short crack’ problem for metals, where anomalous behavior under fatigue loading was observed for cracks extending for, e.g., 10 micrometer, compared to ‘longer’ cracks of several millimeter length and more. At present, evidence for investigating this question quite likely will have to come from structural fatigue tests or from composite structural applications under real fatigue load spectra. A direct experimental verification on laboratory scale specimens does seem difficult, due to, among others, e.g., cracks and other

defects already present in the material after manufacturing and the difficulty of implementing suitable, well defined starter cracks for testing.

In part III of this thesis, it was shown that the use of cold metal transfer (CMT) welded pins as through-the-thickness reinforcement can significantly increase the damage tolerance of composite-composite joints compared to co-cured and adhesively bonded joints. In both, quasi-static and fatigue loading steel CMT pins were able to carry loads even after adhesive failure of the joint's bond line. In quasi-static loading, the level of load stayed at a high level up to high values of strain. In fatigue tests steel CMT pin reinforced joints failed at significantly higher numbers of cycle than unreinforced joints. The joint's stiffness remained at a high level up to high numbers of cycles, when steel CMT pins were used as through-the-thickness reinforcement.

Titanium CMT pin reinforced samples on the other hand did not reach the level of mechanical properties that was reached when using steel CMT pins as through-the-thickness reinforcement. This can be ascribed to the lack of a pronounced ballhead-spike geometry, which would improve the form-fit connection between the titanium and the CFRP.

Based on these preliminary results, the CMT pin joining technology is currently being improved. Welding process improvements for thin titanium sheets are necessary for an increase in the mechanical properties of titanium CMT pin reinforced composite-composite joints. One approach is the use of a laser beam to stabilize the welding arc. Another area of possible improvement is the metal sheet that carried the CMT pins in the preliminary tests in this thesis. The metal sheet, or unused parts of the metal sheet, which were so far left within the joining area between the two composite adherends, will be removed to allow for additional resin bonding. This will increase the mechanical properties of the joint, but on the other hand complicate the positioning of the pins in the CFRP.

Further, there are several open questions concerning CMT pin reinforced joints that will have to be investigated in the future, despite the very positive results in this thesis. In order to receive CMT pin reinforced joints with optimum properties it will be necessary to investigate pin size effects. Thick (large diameter) pins cause detrimental effects such as fiber undulations and large resin pockets in the vicinity of the pin reinforcement. Thin (small diameter) pins will reduce these effects and transfer loads more homogeneously. Given that they do not pull out from the CFRP, because of a properly working form-fit thin pins would be hence ideal for joining composites. But below a critical diameter, they may not be feasible for

automated manufacturing techniques. During draping, thin pins will be bent more easily than thick pins. Additional points that will have to be investigated are the effects of the CMT pins on the in-plane mechanical properties of the CFRP. Significant knockdowns in compressive strength can be expected due to fiber misalignment and undulations [3,4].

In addition, differences in the coefficient of thermal expansion between metal and CFRP (consisting of fiber and matrix resin) cause residual stresses in the metal-polymer interface [5]. These residual stresses may have a negative effect on the joint's mechanical properties and will have to be investigated at different testing temperatures.

Concerning the application of the CMT pin joining technology there are two main areas of interest. On the one hand it may be used to support bolts/rivets in a joint and thereby reduce their amount. This can lead to a significant reduction in weight. On the other hand, CMT pins may even completely replace bolts/rivets in the composite structure. Yet, the above mentioned topics of interest have to be addressed first, before CMT pins can be applied in service.

11.1 REFERENCES

[1] A. Frank, Fracture mechanics based lifetime assessment and long-term failure behaviour of polyethylene pressure pipes. Dissertation, Leoben, 2010.

[2] R. Jones, S. Pitt, A. Brunner, D. Hui, Application of the Hartman–Schijve equation to represent mode I and mode II fatigue delamination growth in composites, Composite Structures 94 (2012) 1343–1351.

[3] D.S. Cairns, T. Riddle, J. Nelson, Wind Turbine Composite Blade Manufacturing: The Need for Understanding Defect Origins, Prevalence, Implications and Reliability, Sandia Report 1094 (2011).

[4] C. Soutis, F. Smith, F. Matthews, Predicting the compressive engineering performance of carbon fibre-reinforced plastics, Composites Part A: Applied Science and Manufacturing 31 (2000) 531–536.

[5] C. Liljedahl, M.E. Fitzpatrick, L. Edwards, Residual stresses in structures reinforced with adhesively bonded straps designed to retard fatigue crack growth, Composite Structures 86 (2008) 344–355.

APPENDIX:

Abbreviations and Symbols

ABBREVIATIONS

Abbreviation	Meaning
3ENF	end-notched flexure in 3 point bending
AITM	Airbus Industrie test method
ALM	additive layer manufacturing
ASTM	American Society of Testing and Materials
BSS	Boeing specification support standard
CAI	compression after impact
CBT	corrected beam theory
CFRP	carbon fiber reinforced polymer
CLS	cracked lap shear
CMT	cold metal transfer
CoJEC	composite-composite joints with enhanced damage tolerance
da/dN	crack growth rate
DCB	double cantilever beam
DIC	digital image correlation
DLS	double lap shear
ECM	experimental compliance method
ENF	end-notched flexure
ELS	end-loaded split

Abbreviation	Meaning
ESIS TC4	European Structural Integrity, Technical Committee 4
FCG	fatigue crack growth
FEP	poly-tetra-fluoro-ethylene-hexa-fluoro-propylene
FKV	Faserkunststoffverrbund
FRMM	fixed ratio mixed mode
FRP	Fibre reinforced polymer
FR-PMC	fiber reinforced polymer matrix composite
GFRP	glass fiber reinforced polymer
FF	first failure
HB	China aviation industry standard
ISO	International Standardization Organization
JIS	Japanese industrial standard
MCC	modified compliance calibration
MMB	mixed mode bending
MMF	mixed mode fracture
NCF	non-crimp fabric
PEEK	poly-ether-ether-ketone
PTFE	poly-tetra-fluor-ethylene
RT	room temperature
RTM	resin transfer molding
SBT	simple beam theory

Abbreviation	Meaning
SLS	single lap shear
SS	shear strength
Ti	titanium
UD	unidirectional
UF	ultimate failure
VARTM	vacuum assisted resin transfer molding

SYMBOLS

Symbol	Unit	Meaning
2h	[mm]	specimen thickness (double cantilever beam specimen)
a	[mm]	crack (delamination) length
A	[J/m²]	toughness like parameter of the Hartman-Schijve equation
		or
	[-]	constant of the Paris law
α	[-]	exponent of the Anderson equation
A_0	[mm²]	Initial bonding area of the SLS specimen
a_e	[mm]	effective crack length in mode II loading
a_{eff}	[mm]	effective crack length in mode I loading
b	[mm]	specimen width
β	[-]	exponent of the Hartman-Schijve equation
C	[mm/N]	specimen compliance
C'	[-]	constant of the Anderson equation
d	[mm]	diameter
δ	[mm]	axial displacement
δ_{cr}	[mm]	critical displacement in the quasi-static test
δ_{max}	[mm]	maximum displacement in cyclic test

Symbol	Unit	Meaning
D	[-]	constant of the Hartman-Schijve equation
Δ	[mm]	correction factor to account for the effects of transverse shear and for deformation beyond the crack tip
da/dN	[mm/cycle]	crack growth rate
ΔG	[J/m²]	strain energy release rate range
ΔK	[MPa $m^{1/2}$]	stress intensity factor range
ΔK_{th}	[MPa $m^{1/2}$]	threshold stress intensity factor range
E_{11}	[GPa]	Young's modulus in fiber direction
E_{22}	[GPa]	Young's modulus transverse to fiber direction
E_{33}	[GPa]	Young's modulus in thickness direction of the laminate
$E_{45°}$	[MPa]	Young's modulus in 45° to the fiber direction
F	[-]	correction factor for large displacements
F^*	[-]	correction factor fpr curved shape of the crack in the three point bending, end-notched flexure test
G	[J/m²]	strain energy release rate
G_C	[J/m²]	critical strain energy release rate
G_{IC}	[J/m²]	critical strain energy release rate in mode I
G_{IIC}	[J/m²]	critical strain energy release rate in mode II

Symbol	Unit	Meaning
$G_{I:II=4:3}$	[J/m²]	critical strain energy release rate in mixed mode I/II with a load ratio of I:II=4:3
G_{12}	[GPa]	shear modulus in 12 direction
G_{23}	[GPa]	shear modulus in 23 direction
G_{13}	[GPa]	shear modulus in 13 direction
G_{dyn}	[MPa]	dynamic shear modulus
G_I	[J/m²]	strain energy release rate in mode I
G_{II}	[J/m²]	strain energy release rate in mode II
G_I^{mixed}	[J/m²]	mode I partition of the strain energy release rate in a mixed mode test
G_{II}^{mixed}	[J/m²]	mode II partition of the strain energy release rate in a mixed mode test
G_m	[J/m²]	mixed mode strain energy release rate
G_{max}	[J/m²]	maximum strain energy release rate
G_{min}	[J/m²]	minimum strain energy release rate
G_{total}	[J/m²]	total strain energy release rate (sum of all modes)
G_{th}	[J/m²]	threshold of strain energy release rate
G_{thr}	[J/m²]	threshold like parameter of the Hartman-Schijve equation

Symbol	Unit	Meaning
h	[mm]	half thickness of double cantilever beam, end-notched flexure, end-loaded split specimen and fixed ratio mixed mode specimen
η	[-]	exponent of the Benzeggagh and Kenane criterion for mixed mode loading
K	[MPa $m^{1/2}$]	stress intensity factor
K_c	[MPa $m^{1/2}$]	critical stress intensity factor
K_m	[MPa $m^{1/2}$]	mean stress intensity factor
K_{11}	[N/mm^3]	cohesive stiffness in 11 direction
K_{22}	[N/mm^3]	cohesive stiffness in 22 direction
k	[-]	slope of S-N curve in the double logarithmic diagram (exponent of the power law)
k_{SLS}	[N/mm]	SLS joint stiffness
L	[mm]	span of end notch flexure specimen
m	[-]	exponent of the Paris law
N	[-]	number of cycles, or
		or
	[-]	load-block correction factor

Symbol	Unit	Meaning
N^*	[-]	correction factor for changes of the specimen compliance in a three point bending, end-notched flexure test
ν_{12}	[-]	lateral contraction in 12 direction
ν_{23}	[-]	lateral contraction in 23direction
ν_{13}	[-]	lateral contraction in 13 direction
p	[-]	number of data points used for calculating da/dN rates according to ASTM E647
P	[N]	axial load
P_I	[N]	load in tensile direction
P_{II}	[N]	load in shear direction
p_x	[mm]	pitch between two rows of pins in loading direction
p_y	[mm]	pitch between two rows of pins in lateral direction
σ_{Imax}	[MPa]	cohesive strength in 1 direction
σ_{Imax}	[MPa]	cohesive strength in 2 direction
τ_{FF}	[MPa]	first failure stress
τ_{max}	[MPa]	maximum of the shear modulus
$\tau_{max,\ 10^6}$	[MPa]	nominal maximum shear stress at 10^6 cycles

Symbol	Unit	Meaning
τ_{SS}	[MPa]	shear strength
τ_{UF}	[MPa]	ultimate failure stress
tanγ	[mm/mm]	shear strain
W_x	[Nm]	dissipated energy during deformation of SLS joints